



**Evaluation of groundwater potential based on hybrid
approach of geology, geophysics, and
geoinformatics: Case study of
Buffalo Catchment area,
Eastern Cape, South Africa**

SOLOMON T. OWOLABI



A thesis submitted in fulfillment of the requirements for the degree of

DOCTOR OF PHILOSOPHY IN GEOLOGY

SUPERVISOR: Dr. K. MADI

CO-SUPERVISOR: Dr. A. M. KALUMBA

**In the
Department of Geology
Faculty of Science and Agriculture
University of Fort Hare**

2019

DECLARATION

This thesis is my own work and has not previously been submitted in fulfillment of the requirement of another degree or to another university.

Signature

A handwritten signature in black ink, appearing to be 'C. M. H.', written over a horizontal line.

.....

.....



University of Fort Hare
Together in Excellence

20thJUNE, 2019

DECLARATION ON PLAGIARISM

—I, Solomon T. Owolabi, student number 201704667, hereby declare that I am fully aware of the

University of Fort Hare's policy on plagiarism, and I have taken every precaution to comply with the regulations.

Signature



University of Fort Hare
Together in Excellence

DECLARATION ON RESEARCH ETHICS CLEARANCE

—I, Solomon Temidayo Owolabi, with the student number 201704667, hereby declare that I am fully aware of the University of Fort Hare’s policy on research ethics, and I have taken every precaution to comply with the regulations. I confirm that my research constitutes an exemption to Rule G17.6.10.5 and an ethical certificate with a reference number is not required.

Signature



University of Fort Hare
Together in Excellence

ABSTRACT

This study focuses on the feasibility of exploring potential groundwater zones through assessment of catchment geo-hydrodynamic processes, using hydro-statistic principles and geographic information system-based approaches. The research work integrated analysis of hydrologic variables, geologic structures, and geomorpho-tectonic processes that provide information on spatial variability of hydrologic units in a watershed. The study is aimed at improving conceptual knowledge and presenting the technical feasibility of exploring potential groundwater zones through geo-hydrodynamic perspectives in hydrogeologically challenged environments. The study adopted a case design approach at the Buffalo hydrologic basin headwater in Eastern Cape, South Africa. The methods used in this study include: field mapping of geologic units and structures, digital processing of aeromagnetic map, cross-section profiling of borehole logs, auto-extraction of lineament, streamflow variability and recession assessment, geomorpho-tectonic analysis of surficial drainage pattern, vertical electrical sounding for imaging shallow subsurface layers, and geospatial integration of thematic maps of groundwater multi-influencing factors. The results indicate that the hydrogeological settings of Buffalo watershed comprised of good, moderate, fair, poor and very poor groundwater potential zones which cover 187 km², 338 km², 406 km², 185 km², and 121 km² respectively. The results report that the groundwater system of Buffalo watershed is mainly hosted by the well-drained fractured dolerite and the shallow unconfined sandstone aquifer. The aquifer is bounded by two parallel impermeable valley walls in the north and south. Also, the Buffalo drainage system constitutes a variable head boundary as a groundwater discharge zone. The groundwater discharge which mostly occurs at the Tshoxa upper course, Mgqakwebe, Quencwe, Yellowwoods upper course and the Buffalo River center influence the status of the Buffalo River as a perennial river system.

The groundwater recharge occurs through the networks of surficial lineaments and fractures concentrated on the sandstone lithosome, mostly in the northern half of the watershed. The surficial tectonic features trend in a WNW-ESE and E-W direction. The groundwater flow system is controlled by the subsurface lineaments which are oriented in west-northwest – east-southeast direction. Most of the groundwater recharge is driven by rain which is extreme at the north. The hydro-climatic pattern of the region influences the dendritic drainage system of Buffalo watershed. The geologic characterization and geomorpho-tectonic analysis indicate that the geologic settings are made up of upward-fining lithologic material and siliciclastic materials that were deposited as fill in paleochannels by braided and meandering fluvial systems. The variability in dissection property and the fluvial system indicates that Buffalo hydrologic and geomorphic systems are heterogeneous and complex. The possible impact of these variabilities aligns with the report of geoelectric sections which revealed the heterogeneity of the aquifer intrinsic properties and variability in groundwater yield. The electric resistivity tomography revealed the existence of a fault system and variation in the thickness of the aquifer. Hydrologic characterization indicates the vulnerability status of the rivers within the watershed. In particular, the Ngqokweni River is vulnerable to diminution while Quencwe River has the potential for a flash flood. Buffalo station is an important surface water capture zone. Delineation of groundwater potential zone should incorporate geologic, hydrologic, geophysical, geomorpho-tectonic, and environmental perspectives due to the inherent relationship among influencing factors. The study therefore identifies groundwater capture zones which can be further explored for groundwater development and to mitigate the stake of water shortage. The study therefore recommends the approach here to the department of water affairs for adoption to map the zones of groundwater potential at a regional scale. The study also provides resourceful information on

groundwater recharge zones and therefore recommends that the environment and water stakeholders work together to protect the recharge zones from groundwater contamination due to land use.

Keywords: Geohydrodynamics; Hydrologic time-series; Basement configuration; River catchment; Balfour formation; Groundwater potential zones; Morphometric analysis; Lineaments; Flow duration curve; recession analysis; Buffalo river; and Analytical Heirarchical Analysis



University of Fort Hare
Together in Excellence

ACKNOWLEDGMENT

I am grateful to the Almighty God, my savior, the Lord Jesus Christ, and the Holy Spirit for the life, grace and intellect that birth the special opportunity to begin and see the PhD programme to this very final stage.

My utmost gratitude goes to my supervisor, Dr. Kakaba Madi, for his kind heartedness towards me. His consistent academic, moral and logistical support throughout every stage of the programme was the major synergy that birthed this achievement. I also want to thank my co-supervisor, Dr. Ahmed Mukalazi Kalumba, for enabling the platform for my analyses, career development and providing the strategic advice that ensued the success of this programme. I like to thank Prof. Anthony Okoh, Prof. Omobola Okoh, Prof. B.F. Alemaw, Dr. Emmanuel Adelabu, and Dr. T. E. Iortyom, the entire staff of Department of Geology and Department of Geography and Environmental Science, for their moral and technical contribution to my advancement.

My heartfelt appreciation goes to my sweetheart, Victoria Olajumoke Owolabi, and to my children, Emmanuel Oluwadarasimi (GIG) and Eleazar Teminijesu (JIM) Owolabi for their sacrificial love and endurance through the academic journey. I am indebted to my parents, Pst. Israel Oluwole Owolabi and Deaconess Rachael Aduke Owolabi, who invested greatly in spiritual, emotional and financial terms into who I am today. I would also like to thank the following families for their support and advice, Prof. Emmanuel Olufemi Owolabi, Dr. and Mrs. Emmanuel Adelabu, and Dr. Goke Adeniji for their prayers and support.

I am grateful to have shared the PhD experience with a number of other postgraduate students in Geography, Geology and Chemistry departments, University of Fort Hare. I am particularly thankful to Gbenga Adesola for their tireless support during the geoelectric survey. I am thankful to Athenkosi Mpemba, Ebenezer Fatumo and Chinemerem Ohoro for their vast support during

the field geologic and hydrologic survey. I am thankful for their moral support, assistance and friendship.

I would like to thank the Govan Mbeki Research and Development Centre for providing me tuition fee waiver and supervisory-linked bursary from the second year. I also wish to express my gratitude to the South Africa Weather Service, and Department of Water Affairs, for making data available for the success of this study.



University of Fort Hare
Together in Excellence

LIST OF ABBREVIATIONS AND GLOSSARY OF TERMS

ACF: Autocorrelation function

ATHR: Angular difference threshold

BFI: Baseflow index

B-P: Box-Pierce

BR: Buishand range test

CMB: Chloride mass balance

CRD: Cumulative rainfall departure

DD: Drainage density

DEM: Digital elevation model



University of Fort Hare
Together in Excellence

DMC: Double mass curve

DTHR: Distance threshold

ERT: Electrical resistivity tomography

FDC: Flow duration curve

FTHR: Fitting threshold

GIS: Geographic information system

GM: Geometrical mean

GPS: Global positioning system

GW: Groundwater

GW – SW: Groundwater – surface water

J-B: Jarque-Bera

KS: Kolmogorov-Smirnov

L-B: Ljung-Box

LD: Lineament density

LST: Land surface temperature

LTHR: Length threshold

LULC: Land use land cover

MA: Moving average

MK: Mann-Kendall

NDVI: Normalized difference vegetation index

N-W-W: Northwestwest

PC: Parde Coefficient

PCA 2: Principal Component Analysis 2

POR: Period-Of-Record

RDF: Recursive digital filter

RS: Remote sensing,



University of Fort Hare
Together in Excellence

RTP: Reduced-to-pole

SD: Standard deviation,

S-E-E: Southeasteast

SNHT: Standard Normal Homogeneity test

SW: Surface water

TDR: Tilt derivatives

TDX: Total horizontal derivative

TWI: Topographic wetness index

TwoPRDF: Two Parameters Digital Filter program,

WGS: World Geodetic System



University of Fort Hare
Together in Excellence

TABLE OF CONTENTS

DECLARATION	ii
DECLARATION ON PLAGIARISM.....	iii
DECLARATION ON RESEARCH ETHICS CLEARANCE	iv
ACKNOWLEDGMENT.....	viii
LIST OF ABBREVIATIONS AND GLOSSARY OF TERMS	x
Table of Contents.....	xiii
LIST OF TABLES	xviii
LIST OF FIGURES	xix
Chapter 1: Introduction	1
1.1 Background.....	1
1.2 Research questions.....	5
1.3 Aims and objectives.....	5
1.4 Research objectives.....	6
1.4.1 Evaluation of geologic structures.....	6
1.4.2 Assessment of streamflow variabilities and correlation with rainfall	7
1.4.4 Correlation of hydro-geomorpho-tectonic settings and lithology attributes	8
1.4.5 Geospatial investigation of groundwater potential zone	8
1.5 Research justification.....	9
1.4.3 Characterization of streamflow recessions.....	9
1.6 Study area.....	10
1.6.1 Geographic setting of the study area	10
1.6.2 Hydro-climatic situation	11
1.7 Thesis structure	12
Chapter 2: Literature Review	15



University of Fort Hare
Together in Excellence

2.1	Introduction.....	15
2.2	Summary of basic principles of geo-hydrodynamics and groundwater development	15
2.2.1	Hydrogeologic studies.....	15
2.2.2	Geohydrological process.....	16
2.2.3	Groundwater recharge and flow system.....	17
2.2.4	Mechanism of groundwater-surface water interaction.....	18
2.3	Global trends of groundwater-surface water interaction studies.....	20
2.4	Trends of groundwater-surface water interaction studies in South Africa.....	22
2.5	Geologic framework	25
2.5.1	Tectonic settings of Karoo Basin	25
2.5.2	Geological settings of the Karoo Supergroup	26
2.5.3	Trends of geologic study on the Balfour Formation	28
2.6	Delineation of groundwater potential zones and geoinformatics.....	31
2.7	Lineament mapping as an important tool in groundwater survey.....	35
2.8	Electrical resistivity tomography for groundwater survey.....	36
2.9	Geomorpho-tectonic analysis for groundwater zone decipherment.....	38
2.10	Hydro-climatic flux and streamflow recession attributes as important metrics	40
2.11	Water-related literature in and around the study area	44
2.12	Scale of analysis.....	45
2.13	Summary	47
Chapter 3: Methodology		48
3.1	Methodological procedures: an overview	48
3.2	Mapping of geologic structures for delineation of hydrogeological settings.....	48
3.2.1	Geologic mapping.....	49
3.2.2	Extraction of lineaments	50
3.2.3	Processing of aeromagnetic data.....	52
3.2.4	Validation of surficial lineaments and analytical signal map for characterization of the hydrogeology of Buffalo catchment	54
3.3	Baseline study of streamflow variabilities: methodologies	55
3.3.1	Variability assessment.....	56
3.3.2	Correlation assessment of streamflow to rainfall.....	60
3.4	Watershed characterization using streamflow recession attributes.....	61

3.4.1	Flow duration curve computations.....	62
3.4.2	Baseflow Separation Procedure	64
3.5	Evaluation of hydro-geomorphological settings for groundwater potential	68
3.5.1	Geomorpho-tectonic analysis.....	68
3.5.2	Electrical resistivity tomography and data processing.....	73
3.6	Investigation for groundwater potential zonation	75
3.6.1	Development of a thematic map	75
3.6.3	Overlay analysis for the delineation of groundwater potential zone.....	79
3.6.4	Evaluation of model performance and validation of groundwater potential zone	79
3.6.5	Hydrogeological conceptualization and delineation of groundwater potential zone	80
Chapter 4: Mapping of geologic structures.....		82
4.0	Introduction.....	82
4.1	Field geologic mapping.....	82
4.2	Lineament extraction.....	86
4.3	Aeromagnetic data analysis	88
4.4	Groundwater recharge zones and aquifer delineation.....	93
4.5	Summary	95
Chapter 5: A baseline study of streamflow variabilities.....		97
5.1	Introduction.....	97
5.2	Hydro-climatic variability analyses	97
	Buffalo Yellowwoods Ngqokweni Quencwe Mqgakwebe Tshoxa Error! Bookmark not defined.	
5.3	Summary	107
Chapter 6: Characterization of streamflow recession attributes		109
6.1	Introduction.....	109
6.2	Results.....	109
6.2.1	FDC Smoothness assessment.....	109
6.2.2	High flow assessment.....	109
6.2.3	Low flow assessment	113
6.2.4	Baseflow separation	115
6.3	Summary	119



Chapter 7: Evaluation of geomorpho-tectonic settings.....	120
7.1 Introduction.....	120
7.2 Results.....	120
7.2.1 Physiographic settings.....	120
7.2.2 Morphometric analysis.....	122
7.3 Summary.....	133
Chapter 8: Investigation for groundwater potential zonation	135
8.1 Introduction.....	135
8.2 Attributes of thematic maps	135
8.2.1 Dominant surficial lithology	135
8.2.2 Lineament density	136
8.2.3 Drainage density	137
8.2.4 Rainfall.....	138
8.2.5 Land use/ Land cover change map.....	139
8.2.6 Land surface temperature.....	141
8.2.7 Soil Topographic Wetness Index map.....	142
8.3 Normalization of features of GWPZ mapping.....	143
8.4 Delineation of Groundwater Potential Zones.....	145
8.5 Validation and corroboration of groundwater potential zones.....	145
8.6 Integrated hydrogeological conceptualization	149
8.7 Summary.....	152
Chapter 9: Discussion	154
9.1 Introduction.....	154
9.2 Evaluation of geologic structures.....	154
9.2.1 Geologic settings of Buffalo catchment.....	154
9.2.2 Surficial and subsurface lineaments of Buffalo catchment.....	157
9.3 Spatio-temporal variability and recession of streamflow.....	160
9.4 Geomorpho-tectonic and geo-electric section analyses of Buffalo catchment	165
9.4.1 Morpho-tectonics of the sub-basins and implications.....	165
9.4.2 Buffalo morpho-tectonics	169
9.5 Eco-environmental analysis of groundwater potential zone mapping	170



9.6. Integrated hydrogeological conceptualization 171

Chapter 10: Conclusions and recommendation 173

References 178

APPENDIX 212

Borehole lithological log used in Chapter 4 and Chapter 7 212

Sub-basins monthly streamflow in Buffalo basin headwater used in chapter 5 and 6 (Courtesy of DWA) 213

King Williams town precipitation information used in Chapter 5 (Courtesy of SAWS) 215

Borehole discharge rate used in Chapter 8 for validation of groundwater potential zone map 215



University of Fort Hare
Together in Excellence

LIST OF TABLES

Table 2. 1: Representative values of hydraulic conductivity for various rock types (Domenico and Schwartz, 1990).....	17
Table 2. 2: Litho-stratigraphy of Karoo Supergroup (Johnson et al., 2006).....	27
Table 3. 1: Peculiar structural features of sedimentary facies of Balfour formation.....	50
Table 3. 2: Description of morphometric parameters of Buffalo watershed analysis.	69
Table 3. 3: Box-and-whisker plots parameters.	80
Table 5. 1: Statistical summary of descriptive statistics.	99
Table 5. 2: Result of descriptive analysis for normality and white noise test of streamflow records (1989 – 2016) for Buffalo watershed.	99
Table 5. 3: Homogeneity test results for Buffalo streamflow records from 1989 to 2016.	101
Table 5. 4: Mann-Kendall trend test and Sen’s slope results for Buffalo watershed involving Rainfall and six streamflow station data of 1989-2016.	103
Table 5. 5: Sensitivity analysis of rivers in Buffalo watershed.	106
Table 6. 1: 7-day mean SFDC for 10 years and 100 years return period using 95th percentile.	113
Table 6. 2: Summary of FDC results.	115
Table 6. 3: Long-term average annual baseflow for streamflow of 1977 to 2016.....	116
Table 7. 1: Calculated drainage network attributes of Buffalo watershed.....	123
Table 7. 2: Calculated characteristic geometry of Buffalo watershed.	124
Table 7. 3: Calculated drainage texture attribute of Buffalo watershed.	126
Table 7. 4: Calculated relief characteristics of Buffalo watershed.	127
Table 7. 5: IPI2WIN inversion results for; A) Quencwe VES, B) Mqgakwebe VES, C) Yellowwoods VES, D) Ngqokweni VES, E) Buffalo VES.....	128
Table 7. 6: Summary of IPI2WIN VES data interpretation for the five sounding stations.	129
Table 8. 2: Pairwise comparison matrix	143
Table 8. 3: Classification of parameters for weighted overlay analysis	144
Table 8. 4: Table indicating the relative value of GWP rate to borehole yield	147
Table 8. 5: Results of the model assessment.....	148

LIST OF FIGURES

Figure 1. 1: Buffalo map showing important locations, the drainage system and surface geology (Modified from Johnson et al., 2006).	11
Figure 2.1: Mechanism of groundwater-surface water interaction (Water-gaining stream) (Modified from Barlow and Leake, 2012).	18
Figure 2. 2: A water-losing stream; A) connected stream, B) disconnected stream, (Not to scale - Modified from Barlow and Leake, 2012).	19
Figure 2. 3: Lithostratigraphic map of South Africa (Modified from the Council for Geoscience, 1990).	26
Figure 3. 1: Plots indicating the extracted Buffalo stream segments, the sub-basins, the physiography of each sub-basin and stream channel topography.....	71
Figure 4. 1: Photograph of the Daggaboersnek Member showing: (A) massive and multistory sandstone; (B) fractured mudrock filled by unconsolidated sandstone; (C and D) fragmented sandstones; (E and F) channel fill features comprising of mudstone; and (G and H) desiccation cracks of channel-filled grey mudstone.	83
Figure 4. 2: Photograph of the Barberskran Members showing: (A and B) Massive sandstone deposit,; (C) Unconsolidated interbedding of overbank deposit of fine sands and mudstone unit; and (D) Highly jointed mudstone fills with crevasse channel interspersed by siltysandstone matrices.	84
Figure 4. 3: Lithostratigraphic map of Buffalo catchment (After Katemaunzanga and Gunter, 2009). 10 units of oxidized mudstone units, 20 units of Elands, 26 Barberskrans units, and 27 Daggasboersnek units.	85
Figure 4. 4: Lineament distribution and lineament density map showing: A) surficial lineament density; B) the swarms of surficial and subsurface lineaments and; C) subsurface lineament density.	86
Figure 4. 5: Buffalo basin lineaments rose diagrams and their statistical information (in meters)	87
Figure 4. 6: Photograph showing lineaments in the study area.	88
Figure 4. 7: RTP magnetization anomaly map; indicating the geologic sources and the regions of low intrusion pressure which coincides with the area of dolerite outcrop.	89
Figure 4. 8: Maps showing the; A) First vertical derivative map, and B) Total horizontal derivatives of Tilt derivatives (TDXTilt) overlain by automatically extracted lineaments.	90

Figure 4. 9: Analytical signal map; indicating the regions of surface/near-surface basement emplacement which visually correlates with the dolerite outcrops in the basin.	91
Figure 4. 10: Depth slice; the corresponding effective anomaly is shown with a blue ring while the deepest (Slice 5) is shown with a red arrow. The red dots in Slice 1 reveal the effective anomaly corresponding to the depth being sliced.	92
Figure 4. 11: Lineament-dolerite Corroboration of the analytical signal map by by borehole lithology cross-section profiling.	93
Figure 4. 12: Borehole lithology cross-section profile for North and West of Buffalo basin.	94
Figure 4. 13: Borehole lithology cross-section profile for northeast, east, and south of Buffalo basin.	95
Figure 5. 1: Double Mass Curve plot of the six stations on the y-axis and the respective stations on the x-axis.	98
Figure 5. 2: Autocorrelation function plot of streamflow time series for the six stations.	99
Figure 5. 3: Parde coefficient plot showing regime variability of streamflow and rainfall data series (1989 – 2016).	102
Figure 5. 4: Result of two-sample Kolmogorov-Smirnov test of Buffalo watershed showing the plot of cumulative relative frequency (CRF) of tested station and rainfall. The red and blue lines correspond to the empirical distribution function of streamflow data of the station tested and rainfall data of Buffalo watershed respectively. The values after the red and black lines in the plot legends report the CRF value of each of the stations and that of rainfall (60.8).	105
Figure 6. 1: FDC plot of rivers in Buffalo catchments for; A) Buffalo, B) Yellowwoods, C) Ngqokweni, D) Quencwe, E). Mgqakwebe and F) Tshoxa stations.	112
Figure 6. 2: Low FDC plot using 95 th percentile time exceeded for; A) Buffalo, B) Yellowwoods, C) Ngqokweni, D) Quencwe, E) Mgqakwebe, and F) Tshoxa stations.	114
Figure 6. 3: Mean Annual BFI plots for; A) Buffalo, B) Yellowwoods, C) Ngqokweni, D) Quencwe, E) Mgqakwebe, and F) Tshoxa stations.	118
Figure 7. 1: Landform map of Buffalo basin headwater showing the geomorphic dissections of landmass (Dijkshoorn et al., 2008).	120
Figure 7. 2: Field photographs showing: (A) thick alluvial deposit; (B) boulders, cobbles and dolerite intrusions in the Quencwe River channel at the hilly terrain; (C) wide channel and gravelly deposits of Buffalo River; (D) boulders, cobbles and pebbles on upper course of Mgqakwebe River channel (West); (E) wide and rapid flow at the lower course of Mgqakwebe River, and; (F) wide channel of lower course of Yellowwoods River with riparian forest.	121

Figure 7. 3: Massive joints in rocks along embankments and channels of the Quencwe River. The direction of joints indicating the effect of extensional stress was indicated with a red arrow. The extensional stress is significant for its productive influence on interflow and recharge from baseflow.	122
Figure 7. 4: Comparative summary of stream orders (Nu) and total stream length (Lu). A. Buffalo drainage B. The sub-basins drainage networks in the watershed. Quencwe and Tshoxa stations are associated with five stream orders while Mgqakwebe, Yellowwoods, and Ngqokweni have four.	123
Figure 7. 5: Calibration of VES curve with borehole-log information for; A) Ngqokweni VES 2, B) Mgqakwebe VES 2, C) Quencwe VES 2, D) Yellowwoods VES 2, and E) Buffalo VES 2	130
Figure 7. 6: Pseudo-sections showing sounding at; A) Ngqokweni, B) Mgqakwebe, C) Quencwe, D) Yellowwoods, and E) Buffalo stations.	132
Figure 8. 2: Map of dominant surficial lithology.....	135
Figure 8. 3: Lineament density map of Buffalo basin headwater showing areas of variable lineament density.	136
Figure 8. 4: Reclassified drainage density map of Buffalo basin headwater showing areas of highs and low drainage density.....	138
Figure 8. 5: Rainfall map of Buffalo basin headwater showing the rainfall variability.	139
Figure 8. 6: Land use/land cover map of Buffalo basin headwater showing variability in land use and cover type.....	140
Figure 8. 7: Land surface temperature map showing spatial variability in land surface hotness and coldness.....	141
Figure 8. 8: Topographic wetness index map of Buffalo basin headwater showing the areas of potential for topographic influence on wetness.	142
Figure 8. 9: Map showing groundwater potential zone of the study area.....	145
Figure 8. 10: Map showing the overlay of borehole yield and GWPZ.....	146
Figure 8. 11: Scattered plots of groundwater potential zone mapping of Buffalo catchment. ...	148
Figure 8. 12: Box-and-whisker plot reporting the relationship between the GWPZ and borehole yield.....	149
Figure 8. 13: Three-dimensional presentation of actual landform (DEM), magnetic anomaly map (analytical signal on total residual magnetic layer) and lineament (TDXtilt) structure within. .	150
Figure 8. 14: Map showing: A. the spatial demarcation of GWPZ in relation to the surficial geology, the watershed drainage, and some townships; B. GWPZ association with drainage. Map B shows that only Ngqokweni River is not connected to an aquifer, Yellowwood River is partially connected while Tshoxa, Quencwe, and Mgqakwebe are directly connected to an aquifer through the alluvial plain.....	151

Chapter 1: Introduction

1.1 Background

Some of the principal issues that control the occurrence and distribution of exploitable water resources need to be investigated. In particular, this study focuses on the application of hybrid approaches (hydro-statistics and geoinformatics) for deciphering the location of exploitable subsurface water components in data-scarce regions like South Africa. This study engages the scope of conjunctive water management. The scope highlights that public policy and management goals can only be achieved through the combined use of groundwater and surface water (Ross, 2017). The scope of this work is based on the entwinement of surface water and groundwater as a single entity.

Over time, water resources have been treated and studied as two distinct components; surface water and groundwater (Chung et al., 2010; Graf et al., 2014). Inadequate knowledge about the linkage between the two components can affect the quality of management and development of the resources. The paucity of data reveals the inadequate knowledge that needs to be addressed in order to achieve effective water resource management. Optimal water resource management depends on the quality and extent of the water resources assessment program engaged.

In the year 2000, South Africa's estimated annual water need was 13.28 billion m³, while the overall water yield from impoundments was 14 billion m³ (De Coning, 2006). This is virtually two-seventh of the total natural runoff of rivers which was estimated to be 50 billion m³. With population growth, an increase in urbanization rate and industrial expansion in the present time, the pre-existing pressure on surface water supply has been compounded. This has led to the increase in physical and economic scarcity, water contamination, uncontrolled

abstraction, loss of rivers, exhaustion of baseflow, diminution of wetlands, loss of springs, and disruption of riparian forests and eco-systems (Caló et al., 2017). As a result, a call has been intensified for the development of alternative water supplies (DWS, 2010).

Long before the 21st century, the water situation in South Africa was managed through ad-hoc data gathering and research on surface water at the primary catchment scale (Cobbing, 2014). However, little or limited efforts were made to gather information on groundwater resource evaluation. This was mainly due to the historical pattern of administration of the resources (Pietersen et al., 2012). Groundwater management was sequestered in policy and regulation from surface water management under the former South African Water Act (Act 56 of 1956). Groundwater status and development were relegated to private operations with no restrictions (Pietersen et al., 2012). As a result, vast numbers of groundwater and surface water researches have been carried out as a separate entity (Tanner and Hughes, 2015).



In the Water Act reform (Act 36 of 1998) amended 20 years ago, groundwater resource was acknowledged, hence, the disjunctive management of the two resource components was depolarised. This brought about the system of licensing and authorization prior to the allocation of the right to groundwater development (Levy and Xu, 2012). As a result, the gap between surface water and groundwater practitioners was bridged. However, quantitative approaches and structures for collating information on groundwater status have not been formally institutionalized (Pietersen et al., 2012). Hence, the water resources reserve is still estimated using surface water information (Tanner, 2013). It is imperative that approaches for quantifying the spatial variability in groundwater distribution are developed for integration with surface water approaches in order to achieve a holistic estimation. In doing this, the allocation of water in accordance with the requirements of the National Water Act would be accomplished.

Almost twenty-one years have gone since the proclamation and enactment of the National Water Act. Meanwhile, regional groundwater status is yet to be defined. Information on processes controlling recharge and distribution of groundwater is still poorly documented (Cobbing, 2018). Institutional framework and arrangement for data collection, private sector data handling, integrated developmental plans, and management strategy for groundwater resources are issues yet to be properly accounted for (Pietersen et al., 2012). Till present, few aquifers have been assessed for groundwater potential. These include the Zululand coastal plain aquifer, Maputaland coastal aquifer, Table Mountain group aquifer, Grootfontein aquifer, and Cape flats aquifer (Kelbe and Germishuysen, 2010; Cobbing and de Wit, 2018). Since groundwater availability is dispersed, it is equally an advantage for meeting the domestic needs of rural communities. Due to limited information on the resource, its development has faced administrative issues such as developmental funding, insufficient technical skill, poor maintenance strategy, and weak capacity building (Pietersen et al., 2012).



University of Fort Hare
Together in Excellence

Many factors have been identified to be responsible for the poor information on groundwater. Among them is the scientific uncertainty associated with the exploration and quantification of groundwater availability (Tanner, 2013). The uncertainty extends to the complexity of processes controlling surface and groundwater interaction. In regions where groundwater recharge is mainly driven by rainfall, understanding of the groundwater flow-path and morphotectonic arcs that enhance geo-hydrodynamic processes for groundwater storage are necessary. Knowledge of hydrodynamic response of streamflow to baseflow due to possible hydraulic connection between aquifer and streams/rivers is also essential for effective allocation and abstraction management (Ross, 2017).

Much literature has revealed the complexity of geology of South Africa for groundwater exploration, especially as a result of widespread fractured rock (MacDonald and Davies,

2000; Holland and Witthüser, 2011; Dhansay et al., 2016). As a result of the complexity, hydrogeology has been studied at a local scale meanwhile surface water hydrology can be studied at a regional scale (Tanner, 2013). Groundwater hydrology focuses largely on the geologic environment and flow system within the saturated zone, which could not be readily quantified except through a physics-based model (Shaw, 2014). On the other hand, surface water hydrology focuses on rainfall-runoff assessment, which could be virtually estimated and usually at the catchment scale (Shaw, 2014). The complexity of geology, the difference in scale of groundwater monitoring and technicality involved in data collection add to the unparalleled objective of water resources management in South Africa. These differences also contribute to the difficulty in integrating the two components of water resources for researching and modeling (Hughes et al., 2010).

As a result of limited large scale integrated assessments of water resources, most common evaluations have adopted the baseflow estimation technique and the Pitman model (Hughes et al., 2013). The baseflow separation method depends solely on streamflow data and, as a result, cannot provide detailed information on geologic and geomorphological settings (Kapangaziwiri and Hughes, 2008). While the Pitman model caters to some of the inadequacy of the baseflow method, its reliance on physical and hydro-climatic predictors (model inputs) makes its estimation process vulnerable to uncertainties (Beven, 2012). Furthermore, the Pitman model provides an approximated result as is the case of every numerical model (Beven, 2012). It is therefore imperative to devise analytical approaches that are capable of providing first-hand information on groundwater occurrence, addressing groundwater assessment problems and also providing holistic information on groundwater surface water interaction.

1.2 Research questions

Some of the key research questions that guide these exploration exercises are as follow:

- Is it possible to develop a simpler analytic exploration program for dominant geologic structures that control groundwater recharge and storage at the regional scale in semiarid areas with complex geology?
- To what extent can Spatio-temporal variability of streamflow and its correlation to rainfall provide information on subsurface water distribution?
- How can the information on surface water recession and groundwater discharge be analyzed for the purpose of regional characterization of subsurface geo-hydrodynamic attributes?
- Can the evaluation of geomorpho-tectonic features corresponding to the development of drainage networks and lithological succession be inferred for three-dimensional assessment of groundwater availability?
- Can the information on the geologic property of an area be integrated with other groundwater influencing factors in the environment for groundwater potential zone mapping?



University of Fort Hare
Together in Excellence

1.3 Aims and objectives

The aim of this study is to improve the conceptual knowledge and present the technical feasibility of exploring groundwater potential zones through geo-hydrodynamic perspectives in a complex environment.

In order to achieve this, the following sub-objectives are addressed:

- i. Evaluation of geologic factors that control groundwater accumulation and delineation of hydrogeological settings;

- ii. Assessment of spatio-temporal attributes of streamflow variabilities and the correlation with rainfall;
- iii. Characterization of streamflow recessions with respect to high flow, low flow, and baseflow index;
- iv. Correlation of hydro-geomorpho-tectonic settings with respect to lithology geophysical attributes; and
- v. Geospatial investigation of groundwater potential zones with respect to multi-influencing factors.

1.4 Research objectives



1.4.1 Evaluation of geologic structures

University of Fort Hare
Together in Excellence

Lithology, aquifer properties, geologic structures, and tectonic arcs are the major hydrodynamic factors that control redistribution, yield, flow, and quality of groundwater (Vittecoquet et al., 2015). Groundwater occurrence in rock depends on the hydraulic conductivity of lithologic materials. This is a function of openings, joints, fractures, pore spaces and interconnectivity of the pores. It is essential to be able to analyze their spatial distribution and to interpret them for hydrogeological characterization purposes. Geologic settings vary considerably both in scale and depth. These variations influence the locality of aquifers as well as the suitability of methods for the exploration of such aquifers. The majority of the geologic environments are characterized by two major types of aquifers; the deep regional aquifer and the shallow localized aquifer. Deep regional aquifers are not often exploited for groundwater use due to their cost of exploration and quality except in

waterscarce areas where their exploitation is the only possible option (Suter et al., 2019). Small localized aquifers or springs are often the major targets for water resource provision (Vittecoq et al., 2015). Consequently, knowledge of lithostratigraphic settings, geologic structures and decipherment of fracture networks are important for the delineation of aquifers. In doing so, it is necessary to consider the mapping of field geologic structures, extraction of lineaments, aeromagnetic data analysis, and borehole log profiles.

1.4.2 Assessment of streamflow variabilities and correlation with rainfall

Streamflow is an important metric for assessing geo-hydrodynamic attributes of a subwatershed to rainfall. In areas where borehole information is lacking, surface water information has been analyzed for information on its baseflow component, especially during dry hydrologic regimes (Kalbus et al., 2006). More so, many groundwater systems in semiarid areas depend on rainfall input as the main source of groundwater recharge (Kelbe and Germishuys, 2010). It was recognized that comparative analysis of the streamflow trend across hydrologic regimes could provide baseline information on factors that influence the spatial distribution of groundwater. Due to the entwinement of surface water and groundwater, information on spatio-temporal attributes of streamflow and watershed influencing factors is relatively limited (Barlow and Leake, 2012). In the South Africa case, where groundwater data monitoring is poor, inference of information from streamflow may be necessary. The hydrologic response of a watershed depends on the intrinsic properties of the watershed. Hence, baseline trends of groundwater potential in hydrologic regimes were inferred from variability and correlation analysis with respect to sub-watershed hydrologic attributes. The exercise helped to identify the factors influencing the hydrologic pattern across the watershed.

1.4.4 Correlation of hydro-geomorpho-tectonic settings and lithology attributes

Hydro-geomorpho-tectonic settings is another physical feature that is of significance to both surface and subsurface hydrologic systems aside from hydro-climatic and geologic properties (Mahajan and Sivakumar, 2018). It carries historical imprints of water transmission, infiltration and ponding information, moisture accumulation and release, neotectonic lineaments that determine aquifer development, relief system and drainage networks (Gebre et al., 2015). It is an altered morphogenetic medium that contains information on the evolution and process of groundwater-surface water interaction (Evangelin et al., 2015). Hence, the analysis of morphometric parameters is essential for the critical understanding of conjunctive management of water resources. The central aim of this objective is to evaluate the properties of hydro-geomorpho-tectonic settings to provide information on groundwater potentials. In order to complement the findings in a holistic manner, the morphometric parameters were correlated with geoelectric attributes of each sub-watershed investigated.



University of Fort Hare
Together in Excellence

1.4.5 Geospatial investigation of groundwater potential zone

Going by the goal of exploring groundwater availability through the geo-hydrodynamic perspective, it is essential to devise an approach that integrates all the major factors that influence groundwater development. In doing so, the geologic system, hydro-climatic factors, and hydro-geomorpho-tectonic settings were computed with other essential environmental factors. Environmental factors such as land use/land cover change, vegetation index, topographic wetness index, and soil distribution are important indicators for the assessment of groundwater-surface water interaction (Das, 2017; Kanagaraj et al., 2018). With the advent of geospatial technology, integrating these factors through knowledge-based multiinfluencing indices and overlay analysis enables a cost-effective solution to the delineation of groundwater potential zone at the catchment scale.

1.5 Research justification

This study intends to present the technical feasibility of exploring regional groundwater potential zones using cost-effective means through fragmented approaches and the integrated approach. The fragmented approach involves a disjunctive exploration of groundwater through analysis of the geologic system, hydrological system, and geomorphological system. The integrated approach involves the use of non-invasive geospatial technology to integrate every essential environmental factor that contributes to groundwater development. The advent of the geographic information system and remote sensing technology has enabled a thorough assessment of inaccessible locations possible. The remote sensing logic of large scale geology and the environment has also been made easy and possible, where previous approaches required sophisticated appliances and highly skilled and experienced technicians. Meanwhile, due to the complexity associated with the development of groundwater, especially at the regional scale, regional exploration of groundwater has faced setbacks in South Africa. The study, therefore, endeavors to contribute to the knowledge of groundwater exploration and to increase the confidence in the use of geospatial technology for integrated studies of surface water and groundwater interactions.



University of Fort Hare
Together in Excellence

1.4.3 Characterization of streamflow recessions

Understanding of recession attributes of streamflow is essential for the integrated assessment of groundwater-surface water interaction. It provides information on streamflow dynamics, hydrologic response variability, lithologic properties of the watershed, storage potential and discharge properties of the subsurface (Yokoo and Sivapalan, 2011). These are crucial properties that enable the characterization of the watershed for zones of groundwater potential (Kienzle, 2006). This approach tends to satisfy the need for the affordable and noninvasive approach for watershed characterization in hydrologic regions. The recession analysis was established through high flow, low flow, and baseflow indices evaluation.

1.6 Study area

1.6.1 Geographic setting of the study area

The study area is situated in the headwater of the Buffalo catchment, Eastern Cape, South Africa. It lies between latitude S32°40' and S32°59' and longitude E27°00' and E27°33', covering an approximated area of 1237 km², with a length of 36 km and a width of 41 km (Figure 1.1). It is drained by the Buffalo River, which runs south-eastward from E27° 17' 1.9"; S32° 40' 51", (Isidenge State forest) to the Indian Ocean at E27° 54' 54.6"; S33° 0.1' 42.3". The river stretches across an approximated length of 126 km. It is impounded at three different locations, namely, Rooikransdam, Laing Dam and Bridle Dam. The study area incorporates the areas around the metropolis of Bhisho in the center, King Williams Town at the south center, Zwelithsa at the extreme south, Dimbaza in the extreme south-west, Pirie Mission in the west and Isidenge nature forest reserve in the extreme north. In general, accessibility is fair, especially due to well-planned towns and communities. Areas of accessibility challenges, where traverse mapping is limited, include some of part of the nature reserve areas, fenced farmland, and areas of thick vegetation cover. The poorly urbanized area of the north is covered by woodland and deciduous trees. The landform is characterized by three main terrain types; the medium gradient mountain in the north-west, the dissected plain which flanks from the west to the north-east and east, and the plain which spreads across the south-west, south, and south-east (Bailey et al., 2011). The relief of the area has a range of 258 – 1370 m above mean sea level.

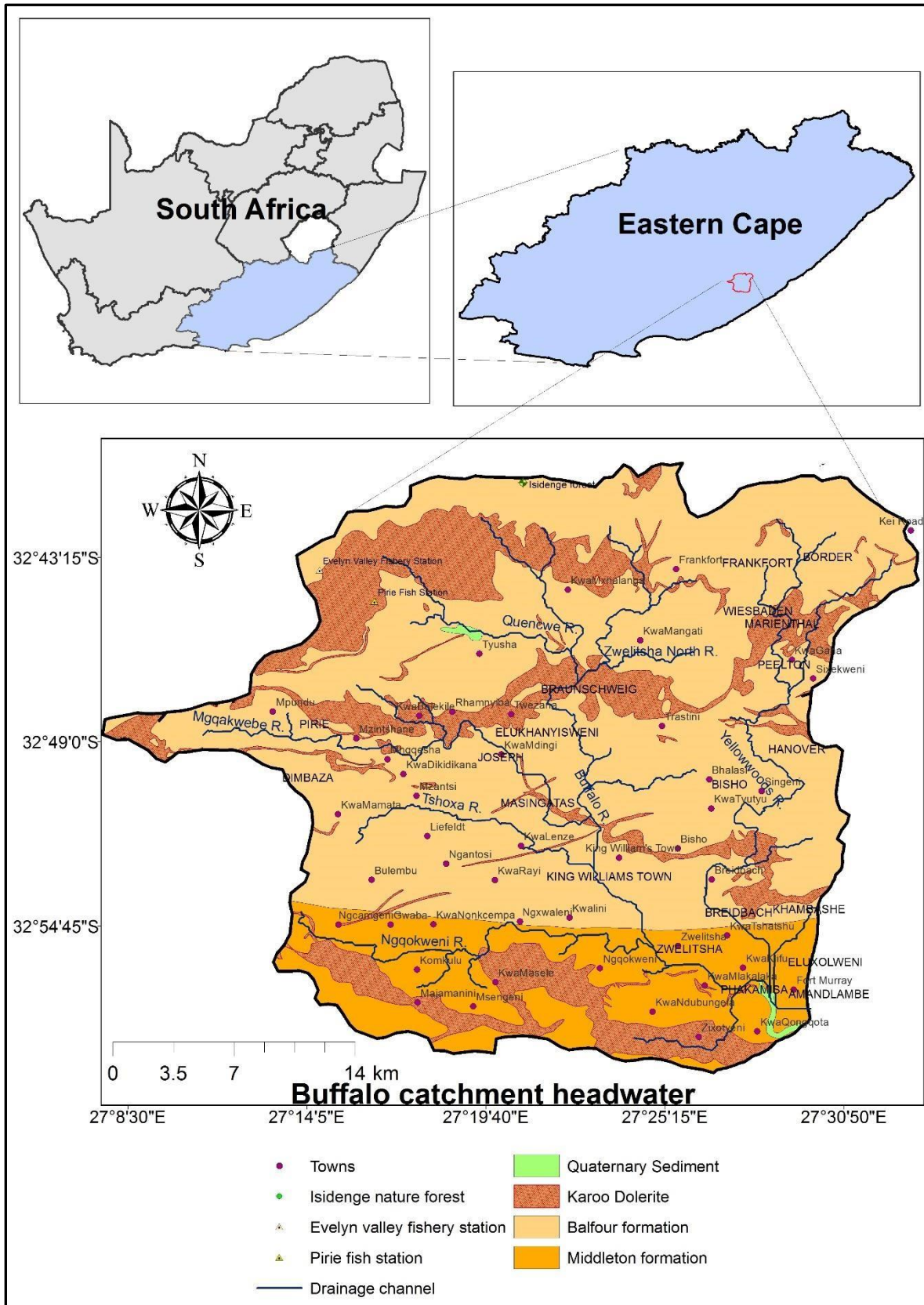


Figure 1. 1: Buffalo map showing important locations, the drainage system and surface geology (Modified from Johnson et al., 2006).

1.6.2 *Hydro-climatic situation*

The hydrologic periods run across four seasons from August to July; spring (September to November); summer (December to February); autumn (March to May); and winter (June to August). The mean annual rainfall from the central station at Bhishe is estimated to be 590 mm/year for 1989 to 2016. Rainfall varies from the hilly terrain and natural forest to the plain in the north-western to south-eastern direction. The average minimum temperature is 13.5° in general, and as low as -3° in winter at the hilltop (Slaughter et al., 2014). The average maximum temperature is 22.3° across the environment, while the maximum summer temperature is 38° (Slaughter et al., 2014). Due to the frequent drizzle and gentle rain in the winter months, soil moisture is raised in spring, the beginning of the hydrologic regime (DWA, 2010). Infrequent extreme downpours in November, January, and February raise the streamflow and dam levels in the summer while dry spell in the summer lead to a decline in streamflow and dam level (DWA, 2010).



University of Fort Hare

Buffalo River is perennial in nature and supported by six reaches; Ngqokweni, Tshoxa, Mqgakwebe, Quencwe, Zwelitsha North, and Yellowwoods Rivers (Bailey et al., 2011). The section of Buffalo River catchment captured within the study area terminates at the river mouth to the Laing Dam, approximately 54 km in length. Its drainage network is dendritic in style and oval in circularity.

1.7 **Thesis structure**

The thesis spreads across ten chapters. Chapter 4 to chapter 8 report the results obtained from concise analysis conducted in accordance to each objective of the research. This was done for easy coupling of approaches while contributing to the realisation of the overall aim of the study.

Chapter 1 introduces the research, provides the background, outlines, objectives, and scope of the thesis.

Chapter 2 sets out to establish the literature about surface water-ground water interaction studies. The topics addressed include the trend of literature on the interaction of the two water components, physical mechanisms influencing water hydrodynamics, flow mechanisms over permeable stratum, conceptual processes that define river-aquifer interaction and summary of the existing methods used for quantifying hydrodynamic attributes of the groundwater system.

Chapter 3 gives an account of the methodology and materials used in relation to the objectives of the study. The chapter contains five sections that are used to describe submethodologies of each of the objectives. Applications used to explore each set of objectives vary with respect to the data used and the specific aim to be addressed.



Chapter 4 reports the results of analyses of geologic settings for groundwater development. The chapter is divided across four sections; geologic structures, analysis of magnetic susceptibility, automatic extraction of lineaments and borehole cross-section profiling. To this end, the gap between structural details on the surface is compared with geospatially and digitally processed aeromagnetic data for the characterization of groundwater signatures.

Chapter 5 establishes the baseline study of spatio-temporal attributes of rainfall and streamflow variabilities for the study area. In elucidating the hydrological processes, results of time series analysis, regime variability, and trend analysis of hydro-climatic patterns are reported. Also, correlation analysis of streamflow data to the main rainfall station was carried out. The entire findings are encapsulated to explore the streamflow variability and to characterize watershed with respect to trend and productivity.

Chapter 6 provides information on streamflow recession analysis. The study entails the application of the flow duration curve and baseflow index analyses to characterize the high flow, low flow and baseflow attributes of sub-basins. The reports addressed involve the characterization of subsurface flow dynamics from the perspective of environmental flow. The different approaches of flow duration curve employed are compared with baseflow indices to establish the validity of the findings.

Chapter 7 provides an account of groundwater delineation from geomorpho-tectonic arcs analyses. Analyses of altered surficial morphogenesis were classified into four basic characteristic units, namely, drainage network, basin geometry, drain texture and relief characteristics. Results of sub-basin morphometric analyses were visually correlated with deductions of electric resistivity tomography. The findings address the gap in groundwater delineation from hydro-geomorpho-tectonic analysis perspectives.

Chapter 8 provides an account of the integrated analysis of groundwater potential zones. The application of geospatial technology for the extraction of major groundwater influencing factors in the environment is presented. Approaches adopted for the integration of eleven major contributory factors are detailed. The entire exercise reports the results of regional groundwater potential zone mapping using the integration of geologic, hydrologic, geomorphic and environmental factors. The findings are validated through the overlay of results with georeferenced data of borehole yields.

Chapter 9 provides the synthesis of the main findings from this study and the general discussion.

Chapter 10 provides information on conclusions drawn from the entire findings.

Recommendations are provided for future research.

Chapter 2: Literature Review

2.1 Introduction

The interaction between surface water and groundwater remains vaguely understood in many catchments globally. This gap is one of the major issues confronting the complexity of the groundwater system globally. Numerous perspectives on groundwater-surface water interaction have been generated as a result (Woessner, 2000; Sophocleous, 2002; Krause et al., 2014). Essentially, for an accurate understanding of this interaction, there must be a proper integration of knowledge of hydrological processes with the geologic systems. This is fundamental to the understanding of groundwater development and the identification of the groundwater potential zone. However, the majority of the researches on water resources in South Africa have focused mainly on water management issues (Xu et al., 2002; Le Maitre and Colvin, 2008; Levy and Xu, 2012; Pieterse et al., 2012; Cobbing, 2014; Conway et al., 2015; Entholzner and Reeve, 2016; Cobbing and de Wit, 2018). Researches that address physical processes and factors controlling groundwater-surface water interaction are few (Kelbe and Germishuys, 2010; Stroebel et al., 2018). To respond accurately to these deficiencies, this chapter intends to present the definition of key processes underpinning groundwater-surface interaction and provide an overview of these processes. This chapter presents information on the basic knowledge of exploration of groundwater potential.

2.2 Summary of basic principles of geo-hydrodynamics and groundwater development

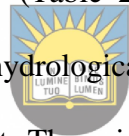
2.2.1 Hydrogeologic studies

The geo-hydrodynamic factors of subsurface water are the geologic processes controlling the response and transport of water in the flow-path within the catchment sub-terrain (Li et al.,

2013; Ochoa-Rodriguez et al., 2015). It entails a conjunctive study of the interaction between the geologic properties of the environment and hydrological processes in the subsurface. Earlier, hydrodynamic studies were restricted to the surface water components only (Hu et al., 2003; Tang et al., 2006). In recent time, the impact of hydrogeological settings on surface water processes, especially for influencing variability in streamflow across watersheds, are now being recognized and emphasized in various literature (Viezzoli et al., 2010; Demers et al., 2013; Hayashi et al., 2016; Luo et al., 2018).

The extent of hydraulic connectivity and fracturing determine the size of an

(Bracken et al., 2013). Taylor and Greene (2008) elaborated that the hydrogeology of a groundwater system is influenced by numerous geological and hydrological factors. These factors include hydraulic conductivity (Table 2.1), topographic condition, and lineament density. White (1999) highlighted the hydrological factors that control subsurface water flow and storage in a fractured environment. These include basin morphometry, recharge, flow-path capacity, and aquifer hydrodynamic responses. Detailed geologic information on the area of catchment hydrodynamic studies is therefore imperative.



University of Fort Hare
Together in Excellence

2.2.2 *Geohydrological process*

A hydrologic process begins with precipitation as the principal water input into the subsurface (Shaw, 2014). Within the vadose zone, subsurface water is unsaturated due to the presence of air and water within the pore space. Below the vadose zone is the water table, which acts as an interface between the vadose zone and the phreatic zone. The phreatic zone is the zone of groundwater, whereby the pore spaces are filled with water only. The phreatic zone is the main target for groundwater development (Barlow and Leake, 2012).

Table 2. 1: Representative values of hydraulic conductivity for various rock types (Domenico and Schwartz, 1990).

Rock type	Material	Hydraulic conductivity (ms ⁻¹)
Unconsolidated (Sedimentary) Material	Marine clay	8×10^{-13} to 2×10^{-9}
	Clay	1×10^{-11} to 2×10^{-9}
	Till	1×10^{-12} to 2×10^{-6}
	Silt	1×10^{-9} to 2×10^{-5}
	Fine sand	2×10^{-7} to 2×10^{-4}
	Medium sand	9×10^{-7} to 5×10^{-4}
	Coarse sand	9×10^{-7} to 6×10^{-3}
	Gravel	3×10^{-4} to 3×10^{-2}
Sedimentary Rocks	Shale	1×10^{-13} to 2×10^{-9}
	Anhydrite	4×10^{-13} to 2×10^{-8}
	Salt	1×10^{-12} to 1×10^{-10}
	Siltstone	1×10^{-11} to 1.4×10^{-8}
	Sandstone	3×10^{-10} to 6×10^{-6}
	Limestone/ Dolomite	1×10^{-9} to 6×10^{-6}
	Karst/ Reef limestone	1×10^{-6} to 2×10^{-2}
Crystalline rock	Unfractured igneous and metamorphic rock	3×10^{-14} to 2×10^{-10}
	Basalt	2×10^{-11} to 4.2×10^{-9}
	Weathered gabbro	5.5×10^{-7} to 3.8×10^{-6}
	Weathered granite	3.3×10^{-6} to 5.2×10^{-5}
	Fractured igneous and metamorphic rock	8×10^{-9} to 3×10^{-4}
	Permeable or vesicular basalt	4×10^{-7} to 2×10^{-2}



University of Fort Hare
Together in Excellence

2.2.3 Groundwater recharge and flow system

Groundwater recharge depends on the infiltration of water from the source into the vadose zone and percolation through the vadose zone into the groundwater system. Sources of water for groundwater recharge include; direct rainfall, condensational water, overland flow,

instream and wetland (Barlow and Leake, 2012). After percolation into the phreatic zone, groundwater moves continuously from recharge centers through the aquifer to discharge points such as streams, wells, lakes, estuaries, springs, wetlands or directly to the oceans (Shaw, 2014). The residence time of groundwater can vary from days to years for shallow or local groundwater systems and centuries to millions of years for regional groundwater systems traveling at great depth in lithologic materials with low hydraulic conductivity (Stephens, 2018). Generally, groundwater flow is controlled by a hydraulic gradient, and the hydrogeologic boundary conditions (Fetter, 2018). At the regional scale, the groundwater flow net may be similar to the surface water flow net; however, at the shallow or local scale, groundwater flow direction may be altered by the cone of depression produced from excessive pumping (Barlow and Leake, 2012).

2.2.4 Mechanism of groundwater-surface water interaction

Figures 2.1 and 2.2 A and B provide a summary of groundwater-surface interaction. Information on groundwater-surface water interaction can be best deduced from streamflow recession assessment and analysis of baseflow estimates (Fetter, 2018). Simple hydrological processes and water distribution are summarized in Figures 2.1 and 2.2.

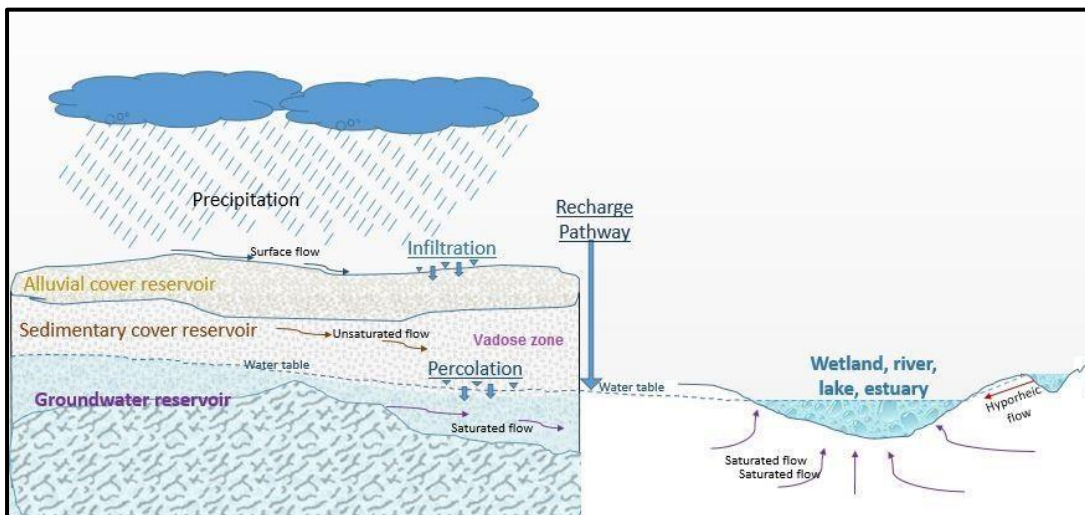


Figure 2.1: Mechanism of groundwater-surface water interaction (Water-gaining stream) (Modified from Barlow and Leake, 2012).

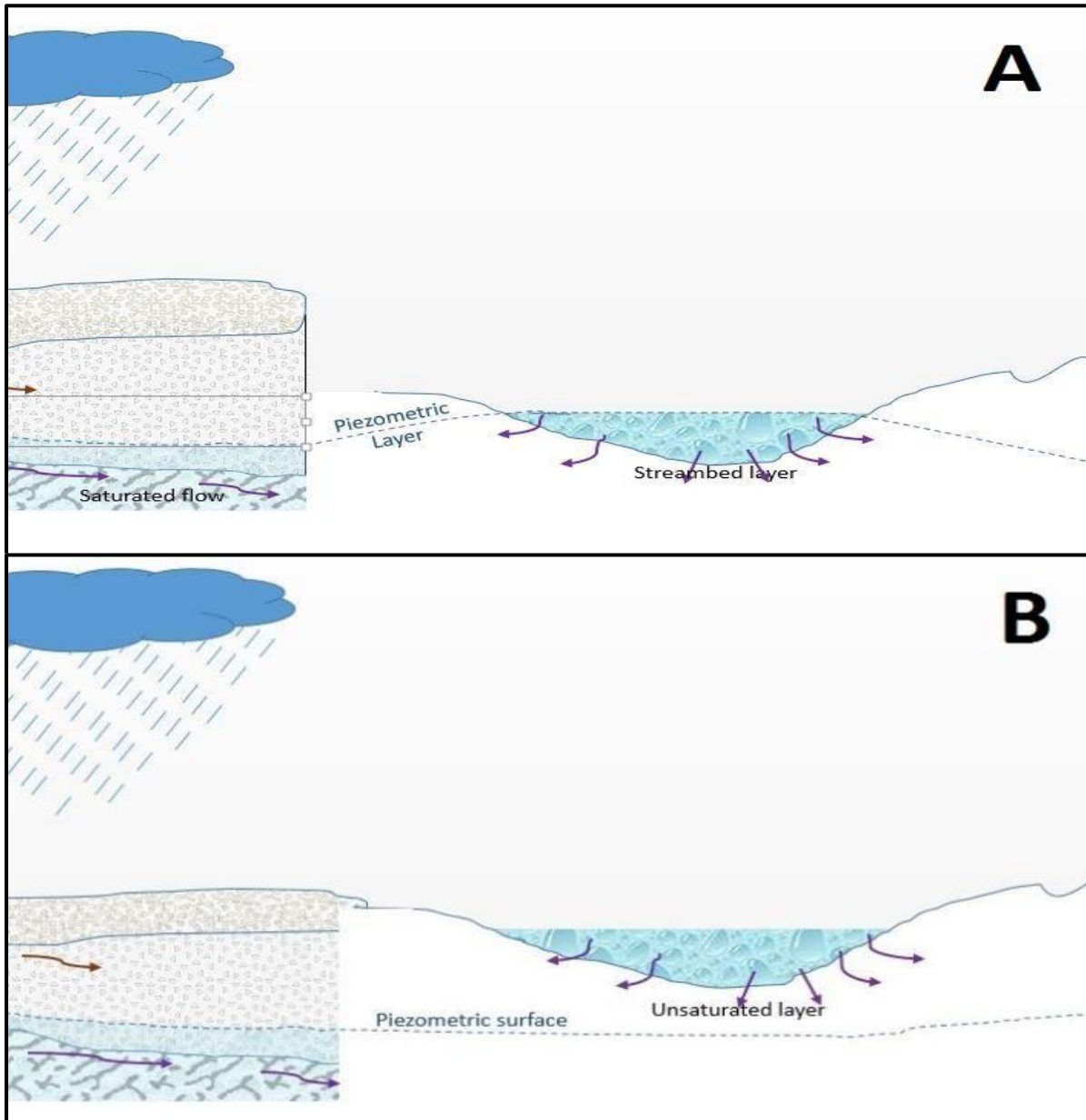


Figure 2. 2: A water-losing stream; A) connected stream, B) disconnected stream, (Not to scale - Modified from Barlow and Leake, 2012).

A stream is recharged by baseflow when the water table connected to the stream is at the higher hydraulic head (Barlow and Leake, 2012). Conversely, water recedes from the stream into the groundwater system when the water table is at a lower gradient to the connected stream (Pacheco and Fallico, 2015). Groundwater recharge from streams can still occur when the water table is disconnected, depending on the hydraulic property of the stream embankment and floor (Woessner, 2000).

This spatial variability in surface-subsurface water interaction process determines the perennial attributes of some downstream reaches and ephemeral attributes of some upstream or headwater reaches where the altitudinal variation is large (Barlow and Leake, 2012). Temporal variability may also influence the interaction between stream and groundwater. During the high flow of a stream, overbank flow from the stream may be stored in the riparian zone and discharged back when the streamflow subsides (Winter et al., 1998).

Hyporheic flow is another type of subsurface-surface water interaction, which is similar but not exactly groundwater-surface water interaction; hence, its knowledge is important (Sawyer and Cardenas, 2009). It is the flow type whereby surface water which seeps through the bed sediments at the upstream, returns to the surface at the downstream. A hyporheic flow path is developed as a result of changes in the meandering nature of the river or variation in bed gradient (Sawyer and Cardenas, 2009). Ripples and pools may constitute a divide and hyporheic flow across the flow-path in which the surficial flow re-emerges downstream (Sawyer and Cardenas, 2009). Sedimentation eroded debris and heterogeneity in streambed sediments may deflect the flow along its path into a new channel (Pryshlak et al., 2015).

2.3 Global trends of groundwater-surface water interaction studies

Toth (1963) was one of the first to report on surface water and groundwater interaction. The report highlights the spatial control of climate, topography, and geology on the groundwater systems. McBride and Pfannkuch (1975) also built on this with a theoretical investigation of groundwater-lake and groundwater-wetland interaction. Approaches for assessment of streamflow components from bank storage and aquifer were initiated by Rorabaugh (Rutledge, 2007). By 1980, one of the first numerical approaches in a computer program for assessing the GW and SW linkages, which is the hydrograph-separation methods (fixed and

local minimum) was developed by Pettyjohn and Henning (1979). Meanwhile, by the end of the decade, the work was built upon by Prudic (1989). More modules were included in the numerical approach in order to better simulate GW-SW interaction. Applications of the model thereafter were focused mainly on the quantification of the two components. Efforts were made to develop a robust model that could address the deficiencies in the first GW-SW model. Deficiencies identified include; inability to handle a large-scale investigation, poor and incoherent spatio-temporal resolution, system simplification, and inability to classify aquifer and streambed units. The decade 1980-90 also witnessed the incorporation of eco-services and biogeochemical processes into hydrologic dynamic models of GW-SW interaction (Grimm and Fisher, 1984; Stanford and Ward, 1988). The starting point of intensive research on hyporheic exchange and solute storage on solute transport began with the introduction of the transient storage model (Bencala and Walters, 1983).



The following decades witnessed a breakthrough in GW-SW interaction. Among the significant publications on GW-SW interactions in recent decades is Sophocleous (2002). The work elaborated on the fundamental concepts and significance of GW-SW interaction from the hydraulic and hydrogeological points of view. Winter (1998) takes his view from hydraulic conditions controlling diversities in surface waters. Hayashi and Rosenberry (2002) worked on the ecological significance of GW and SW interaction. Kalbus et al. (2006) elaborated on the field techniques for appraising the numerical interchange between GW and SW at varying scale. Anibas et al. (2012) extended the GW-SW fluxes to the regional modeling of wetlands. Werner et al. (2013) applied GW-SW interaction concepts to the study of the interaction between subsurface flow and seawater. Dahl et al. (2007) proposed a new typology for GW-SW interaction which stems from the establishment of a classification system for the GW-SW interaction process. GW-SW interaction study has been extended to the study of hyporheic zones (Banzhaf et al., 2013; Wang et al., 2018). In the present time,

reviews of methodologies and models are being consulted and redeveloped as a precursor to improve, build on or widening the scope of GW-SW interaction (Barthel and Banzhaf, 2016; Glose et al., 2019).

2.4 Trends of groundwater-surface water interaction studies in South Africa

Studies involving groundwater and groundwater-surface interaction are limited in South Africa. The major challenge arises from data unavailability; however, basic knowledge on the South Africa groundwater system and its development are still presented in the literature (Xu et al., 2002; Smakhtin 2001; Vegter and Pitman, 2003; Kelbe and Germishuise, 2010; Van Wyk et al., 2012). The earliest and popular study on the groundwater system of South Africa was initiated by Bredenkamp and Vogel (1970), followed by Bredenkamp et al. (1974) in Western Transvaal and Smit (1978) in the Northern Cape.

A significant research breakthrough in groundwater studies was the one by Bredenkamp et al. (1995) which focused on the application of some semi-empirical methods for groundwater recharge quantification. Of the methods he proposed, chloride mass balance (CMB), cumulative rainfall departure (CRD) and groundwater modeling were widely adopted (Xu and Beekman, 2003). CMB is based on mass conservation of atmospheric chloride and chloride flux in the subsurface. It is used for the estimation of moisture flux in the unsaturated zone; however, the flux may be overestimated (Bredenkamp et al., 1995). For recharge estimation in the saturated zone, the application of CMB is limited by the presence of evaporites or saline water intrusion due to chloride concentration (Xu and Beekman, 2003). Its application in areas with fractured rock may be complicated due to the potential for the development of new chloride concentration equilibrium (Cook, 2003). The CRD method is based on the rationale that the groundwater influx is influenced by rainfall (Bredenkamp et

al., 1995). The methodology was revised to incorporate rainfall time series by Xu and Tonder (2001). However, it cannot be applied to a confined aquifer (Xu and Beekman, 2003).

Smakhtin (2001) identifies the sustainability balance of baseflow between groundwater and surface water. The work outlined that: a) seasonal recharge of an interacting aquifer must be more than the baseflow rates; b) interaction of the stream with the aquifer depends mainly on the extent of the shallowness of the draining aquifer; c) aquifer size and hydraulic properties are a major factor for sustainable baseflow in the dry season. Le Maitre and Colvin (2008) extend the argument that the significant aquifer properties for sustainable discharge are storativity and transmissivity, while high hydraulic conductivity is simply a necessary condition.

Xu et al. (2002) presented geomorphological stages of streams in South Africa and then related them to hydrogeological settings for baseflow discharge estimation. The stages were classified as upper, middle and lower courses as well as special cases of endorheic drainage, and were related to specific simple hydrographs (Xu et al., 2002). This enables easy separation of baseflow based on Herold's (1980) formula on average groundwater contribution. The work revealed that direct correlation exists between groundwater recharge and stream discharge peak.

As a sequel to Xu et al. (2002), Xu and Tonder (2002) addressed the inadequate knowledge of a numerical model of dyke-influenced aquifer. The work entails the development of an applicable and accurate approach for simulating groundwater flow behavior and modeling capture zones using the line sink concept (Haitjema, 1995). Vegter and Pitman's (2003) work is another important contribution to groundwater-surface water interaction. The work classified South Africa streams into three types; ephemeral, seasonal and perennial. They also build on the classification to characterize their interaction with the groundwater system.

The work identified two types of disconnected streams in South Africa: A) detached stream, which is disconnected because their intervening materials are impervious, and B) famished stream, which is disconnected because the connecting groundwater flow path is affected by the evaporation rate that exceeds the recharge rate.

Xu and Beekman, (2003) investigated the response of South Africa's groundwater systems to rainfall recharge. The result identified depth, structure, and texture of the unsaturated zone as the main factor that determines the aquifer response. The result led to identification of three types of responses: a) Rapid response (for cases where recharge occurs in hours, days or months due to preferential flow path); b) Intermediate response (for cases where recharge occurs over a year or two through direct and indirect flow path); and c) Slow response (for cases where recharge takes longer than two years through direct flow path).



University of Fort Hare
Together in Excellence

Van Wyk et al. (2012) established through the hyetograph-hydrograph time series data set that summer and winter rainfall is responsible for sustainable groundwater recharge, especially in fractured rocky terrain. The research observed evidence of the time-bound infiltration phase during early summer rainfall. The recharge potential of a groundwater system depends on the status and field capacity of the unsaturated zone reservoir as well as the growth of the local vegetation (Van Wyk et al., 2012).

Tanner (2013) investigated the hydrological systems of South Africa with the aim of defining their potential for the conceptual examination of groundwater-surface water interaction and the accuracy of the Pitman model to the hydrological systems. In doing so, the work classified the hydrological system into the following class of environments, namely, karst, primary, fractured (secondary), and alluvial environments.

Barath (2015) explores the hydrogeologic potential of four hydrostratigraphic units in Zululand. His work quantifies surface water and groundwater interaction using Herold's

curve fitting and saturated volume fluctuation. His findings established that shallowness and unconfined status are a major issue for the vulnerability of some of the aquifers to pollution. However, the aquifers sustain some of the lakes and streams, hence the need for controlled abstraction in order to avoid diminution of the streams (Barath, 2015).

2.5 Geologic framework

Hydrostratigraphy and paleo-environment attributes provide important information that can be linked with the groundwater potential of a geologic system. The deposition that led to the emplacement of the Balfour Formation began with the initiation of the Karoo Supergroup. A number of researches have been focussed on the geologic settings at a higher lithostratigraphic scale, within Karoo Supergroup.

2.5.1 Tectonic settings of Karoo Basin

The eventful episodic history of Balfour Formation began with the initiation of the Karoo Basin, through mantle-driven subsidence and supralithospheric loading across the southern margin of Gondwana in the late Palaeozoic to early Mesozoic period in response to subduction and compression of the Panthalassan plate underneath the Gondwana plate (Catuneanu and Elango, 2001; Lanci et al., 2013). This resulted in the formation of a retro-arc foreland system, prior to the orogenic event that initiated the Karoo sediment accretion (Dickinson, 1974; Baiyegunhi et al., 2017a, b). To date, there is controversy surrounding the development of the Karoo Basin. Several models have been proposed for the formation of the Late Carboniferous-Middle Jurassic Karoo Basin (Catuneanu et al., 1998; 2002; Catuneanu, 2004; Johnson et al., 2006; Tankard et al., 2009; 2012; Lindeque et al., 2011; Pángaro and Ramos, 2012). Veevers et al. (1997) envisaged that the continued subduction of the Panthalassan (palaeo-Pacific Ocean) beneath the Gondwana plate led to northward

compression as well as the eventual development of a fold-thrust belt inboard of the magmatic arc.

2.5.2 Geological settings of the Karoo Supergroup

Sedimentation in the Karoo Basin started with the deposition of diamictite of the Dwyka Group, followed by turbidite and shale-rich succession of Eccca Group (Broquet, 1992; Tankard et al., 2009; Figure 2.3 and Table 2.2). Overlying the Eccca Group is the sandstonerich Beaufort Group, which is subdivided into the Adelaide and Tarkaskad subgroups. The Adelaide subgroup comprises the Koonap, Middleton and Balfour Formations, while the overlying Tarkastad subgroup is made up of the Katberg and Burgersdorp Formations (Hiller and Stavrakis, 1980; Baiyegunhi and Gwavava, 2017b).

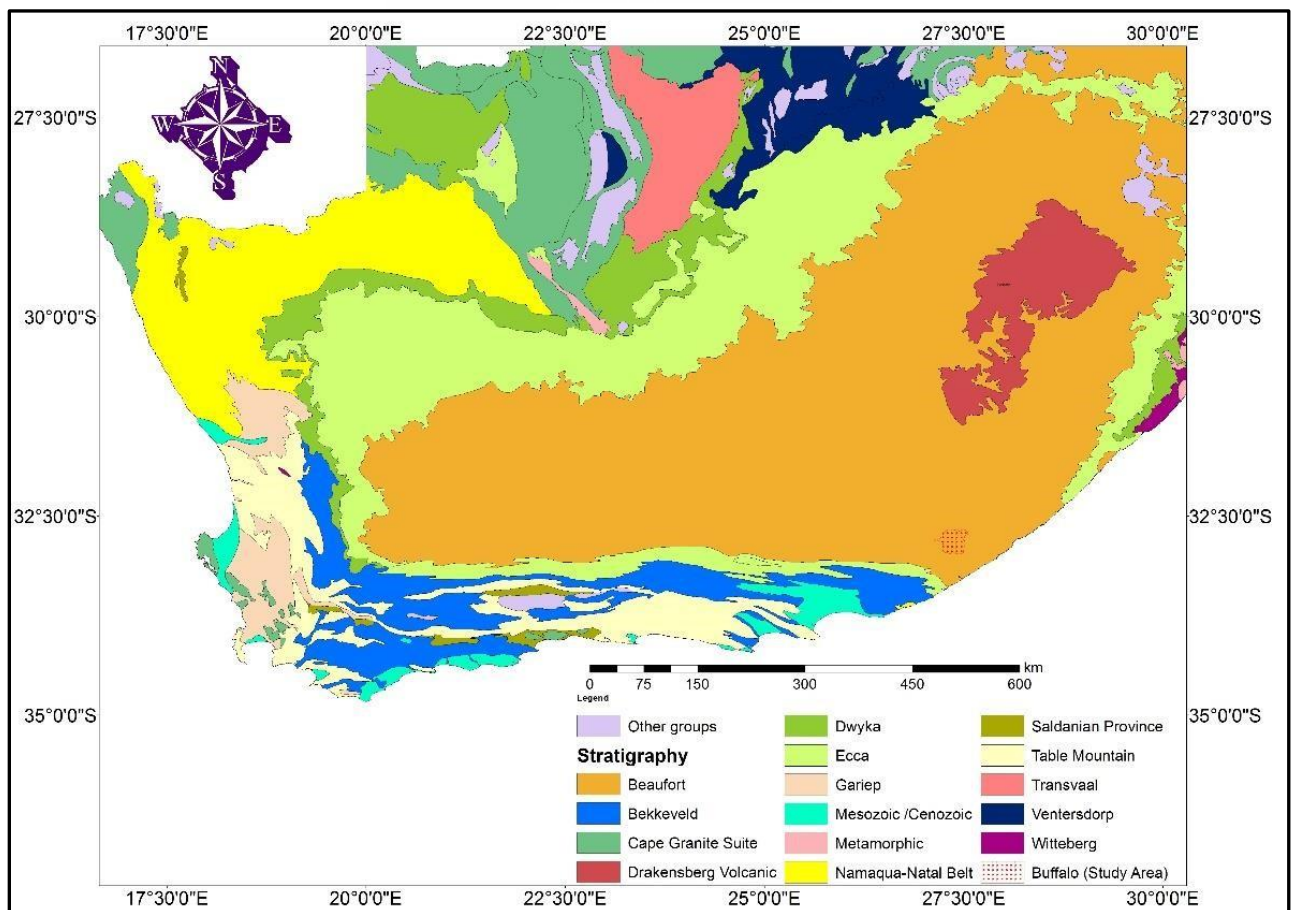


Figure 2. 3: Lithostratigraphic map of South Africa (Modified from the Council for Geoscience, 1990).

Table 2. 2: Litho-stratigraphy of Karoo Supergroup (Johnson et al., 2006).

SUPER GROUP	GROUP		FORMATION (Members)		Epoch		Period				
Karoo	Stormberg		Drakensberg		JURASSIC		Dogger				
			Clarens				Lius				
			Elliot				TRIASSIC	Late Triassic	Norian		
			Molteno						Carnian		
			Beaufort	Tarkastad			Burgersdorp		TRIASSIC		Middle Triassic
	Katberg				Early Triassic	Anisian					
	Adelaide	Balfour		Palingkloof		PERMIAM	Late Permian				Tatarian
				Elandsberg							
				Barberskrans							
				Daggaboersnek							
				Oudeberg							
	Middleton			Kazanian							
	Koonap			Ufimian							
	Ecce	Waterford (Not present in ECCA Pass)							Early Permian		Kungurian
		Fort Brown									Artinskian
		Ripon									Sakmarian
		Collingham				Asselian					
		Whitehill									
		Prince Albert									
		DWYKA				Late Carboniferous					

The Stormberg Group overlies the Burgersdorp Formation and it is made up of fluvial and aeolian-lacustrine successions of the Molteno, Elliot and Clarens Formations (Johnson et al., 1996). The Molteno Formation is made up of medium to coarse-grained sandstones that alternate with grey mudstones. The Late Triassic Elliot Formation is a typical "red bed"

fluvial deposit and consists of an alternating sequence of mudstone and subordinate fine to medium-grained sandstone (Johnson et al., 1996; Catuneanu et al., 1998).

The final stage of the Karoo sedimentation is represented by the Late Triassic - Early Jurassic Clarens Formation consisting of fine-grained sandstones and mudrocks (Catuneanu et al., 1998). The Drakensberg Group lava overlies the Clarens Formation and is believed to have terminated sedimentation within the Karoo Basin in the Middle Jurassic, signifying the breakup of the Gondwana Continent (Catuneanu et al., 1998; Johnson et al., 1996; 2006; Smith and Botha-Brink, 2014). The Group is made up of a thick succession of basalts that cap the Karoo sedimentary succession and covered a large area of central South Africa and Lesotho (Johnson et al., 1996).

2.5.3 Trends of geologic study on the Balfour Formation

Johnson (1976) who pioneered the research on Karoo Supergroup in the Eastern Cape Province described the Balfour Formation explicitly. The litho-stratigraphic succession of the Balfour Formation was detailed with respect to the hydrogeochemical uniqueness of the Karoo sequence in the Eastern Cape Province in the work of Tordiffe (1978). Visser and Dukas's (1979) study on the Beaufort group opined that the Balfour Formation is emplaced as an upward-fining fluvial cycle owing to its braided and meandering structural style. Smith (1997) builds on the argument of fluvial style that the braided river system has low sinuosity while the meandering river system has high sinuosity.

Investigation of litho-facies within the stratigraphic layout of Ecca-Beaufort contact by Rubidge et al. (2000) addressed the gap on the paleo-current pattern and paleontologic sequence of the Balfour Formation. Catuneanu and Elango (2001) established their argument on the fluvial style and outlined the elements of the fluvial style accordingly; 1) Perennial sand-bed braided system, 2) sand-bed meandering system, and 3) fine-grained meandering

system. Catuneanu and Elango (2001) identified that the paleoclimate, based on biostratigraphy record, is temperate to humid as opposed to previous findings that suggested dry and semi-arid climate.

However, Catuneanu et al. (2005) discovered that there were shifts in tectonic and climatic conditions during the Late Carboniferous-earliest Permian during the Karoo interval. The shift led to a change in climatic conditions and suggests that the transformation from warm and humid climatic conditions to cold and semi-arid conditions must have taken place in the south-eastern Karoo. The study on the Permian-Triassic boundary, which is the geologic age of deposition of the Balfour Formation, was covered in the geochemical and mineralogical investigation of Southern Karoo Basin by Coney et al. (2007).

Katemaunzanga and Gunter (2009) classified the architectural elements of the Balfour Formation into two elements; channel deposits and overbank deposits. Each element of the Balfour Formation is associated or predominated by one or more of the features of the architectural elements (Katemaunzanga and Gunter, 2009). Channel deposits are associated with channel fill, sandy bed, laminated sheets, lateral accretion, and downstream accretion. Meanwhile, overbank deposits are associated with floodplain fines, crevasse-channel, abandoned channel and levees. Katemaunzanga and Gunter (2009) established that the Oudeberg and Barberskrans Members were dominated by sandstones while Daggaboersnek, Elandsberg and Palingkloof Members were dominated by mudstone.

Oghenekome (2012) builds on Katemaunzanga and Gunter's (2009) work by characterizing the lithofacies of the Balfour Formation. The Oudeberg Member was inferred to be dominated by massive sandstone which alternates with thin laminated siltstone and mudstone. The Daggaboersnek Member was associated with non-lenticular mudstone. Barberskrans Member was associated with sandstone lithosomes. The Elandsberg Member

was characterized as an argillaceous unit. Palingkloof was inferred to comprise of red mudstone. Findings of Oghenekome (2012) revealed that the sandstone-dominated units of the Balfour Formation were transported by the river system.

Wilson et al. (2014) investigated the architecture and sedimentology pattern of the lower Beaufort Group (Adelaide subgroup), which comprises of Koonap, Middleton and Balfour Formations and seven fluvial styles. These include; flat-topped sheets, concave-up topped sheets, heterolithic ribbons, flat-topped ribbons, unconfined concave-up topped complexes, unconfined strongly amalgamated sheet complexes, and valley-confined strongly amalgamated ribbon complexes. The work established that the fluvial style of the Adelaide subgroup was due to semi-arid climate, local variability in subsidence rate, the relative position of megafan and relative sea-level changes.

The semi-aridity of the Balfour Formation paleo-environment identified by Wilson et al. (2014) was inferred as low energy paleo-current in the work of Catuneanu and Elango (2001). In conformity with this, Baiyegunhi's (2015) findings established that the Balfour Formation is characterized by premature, greywacke and heavy mineral assemblages. This typifies insufficient transport energy for the sandstone mobilization. From the analysis of the aeromagnetic map of the Eastern Cape Province, Baiyegunhi (2015) identified shallow and deep sources of magnetic susceptibility. The shallow sources were associated with magnetic minerals of the Beaufort group while the deep sources were associated with the basement (Baiyegunhi, 2015).

Johnson et al. (2006) produced a detailed regional litho-stratigraphic map with limited detail on the Balfour Formation. Katemaunzanga and Gunter (2009) narrowed their geologic exploration of the sedimentary facies of the Balfour Formation. However, Katemaunzanga and Gunter's (2009) map was 30 km to the west of the Buffalo catchment area, covering Fort

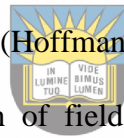
Beaufort to Queenstown. Also, information on surficial tectonic arcs for the study area was uncovered. The work on magnetic sources and lineaments of the Eastern Cape by Baiyegunhi (2015) is considered over-generalized in the catchment scale. Gaps on catchment-scale magnetic sources need to be covered, for both outcropped, near-surface, shallow and deepseated signatures.

2.6 Delineation of groundwater potential zones and geoinformatics

Groundwater potential zones are areas enclosing occurrences of considerable and economically exploitable quantities of groundwater resources. They are explored conventionally through field geologic, hydrologic and environmental mapping (Marghany et al., 2009). Data like borehole log, aquifer test, divide, tectonic arc observation, and drawdown assessment and aquifer recovery through pumping tests are commonly obtained from field and aerial photographs. Data collection processes are rigorous, robust, timeconsuming, expensive, and have serious environmental implications (for example, borehole drilling and pumping test). One of the widely employed geophysical methods for exploring the resource is a geo-electric survey. However, its application is limited in terms of spatial coverage as it provides point information in a regional scale context. It is also quite laborintensive (Oshmarin et al., 2016). The use of gravimeter and magnetometer is also associated with similar limitations to the geoelectric survey. In addition, they require high technical skills and are expensive to manage. The use of ground penetration radar has been limited due to its limitations in clay-rich environments and its resolution with great depth (Oshmarin et al., 2016). The use of airborne gravity, aeromagnetic and seismic surveys enables wider spatial coverage. However, they are sophisticated equipment that requires highly technical skills and huge budgets (Sakher et al., 2015; Feijth et al., 2019). Meanwhile, the logging of borehole cores, sampling of intrinsic properties of borehole, and aquifer

recovery through pumping tests were only obtainable in the field. They are also time-consuming and expensive (Wendt et al., 2016). The evolution of remote sensing in the form of aerial photography, satellite imagery and the non-invasive induction process of geophysics was timely and enabled spatial solutions to the regional exploration of groundwater potential zones (Lyle and Stutz, 1983). The easy, time-smart and accessibility power of geophysical methods for inaccessible areas, which was further amplified by world wars, were major breakthroughs in exploratory science (Lyle and Stutz, 1983).

The popularity of environmental exploration studies with the aid of geoinformatics began to grow in the late 1970s, especially when it was applied for moon surface environmental exploration (James and Hedenquist, 1978). The usefulness of remote sensing (RS) and geographic information systems (GIS) is now well recognized for reconnaissance surveys in geologic and hydrogeological studies (Hoffmann and Sander, 2007). They have enhanced traditional mapping and interpretation of field observations in a cost-and-time effective manner.



University of Fort Hare
Together in Excellence

Historical use of GIS became more intensified with Hill et al. (1983) on environmental data. Gimblett's (1989) review of the benefits of GIS in the modeling of the earth's surface was an eye-opener in geoscientific studies. Robinson et al. (1989) built on these advances with the elaboration of the evolution of hybrid use of GIS and RS. The concurrent evolution of geospatial technology with computer technology was a remarkable innovation in science at large (Shamuyarira, 2017). The development of faster computer processors was concurrent with GIS capability improvement for analysis of basement complex (Shamuyarira, 2017). More information on geoinformatics application to basement rocks is provided in Machiwal et al. (2011) and Vasanthavigar et al. (2011). The use of geoinformatics was equally

extended and improved for lineament mapping and geomorpho-tectonic alteration analysis (Corgne et al., 2010; Masoud, 2016; Abdulkareem et al., 2018).

The development of geospatial technologies such as an integration of remotely sensed satellite imageries and geographic information system (GIS) enables the mapping of groundwater potential areas with spatially accurate performance and pocket-friendly cost. Importantly, satellite imagery such as Landsat 8 operational land imager and digital elevation model (DEM) present the opportunity to analyze the real-time spatial status, distribution and changes in the environment (Lillesand et al., 2014). For example, Landsat 8 OLI enables a spatial analysis of changes influenced by environmental factors such as vegetation indices and land use/land cover changes, surficial lineament and climatic factors such as land surface temperature (Roy et al., 2014). DEM enables a spatial analysis of the status of the environment such as the landform, drainage pattern, topographic wetness index and slope (Nampak et al., 2014). The interface of GIS tools presents the opportunity to integrate spatially encoded groundwater influencing factors in a single map (Lillesand et al., 2014). Depending on the plug-ins and geoprocessing tools such as clipping, editing, interpolation, buffering, overlay, rescaling, reclassification, and color coding can be carried out on groundwater zone delineation (Dixon et al., 2015). The efficiency and effectiveness of this method are well documented in the works of Srivasta and Bhattacharya (2006), Sahoo et al. (2016), Naghibi et al. (2017) and Kanagaraj et al. (2018).

Quite a number of statistical methods have been developed to improve the spatial resolution of the thematic layers to be integrated. These include; multi-criteria decision analysis (Kan et al., 2012), artificial neural network model (Lee et al., 2012), analytical hierarchical process (Sahoo et al., 2016), frequency ratio, and weight of evidence method (Ozdemir and Altural,

2013; Hong et al., 2018). To incorporate the statistical approach, the attributes of thematic layers are identified by assigning weighted average.

In these studies, thematic layers such as rainfall, lineament density, drainage density, lithology, slope, wetness index, water index, vegetation index, soil type, land use/land cover (LULC), geomorphology, and land surface temperature (LST) were selected. The selection of these unique parameters is based on their inherent influence on groundwater development. The identified factors have been validated in numerous literature (Das et al., 2017; Kanagaraj et al., 2018). Lineament density (LD) indicates surficial inlet for an appreciable quantity of groundwater influx into spaces within geologic discontinuities and tectonic arcs (Fenta et al., 2015). Degree of drainage density (DD) has an inverse relationship with permeability and infiltration and, as a result, it informs on the degree of ponding in such environmental units (Srivastava et al., 2008). The lithological type of area provides information on the inferable hydraulic properties of such areas for groundwater potential (Burbery et al., 2018). Soil type also provides information on hydraulic conductivity properties and infiltration potential for groundwater development (Wysocki and Schoeneberger, 2016). Terrain configuration indicates the potential of surface water to develop into an overland flow rather than infiltrate as a result of surface topography (Neilson et al., 2018). Basically, landform informs on the degree of alteration of the morphogenetic property of an environment. It presents the summation of the influence of relief on the conversion of surface water into groundwater/overland flow (Wysocki and Schoeneberger, 2016; Fetter, 2018). Topographic wetness index (TWI) reveals areas with the relative potential of a hillslope factor to influence hydrologic processes (Hojati and Mokarram, 2016). Land use and land cover map summarise the environmental modification influenced by human interaction, urbanization and socioeconomic changes (Aquilué et al., 2017). Land surface temperature indicates zones of poor saturation thickness as well as areas of high potential for evaporation and

evapotranspiration potential (Urqueta et al., 2018). This is of particular importance in a semi-arid/arid environment where water conservation is a major priority.

2.7 Lineament mapping as an important tool in groundwater survey

The major target zones in groundwater exploration are often areas of secondary porosity such as shear zones, trenches, joints, faults and fractures, generally referred to as natural lineaments (Singhal and Gupta, 2010). Lineaments are tectonics structures developed by stress concentration or strains due to the initiation and evolution of rift and orogeny (Kazemi and Davoodi, 2011). Lineaments are often concentrated in areas with complex landform and heterogeneous lithostratigraphy developed over geological time (Galloway, 2010).

Mapping of lineament as a remote sensing application in geology has an age-long history, for example, O'Leary et al. (1976) opined his view of lineament as extractible features of the earth with linear or curvilinear orientations on weak points of the earth surface. In order to ascertain the inception point of Laramide orogeny in the Beartooth Mountain block, Wilson (1936) employed the extraction of lineaments to uncover the situation surrounding the NyeBowler tectonic activity and structural alignments on the historic sedimentary deposits in the region, ranging from Pennsylvanian sandstone of Permian Clear Fork Formation to the variegated shale of the Eocene Wasatch Formation. Wilson (1950) employed extracted lineaments for the interpretation of elements of orogenesis and arcs of North America. Moody and Hill (1956) employed lineament extraction to study tectonic activities associated with stresses on large wrench faults such as that of San Andreas of California, which may have generated other smaller faults such as the thrust faults, anticlinal folds and wrench faults. Gilluly (1976) disagreed on the application of surficial lineament, especially those that span more than ten miles wide, for exploration of ores in contrast to preceding literature on extensive application of lineaments. He supported his argument with facts that most exploitations using lineaments are negatives and non-existent. Maughan and Perry (1986)

evaluated the tectonic activities of middle Phanerozoic sedimentation that account for the development of the Williston Basin, Big Snowy Trough, Zuni Uplift and the Ancestral Rocky Mountains on the Cordilleran continental shelf using a combination of geologic mapping and extracted lineaments. Other works that documented the application of lineament extractions for interpretation of geologic signature include Mwaniki et al. (2015), Steven et al. (2018), and Lesage et al. (2019).

Geophysical prognosis involving aeromagnetic mapping offers a faster economical and versatile means to encroach densely vegetated landmass of varying altitude and depth. Its capability to resolve varying scales of features such as magmatic intrusions, volcanic rocks, fault structures and variation in basement types makes it of particular interest in geologic studies for groundwater prospects.



University of Fort Hare
Together in Excellence

Many approaches involving the use of satellite images, aerial photographs and digital elevation models (DEM) for the extraction of structural signatures such as lineament have been documented. These can be categorized into manual extraction (Scheiber et al., 2015), semi-automatic extraction (Bonetto et al., 2017), and automatic extraction (Hashim et al., 2013; Adiri et al., 2017). The automatic extraction approach appears to be much more reliable as the other methods depend on the analytic perception of the mapper. The quality of automatic extraction also depends on algorithm efficiency and image quality. Mapping of lineaments is vital in hydrogeological studies for delineation of groundwater potential zones, groundwater vulnerability mapping, water resources management and evaluation of groundwater-surface water interaction (Corgne et al., 2010).

2.8 Electrical resistivity tomography for groundwater survey

Geophysical methods like electrical resistivity tomography (ERT) have been extensively applied to address lithological profiling problems in environmental, engineering, and

reservoir geological explorations. The chances of successful results with the application of geophysical tools have been dependent on correlative verification of findings (Mohammed et al., 2012). In particular, ERT has yielded reliable results for prospecting of subsurface layer and groundwater potential. Important information such as the subsurface structure, composition, and buried Formation have been successfully surveyed. ERT works by measuring and inferring the electrical resistivity properties of subsurface fluid content, rock (bulk density, thickness, porosity, and conductivity) and temperature on geoelectrical sections (Mohamaden et al., 2016). The sections are differentiated into different geoelectrical units based on the difference in the humidity percentage of the geological units (Parasnis, 1997). Field results of geoelectrical surveys have been interpreted in two ways: 1). Generalized Cagniard graph method (Koefoed, 1965) which depends on curve matching technique; and 2) Analysis of ERT results using computer software such as IPI2WIN and RES2DINV.



Electrical resistivity tomography has been integrated with other GIS methods, most importantly, morphometric analysis, in order to address many geomorphological and geologic-related problems. Literature such as Attwa et al. (2016), Sultan et al. (2017), Attwa and Ali (2018), and Bastawesy et al. (2019) employed the combination of ERT and morphometric parameters approach in varying water-related exploration capacity. For example, Attwa et al. (2016) employed the integrated approach of GIS-based geomorphological analysis with direct current resistivity sounding for characterization of hydrographic basins and hydrogeological conditions at Luxor, Egypt. The results reveal five hydrographic basins, the profile of the subsurface layers and also enable the delineation of groundwater sweet spots. Sultan et al. (2017) employed morphometric parameters for the deduction of the hydrological model of alluvial active channels, while ERT was employed to delineate the lithostratigraphy thickness together with well-log information in an effort to

evaluate the groundwater potential of the north-western part of the Gulf of Suez region. Attwa and Ali (2018) successfully deployed the hybrid approach for characterization of the subsurface layer and zones of groundwater potential in the Wadi-Ramleiya basin, the eastern desert of Egypt. The combined impact of landforms and lithostratigraphic units on the development of flash floods was assessed by Bastawesy et al. (2019) using morphometric analysis and ERT. However, the hybrid method has not been applied in South Africa for the integrated characterization of hydrographic basins and groundwater potential areas, despite the severity of water scarcity, especially in the Eastern Cape, where surface water is the major source of potable water supply. All these reveal the potential of the hybrid approach of geomorphological analysis and electric resistivity tomography to decipher groundwater zones through subsurface structural variability analysis.

2.9 Geomorfo-tectonic analysis for groundwater zone decipherment

Studies on the evolution of watershed have received attention in recent times due to the significance of watershed management for water resource provisioning and disaster risk management. Nevertheless, the need to develop watershed for the understanding of its potential for groundwater prospect, river basin resource management and sustainable development of water resources is equally a major priority in semi-arid environments. By undertaking the prioritization of watershed streamflow with respect to its spatial variability, evolution process, and flow attributes, useful information on water resource management can be provided (Evangelin et al., 2015). In order to arrive at this, a watershed assessment approach that encapsulates the analysis of topography, hydrologic alteration of morphotectonics, soil reconfiguration, groundwater-surface water interaction hydrodynamics and basin transformation would be essential. Evaluation of these essential components is wrapped up in the morphometric study of drainage basins (Rai et al., 2014).

Morphometric analysis is the quantitative description of drainage systems, landform geometry, and morphology (Pareta and Pareta, 2011). It provides information on the geohydrodynamic changes in drainage networks. This is influenced by physical, erosional, geologic, hydrologic and geomorphological processes within the confinement of a watershed (Rai et al., 2017). Essentially, it reveals the numerical dimensions in the river basin landscape in relation to the lithological attributes of the basin. Its value as a geoinformatics tool for projecting rainfall-runoff behavior, soil characteristics, morpho-tectonic changes and fluvial system imprinted on lithological assemblages in the watershed have been revealed in the literature (Prabu and Baskaran, 2013; Samal et al., 2015; Mahajan and Sivakumar, 2018).

The morphometric parameters were based on the work of Horton (1945), Strahler (1957), Pareta and Pareta (2011), Masoud (2016) and Abdulkareem et al. (2018). The parameters were classified into four attributes, namely, drainage network, basin geometry, drainage texture, and basin relief attributes (Rai et al., 2014). Drainage network analysis is based on characteristics of stream order that reveal the impact of topography, geologic structures and lithological type on drainage configuration (Sreedevi et al., 2005). The analysis provides information associated with the attribute of watershed porosity, ponding property of basin cover, topographic complexity, and geologic settings to drainage architecture. Watershed geometry analysis is based on the parameters of a basin's orientation. It reveals the impact of lithologic material type, relief and climate on catchment orientation (Avinash et al., 2014). It reports the permeability property of the geologic materials, infiltration and groundwater potential of underlying lithology, the efficiency of runoff, and the hydrodynamic response of basin to flow. The drainage texture analysis is used to define the depth of landscape dissection by the drainage network. It is based on the structural progression of stream polylines with respect to geomorphological evolution. Computation involving drainage texture analysis has been used to establish the impact of land use/land cover, climatic



University of Fort Hare

contribution to geomorphological evolution, basin's response to rainfall-run property, permeability of the basin cover, sustainability need of the basin for water resource development and groundwater potential of the basins (Pareta and Pareta, 2011). Relief characteristics of a basin provide information on geomorphological changes influenced by drainage network development, overland flow and erosional attributes of the terrain (Sahu et al., 2017). It has been used to infer impacts of variability in climates, heterogeneity of geology, infiltration capacity of the basin and variability of soil materials in relation to the lithology of the basin. The stream orders indicate the potential for flash floods (Pareta and Pareta, 2011).

2.10 Hydro-climatic flux and streamflow recession attributes as important

metrics

Fluxes in hydrologic events are important metrics for assessment of water availability and viability. The influence of these fluxes on streams and hydrologic drainage systems makes streamflow frequency a valuable environmental tool for assessment of water availability and environmental sustainability. Among the uses of metrics of hydrologic flux are; (i) prediction of stream periods and temporal sequences; (ii) study of river equilibrium; (iii) assessment of discharges from groundwater; (iv) assessment for flux in the water cycle, hydrologic regime and seasonality; and (v) exploration of future water needs (Faiz et al., 2018). In the semi-arid environments, hydrologic fluxes are compounded by climate changes and extremities of weather patterns among other factors such as geology, soil type, physiography, watershed size and land use/land cover. Exploration of the variabilities of these hydro-meteorological elements has been one of the major scientific approaches for theorizing, regionalizing, and controlling the impact of hydrologic processes.



In particular, entwinement of groundwater and surface water indicates that the existence of one could serve as a predictor of the other (Ross, 2017). Consequently, the hydrodynamic fluxes of one of the components can provide information on the variability of the other. Hydrologic response of a catchment to these fluxes depends on geomorphological and hydraulic properties of the catchment (Barros et al., 2017). The response results in variability and non-linearity across hydrological units due to the heterogeneity of catchment lithologic materials. Although rainfall also varies in non-linear patterns, the impacts of antecedent soil moisture conditions have been revealed to influence the amount of water stored and later discharged as baseflow (Montgomery, 2002). The streamflow hydrodynamics can serve as the means of quantifying the variability in groundwater performance, storage potential and the discharge properties across hydrologic sub-basins (Wittenberg and Sivapalan, 1999; Kienzle, 2006). Estimation of streamflow hydrodynamics is based on the property of baseflow and interflow, associated with the delayed signature in the stream hydrograph.



University of Fort Hare

The understanding of seasonal and long term changes in baseflow is essential for water resource development, management and use (Esralew and Lewis, 2010). Knowledge of baseflow rate (index) enhances the understanding of hydrologic budget, low-flow dynamics, intrinsic hydraulic properties of the subsurface, and environmental flow condition (Barlow et al., 2015). Vogel and Kroll (1992) underpin the relationship between low-flow deductions and the product of average watershed slope, baseflow recession constant and catchment area. Their analysis reveals that the constant of baseflow recession can serve as an important indicator and surrogate for catchment hydraulic conductivity and soil porosity. The study by Chapman (1999) reveals that the streamflow recession can serve as an important estimator of environmental flow processes.

Kienzle (2006) established that the recession index indicates the integral response of catchment in a low rainfall regime, it provides information on the storage capability of a

catchment and serves as an indicator for streamflow recovery. A time-series evaluation of the recession rate by Mair and Fares (2011) reported a major slump in baseflow and this was linked with the impact of urbanization. The study by Barros et al. (2017) reveals that the decadal component of baseflow can be used to forecast drought events. Recession analysis is a major research tool for assessing streamflow-groundwater interaction in the hydrological analysis.

Flow duration curve (FDC) is the plot of the observed historical variation of flow with the percentage of time resolution in order to typify the probability of exceedance flow over a given value (Verma et al., 2017). It involves the computation of the cumulative density function of flow at a defined time domain. The time resolution can be prepared as mean daily, weekly, monthly or seasonal discharge. The shape of the curve can be used to deduce information on the regime property of the river in the high flow, and the sustenance of the river in the low flow. In general, it provides information on the stochastic fluctuation potential of streamflow and storage capability of the catchment for river basin maintenance (Müller et al., 2014). The general procedure for deducing low flow in FDC involves an analytical study of the recession part, usually between 70 – 95% percentiles. Computation of FDC using a 7-day moving average and extraction of 95% percentile for low flow threshold has been widely recognized for assessment of the risk of extremely low flow (Smakhtin, 2001). Interestingly, both the low flow and high flow section of FDC could suggest information on the subsurface properties of an environment influencing flow patterns (Yokoo and Sivapalan, 2011).

Baseflow is basically deduced from the investigation of streamflow time-series hydrographs. Varieties of methods have been proposed for baseflow separation. These include; smoothed minimum technique, popularly known as constant-discharge method (Institute of Hydrology,

1980), half-linear minimum/maximum technique, popularly referred to as the concave method (Bates and Davies, 1988), efficient subsurface flow technique, (Raudkivi, 1979), constant-slope method, Wittenberg technique (Wittenberg, 1999), and the master curve method (Cimen and Saplioglu 2004). However, these procedures were improved upon through the development of the automated baseflow separation techniques based on the following approaches, namely, recession curve method, filter-based method, and mass balance method.

The recession curve method involves the deduction of recession constant, which can be estimated from the slope of the falling limb of stream hydrograph. The most common recession curve methods include the baseflow index method, hydrograph-separation method, and PART method. The filter-based method is based on signal processing theory. In this method, the low-frequency signal component is separated from the high-frequency signal component. The filter-based method can be further subdivided into two types; recursive digital filter and runoff-stoppage-time method. The recursive digital filter (RDF) was developed by Eckhardt (2005). The RDF works in a unique way compared with others. It employs recession analysis and backward-moving filter in processing quick flow and baseflow attributes (Collischonn and Fan, 2013). It is associated with the key assumption of linearity between storage and aquifer water outflux (Zhang et al., 2017). Their estimations are based on discharge records only and they compute using moving time-window algorithm and basin drainage area only (Lott and Stewart, 2012). The mass balance method, also known as the geochemical or natural tracer method, is carried out using the estimation of the concentration of conservative chemical constituents in the flow components of streamflow, such as hydrogen or oxygen isotope ratios (Stewart et al., 2010). In this method, streams are sampled at intervals while discharge and chemical concentrations are assessed concurrently.

However, the method is laborious and expensive while extreme caution is required on the choice and composition of isotopic tracers as well as the procedure of experimentation to be followed for accurate results (Lott and Stewart, 2013).

The assessment of climatic variabilities using hydro-meteorological elements has often employed the metrics of rainfall and streamflow (e.g. Renner et al., 2011; Zhou et al., 2015; Chen et al., 2016). To this end, quite a number of statistical approaches have been employed in the assessment of rainfall and streamflow variability. These include (a) the nonparametric methods such as Mann-Kendall analysis, sensitivity analysis, Spearman Rho and Sen's slope; (b) the parametric methods such as t-test, principal component analysis, hierarchical cluster analysis, regression analysis, autocorrelation, and the Pearson correlation coefficient test to mention but a few of them. However, non-parametric approaches have been favored over parametric, owing to the stochastic and nonlinear attributes of hydro-meteorological elements. More so, parametric tests are sensitive and distorted by outliers and missing data during normality and variance homogeneity assessment (Asfaw et al., 2018). Time-series assessments of these elements have been a significant tool for evaluating the impact of climate change and variabilities. It reveals the degree of independence within the series, and the strength of trend and periodicity within a regulated frequency (Machiwal and Jha, 2009). The study of trends has also proven valuable for inter-annual variability studies. The Mann-Kendall test for monotony and trend detection has been widely favored over others in hydrology and meteorology due to its ability to normalize outliers that influence skewness (Chen et al., 2016).

2.11 Water-related literature in and around the study area

Numerous research gaps pertaining to geologic, hydrologic, and integrated water exploration have been highlighted in the previous sections for further study. Literature with relevant

information on groundwater is relatively scarce in the study area. However, there are two significant studies with information on groundwater potential in the Buffalo catchment. These include; Madi and Zhao (2010, 2013), Cobbing (2014) and DWA (2010). The work of Madi and Zhao (2010) in the proximity of the study area revealed that the southern neotectonic belt constitutes some important geologic structures that indicate the potential for the development of the groundwater system. Further investigation with the use of seismic data and other noninvasive geophysical methods flagged the existence of the fault, ingrained quartz vein in dolerites, weathered dolerites and Quaternary sediments with potential for a groundwater system (Madi and Zhao, 2013). Cobbing (2014) highlighted the existence of groundwater production boreholes which were closed down as a result of poor management. In Vegter and DWAFs' (2010) classification of hydrogeological region, the study area falls within Ciskeian coastal foreland. The catchment groundwater was reported to be hosted by intergranular and fractured aquifer, while the groundwater yield ranged between 0.5 and 2.0 l/s (Vegter and DWAF, 2010). The hydrogeological mapping for groundwater prospect reported by Vegter and DWA (2010) was suggested to be poor in development.

2.12 Scale of analysis

Environmental studies involving spatial analysis are often associated with scale definition. Barthel and Banzhaf (2016) expanded on the scale of studies pertaining to groundwater surface water interaction and outlined three types; point, local and regional studies. The point scale was defined as a single location within a spatial reference that provided a detailed analysis of unique processes within geographic confinement. Barthel and Banzhaf (2016) stated that point scale analysis enables fundamental analyses of distinct features that cannot be possibly generalized in a discrete manner. Barthel and Banzhaf (2016) defined local scale as the scale of small geographic area coverage where parameters of point

data are integrated. Further, the work expanded that analysis done at a local scale enables expression and comparative assessment of fundamental processes gathered at discrete points. The work revealed that regional-scale may span across hundreds to several millions of square kilometers and as a result enable a wide range of possible combinations of factors.

In general, geological scales are geo-chronologically and spatially bounded. The geological scale is regional in extent. In hydrogeological studies, aquifer or watershed scale is often used to describe flow-net (Fetter, 2018). Meanwhile, the smallest unit of hydrological scale is the hydrologic unit (Strahler, 1957). Hydrologic unit is the area of influence of a single stream order (Strahler, 1957). The largest single hydrological boundary is the primary catchment scale (Vegter, 2001). However, the scale of management can be politically modified into water management boundaries as is the case in South Africa (Vegter, 2001). Primary catchment can be fragmented into secondary, tertiary, quaternary or much smaller basin sizes (Vegter, 2001). An increase in coverage leads to an increase in complexities and uncertainty (Tanner, 2013).



University of Fort Hare
Together in Excellence

Scales of hydrologic studies vary with the choice of model. Beven (2002) presents the classes of hydrologic models as thus; lumped, distributed, deterministic and stochastic models. The lumped model is a model that approximates variable factors of interest in a catchment area into a representative condition. The distributed model enables critical variability among catchment influencing factors as representative point data within every grid element (Jewitt and Schulze, 1999). In the scientific sense, a cell unit of the distributed model is unrealistic, hence, distributed models have lumped models when compared to a much smaller scale. The deterministic model is a model from which a representative result for a catchment is generated (Beven, 2002). The stochastic model is the model type that enables randomness in outcomes (Beven, 2002). The most appropriate scale for this study is the tertiary catchment scale.

2.13 Summary

In general, the information in this chapter has revealed the current status of researches on groundwater system exploration and features. It also expands on feasibility and limitations in researches, physical information on the study area and gaps of research uncovered. From the review, the hydrostratigraphic unit of the study area comprises of a fractured rock system. The aquifer type based on the dominant lithostratigraphy of the study area is an unconfined aquifer that would be mainly recharged by rainfall. More analytic information is required in order to confirm the status and stages of the river in the catchment. The majority of the gaps within the limits of the study area are entirely wrapped up in the scope of this study.



University of Fort Hare
Together in Excellence

Chapter 3: Methodology

3.1 Methodological procedures: an overview

The conceptual representations of processes occurring in the catchment area are interpreted in the mathematical form of a model. The model development is based on the knowledge of real-world geo-hydrodynamic processes leading to the development of a catchment and aquifer recharge system. These include; precipitation, overflow, development of drainage, infiltration, flow path, interflow, recharge, and discharge. Shallow knowledge of the realworld hydrologic and hydrogeologic processes leads to the development of a highly uncertain conceptual model (Wagner and Gupta, 2005). This chapter focuses on the methodological procedure adopted to meet the highlighted objectives of geo-hydrodynamic researches. The study was achieved through extensive literature study, intensive field investigation for sampling, data acquisition, report taking and ground-truthing where necessary, and desktop analyses.



University of Fort Hare
Together in Excellence

3.2 Mapping of geologic structures for delineation of hydrogeological settings

Objective 1 was designed with the aim to delineate hydrogeological settings at the catchment scale using geologic structure mapping. This entailed hybridization of automatically extracted lineaments, intensive field mapping for sedimentary structures and structural signatures from aeromagnetic data interpretation for groundwater prospecting purposes in the Buffalo basin headwater, Eastern Cape, South Africa. The objective of this section is based on the reconstruction of geologic environment and mapping of geologic structures, extraction of lineaments and analysis of the aeromagnetic maps.

3.2.1 Geologic mapping

The geologic mapping was achieved through a desktop study of existing maps and field investigation. The desktop studies engaged include; field trip planning via Google Map delineation and route study, analysis of borehole core log study for surficial geology, aerial photograph analysis and guidance provided in the literature. The field investigation exercises include; reconnaissance survey, information gathering on the sedimentary structures, mapping of outcrops, ground-truthing in relation to hydrogeological boundaries and extracted geomorpho-tectonic arcs (lineaments) as well as sampling with pictorial evidence. The integration of the map features was used to develop a base map in ArcMap 10.5.1, which was used for the field trip. The geologic raster of South Africa was downloaded from www.waterresourceswr2012.co.za. This comprises of a simplified and detailed geology map of South Africa prepared in 1990 and 2005 by the collaboration of the Council of Geoscience and the Department of Water Affairs and Forestry.



University of Fort Hare

Tools used for field investigation include; geologic hammer, clinometer, hand lens, 30 m rules, hand auger, and global positioning system (GPS). The geological mapping was embarked upon after careful extraction of information for easy navigation. In the field, applicable outcrop exposures are found along road-cuts, natural embankments, sinkholes, and channels, although they are marginal and poor in general. Structural delineation is guided by the dominant facies peculiar to structural features of Balfour Formation which were documented in the literature (Katemaunzanga and Gunter, 2009; Wilson et al. 2014 - Table 3.1). Rocks were chipped to examine weathering depth, depth of cleavages, the extent of hardness, and to enable critical examination of detritus fabrics and textures using a hand lens. Corresponding examinations are noted in field report notes and geo-tagged. Reconstruction of the study area geology was developed from a compilation of findings from field reports,

clippings and inferences drawn from previous work and soil maps, and delineated boundaries in geologic raster.

Table 3. 1: Peculiar structural features of sedimentary facies of Balfour formation

S/N	Dominant structural feature	Dominant lithology	Members
1.	Ripple marks – Oscillation and current ripple marks.	Sandstone	Oudeberg
2.	Overbank deposit – Floodplain fines, levee, crevasse channel	Mudstone	Daggasboersnek
3	Channel deposit – lateral accretion, laminated sheet, sandy bed	Sandstone	Barberskrans
4	Floodplain fines	Mudstone	Elandsberg
5.	Oxidized interbeds	Mudstone	Palingkloof

3.2.2 Extraction of lineaments



Landsat 8 Operation Land Imager (OLI) of April 2018 was downloaded from the earthexplorer.usgs.gov website. Mid-Autumn (April) was selected because it represents the time of the year that rainfall intensity and wind speed are fair enough for soil wetness and cloud clarity, thus favoring clarity of fractures in the raster spectral reflectance. Image selection for the Landsat thematic map (TM) imagery was based on less than 10% low cloud proportion criterion and critical visual inspection for the clarity.

The Landsat 8 image was pre-processed by calibrating its radiometric values and ensuring atmospheric correction. Atmospheric correction is essential for the improvement of reflectance quality of the imagery in order to enhance the visibility of critical properties such as the distribution of aerosol and water vapor. The spatial resolution of the imagery was improved by reducing the panchromatic band from 32 m to 16 m in ENVI 5.4.

The corrected image was exported into ArcGIS 10.5.1 for further processing by clipping the raster into the shapefile of interest. Bands 7, 5 and 3 were extracted and transformed using the second Principal Component Analysis (PCA 2). The resulting images of PCA 2 were mosaicked in order to ensure consistent and seamless spectral response-output.

The resulting raster was stacked accordingly using the false-color composite bands tool in ArcMap 10.5.1. The image was clipped using the prepared study area shape-file. This was followed by the multi-stage algorithm of the Canny edge detector for filtering purpose and contour detection enhancement. The automatic extraction of lineaments was carried out in PCI Geomatica software 2018 version. The procedure was carried out in two stages; contour detection and line detection.

Lines detection is carried out in four sub-stages; first is the specification of the minimum length of the curve which will be considered as lineament using curve length threshold (LTHR) parameter; second is a specification of maximum error using line fitting threshold (FTHR) parameter. The third stage involves the specification of the maximum angle between polylines segment using Angular difference threshold (ATHR) parameter and, lastly, specification of the minimum distance between two polylines using linking distance threshold (DTHR) parameter (Kocal et al., 2004; Hashim et al., 2013). These processes generate the polylines referred to as lineaments. These are saved in the shape-file format in PCI Geomatica and then exported into ArcGIS.

The length of the lineaments was computed in ArcGIS by changing the Geographic Coordinate System (World Geodetic System (WGS) 1984) to the Projected Coordinate System (WGS 1984 World Mercator) and then generating the length for the polylines. Lines were split for vertices in ArcGIS in order to generate the start and end coordinates (X1, Y1, and X2, Y2) of the lines. It was then extracted using CAD format for importation into

Rockworks 17 software in order to plot its Rose diagram. The line data was imported into Rockworks 17. Each column of the imported data was aligned with its corresponding output column (X1, Y1, and X2, Y2) in the Rockworks 17 spreadsheet and then processed from the endpoint. The result generates the rose diagram and its statistical summary.

3.2.3 Processing of aeromagnetic data

The aeromagnetic data used in this work was acquired by Fugro Airborne Surveys in the course of a regional aeromagnetic survey of the Eastern Cape using a proton procession magnetometer of 0.01 nT resolution. The aeromagnetic scanner was flown at a constant height of 60 m in north-south flight direction, within the sampling line of 250 m using line spacing of 200 m. The data was extracted using the American Standard Code for Information Interchange (ASCII) gridded format of Geosoft Oasis Montaj.

The acquired magnetic data was imported into Geosoft software for enhancement using the linear and non-linear filtering algorithm of the Montaj MAGMAP filtering system. The data processing was carried out by preparing the space domain grid, which helps in reducing long wavelength and high amplitude behavior, ensuring an adequate gap for periodicity and maintaining the power and frequency content in the data at the same level. In order to reduce to-pole (RTP), an average magnetic inclination of 63.4667° and declination of -28.6667° was applied after removing the International Geomagnetic Reference Field (Peddie, 1982). Then, two dimensional forward and inverse Fast Fourier Transform (FFT) algorithms were applied in order to convolve and filter the data in the wavenumber domain (Cooper, 2014). Enhancement such as X, Y and Z derivatives, and analytical signals were calculated and projected into a map. Shallow structures were enhanced and mapped using tilt derivatives, TDR.

Analytical signal (AS) was computed using equation 1;

$$AS(x, y) = \sqrt{\left(\frac{\delta T}{\delta x}\right)^2 + \left(\frac{\delta T}{\delta y}\right)^2 + \left(\frac{\delta T}{\delta z}\right)^2} \quad (1)$$

Where T, the total magnetic intensity is the measured field and x, y and z, are the edges of the magnetic structures.

Shallow structures were enhanced and mapped using tilt derivatives, TDR. It was computed as shown in equation 2;

$$TDR = \arctan\left(\frac{VDR}{THDR}\right) \quad (2)$$

Given that VDR is the first vertical derivative and THDR is the total horizontal derivative of the total magnetic intensity T which are expressed as shown in equation (3) and (4) respectively;

$$VDR = \frac{\delta T}{\delta z} \quad (3)$$

$$THDR = \sqrt{\left(\frac{\delta T}{\delta x}\right)^2 + \left(\frac{\delta T}{\delta y}\right)^2} \quad (4)$$

The magnetic depth slicing was carried out using Getech GetGRID. Depth slicing linear filter computes the apparent depth to magnetic source as a plot of magnetic field gradients across the subsidence of magnetic anomaly. The computation procedure is based on Wiener filtering principle whereby the magnetic signal is assumed to be due to two or more invariant arbitrary processes (Fuller 1967; Baiyegunhi and Gwavava, 2017). The components of the magnetic gradient were extracted from the gradient plots by disaggregating the shallow sources from the deeper sources. This was done by fitting trend-lines to join the vertices of major tilts on the plot.

The depth estimation is based on the slope of the fitted trendline as defined in equation (c):

$$h = \frac{b}{-4\pi} \quad (c)$$

Where h is the average depth to the anomalous structure in meters, b is the slope of the Nyquist wavenumber components. Further information on the derivation, manipulation,

tutorials and general discussions on magnetic filtering techniques using Fast Fourier domain filters are documented in Whitehead and Musselman (2008). The result of aeromagnetic enhancement was validated using well-log cross-section profiles mapped using Strater 5. And with respect to the deduction, recharge path and geosynclinals structure revealing the major aquifer and groundwater zone in the study area is delineated. The linear features of the THDTD map were also extracted and computed for its azimuthal information using ArcMap 10.5.1.

The result of the assessment was corroborated with cross-section profiling of shallow borehole lithologic profiles mapped in Strater 5 and field geological survey based on sedimentary facies mapping.

3.2.4 Validation of surficial lineaments and analytical signal map

Field expedition for ground-truthing of surficial lineaments and anomalous landforms depicting perceived ridges allows for the validation and interpretation of geologic structural features depicted in maps. Thirty-two reference points were visited and these were instrumental to the geologic interpretation of the surficial lineaments. These were further compared to the general orientation of magnetic lineaments.

The aeromagnetic spectra of the analytical signal map were verified using borehole lithologic information obtained from the National Groundwater Archive of South Africa. First, the spatial distribution of the boreholes was overlain on the analytical signal map in ArcGIS 10.5.1 in order to enable the selection of boreholes that overlay different spectral amplitudes. Boreholes were selected across the magnetic intensity variation (high and low). Selected boreholes were then imported into Starter 5 software to create a cross-section. The worksheet column was defined, the well selector was created and cross-section data was imported. The

operation generated the borehole cross-sections. These were analyzed comparatively in relation to the varying magnetic amplitude reflectance.

3.3 Baseline study of streamflow variabilities: methodologies

Six gauging stations were identified within the hydrologic basin headwater; Ngqokweni, Tshoxa, Mgqakwebe, Quencwe, Buffalo, and Yellowwoods stations. Hence, their daily streamflow data from 1956 to 2017 were acquired from the Department of Water Affairs and rainfall data was acquired from South Africa Weather Service. The data were inspected for missing records, due to the volume of missing streamflow records from 1987 to 1988, which was more than 3% for some of the basins. This is considered unacceptable for hydrological research (Mishra and Singh, 2010) and, as a result, the dataset range for rainfall and streamflow for the six stations was reduced to 28 years records which spanned from January 1, 1989, to December 31, 2016. This just agrees with the minimum of 25 years of data series requirement for average statistical assessment for trends and variability study in Burn and Elnur's (2002) work. Within the 28 years' record, missing data was less than 0.01%. However, missing days were extrapolated by taking the average of the preceding two days and the succeeding two days. All the data was summed into monthly and seasonal records. Data assessment was achieved through desktop analysis using multivariate statistical approaches. The baseline spatio-temporal trend assessment can be classified into three; temporal variability study, streamflow correlation to rainfall and streamflow recession analysis.

Variability assessment of the streamflow was achieved using the following methods;

- I. The double mass curve for consistency assessment
- II. Descriptive analysis for normality and white noise

- III. Homogeneity test
- IV. Parde coefficient plot for regime variability
- V. Assessment of trends

Correlation assessment of streamflow to rainfall was achieved using the following methods;

- I. Kolmogorov-Smirnov test for comparison of the distribution
- II. Sensitivity analysis of streamflow to rainfall

3.3.1 Variability assessment

3.3.1.1 Double mass curve for consistency assessment

A double mass curve (DMC) was computed using linear plots in Microsoft Excel. Cumulative assessments of the monthly flow records were taken for all the stations. The DMC for each station was produced by plotting a cumulative monthly flow record against the average cumulative monthly flow records of the remaining stations. Hence, six DMC curves representing each gauging station were plotted. Trend-line was extracted and the coefficient of determination value was taken for inference on the strength of linearity. Breaks, deflection points and tilts were also noted.

DMC is a simple plot that illustrates the linear relationship between the cumulative values of two or more hydro-meteorological variables measured at the same length of the timeline (Searcy and Hardison, 1960). It is based on the assumption that linear plots produced from cumulative assessments of the hydrologic variables will produce a straight line graph and depict consistency (Searcy and Hardison, 1960). The slope of DMC depicts the constant of proportionality. A break along the line of proportionality indicates inconsistency in sampling and the period of hydrologic alteration (Sayemuzzaman and Jha, 2014). Factors responsible for such breaks may include; changes in the method of data collection, the effect of physical

changes, instrumentation, gauging location variability and changes in environmental or water management procedure (Sayemuzzaman and Jha, 2014).

3.3.1.2 Descriptive analysis for normality and white noise

Descriptive analysis for normality and white noise was carried out in the XLStat engine. The test was done using Jarque-Bera, Box-Pierce, and Ljung-Box statistics in the XLStat engine. This was done by loading the time series data into the automated descriptive analysis command. Jarque-Bera, Box-Pierce, and Ljung-Box statistics were computed at a 95% confidence limit (Yap, 2015). Autocorrelogram was drawn, and white noise test results were generated for the three tests. The summary of the statistical computations was presented in a table.

White noise is an indication of independence, identical distribution, and non-autocorrelation in a sequence of serially random variables with constant variance and mean. When a time series reveals a white noise, it implies that such series is not deterministic and has no autocorrelation, hence it is said to have been pre-whitened or normalized (Mahan et al., 2015). The normality of a time series distribution indicates the skewness of zero, that is, the data set is said to be perfectly symmetrical around the mean. The results of the test provide information about the linearity of the data set about its mean point as a distinct change point with respect to the identified normal distribution of the data set (Hirsch and Slack, 1984). This may not necessarily indicate the major hydrologic alteration point; however, the streamflow data of the stations within the same region are expected to follow the same regional trend with the exception of hydrologic alteration induced by natural causes or anthropogenic interaction with the stream (Douglas et al., 2000).

3.3.1.3 Homogeneity test

Homogeneity tests were computed using the algorithm of Pettitt, Alexandersson's Standard Normal Homogeneity (SNHT), Buishand and von Neumann's ratio test approaches in XLStat plug-in in Microsoft Excel's package (Santos and Fragoso, 2013). This was done by importing the streamflow time series data into the homogeneity test analysis command. The computation was done at a significant level of 5% while the number of simulations and maximum time were run at default (10000 per item samples for simulation while time depends on a set of tied ranks). The result summary was extracted into a table for each of the test approaches, their change date. The significant results were printed in bold font.

The homogeneity test is the test to examine the degree of independence, sameness and the non-existence of a breaking point in the pattern of distribution of a time series (Ahmad and Deni, 2013). The null hypothesis of a homogeneity test defines that the data is independent and identically distributed while the alternative hypothesis indicates that data is considered non-homogeneous with the remark that there is a break in mean at a certain point of the series (Ahmad and Deni, 2013). The three methods are based on the assumption that there exists a date for a change point in a data series.

3.3.1.4 Parde coefficient plot for regime variability

Parde coefficient is the quotient of the long-term average of monthly discharges to that of the long-term average of annual discharge. It is computed using the equation (3.1) (Parde, 1947);

$$Par_i = \sum_{j=1}^n \left(\frac{Q_{ij}}{\sum_{i=1}^{12} Q_{ij}} \right) \quad (3.1)$$

Where:

Par_i = Parde coefficient

Q_{ij} = Mean monthly streamflow in a month i and year j n = all time steps across the years.

When Par_i is zero, it implies that the mean monthly streamflow is uniformly distributed.

The strength of regime variability was defined with respect to the range of Par_i (Bormann, 2010) using equation (3.2);

$$\Delta Par = \max(Par_i) - \min(Par_i) \quad (3.2)$$

Where; $\max(Par_i)$ and $\min(Par_i)$ are the maximum and minimum values of the Parde coefficient for streamflow respectively.

3.3.1.5 Assessment of trends



University of Fort Hare
Together in Excellence

Assessment of trend is carried out using Mann-Kendall and Theil-Sen's slope in XLStat plugin of Microsoft Excel package, and the significance level is set at 5%. The computation result generates the Kendall-Tau result, Sen's slope, and the p-value. The Mann-Kendall (MK) test is a non-parametric method used for describing the status of monotony and type of trend existing in a non-linear time-series data. It computes using the equations by Mann (1945) and Kendall (1948) presented in equation (3.3);

$$S = \sum_{k=1}^{n-1} \sum_{j=k+1}^n \text{sgn}(x_j - x_k) \quad (3.3)$$

$$\text{Where, } \text{sgn}(x) = \begin{cases} 1 & \text{if } x > 0 \\ 0 & \text{if } x = 0, \\ -1 & \text{if } x < 0 \end{cases} \quad (3.4)$$

n = length of data for time series of $j_1, j_2, j_3, \dots, j_n$.

MK assumes that the measurements over time are independent and identically distributed when the trend is absent (Kisi and Ay, 2014; Pohlert, 2016).

Its variance, σ^2 , is derived as presented in equation (3.5):

$$\sigma^2(s) = \{n(n-1)(2n+5) - \sum_{j=1}^p t_j(t_j-1)(2t_j+5)\} \times 1/18 \quad (3.5)$$

Where p = number of the tied groups in the data set and t_j is the number of data points in the j^{th} tied group. Approximation of normal distribution of MK statistics is based on the Z-transformation in equation (3.6):

$$Z = \begin{cases} \frac{S-1}{\sigma} & \forall S > 0 \\ 0 & \forall S = 0 \\ \frac{S+1}{\sigma} & \forall S < 0 \end{cases} \quad (3.6)$$

Consistent variability in the trend of time series is as thus:

$$-Z_{1-\frac{\alpha}{2}} \leq Z \leq Z_{1-\frac{\alpha}{2}} \quad (3.7)$$

Where $Z_{1-\alpha/2}$ = the critical value of Z from the standard normal table. In this work, the critical value is estimated using a 5% significant level. The null hypothesis is accepted when $Z \leq Z_{1-\alpha/2}$, and rejected when $Z \geq Z_{1-\alpha/2}$. Positive values of Z indicate increasing trends while negative Z values indicate decreasing trends in the time series.

Theil-Sen's slope is an estimator used for quantifying the magnitude of trend acceleration. Just like MK, its operation is not affected by outliers. It is computed using equation (3.8) proposed by Theil, (1950) and Sen (1968);

$$\beta = \text{median} \left(\frac{x_j - x_i}{j - i} \right) \text{ Given that all } i < j \quad (3.8)$$

More information on Theil-Sen's slope is documented in the work of Ohlson and Kim (2015) and Pohlert (2016).

3.3.2 Correlation assessment of streamflow to rainfall

3.3.2.1 Kolmogorov-Smirnov test for comparison of the distribution

Its computation is based on a comparison of cumulative relative frequencies (CRF) of two samples at a definite reaction time for estimation of maximal absolute difference, denoted by D, between the two samples. However, KS also computes the percentage of cases of

deviation from the normal curve. This helps in deciding the side of two hypotheses that applies. The null hypothesis postulates that the two samples are normally distributed, while the alternative hypothesis postulates that the two samples have different projections. The significance level, α , is set at 0.05, hence a higher p-value indicates the normality corresponding to the null hypothesis and vice versa (Djuric and Miguez, 2010). The Kolmogorov-Smirnov test was computed in XLStat pug-in of the Microsoft Excel package. The results and graphs generated were extracted and presented for further interpretation.

3.3.2.2 Sensitivity analysis of streamflow to rainfall

This was done by computing the mean of each of the months over 28 years for both streamflow and rainfall separately, i.e. mean ratio of deviation per mean of streamflow to mean deviation per mean of rainfall. The last stage of the operation involves the computation of the median for each monthly sensitivity series.



University of Fort Hare
Together in Excellence

Its computation is based on equation (3.9) (Schaake, 1990):

$$\epsilon_p = \text{median} \left(\frac{Q_t - \bar{Q}}{P_t - \bar{P}} \times \frac{\bar{P}}{\bar{Q}} \right) \quad (3.9)$$

Where P and Q are rainfall and streamflow at time t, \bar{Q} and \bar{P} are mean of rainfall and streamflow series at a specific regime and ϵ_p is the sensitivity factor. In this study, $\epsilon_p < 0$ are considered to be out of phase, while the higher the sensitivity factor, ϵ_p , the more it is out of phase in elasticity according to the Budyko hypothesis (Sankarasubramanian et al., 2001).

3.4 Watershed characterization using streamflow recession attributes

Objective 3 is structured on the aim to characterize streamflow hydrodynamics recession properties of Buffalo watershed in relation to high flow, low flow and baseflow index properties of the watershed. To this end, flow duration curve (FDC) methods and baseflow

separation methods were employed to assess the extracted and processed twenty-eight years' daily records of streamflow for the six gauging stations. Similar to the time series assessment, data assessment was achieved through desktop analysis.

3.4.1 Flow duration curve computations

The streamflow may be discretized as daily, weekly, monthly or yearly intervals. In this work, flow frequency is discretized into daily, 7 days-moving average (MA), 30 days-MA and 60 days-MA in order to examine and consider the smoothest scenario. Two major assessments were computed as outlined below;

- i. Period-Of-Record FDC
- ii. Stochastic FDC

3.4.1.1 Period-Of-Record FDC



Period-Of-Record (POR) FDC was computed by deducting the cumulative density function of different time scenarios such as daily, weekly, monthly and yearly scenarios in a strategic order. In this work, the cumulative density function was computed using daily streamflow discharge time series as well as with scenarios of 7 days (7D), 30 days (30D) and 60 days (60D) moving average. The computation was achieved through the following steps;

- i. Columns were prepared in a spreadsheet for daily time series, and the moving averages (7 days, 30 days and 60 days) were computed in different columns.
- ii. The daily and moving averages were sorted in descending order.
- iii. Time step interval was created, using the rank of numbers for q_i , where $i = 1, 2, 3, \dots, n$, for which n is the total number of periods of record across the time series, while m is the rank of annual extreme series arranged in descending order of magnitude.

- iv. Weibull plotting formulae (equation 3.10) was employed to compute the corresponding probability, P, of exceeding individual flow, i, from the rank.

$$p = \frac{m}{n+1} \times 100 \dots\dots\dots(3.10)$$

$$P = P(Q > q_i) = 1 - P(Q \leq q_i) \dots\dots\dots(3.11)$$

- v. The plot of flow (using all the scenarios) against the corresponding probability, P, (from equation 3.11) is presented in a log-normal graph. P is drawn on the x-axis against the magnitude of stream discharge as well as the scenarios of flow order (1D, 7D, 30D, and 60D) on the y-axis.

Plots are visually correlated with the smoothest curve in order to avoid the need for adjustment of FDCs (Lane et al., 2005). 5th to 20th percentile was extracted for assessment of variability in high flow. Likewise, the 80th to 99th percentile is assessed for low-flow. Plots of PORFDC provide information on the attribute of stormflow and low flow relative to rainfall events (Ye et al., 2018). The recession pattern of the curve provides information on the characteristics of the terrain and stream channel (Croker et al., 2003).



University of Fort Hare
Together in Excellence

3.4.1.2 Stochastic FDC

Stochastic FDC was computed by disaggregating streamflow daily order into the individual annual record and plotting the cumulative density function in relation to the specific order of the FDC plot. Seven days moving average order was adopted owing to its smoothness among others as obtained from the POR FDC. The computation was achieved through the following steps outlined below:

- i. Annual FDC plots were produced for the six stations using the steps outlined in the preceding section.
- ii. Each 5% probability of exceedance was marked, while, only the 95th percentile of the FDC was extracted across the annual columns of aggregates.
- iii. The extracted values were sorted in ascending order and assigned ranking order; using $i = 1, 2, 3, \dots, n$ for ranking order.
- iv. Probability of exceedance, P , (equation 3.11), was deduced from the rank value using Weibull formulae (equation 3.10).
- v. The deduced Stochastic FDC probability of exceedance, P , was plotted against the sorted percentage characteristics using a trend-line for the derivation of the equation of a best-fit line.
- vi. Return periods of 10-year and 100-year were calculated from the equation of best fit and ranked and then plotted again.



The plot of stochastic FDC and return periods of computation provide information on the temporal changes in flow dynamics and response frequency to the hydro-climatic situation with respect to governing environmental conditions (Verma et al., 2017).

3.4.2 Baseflow Separation Procedure

Due to uncertainties that might be associated with the use of one baseflow separation procedure and the rigor of validating the deductions, five different approaches were employed. Their average value was taken and adopted. Hence, twenty-eight years of streamflow data set, from 01 January 1989 to 31 December 2016, was analyzed using Two Parameters Digital Filter program (TwoPDF), PART program, Hydrograph Separation (HYSEP) local minima program, Standard baseflow index (BFI) program, and BFI modified program within USGS groundwater toolbox package.

The BFI standard computation partitions the streamflow records into intervals (N) of five days. The minimum streamflow value for each of the intervals was compared to the minimum streamflow value of its adjacent partition interval in order to deduce its turning point. The result was also tested using a turning point test factor of 0.9, such that if 90 % of a specific minimum is less than the preceding and the following adjacent minimums, then the specific minimum is a turning point. The turning points were then connected in order to generate the baseflow hydrograph (Wahl and Wahl, 1995). The major difference between the computation of BFI standard and BFI modified is the use of recession constant (K') in place of the turning

point test factor (f) according to the equation (3.12) by Barlow et al. (2015);

$$K' = f^{\left(\frac{1}{N}\right)} \quad (3.12)$$

Where the values of $f = 0.9$, and $N = 5$. Hence, $K' = 0.97915$. More information on the Standard and modified baseflow index are provided by Wahl and Wahl (1995). Baseflow computation based on the two Parameters Digital Filter (TwoPRDF) approach was carried out using the low-pass filter algorithm equation (3.13) (Eckhardt, 2005);

$$B_{k+1} = \frac{(1-BFI_{max}) \times \alpha \times B_k + (1-\alpha) \times BFI_{max} \times Q_{k+1}}{(1-\alpha) \times BFI_{max}} \quad \text{if } B_{k+1} \leq Q_{k+1} \quad (3.13)$$

Where;

BFI_{max} = Maximum baseflow index, the ratio of baseflow to streamflow
 α = Baseflow filter parameter


Q_{k+1} = Streamflow at time step k+1

B_k = Baseflow at time step k.

The filter is passed over streamflow record once in order to smoothen the baseflow hydrograph (Arnold et al., 2000; Barlow et al., 2015), while BFI_{max} was modeled by the

algorithm. The TwoPRDF configuration is based on the assumption that the addition of baseflow and streamflow equals the total streamflow, and that the relationship between aquifer storage and baseflow [into stream] is a direct variation. The default value for the baseflow filter parameter was used ($\alpha = 0.98$) in order to ensure a uniform baseflow extraction condition for the six stations that were assessed. More information on this method is provided in detail in Eckhardt (2012).

The PART program is based on the streamflow partitioning principle. It equalizes baseflow for streamflow on days that are assigned as being unaffected by interflow. This is based on the antecedent streamflow recession, given that other components of the flow, such as evapotranspiration, are negligible. Meanwhile, the remaining parts of the hydrographs are linearly interpolated. The days that are not affected by run-off (N-days) are indicated by the continuous recession, (Barlow et al., 2015). Its response time is expressed in terms of the drainage area, A, (1237 km²) as shown in equation (3.14);



University of Fort Hare
 Together in Excellence (3.14)

$$N = 7A^{0.2} \quad (3.14)$$

The daily values of baseflow were obtained by searching the arrays of streamflow for days that fit the antecedent recession requirement three times for three different values of N. The final result of baseflow for each day was estimated from curvilinear interpolation of the three different values of N. More information on the algorithm of the PART program is documented in Rutledge (1998). This program is run three times for each streamflow for consistency reasons.

The HYSEP program was developed by Pettyjohn and Hennings (1979). It computes in a similar way to the PART program using the algorithm of the relationship between basin drainage area (A) and duration (N days) of the recession limb of the hydrograph (equation 3.14). There are three types of HYSEP programs; fixed block, sliding block and local

minimum method. Each of the methods estimates baseflow with unique algorithms. The baseflow hydrograph is drawn from the line the joined the successive discharge minima. The selection of the discharge minima is based on the computation of numbers of days (N) that follow the peak of the storm hydrograph when the surface run-off subsides (Linsley et al., 1949). It is based on equation (3.14) of the PART program.

The HYSEP fixed block approach computes baseflow by searching the hydrograph for minimum streamflow at an interval of $2N$ days from the first day of streamflow record. The HYSEP sliding block approach computes baseflow by default searching for the minimum streamflow within an interval of $2N$ days between day-3 and day-11. The HYSEP sliding block approach allows the designation of the day of interest where the baseflow computation can begin. The major difference between the previous two methods and the HYSEP local minima method is the fact that the local minima method checks each day within the hydrograph interval to ascertain if the minimum streamflow is the lowest within $0.5(2N - 1)$ days before and after the day. If the check is true, then it is considered the local minimum, while the turning points are joined by linear interpolation (Rudra et al., 2010).

In this work, the local minimum method was employed due to the further process of checking for the local minimum which also further reduces uncertainty. This method began its estimation by building a sequence of local minima for each day recorded with the lowest flow within intervals of days with sequential runoff or recession. For further information on HYSEP, see Barlow et al. (2015).

The results of daily baseflow, daily runoff, and baseflow index were generated for each of the methods. The baseflow index results for each of the five baseflow methods used were extracted and computed to monthly mean across the hydrologic year. This was done in order

to simplify the comparative analysis of the results. The results were projected using line charts. The BFI results were compared to the low flow and recession plots of FDC.

3.5 Evaluation of hydro-geomorphological settings for groundwater potential

Objective 4 is based on the aim to evaluate the potential of watershed hydro-geomorphotectonic settings for groundwater potential. The study employed the analysis of morphometric parameters and electrical resistivity tomography. Hence, the study entails both the use of desktop and field exercises. The desktop analysis involves a morphometric analysis of drainage networks while field investigation is achieved through electrical resistivity tomography.

Advanced Spaceborne Thermal Emission and Reflection (ASTER) Digital Elevation Model (DEM) with 30 m spatial resolution was downloaded from the Earth explorer USGS website for desktop analysis purposes. The analysis together with the geological map of South Africa, acquired from the South Africa water resource website, www.waterresourcewr2012.co.za, was employed to support this research. Field visit entails the hydrological assessment of the sub-basins for characterization of river attributes, channel and stream floor attributes. Both morphometric analysis and vertical electric soundings were carried out for Ngqokweni, Mgqakwebe, Quencwe, and Yellowwoods sub-basins as well as for Buffalo basin.

3.5.1 Geomorpho-tectonic analysis

Geomorpho-tectonic analysis is based on geomorphological and hydrologic modeling using the spatial analyst tool in ArcGIS-10.5.1 software. The selection of geomorpho-tectonic parameters was based on the relevance of their information to factors influencing groundwater development. The parameters and their significance are presented in Table 3.1.

Some of the parameters were extracted directly from ArcMap, while others were derived from the fundamental parameters extracted in the ArcMap (Table 3.2).

Table 3. 2: Description of morphometric parameters of Buffalo watershed analysis.

S/N	Morphometric parameters	Equation	Major interpretation/ inference
A Drainage Network			
1	Number of stream segment (Nu)	$Nu = N1 + N2 + \dots + Nk$	Nu = Extent of runoff and basin vulnerability to flash flood (Ghany, 2015). Rb = dissection properties of drainage basin. Rb > 5 = complex dissection (Ghany, 2015). Luwm = growth stage of stream geomorphology. The higher the Luwm, the younger the basin (Aher et al. 2014).
1b	Stream segment ratio (Nur)	$Nur = Nu + (Nu+1)$	
2.	Bifurcation ratio (Rb)	$Rb = Nu / (Nu+1)$	
3.	Weighted Mean Bifurcation Ratio (Rbwm)	$Rbwm = \sum(Rb \times Nur) / \sum Nur$	
4.	Total stream length per (Lu)	Lu	
5.	Stream length ratio (Lur)	Lur	
6.	Weighted mean strength length (Luwm)	$Luwm = Rb \times Nu$	
B Basin Geometry			
7.	Basin area (A)	ArcGIS estimates	Ff = potential of the basin to be recharged or flooded. Its value ranges between 0.1 and 0.8. 0.1 = Potential for recharge; 0.8 = Potential for flash flood (Yadav et al. 2014). Re = Rate of drainage efficiency; > 0.9 = Circular; 0.8 – 0.9 = Oval; 0.7 – 0.8 = less elongated; < 0.7 = elongated (Yadav et al. 2014).
8.	Basin perimeter (P)	ArcGIS estimates	
9.	Basin Length (Lb)	ArcGIS estimates	
10.	Length from the centre to the river mouth (Lcm)	ArcGIS estimates	
11.	Width from the centre of a watershed (Wcm)	ArcGIS estimates	
12.	Form factor (Ff)	$Ff = A / Lb^2$	
13.	Elongation ratio (Re)	$Re = \text{Diameter of A} / Lb$	

14.	Texture ratio (Rt)	$Rt = N1 / P$	Rt = Rate of influence of lithology, infiltration capacity and relief (Masoud, 2016).
15.	Circularity ratio	$Rc = A / \text{Area of } P$	Rc classifies into young, mature and old dendritic stages of a watershed (Wilson et al. 2012).
S/N	Morphometric parameters	Equation	Major interpretation/ inference
C	Drainage texture		
16.	Drainage texture (Dt)	$Dt = Nu / P$	Dt = Rate drainage development in relation to climate, rainfall intensity, vegetal reworking and relief (Yadav et al. 2014). < 2 = very coarse; 2 – 4 = coarse; 4 – 6 = moderate; 6 – 8 = fine, and; > 8 = very fine.
17.	Stream frequency (Fs)	$Fs = Nu / A$	Fs = Distribution of stream order per unit area.
18.	Drainage density (Dd)	$Dd = Lu / A$	Dd = lesser potential for infiltration (Srivastava et al. 2008). < 0.5 = poor; 0.5 – 1.5 = medium; > 1.5 = excellent
19.	Constant of channel maintenance (C)	$C = 1 / Dd$	C = Strength of lithological control on surface permeability (Abdulkareem et al. 2018).
20.	Drainage intensity (Di)	$Di = Fs / Dd$	
21.	Infiltration Number (IfN)	$If = Fs \times Dd$	If = Inverse of infiltration potential (Rai et al. 2017).
D	Relief Characteristics		
22.	Relief ratio (Rhl)	$Rhl = \text{Relief} / Lb$	Rhl = Overall steepness of drainage basin (Ansari et al. 2012).
23.	Relative relief ratio (Rhp)	$Rhp = \text{Relief} \times 100 / P$	Rhp = Rate of rock resistance (Sreedevi et al., 2005).
24.	Ruggedness number (Rn)	$Rn = Dd \times (\text{Relief}/1000)$	Rn = rates basin vulnerability to erosion (Pareta and Pareta, 2011). < 0.2 = steep ground slope and less infiltration; 0.2 – 0.3 = moderate flow-paths with moderate ground slope and moderate infiltration; > 0.3 = more infiltration and reduced run-off.
25.	Length of overland flow (Lf)	$Lf = 1 / (2Dd)$	Lf = ratio of gentler slope to length of flow path (Patel et al. 2013).

These parameters can be classified into four attributes; drainage network, basin geometry, drainage texture, and basin relief attributes.

Extraction of fundamental geomorpho-tectonic parameters was done using Advanced Spaceborne Thermal Emission and Reflection (ASTER) Digital Elevation Model (DEM) with 30 m spatial resolution, downloaded from Earth explorer USGS website. The study area was clipped from the DEM, while the stream order was generated based on Horton's (1945) approach in ArcGIS 10.5.1. The catchment raster is converted into fil raster. The fil raster was processed for computation of flow direction raster. The flow direction raster was processed for computation of flow accumulation. The flow accumulation raster was computed in the raster calculator for drainage network greater than 500. The calculated drainage network was processed together with flow direction raster in order to generate drainage polyline features. The drainage network raster was transformed into streamflow polylines (Figure 3.1).

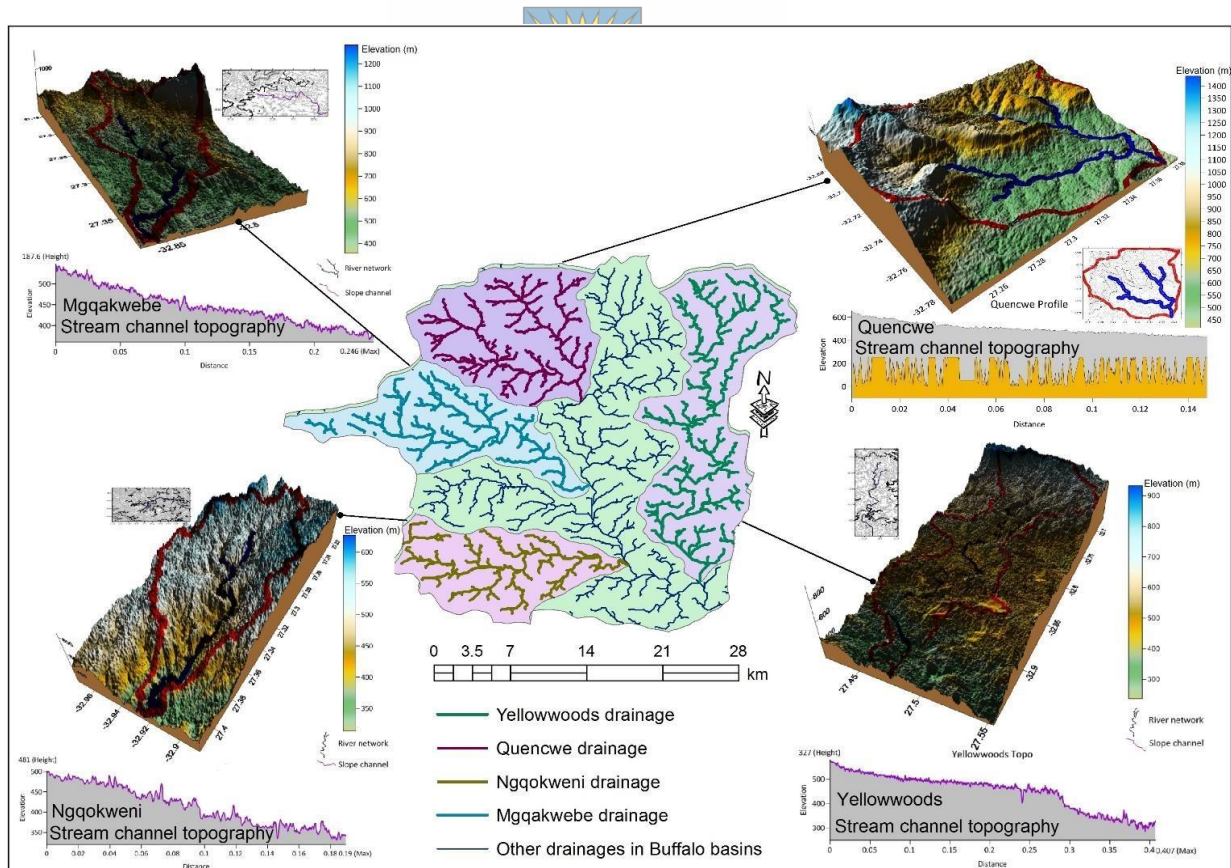


Figure 3. 1: Plots indicating the extracted Buffalo stream segments, the sub-basins, the physiography of each sub-basin and stream channel topography.

The stream order was further created from the drainage network raster and flow direction using the Strahler (1957) ordering approach. The number of stream segments was generated by disbanding the unique values of the grid code of the stream order while the result summary was extracted from the attribute table. Each sub-basin of the watershed was extracted from the computation of the stream basin using the flow direction raster. The computed stream basin was converted from raster format to shapefile format and extracted using the selection process. The derived sub-basin shapefile was used to clip the stream order raster in order to enable easy calculation of stream order for each of the sub-basins. The subbasins used in this research work included Mgqakwebe, Ngqokweni, Yellowwoods, Quencwe, and Tshoxa sub-basins. Information on elevation and relief of the basins was extracted from the map based on the peak elevation calibrated by the DEM map legend.



University of Fort Hare
Together in Excellence

The interface data frame property was converted from the geographic coordinate system into the projected coordinate system in order to ensure that the estimation done in ArcMap was done in Standard International units. For basin area and perimeter, these were calculated geometrically from the attribute tables in meter-square and meter respectively. The total stream length (m) for each order was computed from the stream order attribute table in ArcMap. The coordinate for the head of the main channel of the stream was taken from Google Earth. The Waterhead was located on Google Earth and zoomed down to 20 m elevation view at zero degree tilt in order to ensure accuracy. The coordinate was sought for on the drainage network and calculated from the coordinate to the catchment mouth. Valley length was computed by estimating the drainage path from where the wide river valley developed for each of the sub-basins. The valley head coordinate was also picked up from Google Earth from where the river valley widens out. The extracted coordinate was located on the computed drainage network in ArcMap and computed in a similar way as basin

length. The minimum aerial distance was computed by measuring the straight-line length of the main valley. The center to river mouth was located by estimating the actual center of gravity of the basin by dissecting the shape into approximated four parts. The nearest spot on the main channel was tagged as the center of the river. Hence, length and width from the center of the main channel to the river mouth were estimated through the attribute table in the ArcMap interface. This was done repeatedly for each of the sub-basins while the entire remaining computation of the geomorpho-tectonic parameters was done in Microsoft Excel.

3.5.2 *Electrical resistivity tomography and data processing*

Two-dimensional geoelectrical resistivity tomography was carried out by deploying the techniques of vertical electrical sounding with electrical profiling in the Schlumberger array configuration. The choice of Schlumberger array configuration was due to logistic and performance reasons. The Vertical Electrical Sounding (VES) was performed using ABEM Terrameter SAS1000. The terrameter generates the apparent resistivity directly, hence, no further calculation of apparent resistivity is required. The equipment consists of a current meter and a voltmeter. The choice of reference point for sounding along the river channel was based on the center of gravity of the longest stream order next to the stream mouth. The maximum current electrode spacing (AB) kept in this work was restricted to 200 m. This was due to the need to limit subsurface observation to subsurface depth proximal to the nearest local aquifer within the depth of 30 m. Most importantly, sounding was carried out in triplicates at a 50 m longitudinal interval. Also, the VES was done at 50 m distance away from the river bank based on the accessibility condition of the streambank. The results of the sounding were stored on Microsoft Excel spreadsheets in columns of half-current electrode spacing, potential electrode spacing, and apparent resistivity.

The results were interpreted using IPI2WIN software for semi-automated interpretation and RES2DINV software. For IPI2WIN software interpretation, the data of half-current electrode spacing, potential electrode, and apparent resistivity were imported into IPI2WIN spreadsheets. The model generates two plots; the actual plot impressed by the field activity and a model curve simulated from the master curve. The model also indicates percentage error based on how matching the model curve is to the actual curve. Hence, the model curve was improved by splitting the layer and performing repeated iteration until the curve plot overlays smoothly on the actual plots. In this work, iteration was done until the percentage error was lower than 3.5%. This was performed for each of the VES points across the five stations sampled. The results of data processing were captured and extracted into a summary table showing stations, the number of VES, VES type (based on the curve), layer resistivity, the layer thickness, and the root mean square percentage error.

VES data was processed in RES2DINV by importing the data which was put into a WordPad and stored as a data file. Following the completion of data importation into the software, the data was inverted using the the least-square inversion method. The result generates the pseudo-section corresponding to the inversion of apparent resistivity in the model following a specific number of iterations designed into the software. The resulting model resistivity pseudo-section in RES2DINV and that of IPI2WIN results were validated by establishing a comparative analysis with borehole lithologic information within the vicinity of the sampled VES point. Based on the spatial distribution of the borehole across the watershed as described in section 3.2.5, borehole lithologic logs were compared with the plots of the two software and necessary deductions were made.

3.6 Investigation for groundwater potential zonation

The main objective of this study was to map the zone of groundwater potential at the catchment scale using geospatial themes informed by analytical hierarchical process. In order to arrive at these, a selection of multi-influencing factors guided by an intensive literature review was made. Seven themes of geoscience factors were considered, namely; rainfall spatial distribution, lineament density, drainage density, surficial lithology, topographic wetness index, land use/land cover (LULC), and land surface temperature (LST). Geospatial techniques are geoinformatics approaches adopted for the collection of data associated with georeferenced points. The major technologies of geoinformatics can be grouped into three; global positioning system (GPS), remote sensing (RS) and geographic information system (GIS). In order to adopt geospatial technology in this work, all data was prepared as thematic layers. Some of the data featuring in the multi-influencing factors have been mapped for analysis in the previous sections. These include; lineament map, drainage map, and lithology map.



University of Fort Hare
Together in Excellence

3.6.1 Development of a thematic map

Only two rainfall gauging stations were available for the catchment; Bisho and King Williams Town. In order to produce a rainfall map that represented the actual rainfall spread, data of rainfall from neighboring rain gauging stations was acquired from the South Africa Weather Service. These include; Stutterheim, Cata, Dimbaza, Berlin, East London, Kidds Beach, and Peddie towns. These were summed into the annual average for at least thirty years record, 1987 to 2016. The annual averages were projected for spatial analysis using ordinary kriging interpolation and linear semi-variogram model.

Steps for producing lineament density and drainage density maps are similar. The process involving the extraction of lineament was detailed in Section 3.2.2. The lineament density was processed digitally using line density computation in ArcMap. The computation was

done using the lineament polylines, the Buffalo catchment area as the search radius, 138.58 as the cell size (which is the default cell size based on effective annulus cells) and the Buffalo shapefile as the mask in the raster analysis environment. The extraction of the drainage map was described in detail in section 3.5.1. The drainage density map was computed in a similar way as lineament density using the line density format. In doing so, stream segment polylines are the polyline feature input. The computation was masked using the Buffalo catchment shapefile. The computation was done using the catchment area as the search radius and the cell size of 138.58.

The detailed and updated lithology map produced according to the method described in section 3.2 was used. The analytical signal map was re-computed in order to define the spatial distribution of the dominant surficial lithology. Hence, the analytical signal map was georeferenced. Based on the inference drawn from analytic signal validation, image classification of the analytical signal map was carried out. The resulting signal layer was classified into three; the extremely low, the intermediate, and the high amplitude signal for validation of relative surficial lithology types. The effectiveness of analytical signal for mapping basement configuration and lithology variability have been reported in previous studies (Matter et al., 2006; Baiyegunhi and Gwavava, 2017).

The slope map was prepared from the ASTER DEM downloaded with a resolution of 30 m by 30 m from the Earth Explorer USGS website. This was carried out using the slope method within the spatial analyst interface in ArcMap 10.5.1. The resulting slope map was used to generate the topographic wetness index (TWI) map. Estimation of TWI was done in the raster calculator of ArcMap using equation (3.16) (Hojati and Mokarram, 2016);

$$TWI = \ln \left[\frac{a}{\tan(\beta)} \right] \quad (3.16)$$

Where α , specific catchment area = catchment area, A, per unit contour length, L, (A/L), and $\tan(\beta)$ = slope. This is performed using the raster algebra engine in spatial analysis.

In order to develop the land use/land cover (LULC) map, vegetation map, and land surface temperature (LST) map, Landsat 8 OLI with less than 10% cloud cover was downloaded from Earth Explorer USGS website. The image was rectified for spectral distortion and reflectance quality. The rectified raster was processed to develop thematic maps.

The LULC map was produced through supervised image classification in ArcMap 10.5.1. Classes mapped out include; water bodies, cultivated land, vegetation, woodland, built-up areas (urban), grassland and degraded (bare) areas using maximum likelihood algorithm.

Deduction of LST was achieved in six stages within the raster calculator in the following order (Suresh et al., 2016; Orimoloye et al., 2018);

- 1) Top of atmospheric (TOA) spectral radiance was calculated in raster algebra using equation (3.17);

$$TOA = RF_M \times TIRS_1 + RF_A \quad (3.17)$$

Where RF_M = radiometric multiplicative rescaling factor for TIRS 1 which is 0.0003342, TIRS = thermal infrared sensor 1 which is Band 10, and RF_A = radiometric additive rescaling factor for TIRS 1 which is 0.1.

- 2) TOA was converted to brightness temperature (BT) using equation (3.18);

$$BT = \frac{K_1}{[\ln(\frac{K_2}{TOA})+1]} - 273.15 \quad (3.18)$$

Where K_1 and K_2 = Thermal conversion constant for Band 10 extracted from metadata, 774.885 and 1321.0789 respectively shapefile and 273.15 = constant for temperature conversion from Kelvin to Celsius.

- 3) NDVI was computed for April and October and its average was calculated in raster algebra. NDVI was calculated using the expression in equation (3.19):

$$NDVI = \frac{NIR-Red}{NIR+Red} \quad (3.19)$$

Where NIR (near-infrared) = band 5, and red = band 4 for Landsat 8 OLI.

- 4) Vegetation proportion (Pv) was calculated from NDVI, using equation (3.20);

$$Pv = \left(\frac{NDVI - NDVI_{min}}{NDVI_{max} - NDVI_{min}} \right)^2 \quad (3.20)$$

Emissivity was calculated from Pv, using equation (3.21);

$$\varepsilon = 0.004 \times Pv + 0.986 \quad (3.21)$$

Where 0.004 is downscaling constant for Pv and 0.986 is the correction value of the equation.



- 5) LST is deduced from the integration of BT and Emissivity, ε , according to equation (3.22);

$$LST = \frac{BT}{\left[1 + \left(\frac{0.00115 \times BT}{1.4388} \right) \times \ln(\varepsilon) \right]} \quad (3.22)$$

3.6.2 Computation of priority scores and their consistency ratio

Priority scores of influence of individual factors to groundwater potential is required for weightage computation during the overlay exercise. However, assignment of the priority scores was based on field experience, groundwater experts' advice. The assigned scores were compared against another in a pairwise comparison matrix in Microsoft Excel sheet. This was followed by normalization of the weights using Saaty's AHP. This enables the optimization of priority scale and subjectivity among the GWPZ factors and to enable the assessment of the consistency ratio (Jha et al., 2010). The resulting final criteria weights are considered as the normalized values as long as the consistency ratio lies within the expected limit. The consistency index is computed based on equation 12 (Saaty, 1980):

$$CR = \frac{CI}{RCI} \quad (3.23)$$

where CI is the consistency index based on equation 13 and RCI is the random consistency index obtained from Saaty's 1 – 9 scale (Saaty, 1980).

$$CI = \frac{\lambda_{max} - n}{n - 1} \quad (3.24)$$

where λ_{max} is the principal eigenvalue computed by eigenvector technique and n is the numbers of GWPZ factors. For a consistent normalization, the value of CR is expected to fall within 0.01 to 0.09, otherwise, the priority scores have to be adjusted.

3.6.3 Overlay analysis for the delineation of groundwater potential zone

The overlay analysis of the seven thematic layers was carried out in ArcGIS 10.5.1 as a summation of the effective influence of the factors based on their individual criterion weight to generate the ultimate potential zone. To arrive at these, all the layers were converted an integral raster while their individual character/class were ranked. The groundwater potential zone was calculated based on equation 3.25:

$$GWPI = \sum_{i=1}^{n=7} W_i (R_i) \quad (3.25)$$

where GWPI is the Groundwater potential index, W_i is the criteria weight, R_i is the ranking of parameter factors and i represent each of the seven influencing factors with serial number from 1 to 7.

3.6.4 Evaluation and validation of model performance

The delineated GWPZ was validated using data of groundwater yield of exploration boreholes acquired from the National Groundwater Archive of the Department of Water Affairs, South Africa. The 84 geo-referenced yield data was overlaid on the GWPZ map in order to filter out the corresponding gridcode identity of the borehole spot. The regression equation of the scattered diagram of GWPZ gridcode against the groundwater yield was obtained to simulate the expected yield value. The coefficient of determination (R^2),

coefficient of correlation (R), and the p-value of the relationship between the observed value and the simulated value were calculated in Microsoft Excel. The R value was obtained using equation (15):

$$R = \frac{\sqrt{\sum(E_i - \bar{O}_n)^2}}{\sqrt{\sum(O_i - \bar{O}_n)^2}} \quad (3.26)$$

where O_i is the observed value which is the borehole yield (l/sec), E_i is the expected value drawn from the of simulation of borehole yield, \bar{O}_n is the mean borehole yield and n is the sample size of the borehole yield involved.

The relationship between the derived GWPZ and the actual borehole yield was further interpreted using a box-and-whisker plot. Representative borehole yield for each of the class of GWPZ was computed for their minimum value, lower quartile, median, upper quartile, and maximum value. These were used to derive the estimate for the bottom, 2Q box, 3Q box, whisker- and whisker+ (Table 4; Krzywinski and Altman, 2014).

Table 3. 3: Box-and-whisker plots parameters.

Box-parameter	Formular
Bottom	Lower quartile
2Q Box	Median – Lower quartile
3Q Box	Upper quartile – Median
Whisker-	Lower quartile – minimum value
Whisker+	Maximum value – upper quartile

3.6.5 Hydrogeological conceptualization and delineation

A three-dimensional representation of the magnetic map and a watershed digital elevation model were projected in Surfer 16 in order to depict the structural complexity of the study area. The total residual magnetic map and the analytical signal map in the Tagged Image File (TIF) format were overlain in Surfer 16. Also, the digital elevation model in TIF format and the drainage map in shapefile format were overlain. These were stacked together in order to

conceptualize the hydrogeological settings of the study area. Structural interpretation of the resulting projection together with information on surficial lineament and lithologic properties of the study area enabled the visual decipherment of areas with probable groundwater potential (GWP). The three-dimensional view of the GWPZ map was also projected in a similar way as described above in Surfer 16. The projection was overlain by the drainage network file in order to enable easy conceptualization of hydrogeologic attributes of the area.



University of Fort Hare
Together in Excellence

Chapter 4: Mapping of geologic structures

4.0 Introduction

This chapter reports the findings on structural mapping of surface geology for groundwater potential through a field-assisted structural report, digitally processed Landsat and aeromagnetic images. The chapter presents the results of spatial interpretation of the field structural observation report, residual magnetization analysis, and comparative study of autolineament and magnetic lineament. Also included is the deciphered groundwater potential zone based on low amplitude magnetic anomaly and downhole lithologic material mapping.

4.1 Field geologic mapping



Eighty-three georeferenced points were mapped, most of which were cuts along river channels, trenches, subsidence walls, road cuts, and abandoned channels. Twenty-seven of them were associated with features of Daggaboersnek Member, twenty-six samples were associated with features of Barberskrans Member, twenty samples were associated with features of Elandsberg Member while ten samples were associated with features of Palingkloof Member (Figure 4.1– 4.2).

The south-west, extreme south, and south-east were dominated by extensive mudstones. This is visible along the dry Ngqokweni Riverbank and a construction site where dip cuts were made. From the south-west towards the west around Dimbaza, the mudstone had features of grey desiccation cracks with thin and laminated fine sandstones. Also from the south-east towards the east, the mudstone features appeared as compressed downward accretion of mudstone deposit. This feature is assumed to have graded into deeply fractured multi-story sandstone based on elevation and spot height tracking, especially towards Bhisho.

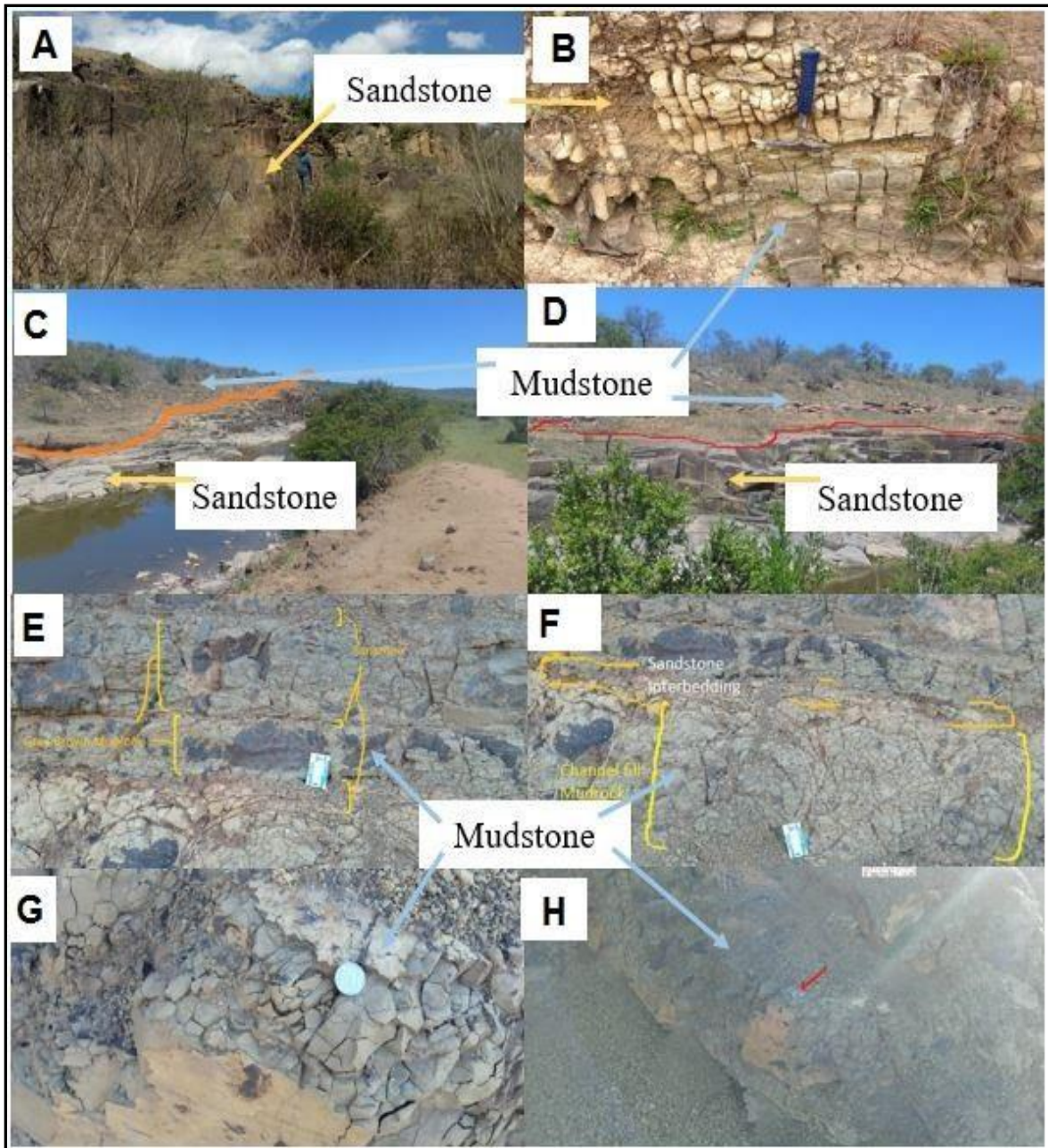


Figure 4. 1: Photograph of the Daggaboersnek Member showing: (A) massive and multistory sandstone; (B) fractured mudrock filled by unconsolidated sandstone; (C and D) fragmented sandstones; (E and F) channel fill features comprising of mudstone; and (G and H) desiccation cracks of channel-filled grey mudstone.

The Bhishe area marked a major transitional zone for facies of the Balfour Formation. A major facie transition was observed from Barberskrans sandstone lithosome, Daggaboersnek mudstone features, and interbeds of mudstone with lenticular sandstone of Elandsberg Members at the Far East of Breidbach town. A similar facies transition was identified around the Pirie fish station in the north-west of the study area. Distinct white features typifying lime

solution which may have been hydrothermally squeezed out were observed. This is considered to be calcrete debris from age-long duricrust of bone or shell-rich fossil. This was not so pronounced in a few sections of the mudstone.



Figure 4. 2: Photograph of the Barberskrans Members showing: (A and B) Massive sandstone deposit,; (C) Unconsolidated interbedding of overbank deposit of fine sands and mudstone unit; and (D) Highly jointed mudstone fills with crevasse channel interspersed by silty sandstone matrices.

The Barberskrans Member is mainly composed of sandstone material, which is thick, unconsolidated at some section, and extensively jointed at many other sections. The unconsolidated feature was observed to be underlain by plate-like dark shale along some sections of Mqgakwebe River, very close to Pirie Mission at the upper central west of the study area. Although the exposure was poor especially due to settlement and vegetation cover, some steeply sloping spots along the river cut showed conspicuous evidence of fine sandstone cross-bedding and horizontal bedding with thin mudstone. This feature extends from central west at Mqgakwebe River center to the north of the Yellowwoods River

sections. The alternation was overlain by a massively jointed grey fine sandstone unit. Based on the mapped features, most of the Daggaboersnek Members are eutric regosols except the ones at the north and the distinct regosol fill cutting across the center of the study area (Figure 4. 3).

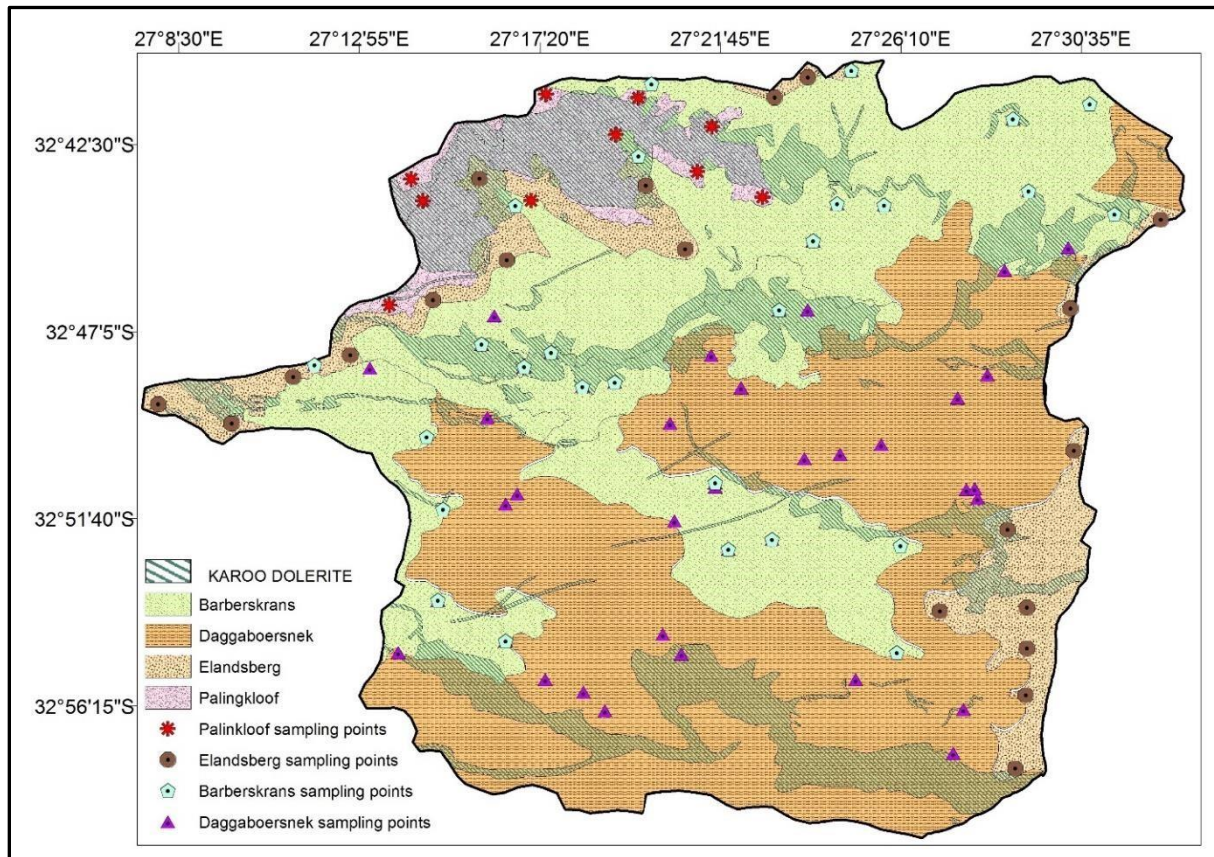


Figure 4. 3: Lithostratigraphic map of Buffalo catchment (After Katemaunzanga and Gunter, 2009). 10 units of oxidized mudstone units, 20 units of Elands, 26 Barberskrans units, and 27 Daggaboersnek units.

The inaccessible north-western hill of the study area which composes of extensive red mudstone cover, and soil type documented as rhodic ferralsol, extends to Queenstown. The red rhodic ferralsol identified as red mudstone overlies the dolerite intrusion. The coloration may have been due to weathering and leaching of oxidized Iron II in the rock. As a result, similar attributes of this area with documented attributes of Queenstown are mapped as Palingkloof Member. Meanwhile, the thin transitional deposit of lithic leptosol soil between Palingkloof and Barberskrans Members were mapped as part of the Elandsberg Member.

4.2 Lineament extraction

Both the subsurface lineament derived from tilt-totally horizontal derivatives enhancement of aeromagnetic data and the extracted surficial lineaments derived from satellite images are overlaid on the Karoo dolerite and tectonic structure map (Figure 4.4).

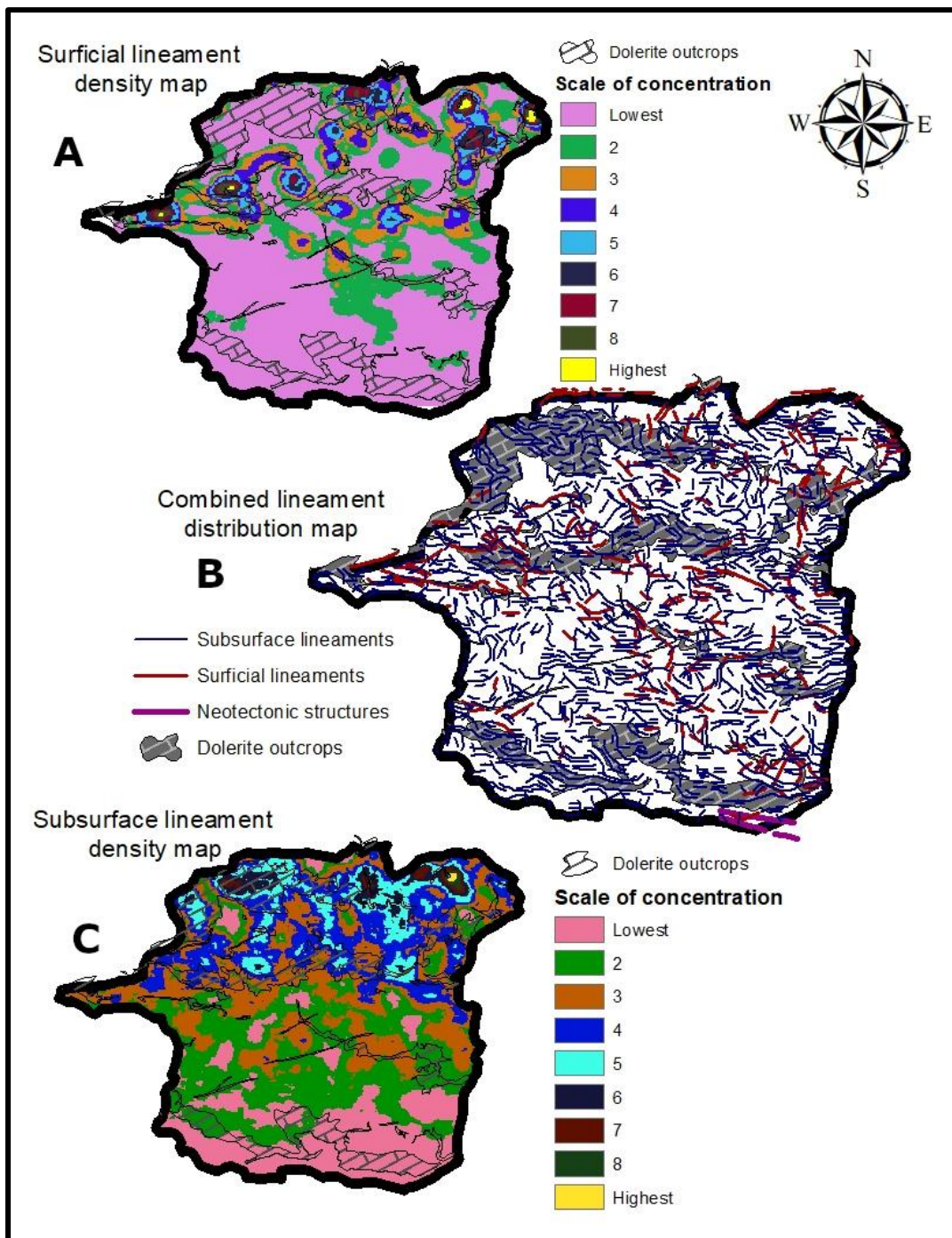


Figure 4. 4: Lineament distribution and lineament density map showing: A) surficial lineament density; B) the swarms of surficial and subsurface lineaments and; C) subsurface lineament density.

The plot shows that the lineaments are concentrated on the regions of the high magnetic anomaly of the RTP map and the altered morphogenetic-hydrological path. The plot, therefore, suggests that the surficial lineament possibly developed from extensional stress induced by dolerite intrusions and hydrologic processes. Most of the delineated magnetic lineaments trends in WNW – ESE direction, the same direction as the surficial lineaments at the range of 12 – 2563 m and 0.83 – 1992 m respectively (Figure 4.5). This was validated by the tectonic lineaments which also trends in WNW – ESE direction at the extreme south of the catchment (Figure 4.4). The conspicuous radial trends of the surficial lineaments compared to the magnetic lineaments suggest the existence of high-density fractures which may facilitate groundwater recharge in the zones of overlapping surficial lineament.

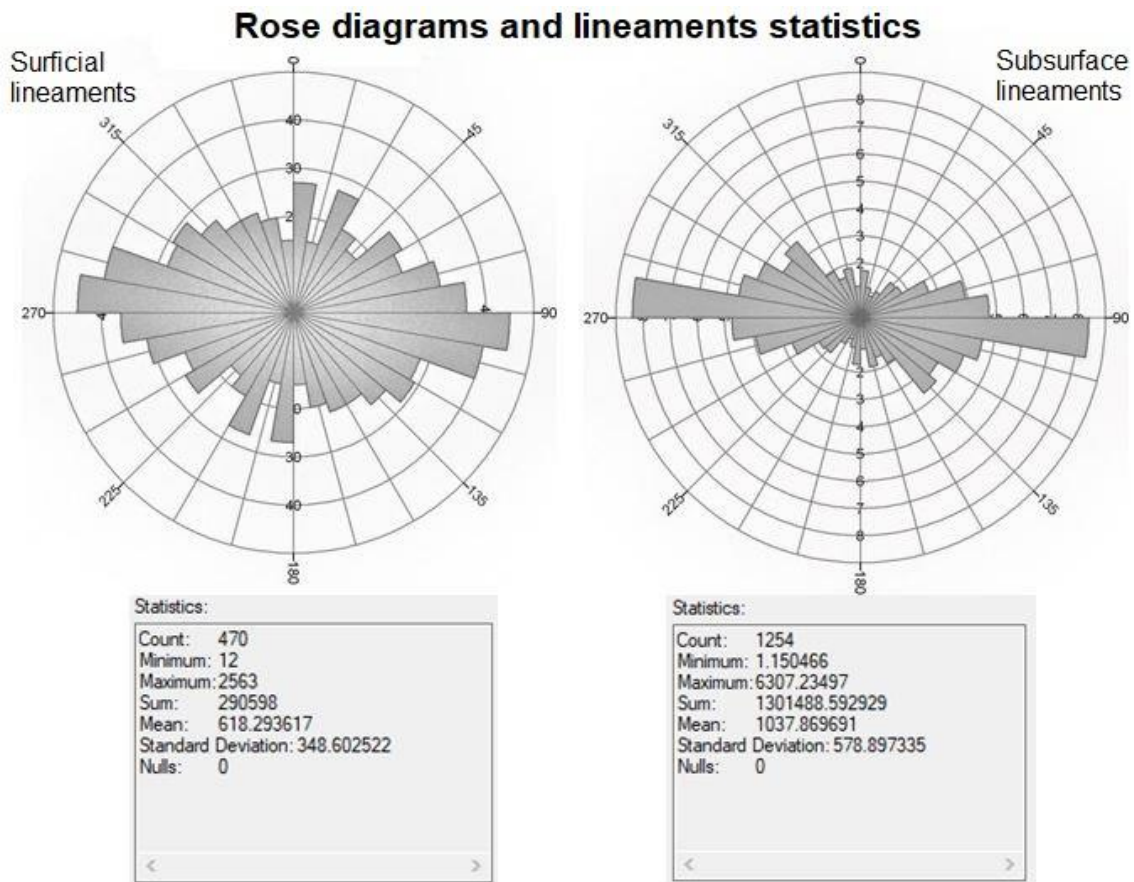


Figure 4. 5: Buffalo basin lineaments rose diagrams and their statistical information (in meters)



Figure 4. 6: Photograph showing lineaments in the study area.

4.3 Aeromagnetic data analysis

4.3.1 Geologic source of basement

The reduction-to-pole map (Figure 4.7) presents the magnetic source distribution whereby the areas of anomalous magnetic intensity indicate the geologic sources of the magnetic information. The RTP map shows that the sources of the magnetic effect, which can be arrogated as the accumulation zones of Jurassic dolerite intrusion, are mainly at the northwest among other dot-like spots in the north, center, extreme west, southwest and south. The areas of extremely low negative magnetic intensity indicate the zones of lesser geologic stress and non-magnetic property. This is supposedly the sedimentary rock successions of the Karoo Supergroup. The RTP map, therefore, shows a negative correlation with the geologic

map of the area such that the low-pressure zones are the areas of the surficial outcropping of the dolerite rocks. Few of the areas showed a positive correlation, like the magnetic ridge running from the southwest to the center and some of the dome-like structures in the northwest.

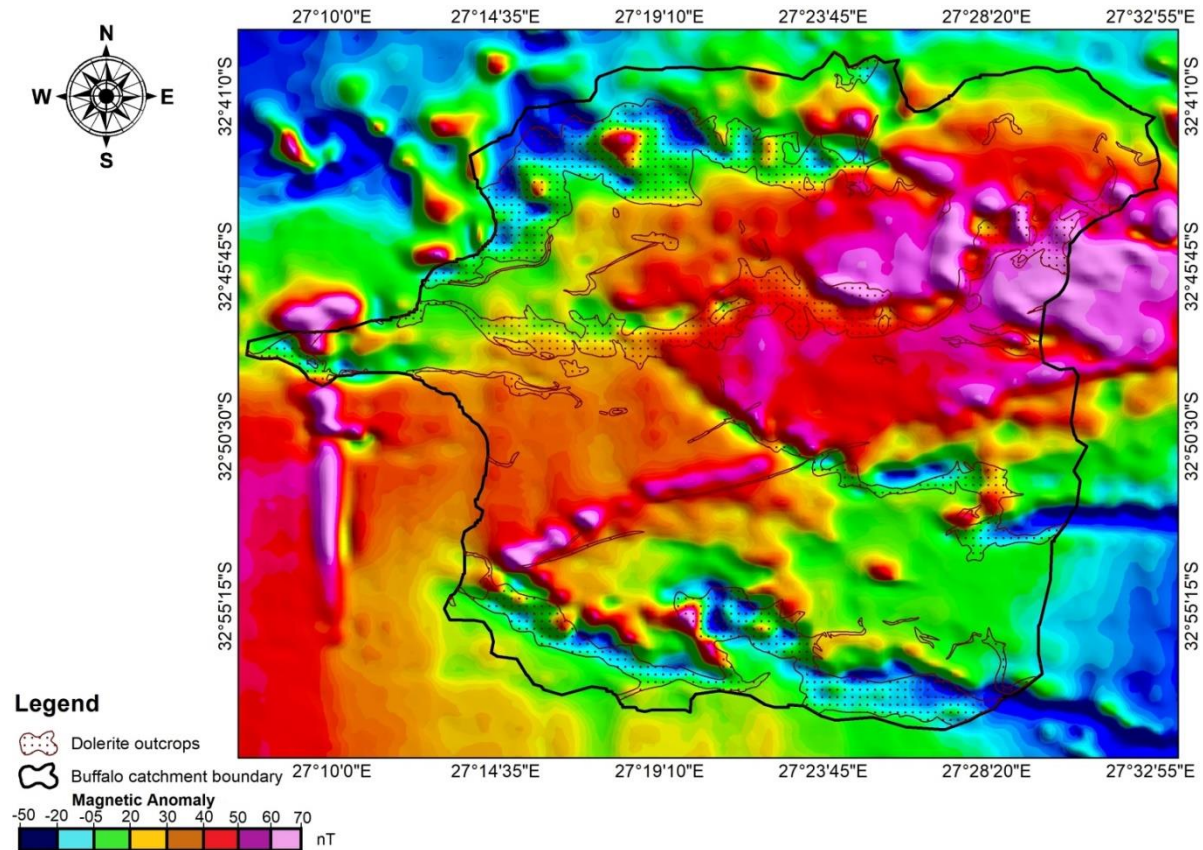


Figure 4. 7: RTP magnetization anomaly map; indicating the geologic sources and the regions of low intrusion pressure which coincides with the area of dolerite outcrop.

4.3.2 First vertical derivative and total horizontal derivatives (TDX)

The need for enhancement of effects of near-surface geology and reduction of anomalies of deeper sources in order to project a better resolution of sources has prompted the calculation of the first vertical derivatives. The vertical derivative is overlain on the area covered by dolerite outcrop (Figure 4.8A). Herein, the anomalous inclusions for the dolerite sills, especially with the ring-ridge structures, are revealed. Also, the neo-tectonic lineament and some other edges can be visibly seen as lineaments. Total horizontal derivatives of tilt

derivatives were calculated and overlain by automatically extracted lineaments (Figure 4. 8B).

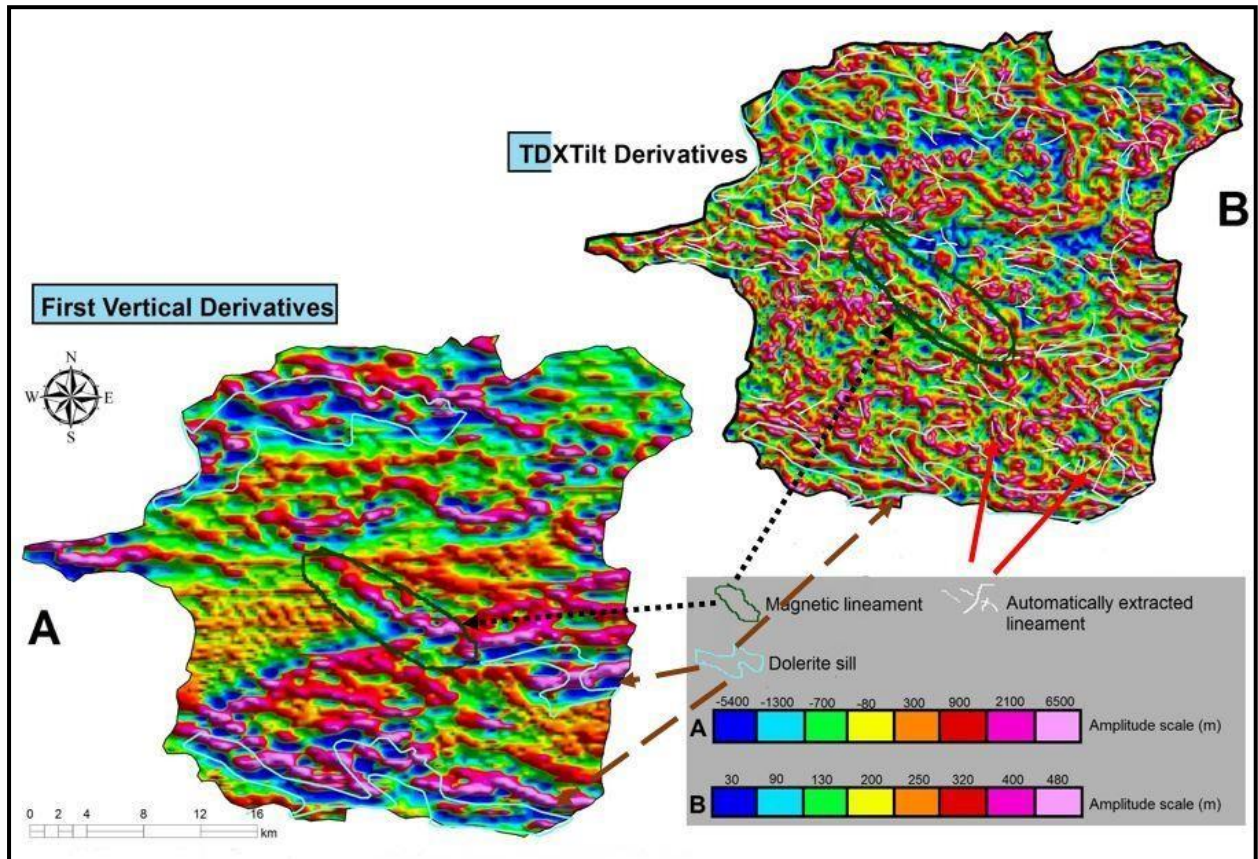


Figure 4. 8: Maps showing the; A) First vertical derivative map, and B) Total horizontal derivatives of Tilt derivatives (TDXtilt) overlain by automatically extracted lineaments.

Vast numbers of the automatically extracted lineaments align with the TDX lineament, implying the extension of surficial structures with subsurface lineaments and possible flow channel for groundwater.

Most importantly, the auto-lineaments are concentrated on the ridge-like edge of magnetic lineaments in the center of the study area (Figure 4. 8). They are also concentrated around the areas where dolerite intrusions are imprinted as sills. These indicate the influence of dolerite intrusion on generations of tectonic structures in the weak areas across the Buffalo catchment. These weak points are important flow-paths for groundwater accumulation and

conduits. Manual extraction of magnetic lineaments was carried out and the lineaments were grouped into three and counted; NW – SE trends (87), E – W trends (60) and N – S (21).

4.3.3 Basement configuration

The analytical signal map presents the magnetic anomaly whose peaks indicate the spots of emplacements of causative bodies in a manner that is independent of induced or remnant magnetization and magnetic inclination or declination (Figure 4.9).

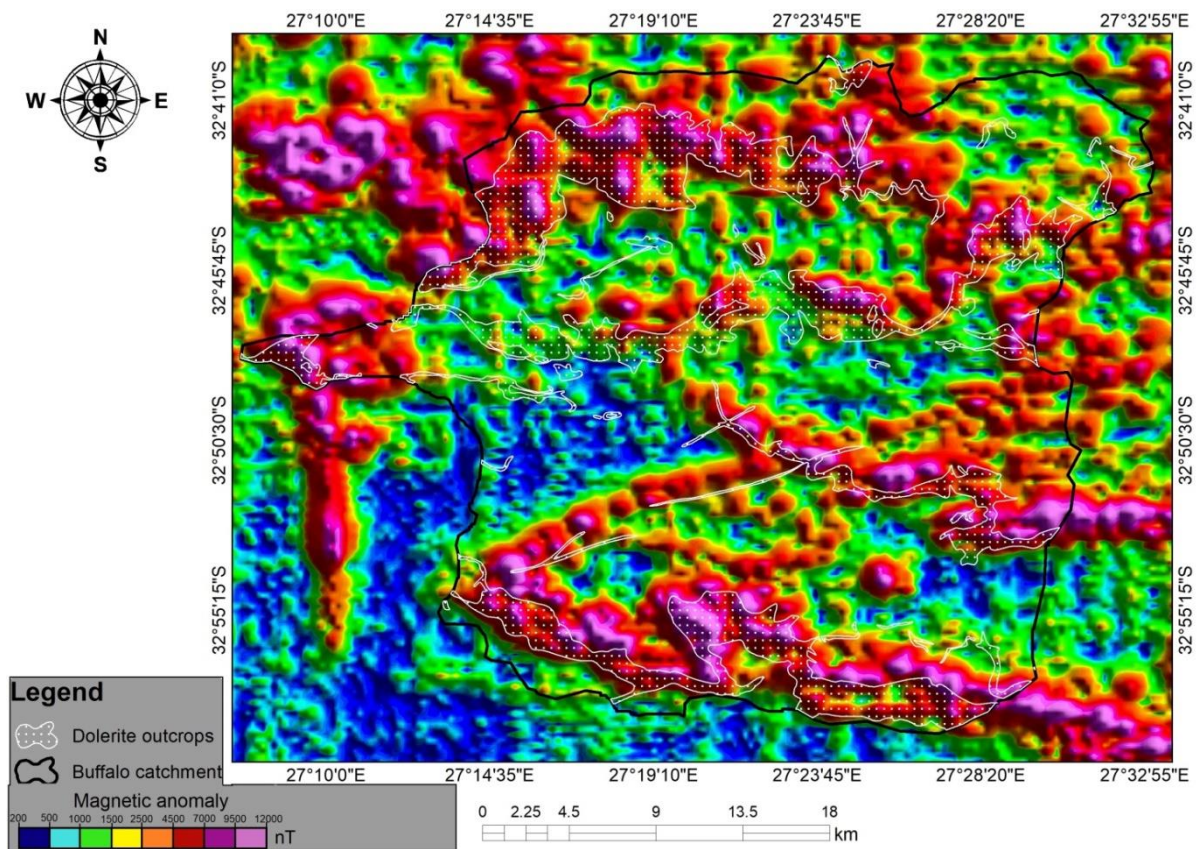


Figure 4. 9: Analytical signal map; indicating the regions of surface/near-surface basement emplacement which visually correlates with the dolerite outcrops in the basin.

The map reveals a strong positive correlation with the geology of the study area, as the dolerite features of the regional geologic map overlays conformably on the areas of the high magnetic anomaly (4000 – 10000 nT) as shown in the composite map (Figure 3). It also correlates strongly with the RTP lineaments which therefore validates the credibility of the AS and RTP maps. The geologic field mapping indicates that the intermediate signals (500 – 1500 nT) indicate the sedimentary sequences dominated by mudstone lithosome. The

extremely low signals (0 – 250 nT) overlays the sedimentary sequences dominated by sandstone lithosome (Figure 3).

4.3.4 *Depth slicing of basement*

The result of the depth variation of magnetic structure sources based on a radially averaged power spectrum is presented in Figure 4.10. Five major structural trends replicate the depth of dolerite structure visibility at the range of 382m – 10.7km were extracted.

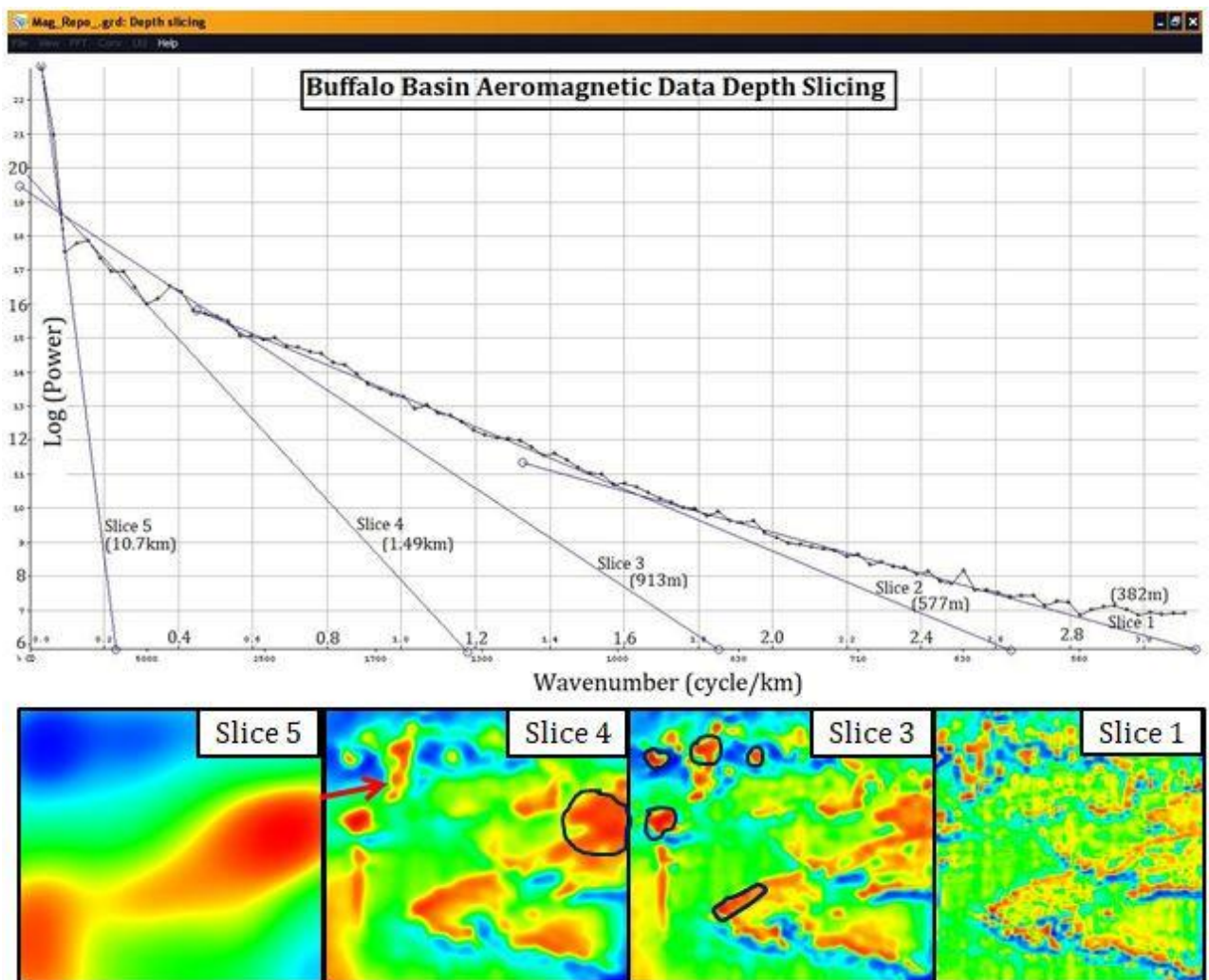


Figure 4. 10: Depth slice; the corresponding effective anomaly is shown with a blue ring while the deepest (Slice 5) is shown with a red arrow. The red dots in Slice 1 reveal the effective anomaly corresponding to the depth being sliced.

Slice 1 indicates that most of the magnetic structures are visible at the depth of 382 m, of which are the magnetic anomalies are trending in W – E, WSW – ENE, and WNW – ESE

directions. A similar view is repeated through Slice 2 (577m) and Slice 3 (913m), thus, suggesting that the anomalous magnetic structure stretches across the great thickness.

Slice 4 (1.49km) presents a shrinkage in the areal magnetic anomaly and indicates the existence of a deep dolerite sill at the west (outside the study area), at the southwest and the northeast of the study area and the disappearance of others. Slice 5 shows that the northwest magnetic structure is the deepest with a depth of 10.7km. The power spectrum, therefore, presents three types of sources; the shallow (382m), intermediate (1.49km), and deep (10.7km) sources.

4.4 Groundwater recharge zones and aquifer delineation

The profile of lithology cross-sections for thirty-four boreholes was grouped into eight and examined as presented in Figures 4.11 – 4.13.

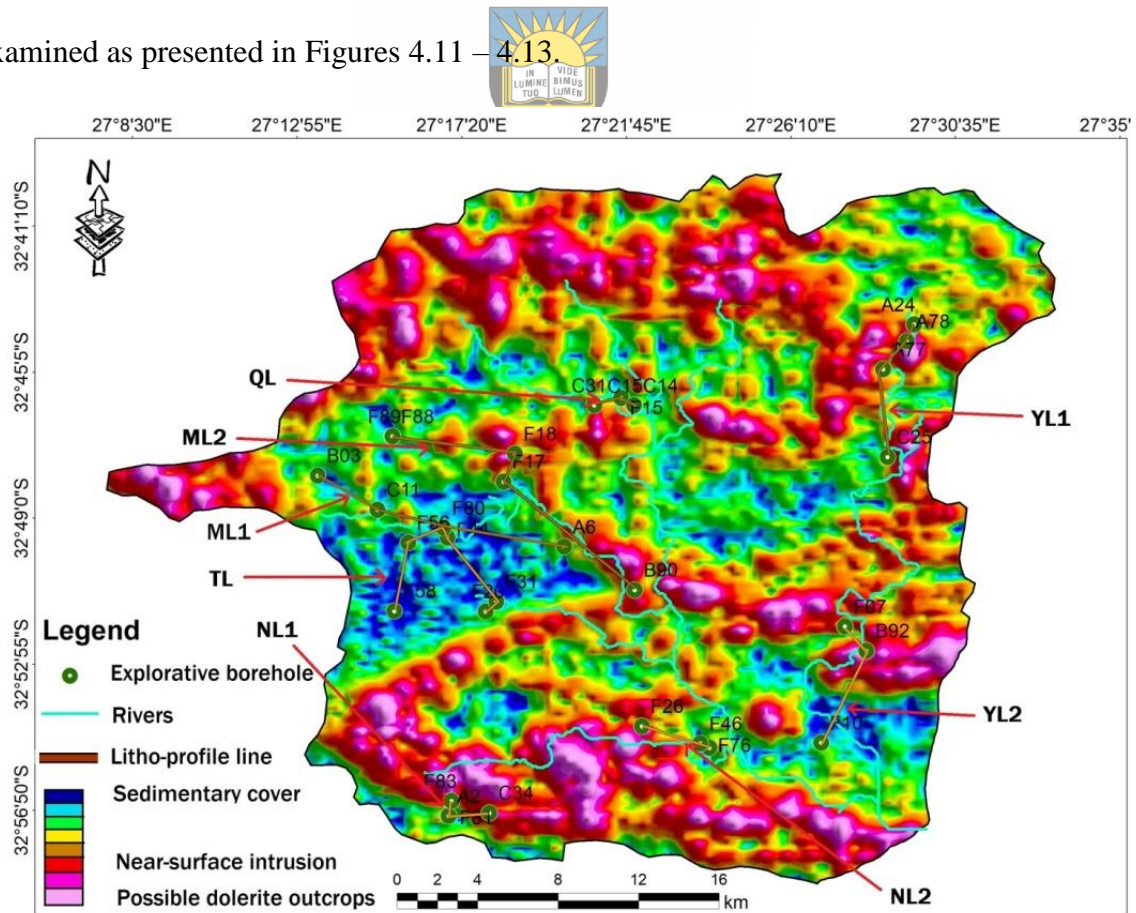
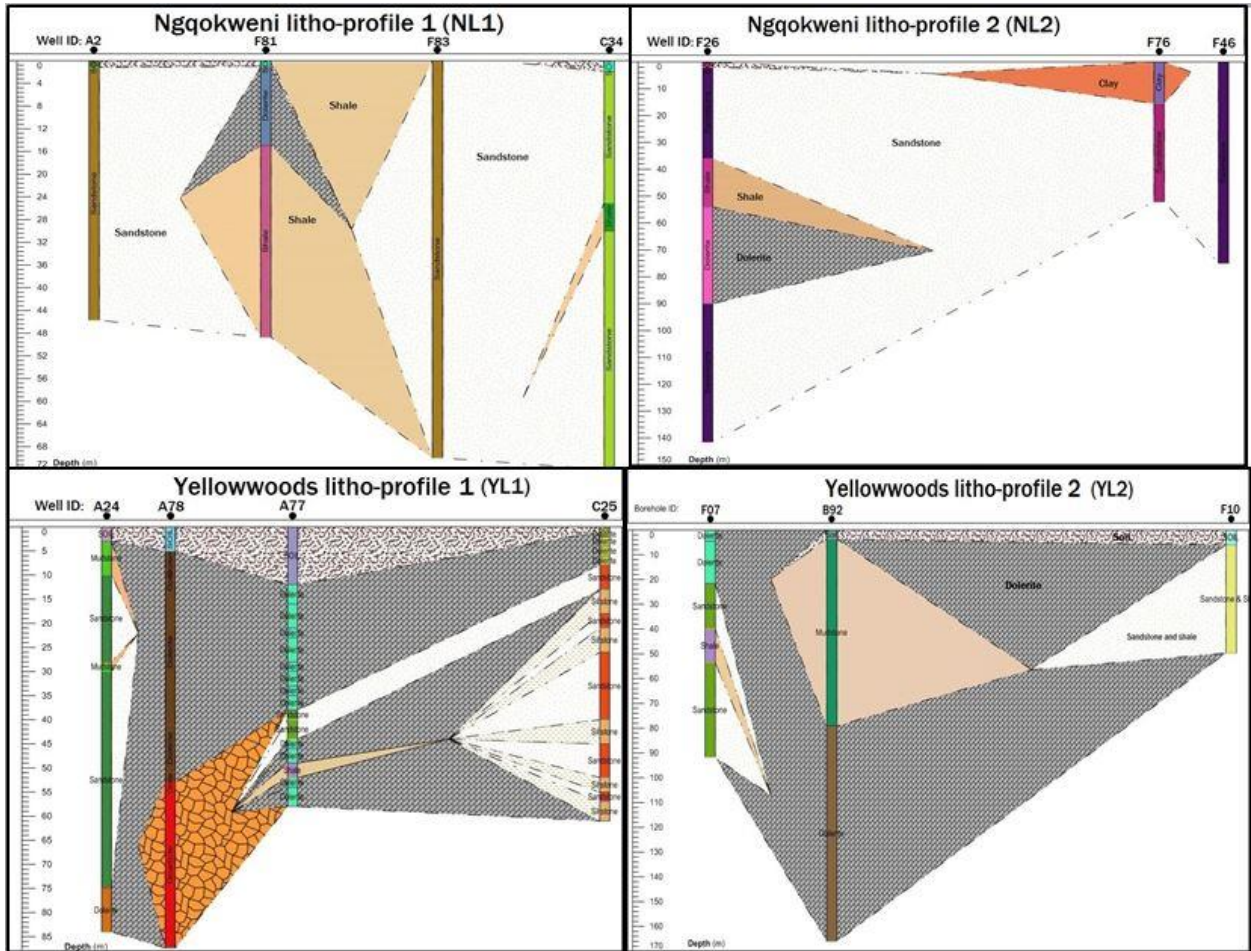


Figure 4. 11: Lineament-dolerite Corroboration of the analytical signal map by by borehole lithology cross-section profiling.



University of Fort Hare
Together in Excellence

Figure 4. 12: Borehole lithology cross-section profile for North and West of Buffalo basin.

The plot shows that the red magnetic anomaly ($4500\text{nT} < AS < 7500\text{nT}$) are near-surface dolerite intrusion (F15, F80, F81, A78, A77). The purple and lilac magnetic anomaly ($AS > 7500\text{nT}$) are possibly outcrops (B03 – C11, F07 – B92). The plot shows that the blue magnetic anomaly ($10\text{nT} < AS < 50\text{nT}$) are mainly sandstones, thus, suggesting that the extremely low magnetic susceptibility is possibly due to the high porosity exhibited by sandstone (F44, F88, F17, A2, and F26). The geology of the northern part drained by Quencwe River, the northwestern part drained by the Mgqakwebe River, and the eastern half of the Buffalo drained by Yellowwoods River are mainly basement (QL, ML1, YL1, and YL2). The overburden of the northern half of the Buffalo basin is mostly characterized by mudstone and sandstone (QL, ML1, and YL1) while the southern half is mostly characterized by sandstone and shale overburden (TL, ML2, NL1, NL2, and YL2). The

cross-section also reveals the possible existence of a fault system in the north profiles (QL, ML1, TL, and YL1) where the dolerite section pinches-out unconformably against another. Ground-truthing confirms the topographic complexity and existence of extensional stress in the northern half of the study area.

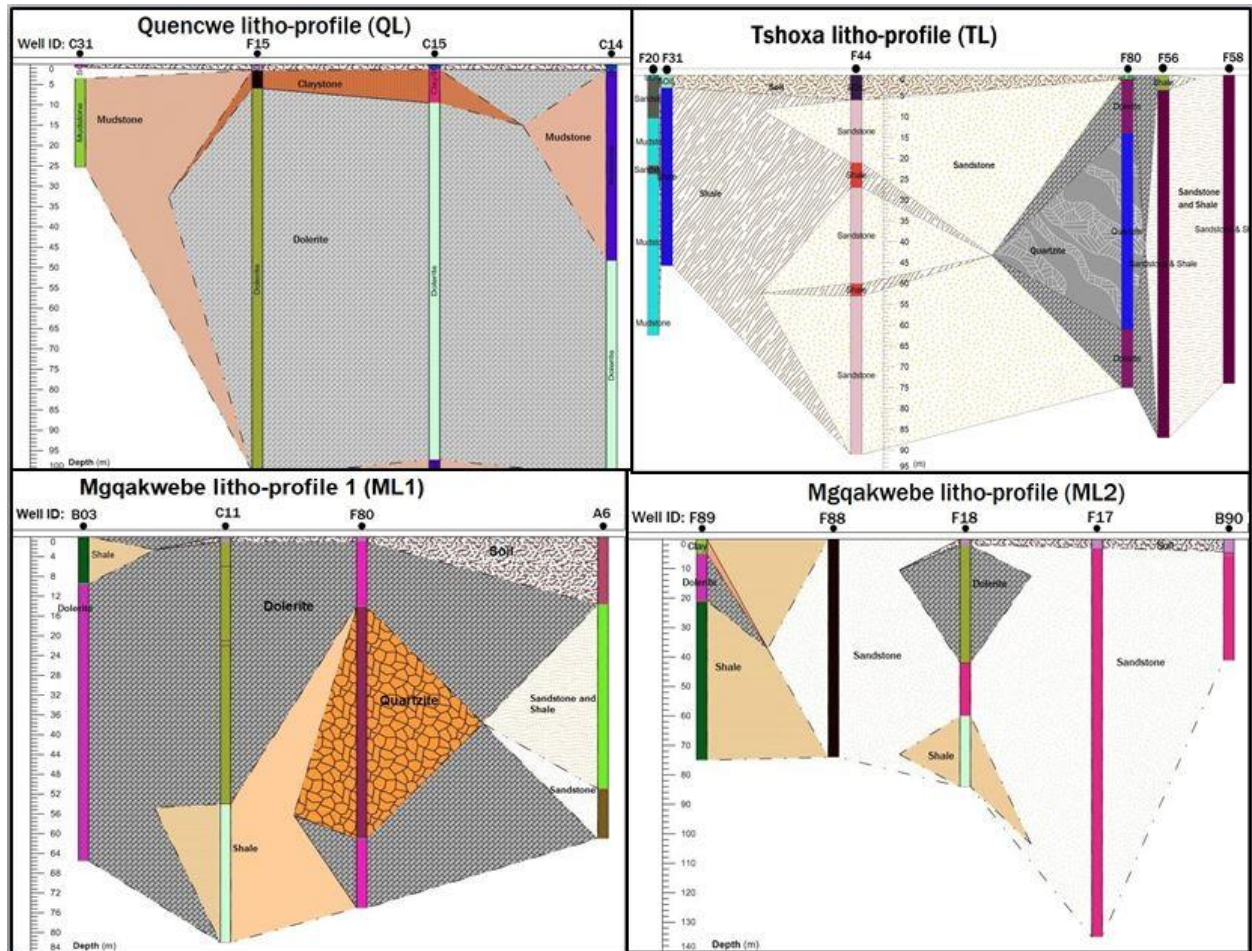


Figure 4. 13: Borehole lithology cross-section profile for northeast, east, and south of Buffalo basin.

4.5 Summary

In this section, the reconstruction of the geology of Buffalo area, mapping of geologic structures, and evaluation of groundwater prospects have been demonstrated through geological field mapping, extraction of lineaments and analysis of aeromagnetic data. The results can then be correlated in order to establish some deductions with respects to previous applications. However, some deductions can be readily inferred from the results;

- RTP mapping reveals patterns that align with the field geologic structures, thus validating the field structural mapping approach,
- The automatic lineament map aligns structurally with lineaments extracted from horizontally tilting derivative maps which further confirms the orientation of possible neotectonic lineament features and applicability of Landsat 8 OLI and the aeromagnetic edge detection combination for delineation of geologic structures,
- Characterization of groundwater potential in the Balfour Formation was defined with Barberskrans Member depicting a high groundwater development potential. This was based on its high lineament density and its sandstone-dominated composition.
- Applicability of hybridization of lineament extraction and aeromagnetic data analysis enhances the location and delineation of synclinal structures, which could make up a groundwater reservoir. This is because the low magnetic amplitude of the unit suggests the likelihood of a thick porous and permeable rock unit. Validation of this unit reveals the presence of quartzite which is characterized by high hydraulic conductivity.
- The outcome of the research reveals evidence of groundwater prospects on the western side of the study area. The discovery implies that the approach can be readily employed for the exploration of groundwater prospects in any environment or geological terrain.

Chapter 5: A baseline study of streamflow variabilities

5.1 Introduction

This chapter presents the results on spatio-temporal variabilities of streamflow and their correlation to rainfall variabilities. The findings attempt to characterize the Buffalo watershed using streamflow dynamics and its sensitivity to rainfall variabilities. Hence, it provides insight into historical trends of surface water availability based on carefully selected multivariate statistical approaches. The inference of findings was linked with environmental factors influencing its seasonality trend.

5.2 Hydro-climatic variability analyses

5.2.1 Consistency assessment



The result of consistency assessment, as inferred from DMC plots of each station against cumulative means of other stations, is presented in Figure 5.1. The result shows that the dataset is consistent and homogenous for all the stations, although smoothness varies for most of the stations (Figure 5.1). DMC for Tshoxa, Mgqakwebe and Yellowwoods stations show considerable linearity while DMC for Buffalo, Ngqokweni and Quencwe stations revealed tilts that reveal an inconsistency in their plots. The coefficient of determination (R^2) reveals that Quencwe station was the most inconsistent. Variability in trend-line linearity in assessing dataset consistency may have been due to basin-specific hydrologic alteration which can be urbanization, land use/land cover system and river basin management.

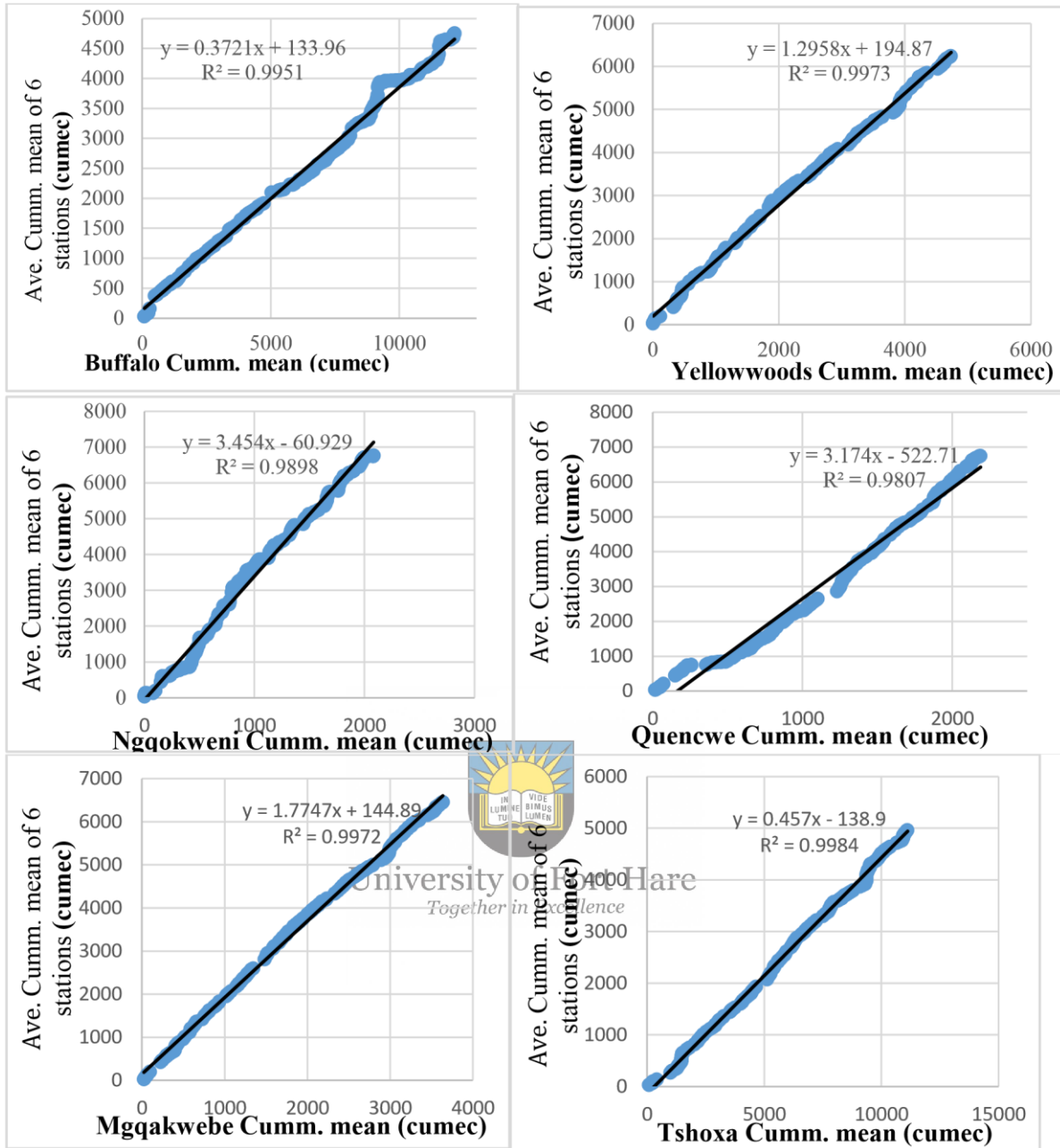


Figure 5. 1: Double Mass Curve plot of the six stations on the y-axis and the respective stations on the x-axis.

5.2.2 Descriptive analysis

Tables 5.1 and 5.2 report the statistical summary for descriptive statistics and descriptive analysis of gauged stations in the study area. Autocorrelation function, ACF, also known as autocorrelogram, is presented in Figure 5.2. The series dependence up to two years of streamflow (lag 2) are significant as noted in Figure 5.2. The descriptive statistic reveals the streamflow variability in response to climatic extremity.

Table 5. 1: Statistical summary of descriptive statistics.

	Range (cumec)	Min (cumec)	Max (cumec)	Mean (cumec)	S. D (cumec)	Variance (cumec)	Skewness	Kurtosis
Buffalo	291.93	2.64	294.56	36.16	43.69	1908.99	2.47	7.97
Yellowwoods	210.26	0.05	210.31	14.09	27.97	782.18	3.75	16.86
Ngqokweni	68.10	0.04	68.13	6.20	11.92	142.19	3.22	11.14
Quencwe	129.44	0.14	129.58	6.51	12.62	159.16	5.09	37.32
Mgqakwebe	138.85	0.08	138.93	10.83	18.43	339.54	3.48	15.68
Tshoxa	592.10	0.04	592.14	33.08	63.12	3983.66	4.32	26.97
<u>Rainfall</u>	<u>324.00</u>	<u>0.00</u>	<u>324.00</u>	<u>49.18</u>	<u>45.78</u>	<u>2095.49</u>	<u>1.70</u>	<u>4.90</u>

Table 5. 2: Result of descriptive analysis for normality and white noise test of streamflow records (1989 – 2016) for Buffalo watershed.

Hydrological stations	J-B (dF=2)	B-P (dF=6)	L-B (dF=6)
Buffalo	1198.857	91.862	92.798
Yellowwoods	4634.913	19.284	19.512
Ngqokweni	2258.638	13.230	13.403
Quencwe	20340.327	12.538	12.695
Mgqakwebe	4007.317	27.455	27.798
Tshoxa	10903.308	36.930	37.340

NB: The Bold figure indicate the period of insignificant change.

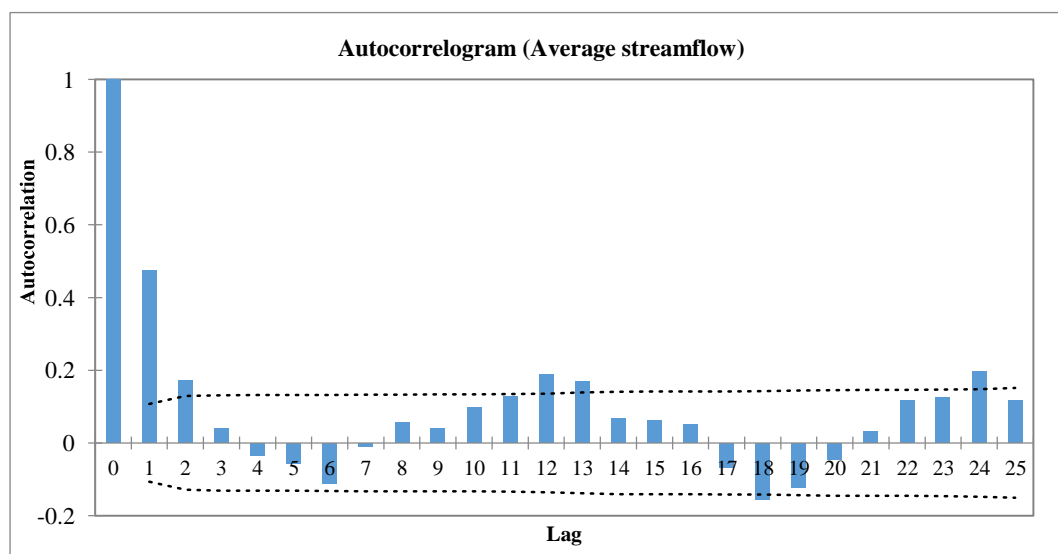


Figure 5. 2: Autocorrelation function plot of streamflow time series for the six stations.

The highest flow, deviation, and variance skewness occur in Tshoxa station while the least occurs in Ngqokweni station. Although Tshoxa station is smaller in size to Ngqokweni, its descriptive statistics suggest that Tshoxa flow receives a higher proportion of baseflow discharge than Ngqokweni flow. The result of kurtosis and skewness reveals the extremity of temporal variability in the statistics of Quencwe station and every other station proximal to the high altitude. The results suggest that the streamflow in high relief has the tendency not to be normally distributed due to its turbulent nature, which is influenced by the hillslope factor. Buffalo flow is the major stream order for most of the stations except Yellowwoods station, hence, this may account for its higher mean discharge than others. Here, the order of response to climate extremity, corresponding to standard deviation and variance, from the highest to the least, are; Tshoxa, Buffalo, Yellowwoods, Mgqakwebe, Quencwe, and Ngqokweni flow. The result of the descriptive analysis (Table 5.2) shows that the p-value is lower than the level of significance for most of the stations. Hence, the test indicates that the data is not normally distributed and it cannot be assumed to be generated by the white noise process. This is also confirmed by the ACF plots.



University of Fort Hare
Together in Excellence

5.2.3 Homogeneity test

The results of the homogeneity test are shown in Table 5.3. The Pettitt test shows that four of the stations - Buffalo, Yellowwoods, Mgqakwebe, and Tshoxa - are significant in alteration and associated with the same change point that occurred in October 1996. Change-point here indicates the period marking a significant deflection from the monotony of the hydrologic record. The change point is evidence of hydrologic alteration. Meanwhile, the test indicates that Ngqokweni and Quencwe are non-homogeneous with change-point in March 1994 and May 2000 respectively.

Table 5. 3: Homogeneity test results for Buffalo streamflow records from 1989 to 2016.

Statistic	Pettitt	SNHT	Buishand
Buffalo	6801.000	5.198	19.426
Change date	Oct-96	Nov-93	Sep-02
Yellowwoods	8230.000	3.652	12.169
Change date	Oct-96	Nov-89	Nov-93
Ngqokweni	1909.000	4.352	9.452
Change date	Mar-94	Nov-89	Jul-04
Quencwe	3015.000	9.952	28.426
Change date	May-00	Apr-00	Apr-00
Mgqakwebe	6730.000	3.069	12.937
Change date	Oct-96	Dec-89	Nov-95
Tshoxa	5341.000	9.672	11.835
Change date	Oct-96	Nov-89	Apr-90

NB: Bold values indicate significant change-point whereby $p\text{-value} \leq 0.05$

However, SNHT and Buishand's tests differ in results as they indicate that most of the stations are non-homogenous. SNHT goes further to show a unique pattern in change point as Yellowwoods, Ngqokweni, Mgqakwebe and Tshoxa stations reveal almost similar change points. The homogeneity test indicates that the stations whose data series produced different change points among others are influenced by site-specific factors. This further validates the results of DMC assessment.

5.2.4 Regime variability and seasonality analysis

The result of seasonality assessment using the Parde plot is presented in Figure 5.3. In this conceptual assessment, it is assumed that precipitation is the major water input in the watershed, hence, its Pc plot is taken as the standard of regional sequence and compared with the streamflow Pc plots for the watershed.

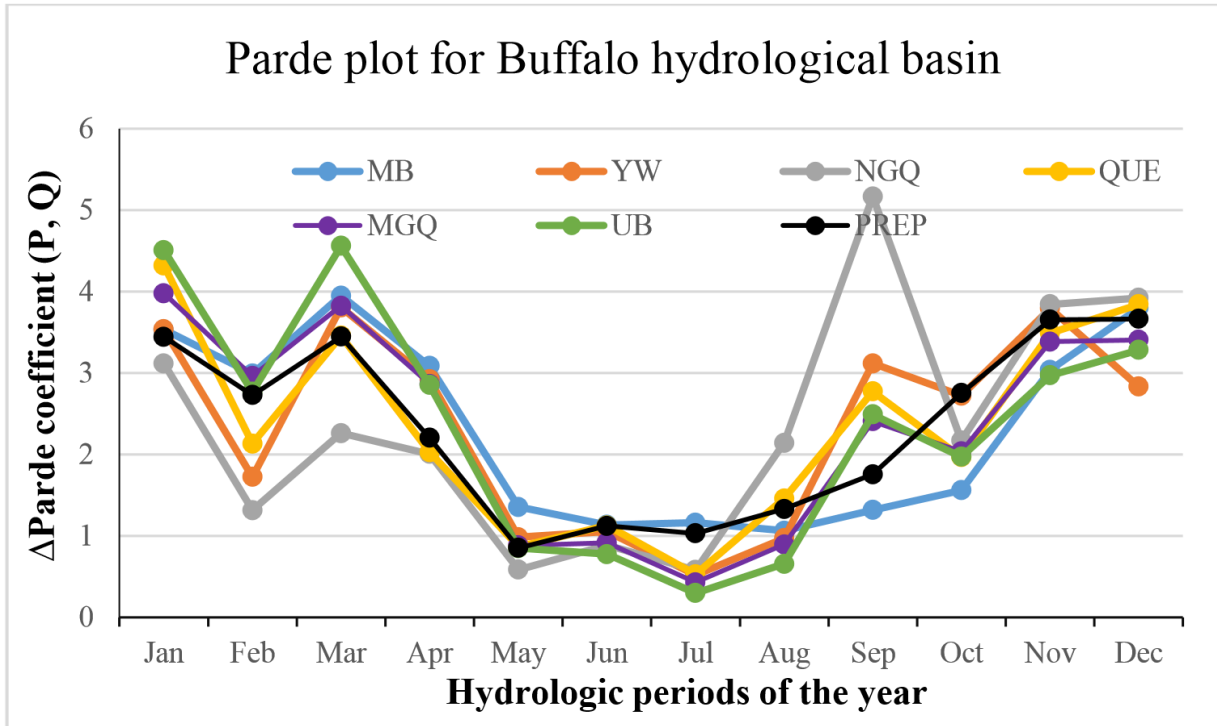


Figure 5. 3: Parde coefficient plot showing regime variability of streamflow and rainfall data series (1989 – 2016).

Peak flow occurs in summer months while seasonality is very weak in the winter months. Flow corresponds to rainfall seasonality in the following order; Tshoxa, Buffalo, Mggakwebe, Yellowwoods, Quencwe, and Ngqokweni station. It indicates that the Ngqokweni regime flow does not align with the standard of regional sequence compared to others, that is, the station has a higher vulnerability and tendency to deflect from the standard hydrologic trend. Tshoxa Pc plots show the strongest alignment across the hydrologic period, and this implies that Tshoxa flow shows the least tendency to vulnerability or diminution owing to its alignment to precipitation trend.

The seasonality of precipitation, $\Delta Par_i = 2.81$, is compared with that of the streamflow. The result indicates that Ngqokweni has the strongest anomalous seasonality ($\Delta Par_i = 4.59$), with anomalously high Par_{Sep} . It has the least variability for most of the first half of the year. The least seasonal station is Buffalo station ($\Delta Par_i = 2.88$). Others are in close average range; Tshoxa ($\Delta Par_i = 4.26$), Quencwe ($\Delta Par_i = 3.79$), Mggakwebe ($\Delta Par_i = 3.55$), and

Yellowwoods ($\Delta\text{Par}_i = 3.28$). Only Buffalo station replicates a high degree of association with precipitation. The results imply that the disruption of the Ngqokweni flow trend from the regional hydro-climatic trend pattern is highly influenced by site-specific factors across the hydrologic year as its Parde amplitude is out-of-phase against the precipitation Parde amplitude. This is revealed by the anomalous result shown in Par_{Sep} . Tshoxa station also revealed a Parde seasonality similar to Ngqokweni station, whereby the amplitude gap between precipitation and Tshoxa implies a strong hydrologic alteration. The seasonality assessment corresponds to the findings of the descriptive statistics with respect to deviation, variance and mean flow.

5.2.5 Trend analysis

The summary of the MK test and Sen's slope analysis is shown in Table 5.4. The streamflow trend in Buffalo catchment shows a mixture of increasing and decreasing monthly trends.



Table 5. 4: Mann-Kendall trend test and Sen's slope results for Buffalo watershed involving Rainfall and six streamflow station data of 1989-2016.

	Series	Aug	Sep	Oct	Nov	Dec	Jan	Feb	Mar	Apr	May	Jun	Jul
Rainfall	M-K	0.12	-0.063	-0.228	0.032	-0.069	-0.048	0.185	0.005	0.026	0.159	0.156	0.16
	S.S	0.296	-0.304	-1.3	0.399	-0.648	-0.348	1.002	0.037	0.175	0.287	0.367	0.394
Buffalo	M-K	0.28	0.185	0.011	-0.011	-0.127	-0.069	0.069	-0.074	0.026	0.122	0.323	0.434
	S.S	0.257	<i>0.128</i>	<i>0.029</i>	<i>-0.025</i>	<i>-0.708</i>	<i>-0.253</i>	<i>0.365</i>	<i>-0.458</i>	<i>0.173</i>	<i>0.139</i>	0.212	0.251
Yelld	M-K	0.255	0.369	-0.043	-0.136	-0.054	0.146	0.049	-0.033	0.092	0.136	0.108	0.211
	S.S	<i>0.039</i>	0.112	<i>0</i>	<i>-0.071</i>	<i>-0.004</i>	<i>0.154</i>	<i>0.002</i>	<i>0</i>	<i>0.034</i>	<i>0.043</i>	<i>0.007</i>	<i>0.017</i>
Ngqo	M-K	0.173	0.195	-0.033	0.038	-0.423	0.081	-0.011	0.114	0.108	-0.114	0.108	0.027
	S.S	<i>0.033</i>	<i>0.05</i>	<i>0</i>	<i>0</i>	-0.348	<i>0.011</i>	<i>0</i>	<i>0.023</i>	<i>0.018</i>	<i>-0.005</i>	<i>0.003</i>	<i>0</i>
Quen	M-K	0.119	0.287	-0.201	-0.114	0.033	0.07	-0.065	-0.423	-0.39	0.005	0.325	0.09
	S.S	<i>0.004</i>	0.033	<i>-0.026</i>	<i>-0.061</i>	<i>0</i>	<i>0.031</i>	<i>-0.004</i>	-0.251	-0.313	<i>0</i>	0.025	<i>0.003</i>
Mgqa	M-K	0.152	0.298	-0.011	-0.125	-0.119	0.038	0.065	-0.065	0.06	0.179	0.347	0.092
	S.S	<i>0.018</i>	0.083	<i>0</i>	<i>-0.061</i>	<i>-0.072</i>	<i>0</i>	<i>0.032</i>	<i>-0.038</i>	<i>0.037</i>	<i>0.052</i>	0.038	<i>0.005</i>

Tshoxa	M-K	0.173	0.39	-0.09	-0.136	-0.125	0.076	-0.027	-0.179	-0.038	-0.005	-0.022	0.022
	S.S	0.021	0.267	-0.009	-0.089	-0.204	0.067	0	-0.94	0	0	0	0

NB: Bold values indicate significant trend given that $\alpha = 0.05$

Slope of trend is not uniform across the catchment. Results indicate that the Buffalo and Mgqakwebe slope trends appear to be synonymous with rainfall slope trends. In general, the stations show characteristic variabilities with altitudes, as stations in low altitudes are characterized by increasing trends while stations in high altitudes are characterized by decreasing streamflow trends. Interestingly, Yellowwoods, Quencwe, Tshoxa, and Mgqakwebe have in common a significant increase in trend and maximum Sen's slope in the September month. The positive trend in the winter months implies that there is an increase in streamflow trends in winter with a decrease in streamflow in the summer. The general increase in the winter and summer streamflow is consistent with the trends in precipitation. The situation implies that there is a shift in hydrologic pattern as the wetness period shifts from summer to winter. The variability in trends across the watershed indicates that there is high variability in climatic pattern and this can be linked with randomness in atmospheric circulation. The result further reveals the deduction of Pc plots.

5.2.6 Rainfall-streamflow distribution comparison

Plots of the Kolmogorov-Smirnov test for comparison of time series distribution of rainfall and streamflow variables are presented in Figure 5.4. The results indicate that the six stations are not normally distributed and, as a result, have some potential variability. The maximum absolute difference indicated that Buffalo streamflow ($D = 0.248$) has the strongest degree of association with precipitation, followed by Tshoxa ($D = 0.376$), Mgqakwebe ($D = 0.525$), Yellowwoods ($D = 0.528$), and Quencwe ($D = 0.621$), while Ngqokweni ($D = 0.645$) has the least degree of association. The results reveal that Ngqokweni has the least degree of

association with precipitation while Buffalo has the strongest degree of association. This reveals that the Ngqokweni flow has the highest vulnerability tendency as its streamflow series reveals a disproportionate association with precipitation and the regional trend.

Meanwhile, Buffalo has the least hydrologic alteration. The result obtained here validates the deductions of Pc, MK and Sen slope.

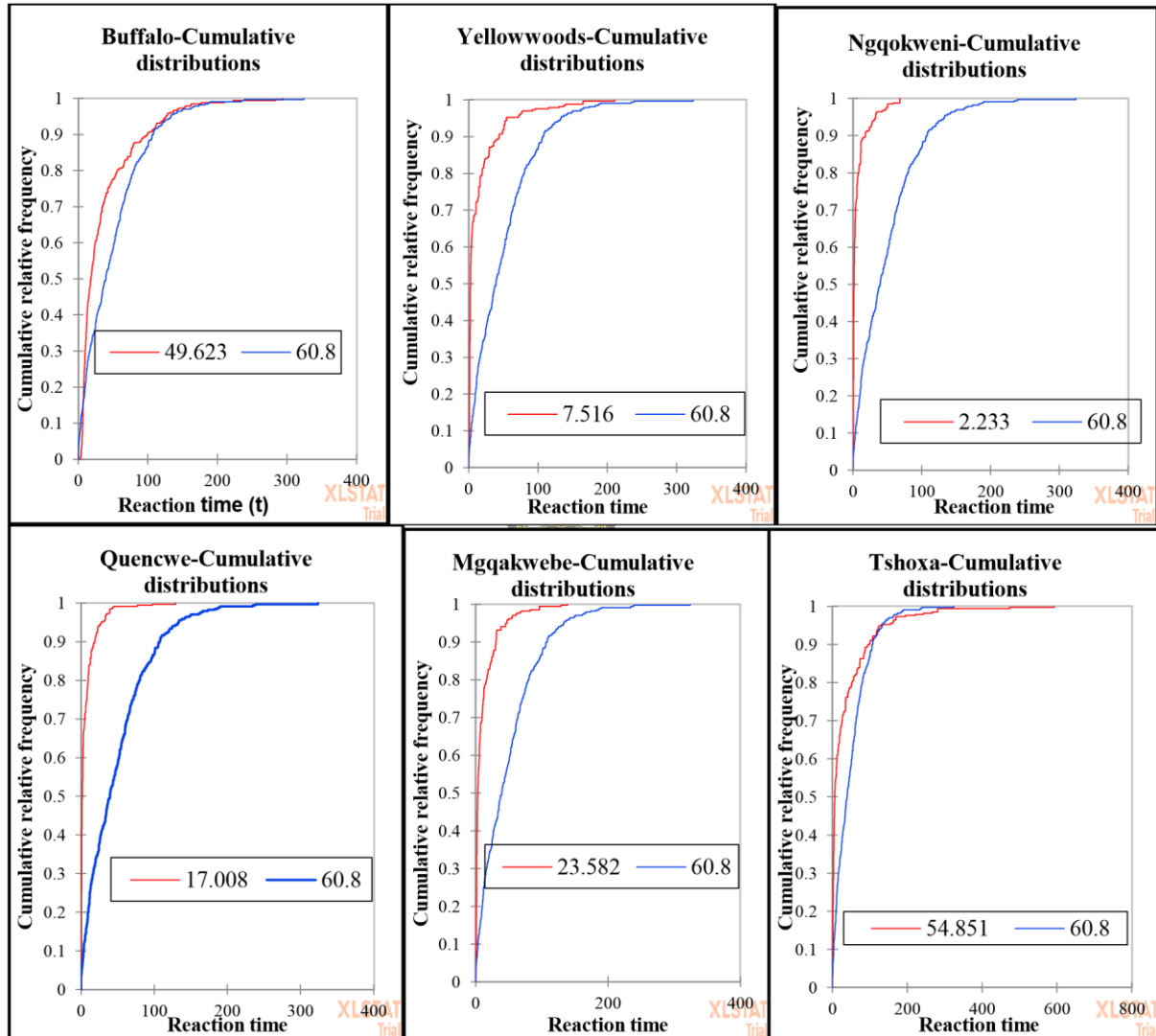


Figure 5. 4: Result of two-sample Kolmogorov-Smirnov test of Buffalo watershed showing the plot of cumulative relative frequency (CRF) of tested station and rainfall. The red and blue lines correspond to the empirical distribution function of streamflow data of the station tested and rainfall data of Buffalo watershed respectively. The values after the red and black lines in the plot legends report the CRF value of each of the stations and that of rainfall (60.8).

5.2.7 Sensitivity analysis test

Table 5.5 reports the summary of streamflow elasticity of rainfall across the hydrologic period. The results show that for most of the months' streamflow records taken at Buffalo station ($\epsilon_p = 0.55$) have the strongest phasal equilibrium to climate. Meanwhile, the Ngqokweni flow ($\epsilon_p = -0.99$), compared to the rest (Tshoxa, Yellowwoods, Mggakwebe, and Quencwe stations) is largely out of phase in a similar pattern to the results obtained from the Kolmogorov-Smirnov test.

Table 5. 5: Sensitivity analysis of rivers in Buffalo watershed.

	Buff	Yell	Ngq	Que	Mgg	Tsh
Aug	0.98	3.15	2.23	4.74	3.93	1.80
Sep	0.25	0.60	-0.46	0.35	0.83	0.69
Oct	-0.65	-1.38	-3.37	-4.09	-2.34	-0.60
Nov	0.49	0.27	-0.76	-1.60	0.30	0.52
Dec	1.02	-1.49	-4.61	-2.99	-1.01	1.40
Jan	0.03	-0.61	-15.06	-4.70	-2.55	-0.02
Feb	0.36	-5.06	-32.63	-8.12	-3.26	0.42
Mar	0.90	1.59	-6.72	-2.27	-0.82	1.59
Apr	0.78	4.54	12.97	10.96	5.27	1.35
May	0.62	2.52	10.97	8.52	4.00	0.98
Jun	0.96	3.92	11.57	10.72	6.02	1.80
Jul	0.82	8.22	14.01	21.96	16.16	5.88
Annual	0.55	1.36	-0.99	2.79	2.21	1.32

All the stations are shown to be out of phase for the month of October and slightly in July. This suggests that atmospheric circulation is probably stronger in October due to extreme rainfall and stormy incidence, while in July the extremity of winter temperature varies with relief. The tables also show a negative sensitivity in the summertime, that is, a negative streamflow situation that does not align with to trend of precipitation while the winter flow shows a positive sensitivity. The results reveal that Quencwe has the strongest sensitivity to rainfall events. The result also suggests that the streamflow at Ngqokweni station is possibly insensitive to a rainfall event (Table 5. 5). The major difference between these two stations is

their relief. This, therefore, suggests that the rainfall variation in the study area is largely influenced by relief.

5.3 Summary

This study presents the variability in the hydrodynamic response of Buffalo streamflow to the hydro-climatic situations using the multivariate statistical approach and non-parametric tests. Numerous findings were reported with further discussion provided in chapter 9. However, the results established that Buffalo watershed is extremely complex with respect to climate variability. Streamflow attributes vary to a great degree with topography, altitudes, and sources. Streamflow stations at higher altitudes are associated with extreme climatic conditions and are more sensitive to climatic variability.

This study revealed that there are strong inter-relationships among Parde coefficient estimates, the Kolmogorov-Smirnov test, and sensitivity analysis as some of the methods reported similar variability across the stations. It, therefore, implies that careful selection of the methods can be an effective tool for regionalizing or characterizing a hydrologic environment. Positive correspondence of streamflow attributes to regime variability of rainfall and hypothetical statements of tests guide the inference on hydrologic viability of streamflow.

Buffalo station stood out as the most consistent flow with precipitation trends across the hydrologic regime. The hydrodynamics and viability of its streamflow can considerably be linked to the density of tributaries feeding its flow. Quencwe station also stood out as the most complex with respect to the extremity of climate variability. The reports on Quencwe flow indicate the influence of the hillslope factor. The Ngqokweni River must have been influenced by site-specific factors. It was shown to be vulnerable to diminution. Headwater

source, plain topography, and vadose zone connectivity are likely contributors to the vulnerability of flow in the Ngqokweni basin to diminution.



University of Fort Hare
Together in Excellence

Chapter 6: Characterization of streamflow recession attributes

6.1 Introduction

This chapter reports the results of streamflow recession assessment based on the flow duration curve and baseflow index approaches. The results of high flow, low flow, and baseflow index assessment were compared across the sub-basins in order to infer factors influencing the variability in patterns of environmental flow and the contribution of baseflow as a basis for the decipherment of groundwater availability.

6.2 Results

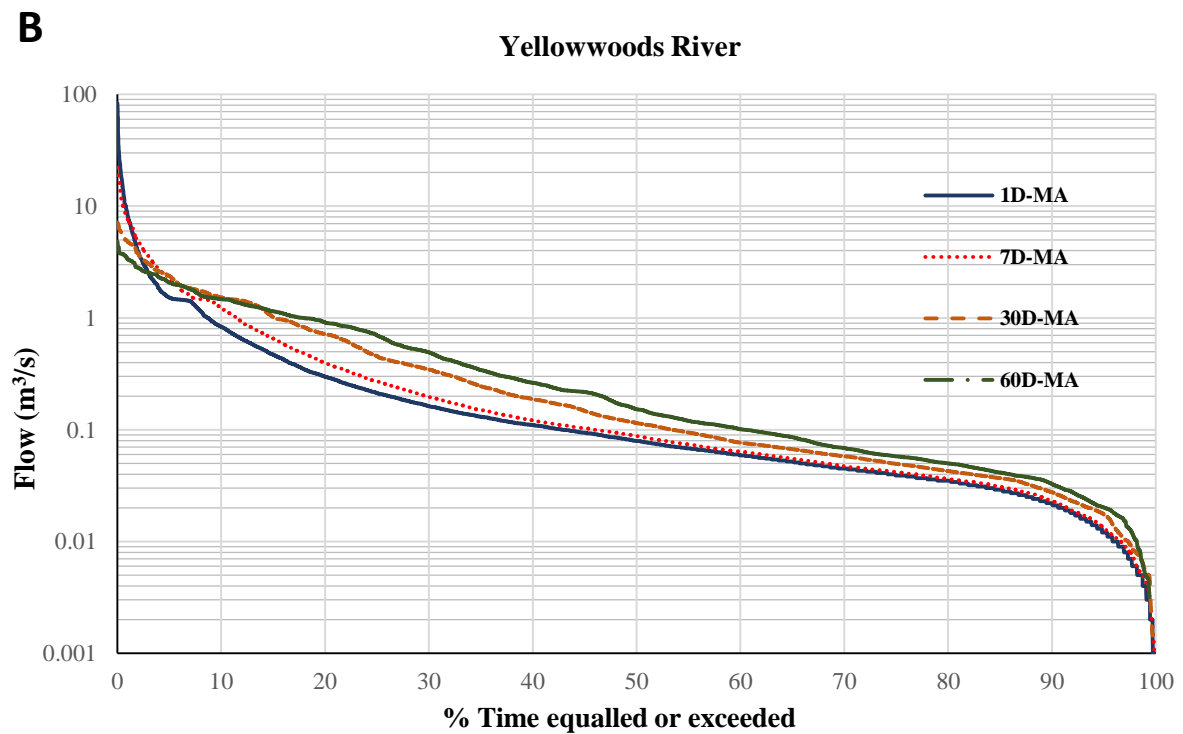
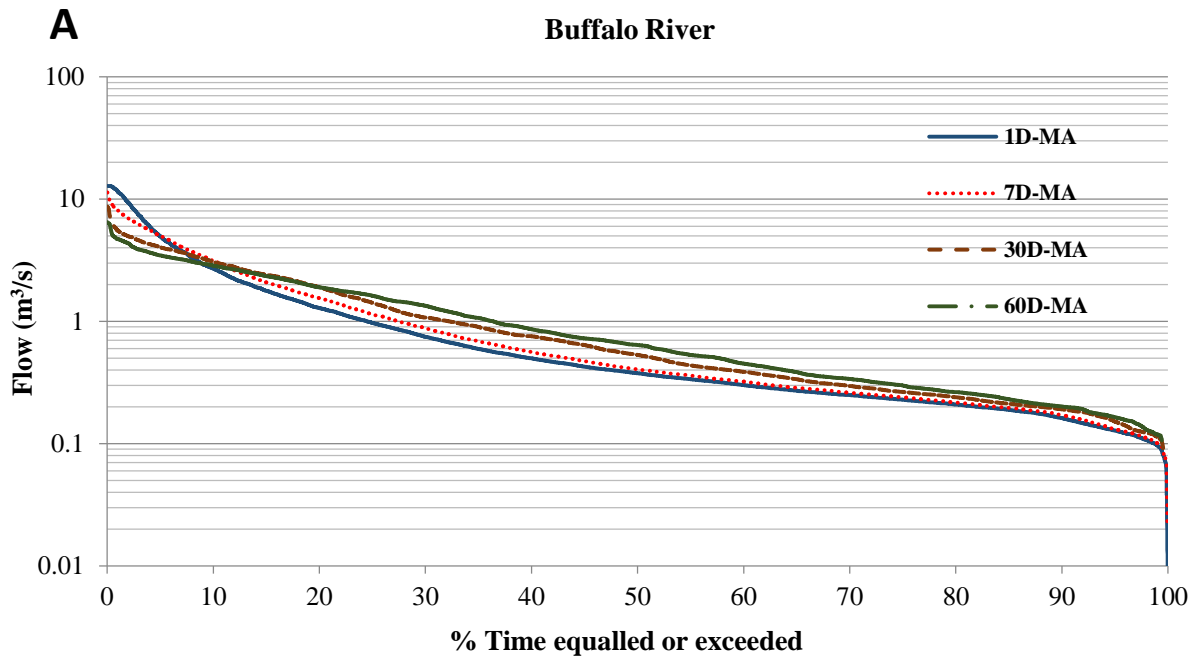
6.2.1 FDC Smoothness assessment

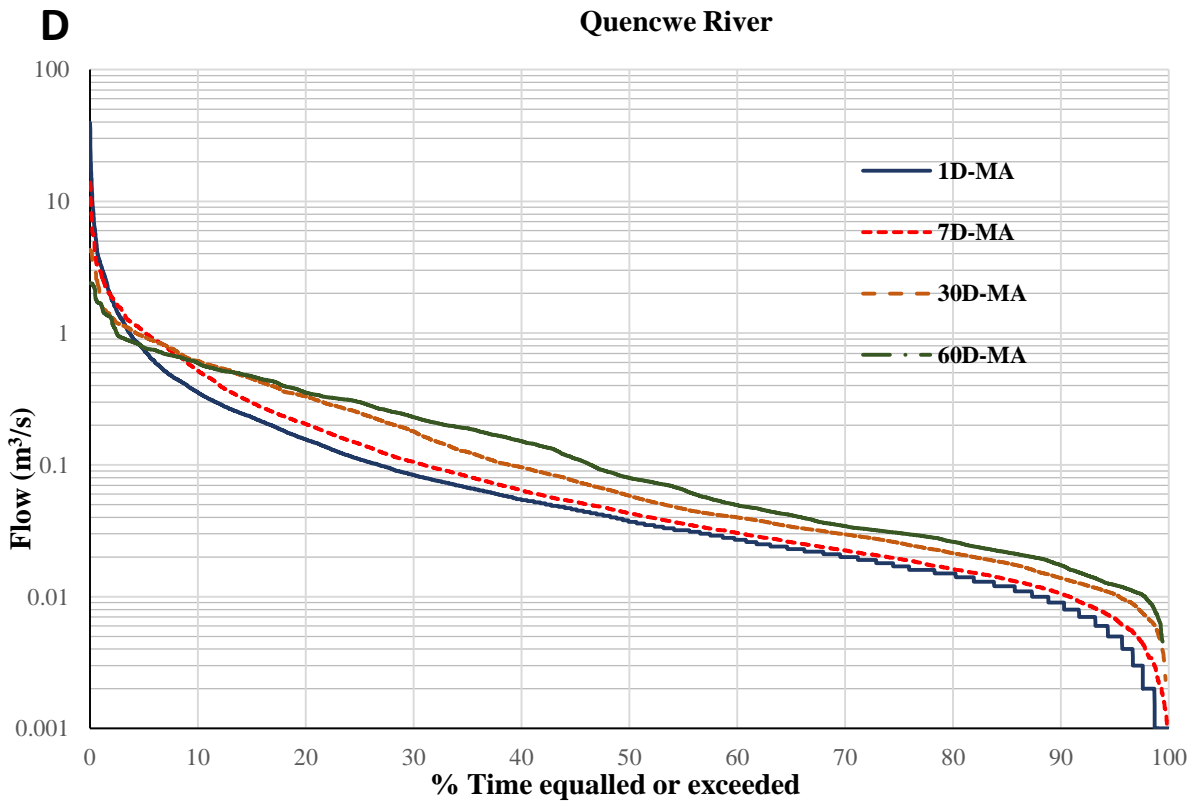
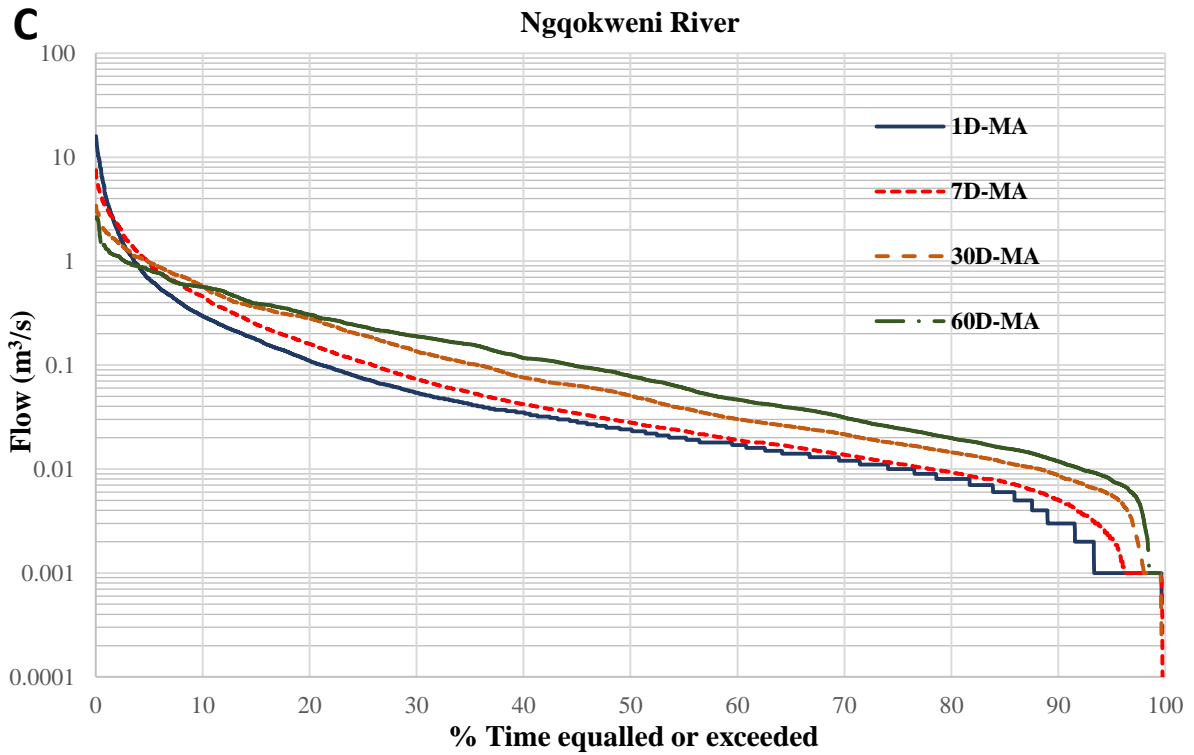
The plots of FDC for streamflow gauging stations are presented in Figure 6.1A - F. The result shows that for all the FDC plots 7D-moving average is the smoothest. The breakage in trend is very much obvious for 1D-frequency especially in the Ngqokweni and Quencwe plots. Meanwhile, 30D- and 60D- showed excessive deviation from the daily record, especially from 20th to 60th for most of the rivers.

6.2.2 High flow assessment

The high flow section of FDC reveals information on the type of flood regime in a catchment. The PORFDC plot shows that high-flow (1st to 10th percentile) recession in streamflow stations are in the following order of gradients; Tshoxa (-5.55), Yellowwoods (-2.10), Quencwe (-1.35), Mgqakwebe (-1.02), Buffalo (-0.84) and Ngqokweni (-0.73) stations. This points to the variation in stormflow potential of the study area which may not be necessarily linked with the size of the basin. The high potential in the Tshoxa basin may be linked with drainage density (Wilson et al., 2012). Yellowwoods station stormflow potential may be due to its size and length of the stream. Stormflow potential in Quencwe

station reveals the possibility of high rainfall intensity which is peculiar to a basin with high relief (Ghany, 2015).





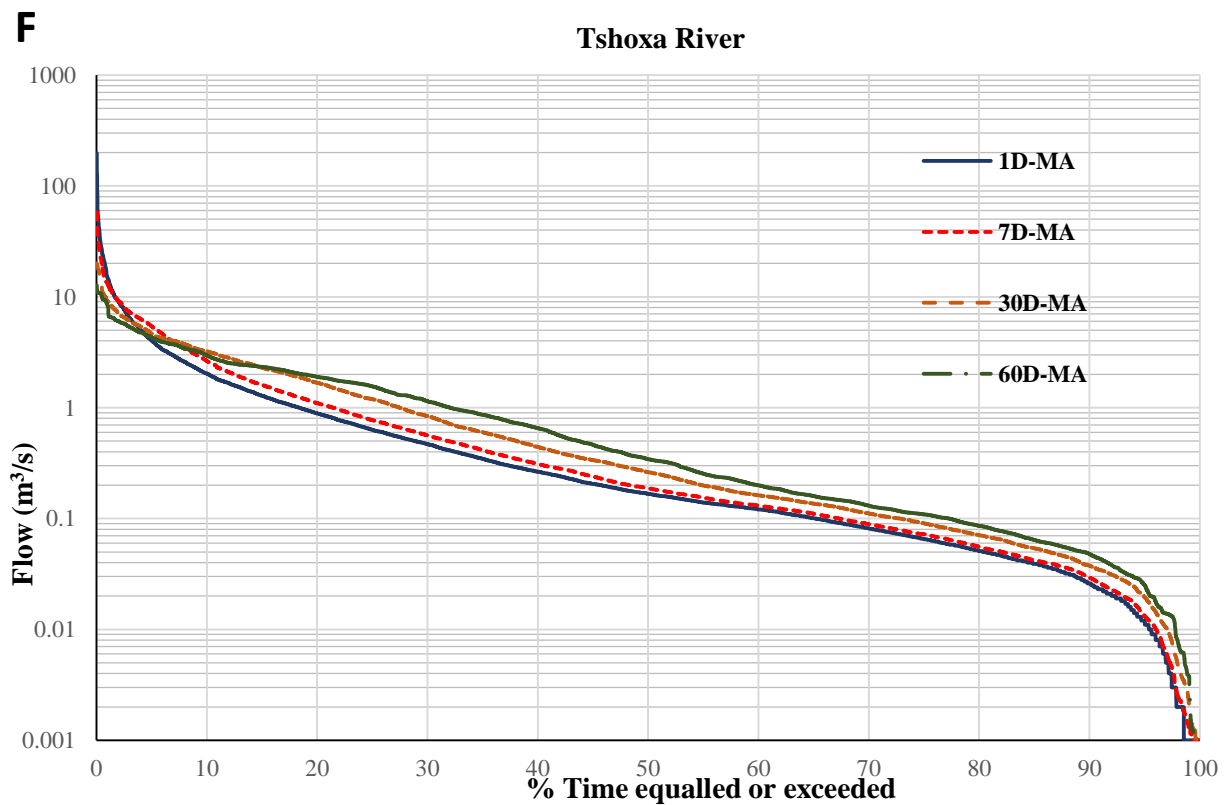
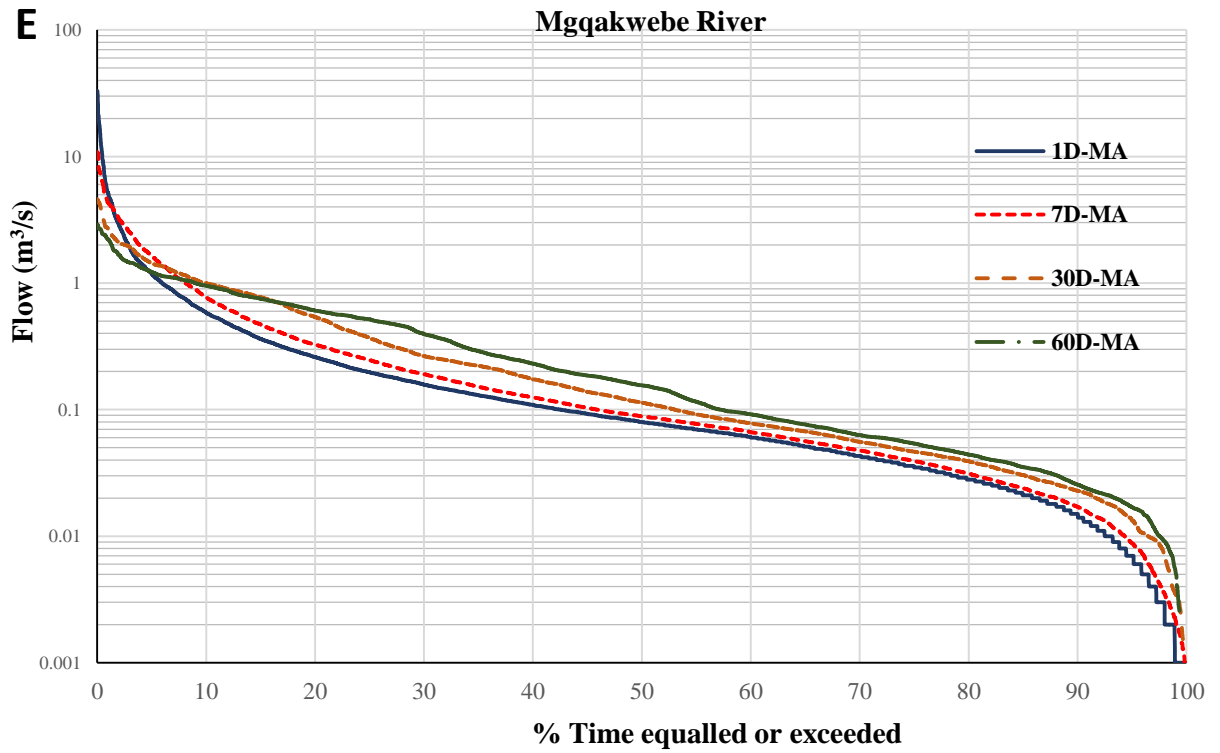


Figure 6. 1: FDC plot of rivers in Buffalo catchments for; A) Buffalo, B) Yellowwoods, C) Ngqokweni, D) Quencwe, E). Mgqakwebe and F) Tshoxa stations.

6.2.3 Low flow assessment

The low flow section of the FDC provides information on the extent of groundwater discharge to support environmental flow in the dry season. The result as indicated on the PORFDC plot for the low-flow region (90th to 99th percentile time exceeded) in the order of decreasing recession are presented as thus (Figure 6.1A - F); Buffalo (-0.0113), Tshoxa (0.0029), Yellowwoods (-0.0022), Mgqakwebe (-0.0017), Quencwe (-0.0009), and Ngqokweni (-0.00049).

The summary of the 7-day mean SFDC for 10 and 100 years' return period using 95th percentile results are presented in Table 6.1. Interestingly, the order of low flow results strongly agrees with the results of the 95th percentile time exceeded of the SFDC and 7-day mean SFDC for 100 years return period (Table 6.2 and Figure 6.2A - F). 95th percentile SFDC plots and 100 years 95th percentile plots would be valuable tools for classification and evaluation of environmental flow. The 95th percentile SFDC table reports the status of extremely low flow events based on the 28 years records while the 100 years plots project the probable extent of low flow recurrent in the next 100 years.

Table 6. 1: 7-day mean SFDC for 10 years and 100 years return period using 95th percentile.

Period	Buffalo	Yellowwoods	Ngqokweni	Quencwe	Mgqakwebe	Tshoxa
7D-10years	0.096	0.0041	-0.0001	0.0014	-0.0007	-0.0089
7D-100years	0.33	0.0761	0.0089	0.0194	0.0623	0.1351

The low flow results, therefore, indicate that groundwater discharge to support streamflow is higher at Buffalo station than other stations. This may be consequential to its stage, as the last stream order for the watershed was where accumulated flow occurs. The trend of decline in the low flow recession at Tshoxa to Ngqokweni station indicates the possible order of baseflow contribution to streamflow across the watershed.

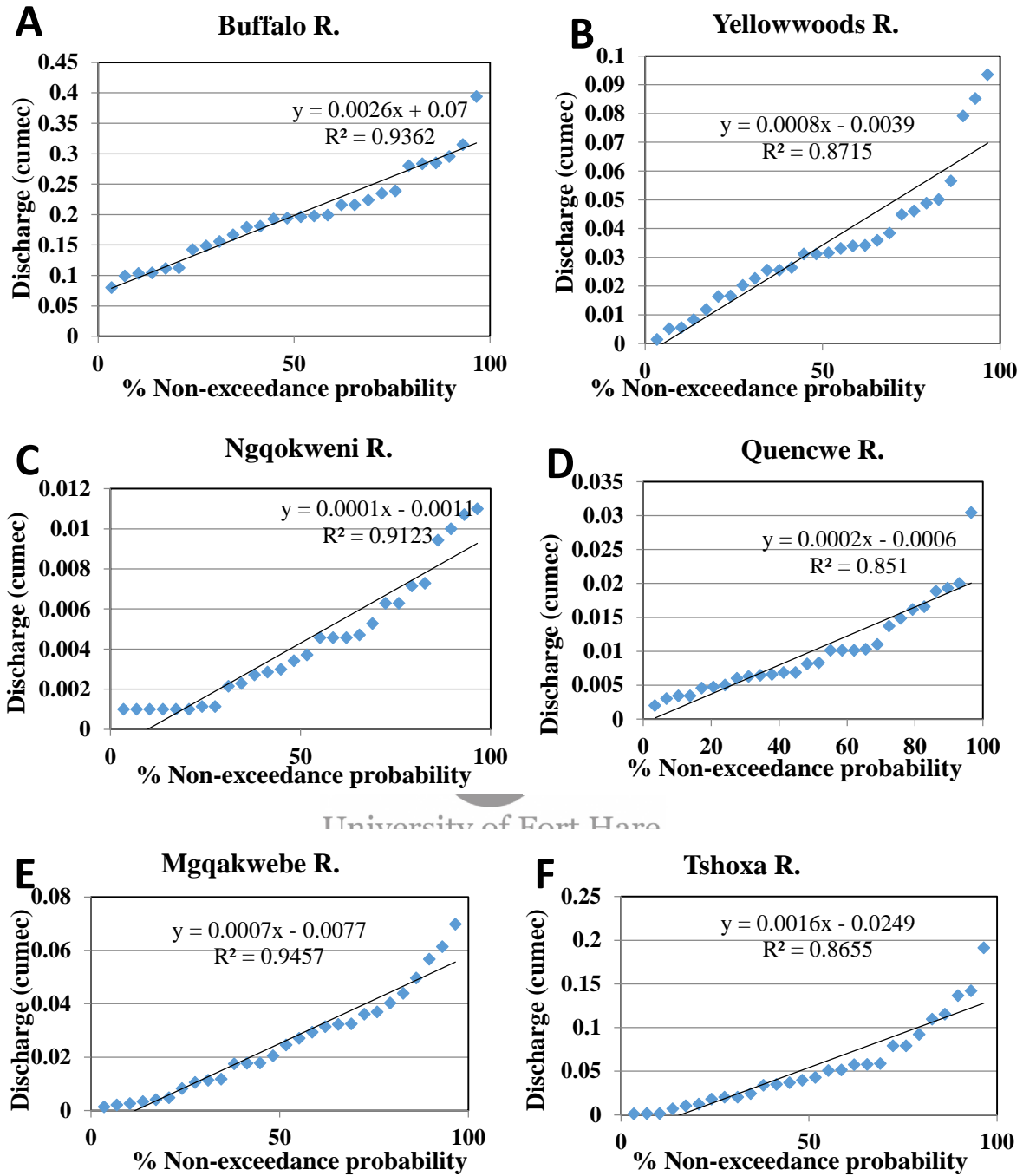


Figure 6. 2: Low FDC plot using 95th percentile time exceeded for; A) Buffalo, B) Yellowwoods, C) Ngqokweni, D) Quencwe, E) Mggakwebe, and F) Tshoxa stations.

The potential for groundwater discharge is majorly controlled by hydraulic conductivity which is possibly low for the Ngqokweni basin compared to the Tshoxa basin. More so, Tshoxa has a smaller area cover of dolerite and is likely to retain most of its rainfall-induced groundwater recharge due to its sandstone-dominated basin lithological property. The fraction of sandstone-rich lithologic materials and fractured and weathered dolerite sections

within the Yellowwoods basin may have favored the groundwater discharge that supports Yellowwoods flow in low-flow periods. Quencwe basin has a larger area cover of dolerite than others and steep relief. It also has more throughflow tendency due to hillslope which may limit the development of the aquifer. The poor streamflow rate in Ngqokweni station may be due to the low hydraulic conductivity of soil and lithologic material in the area.

Table 6. 2:Summary of FDC results.

Period	High flow slope	Low flow slope	95th percentile time exceeded	7D-10years	7D-100years	
Buffalo	-0.84	-0.0113	0.0026	0.096	0.33	
Yellowwoods	-2.1	-0.0022	0.0008	0.0041	0.0761	
Ngqokweni	-0.73	-0.00049	0.0001	-0.0001	0.0089	
Quencwe	-1.35	-0.0009	0.0002	0.0014	0.0194	
Mgqakwebe	-1.02	-0.0017	0.0007	-0.0007	0.0623	
Tshoxa	-5.55	-0.0029	0.0016	-0.0089	0.1351	
Color legend						
Color rank	1	2	3	4	5	6

6.2.4 Baseflow separation

BFI plot provides information on watershed hydraulic properties controlling storagedischarge attributes of the aquifer to support environmental flow, such as transmissivity, porosity, permeability, and hydraulic gradient. Results of the mean annual baseflow separation are presented in Table 6.3. Two parameter digital filter (TwoPDF) approach provides the reading with the highest estimation while the baseflow index modified (BFI modified) approach provided the lowest estimation.

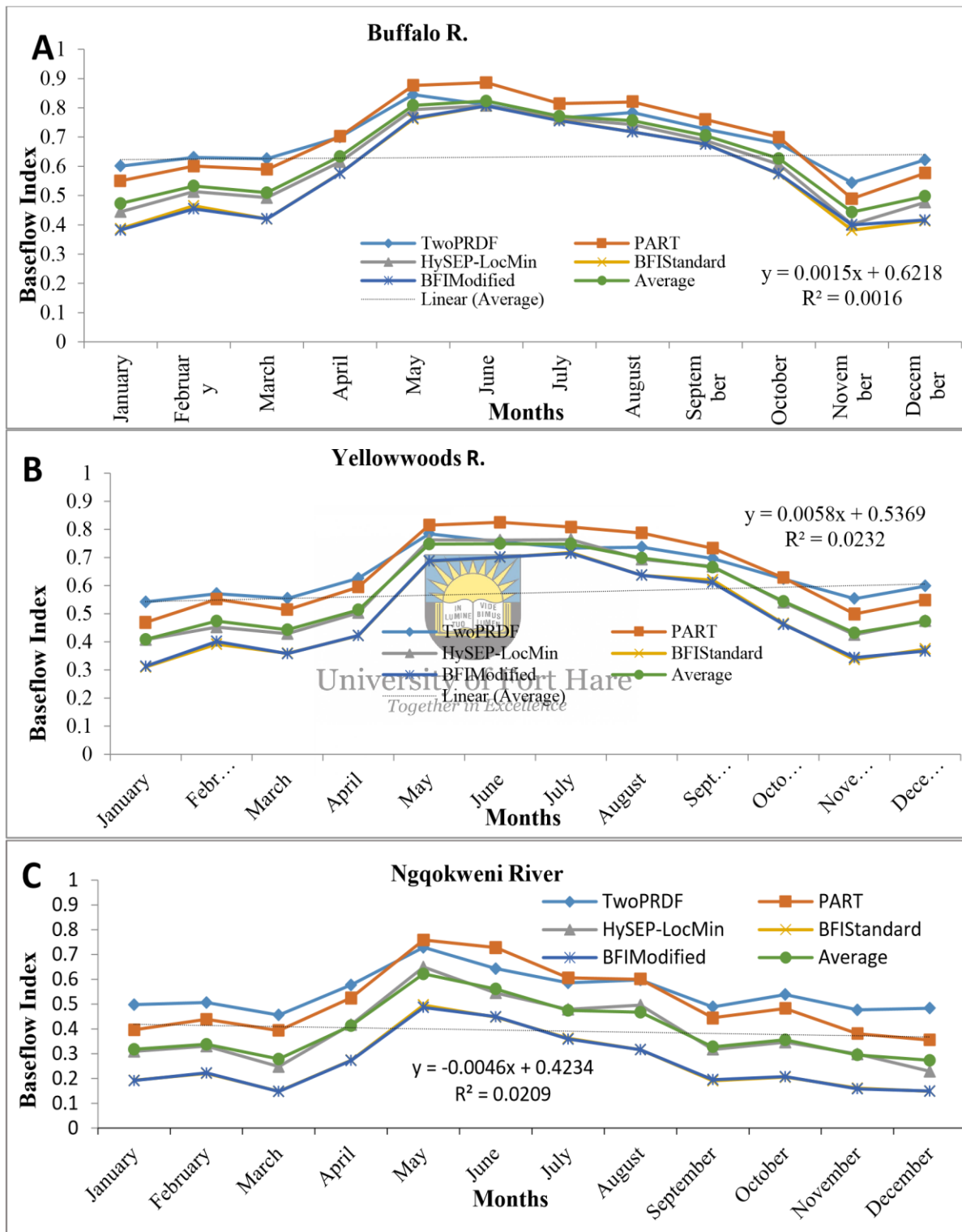
Table 6. 3: Long-term average annual baseflow for streamflow of 1977 to 2016.

Station	Two PRDF	PART	HySEP- Loc Min	BFI Standard	BFI Modified	Average Baseflow
Buffalo	0.596	0.599	0.525	0.492	0.491	0.541
Yellowwoods	0.551	0.551	0.487	0.426	0.426	0.488
Ngqokweni	0.460	0.432	0.327	0.218	0.217	0.332
Quencwe	0.502	0.484	0.448	0.318	0.321	0.415
Mgqakwebe	0.529	0.515	0.450	0.361	0.358	0.443
Tshoxa	0.541	0.512	0.460	0.369	0.368	0.450

Plots of monthly variation of BFI are presented in Figure 6.3A - F. From the plots, streamflow composing of a baseflow index of 0.5 or greater ($BFI \geq 0.5$) implies that the streamflow is dominated by 50% and more of baseflow discharges. Hence, the information on the $BFI \geq 0.5$ significantly highlights the streamflow with viability for environmental flow sustenance through the dry season of the hydrologic regime. Figure 6.3A - F reports that the months of dominant baseflow discharge across the watershed begins in June through August. The increase in run-off proportion in the spring indicates the inception of rainfall events in the watershed.

Specifically, Buffalo station has the highest baseflow discharge across the hydrologic period (Figure 6.3A). The discharge is dominant from February ($BFI = 0.532$) through October ($BFI = 0.626$). The station reported the maximum relative baseflow discharge in the watershed in June ($BFI = 0.823$). The result suggests that the watershed is heavily sustained by baseflow across the hydrologic period. The dominant baseflow discharge in Yellowwoods flow occurs in April ($BFI = 0.513$) through October ($BFI = 0.543$). For Mgqakwebe flow, it occurs in April ($BFI = 0.503$) through September ($BFI = 0.521$). For Tshoxa flow, it occurs in May ($BFI = 0.721$) to September ($BFI = 0.637$). For Quencwe flow, it occurs in April ($BFI =$

0.500) through August (BFI = 0.555). Meanwhile for the Ngqokweni flow it occurs in May (BFI = 0.621) and June (BFI = 0.561).



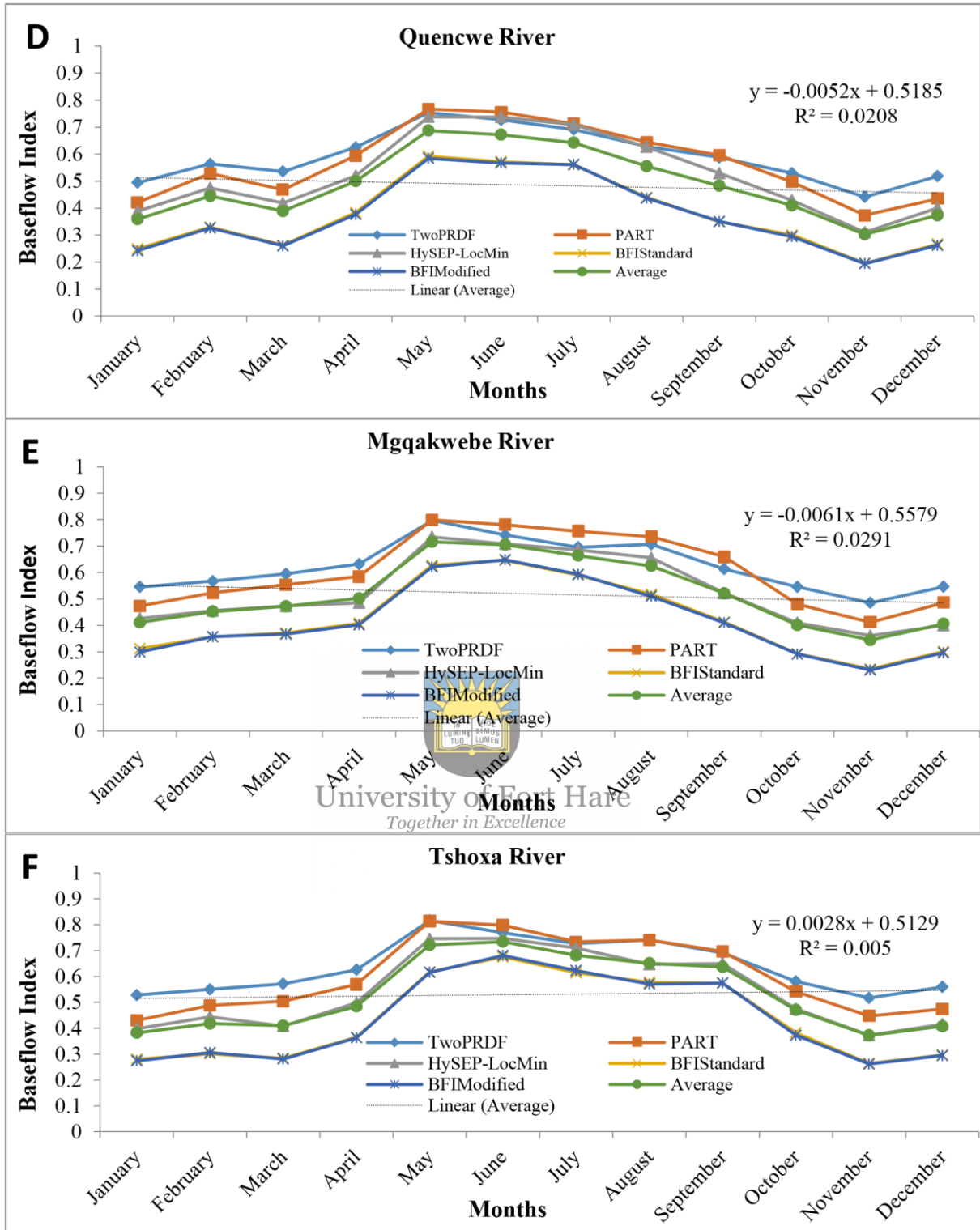


Figure 6. 3: Mean Annual BFI plots for; A) Buffalo, B) Yellowwoods, C) Ngqokweni, D) Quencwe, E) Mggakwebe, and F) Tshoxa stations.

The results report Ngqokweni as having the least baseflow discharge. It also indicates that Ngqokweni drainage is highly vulnerable to drought owing to the few months of baseflow discharge. Baseflow discharge depends on the hydraulic conductivity of the lithology materials in the hydrologic basin. The result implies that surface lithology of the Ngqokweni basin is dominated by lithologic material with low hydraulic conductivity. The BFI results also indicate Yellowwoods as having a sustainable streamflow structure owing to the extent of baseflow discharge across the hydrologic period.

6.3 Summary

Recession attributes of rivers in the Buffalo basin headwater have been evaluated using FDC and BFI analysis. Comparison across the results of the methods employed and previous literature findings are extensively discussed in chapter 9. Meanwhile, the following deductions can be made from the study;



University of Fort Hare

- i. Seven days moving average is recommended for smoothening of FDC plots.
- ii. The order of high flow variability suggests the influence of rainfall variability and hillslope factor, especially at the high altitude.
- iii. 95th percentile exceeded plot and the low flow section of FDC validates the applicability of 100-year return plots for environmental flow assessment.
- iv. The results of low flow assessment conform to the results of BFI plots and indicate the influence of variability in sub-basin hydraulic properties.
- v. The results reveal the viability of Buffalo station as an important surface water capture zone as the BFI results indicate abundant streamflow sustenance across most of the hydrologic periods.
- vi. The hybrid approach of FDC and BFI may be required for holistic streamflow recession study and river classification.

Chapter 7: Evaluation of geomorpho-tectonic settings

7.1 Introduction

This chapter reports the result of the evaluation of subsurface structural variability of the watershed for groundwater exploration potential. Detailed findings of the explored parameters, comparative deductions with other morphometric parameters, their implication to geomorphological settings, environment and for the decipherment of aquifer interaction were established.

7.2 Results

7.2.1 Physiographic settings

The physiographical settings of the Buffalo basin can be classified into three main zones – the hilly terrain (north-west/north), the dissected plain (south-west/central north-east), and the plain (south/south-east) (Figure 7. 1).

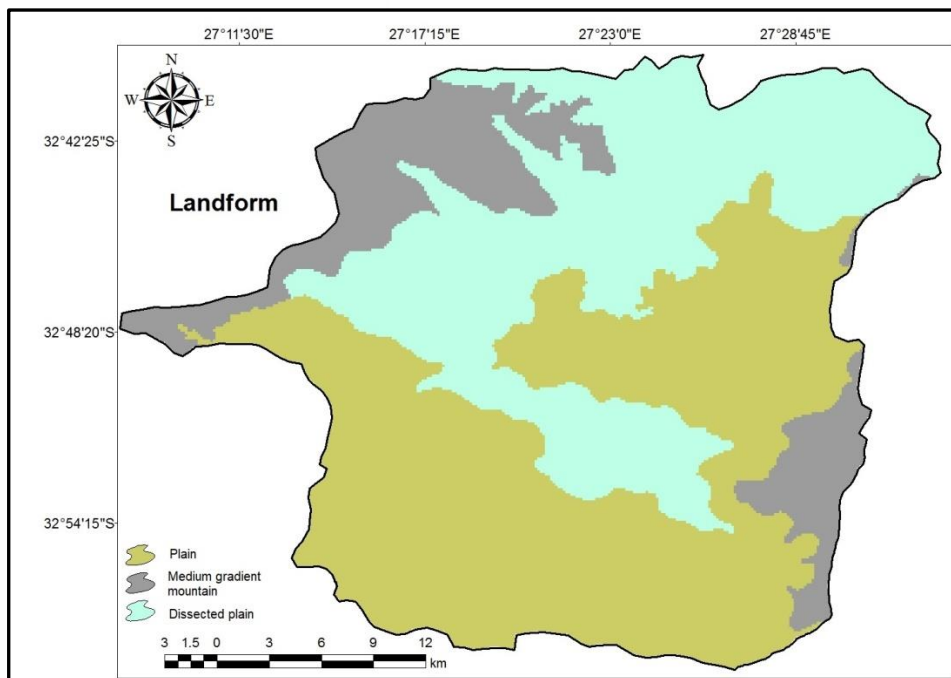


Figure 7. 1: Landform map of Buffalo basin headwater showing the geomorphic dissections of landmass (Dijkshoorn et al., 2008).

Field assessment for the features of river stages and river channel characteristics were summarized in the field grouped based on field information as shown in Figures 7.2 A – F and 7.3. The hilly terrain covers the entire Quencwe and major part of Mgqakwebe sub-basins. It is characterized by extensive dissection, sloping terrains and surficial lineaments orienting in NWW to SEE in the direction of the drainage network. The sediments towards the hilly terrains are massively covered by alluvial deposits (Figure 7.2 A, B & D).



Figure 7. 2: Field photographs showing: (A) thick alluvial deposit; (B) boulders, cobbles and dolerite intrusions in the Quencwe River channel at the hilly terrain; (C) wide channel and gravelly deposits of Buffalo River; (D) boulders, cobbles and pebbles on upper course of Mgqakwebe River channel (West); (E) wide and rapid flow at the lower course of Mgqakwebe River, and; (F) wide channel of lower course of Yellowwoods River with riparian forest.

The river channel at the hilly terrain is mainly covered by boulders and cobbles especially across most of the length of Quencwe River and the upper course of Mgqakwebe River (Figure 7.2 B & D). Most of the outcrops across the Quencwe River were densely fractured and jointed (Figure 7.3). Fractures and joints indicating induction of extensional stress were

visible on the outcrops. Fractures developed from extensional stress constitute pathways for infiltration and percolation for local groundwater and surface water interaction. The plain is characterized by a gentle slope and wide river channel (Figure 7.2F). The embankment is characterized by either visible fine sediment deposit or riparian vegetation. The sediments of dissected plain range in grain size from cobbles to gravel sediments depending on the gentleness and linearity of the channel (Figure 7.3 C & F).



Figure 7. 3: Massive joints in rocks along embankments and channels of the Quencwe River. The direction of joints indicating the effect of extensional stress was indicated with a red arrow. The extensional stress is significant for its productive influence on interflow and recharge from baseflow.

7.2.2 Morphometric analysis

The morphometric estimation summary is represented in Table 3.2 and Tables 7.1 – 7.4. The summary of drainage network analysis consider in this work is presented in Figure 7.4 and Table 7.1. Buffalo drainage is fifth-order drainage which implies a moderate potential for flash floods. This implies that the drainage pattern in Buffalo is influenced by five unique hydrostratigraphic layers whose variation in relief and lithology may influence the hydrodynamic response of stream at the catchment mouth (Figure 7. 4A). The proportionate relationship between stream order and the stream length for the study area indicates the tendency for groundwater discharge (Pareta and Pareta, 2011). Considering the size of

Buffalo basin, there is a major control over the occurrence of flash floods. The bifurcation ratio ($R_b = 2.0$) of the basin suggest a minimum structural disturbance of drainage, which implies that the flow is gentle and steady.

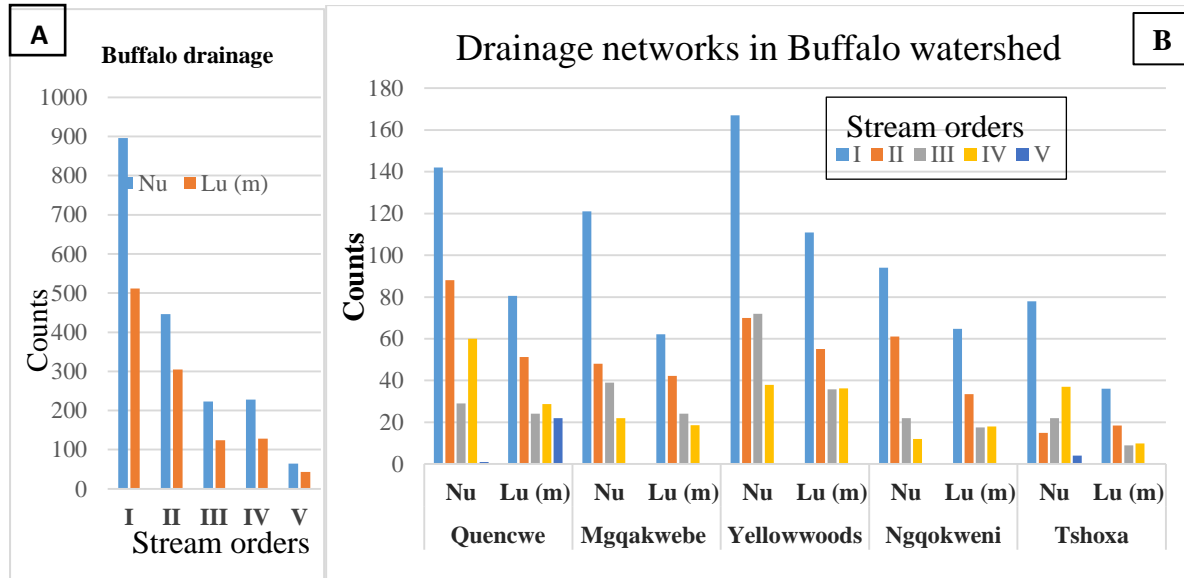


Figure 7. 4: Comparative summary of stream orders (Nu) and total stream length (Lu). A. Buffalo drainage B. The sub-basins drainage networks in the watershed. Quencwe and Tshoxa stations are associated with five stream orders while Mgqakwebe, Yellowwoods, and Ngqokweni have four.

Table 7. 1: Calculated drainage network attributes of Buffalo watershed.

Drainage network	Buffalo	Quen	Mgqa	Yell	Ngqo	Tsho
Number of stream segment, Nu	1857.00	320.00	230.00	347.00	189.00	156.00
Total stream length per, Lu (km)	1112.07	206.75	147.18	238.07	133.64	73.49
Weighted Mean Bifurcation Ratio (Rbwm)	2.00	8.91	2.02	1.86	1.95	4.01
Weighted mean stream length (Luw _m)	1.07	8.39	75.03	105.10	52.96	1.51

Similarly, the fifth-order attributes exhibited by Tshoxa and Quencwe basins indicate that the two basins have a highly variable hydrogeologic property which may influence hydrologic attributes of the drainage (Figure 7. 4B). However, the bifurcation ratio of the two basins indicates the influence of basin structure on the streamflow. Hence, the streamflow in the two stations is possibly turbulent while that of Quencwe indicates the tendency for flooding. The

streamflow at Mgqakwebe, Yellowwoods, and Ngqokweni drainage are possibly gentle based on the report of the Bifurcation ratio (Table 7. 1). The flow in the Quencwe basin is either influenced by the hillslope factor or dam release. However, the high relief plays a major role in the run-off velocity.

A summary of the watershed geometry analysis with information on the form factor is presented in Table 7.2. For Buffalo basin as a whole, the form factor estimate implies the tendency for occasional flooding as a result of a high discharge rate at the catchment mouth. The account of the texture ratio of Buffalo basin indicates Buffalo basin is dominated by impermeable lithologic materials. Its elongation ratio is the circular type and this indicates the efficiency of its runoff. Its circularity ratio indicates that its hydrologic property is mature.



Table 7. 2: Calculated characteristic geometry of Buffalo watershed.

Watershed Geometry	Buffalo	Quen	Mgga	Yell	Ngqo	Tsho
Basin area, A (km ²)	1237.00	200.89	172.56	264.37	149.32	93.13
Basin perimeter, P (km)	170.96	60.00	74.74	97.43	58.55	45.16
Basin Length, Lb (km)	42.97	19.36	29.34	36.50	23.74	16.77
Form factor (Ff)	0.67	0.54	0.20	0.20	0.27	0.33
Elongation ratio (Re)	0.92	0.83	0.51	0.50	0.58	0.65
Texture ratio (Rt)	5.24	2.37	1.62	1.71	1.61	1.73
Circularity ratio (Rc)	0.53	0.70	0.39	0.35	0.55	0.57

Form factor estimation for Quencwe station suggests that the basin has the potential for flooding. The proximity of Quencwe station to the great escarpment has been reported for the extremity of rainfall in the sub-basin (Slaughter et al., 2014). This finding aligns with the result of the bifurcation ratio, indicating the influence of topographic complexity on the turbidity of flow in the Quencwe basin compared to the rest. As for Tshoxa sub-basin, the form factor indicates a balance between the potential for recharge and flooding. This result reveals the evidence of flow regulation which can be linked with regulated and perennial

discharge from baseflow since the drainage station is not fed by headwater from high relief. The turbidity of its flow may only result during excessive groundwater discharge and dam release influence on runoff. The results of form factor for other stations (Ngqokweni and Mgqakwebe) reveal wholly accommodated flow, the higher potential for recharge rather than discharge and more frequent laminar flow. The form factor of the Yellowwoods basin indicates that its storm generation potential is extremely under control, hence, its flow is more often laminar while its high stream segment suggests high streamflow accumulation.

Information on texture ratio across the sub-basins further reveals variation in the impact of lithology and relief on infiltration. Tshoxa, Quencwe and Yellowwoods stations reveal the potential for infiltration and development of drainage. For the Tshoxa basin, it is possibly due to large sections of the basins' lithology dominated by sandstone lithosome while in Yellowwoods it is possibly due to high weathering and fracture of dolerite and sandstone at the northern half of the basin. The southern half is dominated by mudstone and sandy silt. Mgqakwebe and Ngqokweni stations have higher infiltration capacity due to their lithology influence in accordance with their texture ratio. The elongation ratio reveals that Quencwe is oval while Tshoxa may as well be considered being oval. This implies efficiency of run-off in the two sub-basins, meanwhile, other sub-basins are elongated, and are therefore inefficient in a run-off. In terms of circularity ratio, Quencwe drainage revealed the strongest impact of geologic, land use/land cover, climate and relief evolution of its sub-basin and is therefore described as being at its old dendritic stage. Mgqakwebe and Yellowwoods sub-stations are young in impact with respect to this, while others are described as being mature with respect to this impact.

A summary of the drainage texture analysis is presented in Table 7.3. The drainage texture for Buffalo watershed varies from coarse to fine in drainage network texture. Holistically, the watershed possesses very fine drainage network texture and a moderate tendency for stream

discharge. Only Quencwe reveals a fine texture while others are moderately coarse. The stream frequency reported by the Tshoxa basin exhibited a negative correlation with drainage density as compared to others, that is, the impact of stream dissection favors streamflow productivity in Tshoxa (Singh et al., 2013). The low drainage density indicates the potential for infiltration in the basins. Although all the sub-basins indicate low drainage density, there is higher resistance in Quencwe station which can be linked with the impact of dolerite intrusion of the drainage. Tshoxa low drainage density indicates the dominance of fractured sandstone within its basin.

Table 7. 3: Calculated drainage texture attribute of Buffalo watershed.

Drainage texture	Buffalo	Quen	Mgqa	Yell	Ngqo	Tsho
Drainage texture (Dt)	10.86	5.33	3.08	3.56	3.23	3.45
Stream frequency (Fs)	1.50	1.59	1.33	1.31	1.27	1.68
Drainage density (Dd)	0.90	1.03	0.85	0.90	0.90	0.79
Constant of channel maintenance (C)	1.11	0.97	1.17	1.11	1.12	1.27
Infiltration Number (IfN)	1.35	1.64	1.56	1.18	1.13	1.32

With respect to the constant of channel maintenance, Tshoxa sub-basin is flagged as the most maintained with respect to lithological control on surface permeability. Estimates reveal that Quencwe station is the least maintained with respect to natural drainage development. The infiltration potential validates the texture ratio deduction on the tendency for discharge rather than infiltration in the Buffalo watershed. The same goes for Quencwe sub-basin. Ngqokweni shows a higher tendency for infiltration due to the low infiltration number.

A summary of the relief characteristics of the basin is presented in Table 7.4. The relief ratio estimation revealed that the flow in the Quencwe basin is more likely to be converted into run-off and this is possibly due to the hillslope factor. The relief ratio indicates that the Ngqokweni basin has the least tendency to develop run-off and this can possibly be due to its

planal physiography. In general, Buffalo basin has moderate physiography with a varying spatial tendency for run-off and storage. Length of overland flow specifically indicates that all the sub-basin have the tendency to infiltrate its flow content owing to their long flow-path being higher than 0.3. The ruggedness number of Buffalo basin reveals that the entire basin has a high susceptibility to erosion. Across the sub-basins, Quencwe has the highest tendency and Tshoxa has the least tendency for erosion.

Table 7. 4: Calculated relief characteristics of Buffalo watershed.

Relief Characteristics	Buffalo	Quen	Mgqa	Yell	Ngqo	Tsho
Relief, R (Km)	1.112	0.943	0.914	0.670	0.285	0.280
Relief ratio (Rhl)	0.0259	0.0487	0.0312	0.0184	0.0120	0.0167
Relative relief ratio (Rhp)	0.650	1.572	1.223	0.688	0.487	0.620
Ruggedness number (Rn)	1.00	0.97	0.78	0.60	0.26	0.22
Length of overland flow (Lf)	0.56	0.49	0.59	0.56	0.56	0.63

University of Fort Hare

7.2.3 Electrical resistivity tomography survey

The plot of apparent resistivity against half current electrode spacing indicates that the study area is characterized by four-layered structures, specifically VES-type HA. The layer resistivity, thickness, and root mean squared error for the fifteen VES stations are presented in Table 7.5 (Figure 7.4). The pseudo-sections were drawn in RES2DINV software and are presented in Figure 7.5. The results of the lithologic log drawn using IPI2WIN software indicate the presence of four subsurface layers for the shallow subsurface sections.

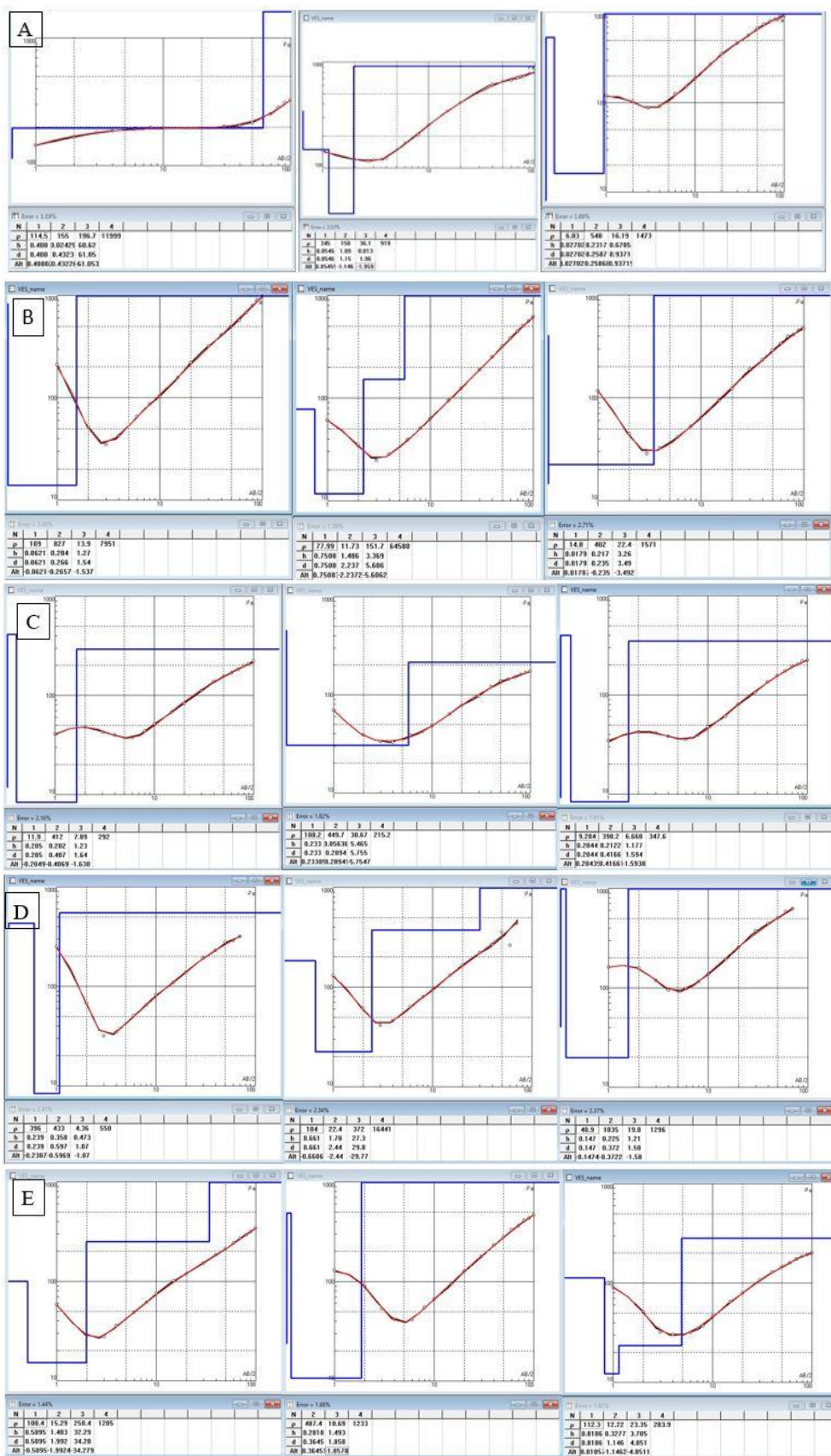


Table 7. 5: IPI2WIN inversion results for; A) Quencwe VES, B) Mggakwebe VES, C) Yellowwoods VES, D) Ngqokweni VES, E) Buffalo VES.

Table 7. 6: Summary of IPI2WIN VES data interpretation for the five sounding stations.

VES No.	Stations	VES type	ayer resistivity (Ωm)				Layer thickness (m)			Root mean square
			ρ_1	ρ_2	ρ_3	ρ_4	h1	h2	h3	%
1	Ngqo	HA	186	62.4	42.5	527	0.35	2.10	3.33	1.10
2		HA	182	25.8	396	16441	0.64	2.09	29.76	1.81
3		HA	181.9	45.01	17935	1186	1.45	2.69	0.51	1.25
1	Mgqa	HA	99.3	771	14.4	63339	0.05	0.22	1.34	3.22
2		HA	59.31	778.6	21.8	27849	0.19	0.08	2.21	1.99
3		HA	14.5	404	22.6	2710	0.02	0.22	3.61	2.66
1	Quen	HA	114.5	155	196.7	11999	0.41	0.02	60.62	1.19
2		HA	345	150	36.1	919	0.05	1.09	0.81	2.12
3		HA	6.83	540	16.19	1473	0.03	0.23	0.68	1.69
1	Yell	HA	11.9	412	7.89	292	0.21	0.20	1.23	2.16
2		HA	100.2	449.7	30.67	215.2	0.23	0.29	5.76	1.82
3		HA	9.28	398.2	6.67	347.6	0.20	0.21	1.18	1.91
1	Buff	HA	120.5	128.1	20.99	453.2	0.17	0.23	2.39	1.87
2		HA	20.8	768	32	20243	0.06	0.15	5.57	2.13
3		HA	10.9	373	26.4	276	0.03	0.17	4.84	2.05

By inferring the hydraulic conductivity from the inverse of resistivity property of the area, variation in aquifer property of the sub-basins represented can be deduced. Only Ngqokweni station has its aquifer properties in the second layer. Its aquifer thickness varies from 2.0 – 5.0 m. Aquifer thickness in Mgqakwebe station varies from 2.0 m to 8.0 m. It varies from 1.5 m – 8.0 m in Quencwe station, 1 – 10 m in Yellowwood station and 0.5 – 6.0 m in Buffalo station. An attempt to align the results with borehole log information shows that baseflow into the river channels were mostly from the alluvial cover and weathered sandstone. Reconciliation of thickness generated from IPI2WIN deductions to the borehole lithologic log is quite difficult and this further reveals the weakness of the IPI2WIN results.

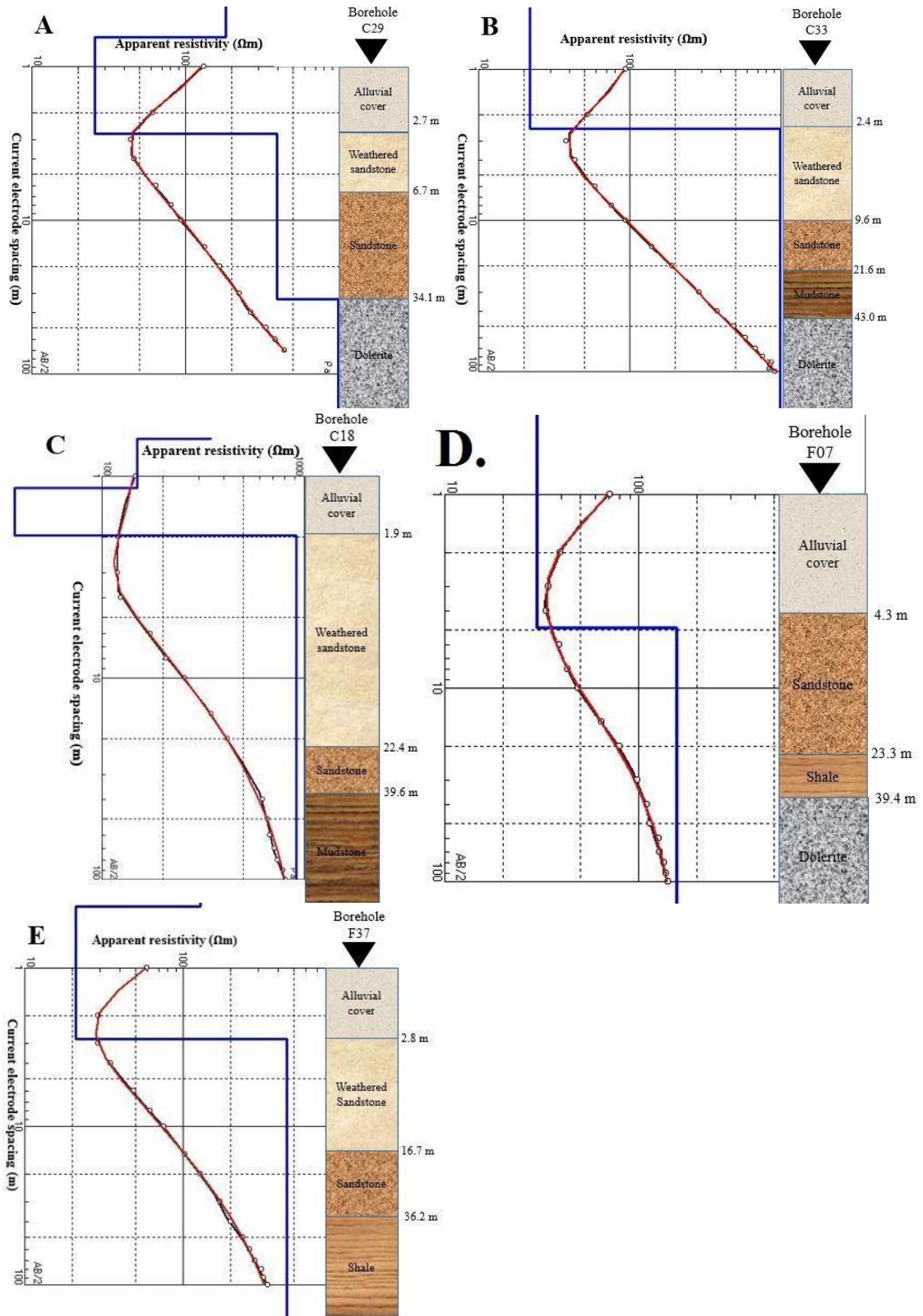
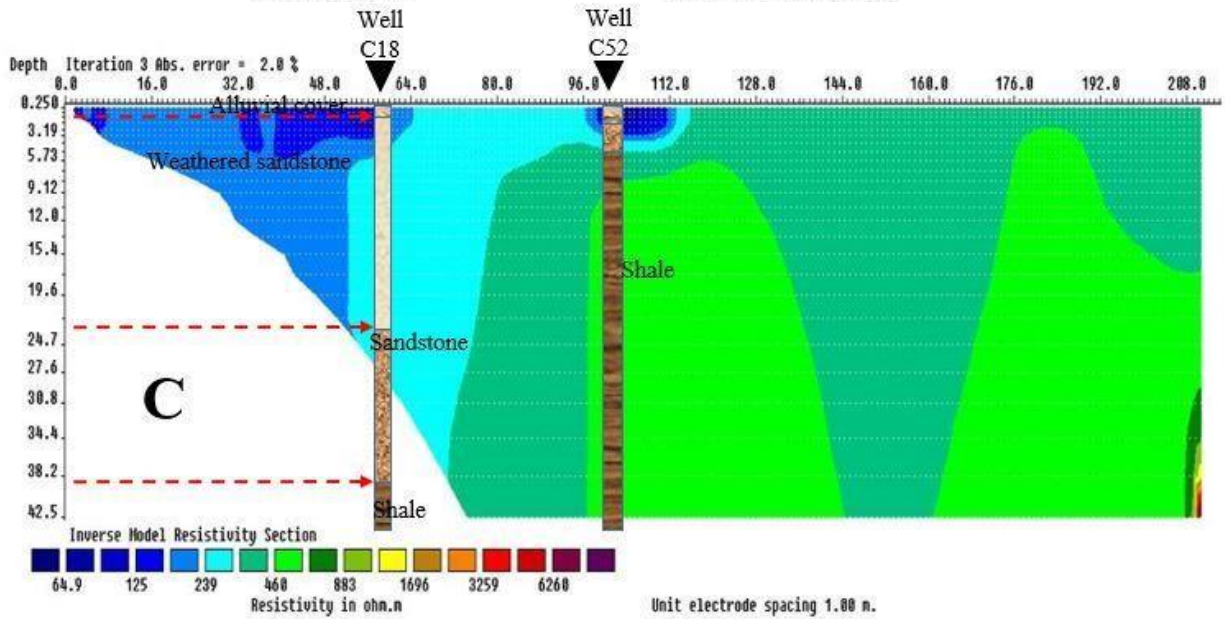
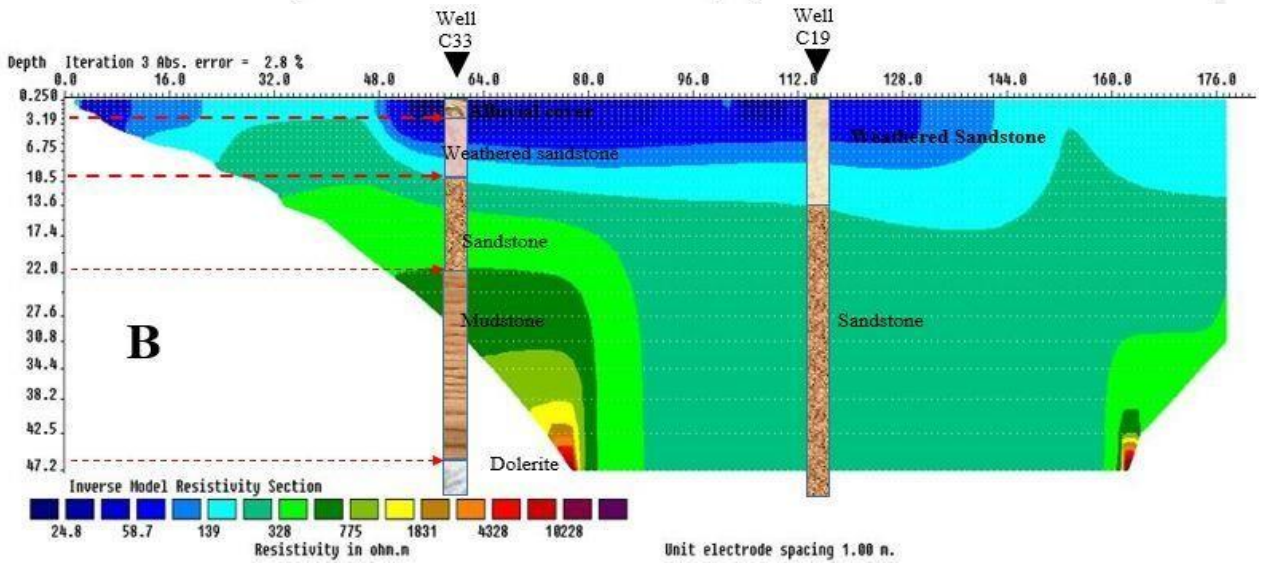
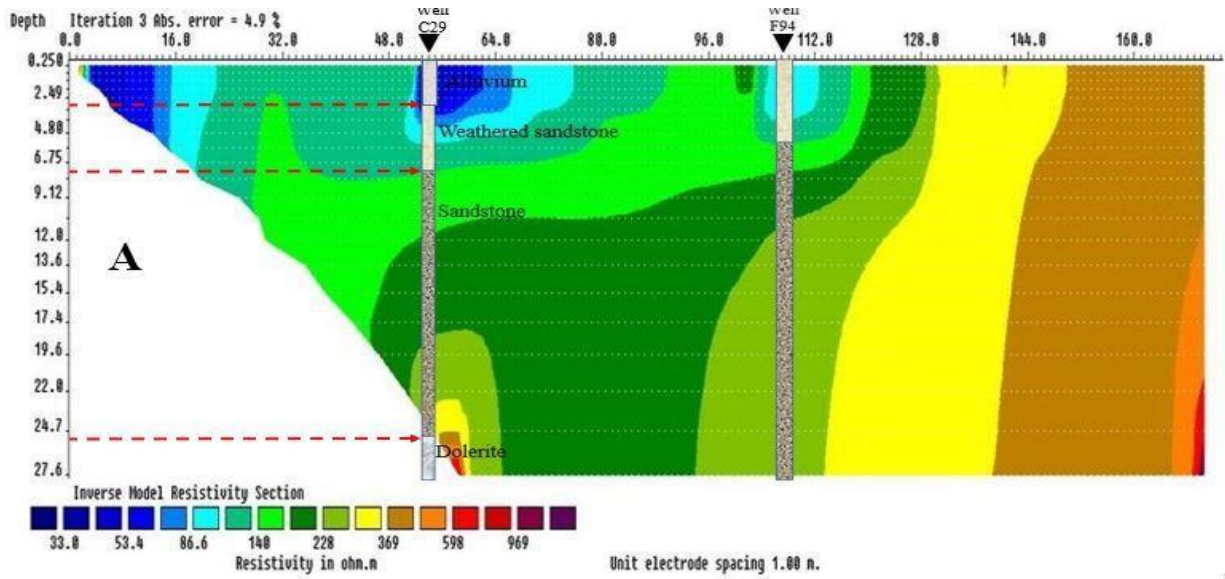


Figure 7. 5: Calibration of VES curve with borehole-log information for; A) Ngqokweni VES 2, B) Mgqakwebe VES 2, C) Quencwe VES 2, D) Yellowwoods VES 2, and E) Buffalo VES 2 .



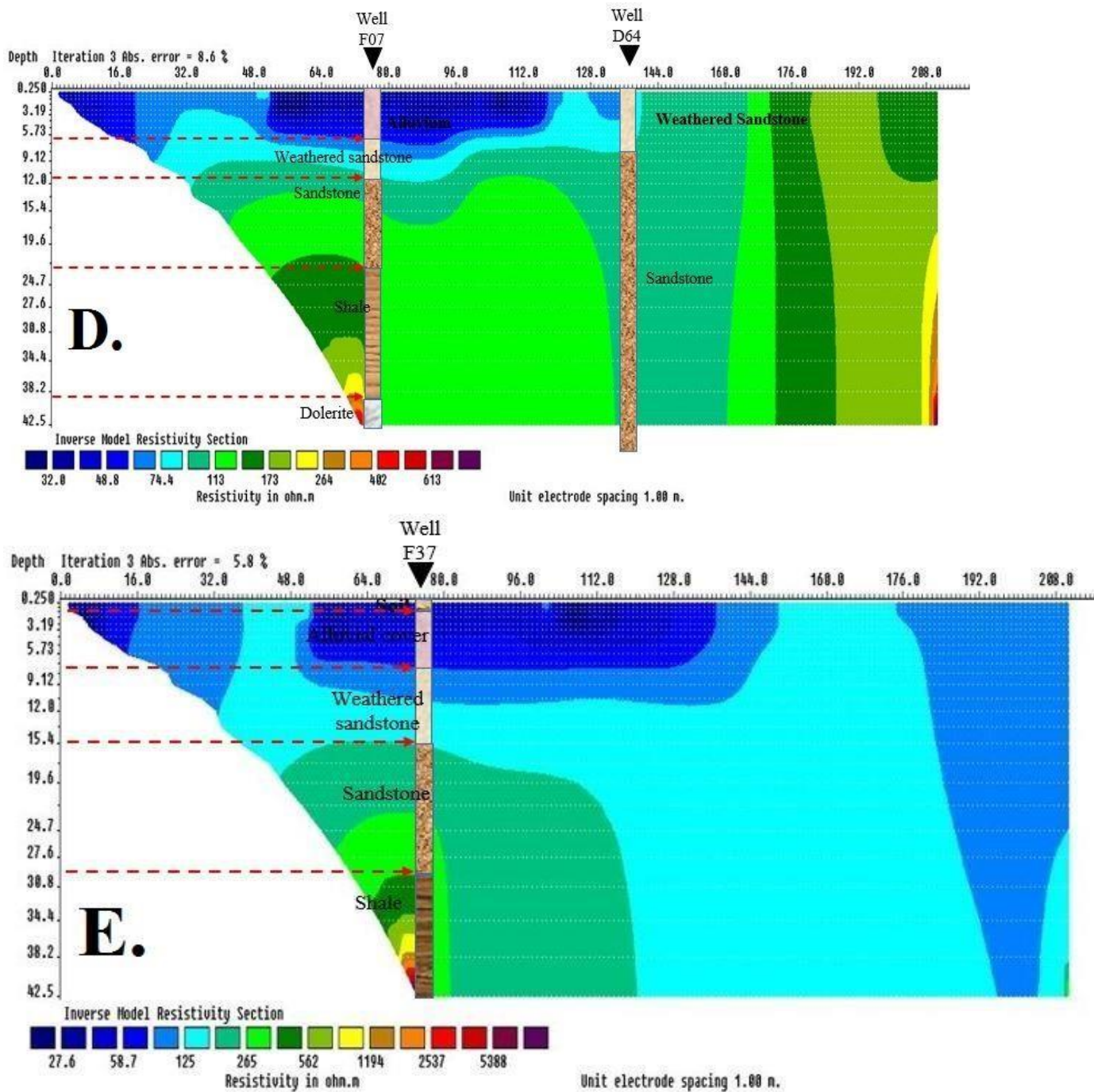


Figure 7. 6: Pseudo-sections showing sounding at; A) Ngqokweni, B) Mgqakwebe, C) Quencwe, D) Yellowwoods, and E) Buffalo stations.

A comparison of the curve with borehole-log information is presented in Figure 7.5. In the RES2DINV result, the variation in electrical resistivity can be aligned with the lithological profile of proximal boreholes. The pseudosections indicate that Buffalo watershed is sustained by groundwater from a shallow unconfined aquifer. Many of the pseudosections

reveal a fault system within the geologic system of the watershed which could facilitate an important groundwater conduit.

Buffalo pseudosection reveals that the aquifer is well-drained at the catchment mouth. The section reports the thickest low resistivity layer (≥ 15 m) compared to other points in the watershed. The low resistivity section indicates high porosity and permeability and these are possibly due to the thickness of alluvial cover as well as the weathering and complex fracture system of Balfour sandstone. Hence, the mouth of the Buffalo catchment can serve as a viable capture zone for groundwater flow. Mgqakwebe pseudosection also reports a low resistivity layer across its top lithological layer. This is possibly due to the weathered sandstone lithosome that dominates the basin. The pseudosection also suggests that the porous hydrostratigraphy is well-drained with a minimum aquifer thickness of 19.3 m. The Yellowwoods pseudosection revealed a well-drained low resistivity section which indicates the existence of a fracture system that facilitates high groundwater drainage potential within a 12 m thick section of the aquifer. Quencwe and Ngqokweni pseudosections showed the poorest potential for groundwater flow. Quencwe section indicates high variability in groundwater flow section. The Ngqokweni pseudosection indicates a complex geologic system that is possibly dominated by fine-grained geologic materials. Its poor groundwater drainage is possibly due to poor atmospheric circulation or a high rate of groundwater evaporation.

7.3 Summary

Integration of the geomorpho-tectonic perspective using morphometric parameters and geologic assessment using ERT has been carried out. This was done with the intention to infer the geomorphic and the hydraulic conductivity properties of the catchment lithology in

relation to sub-basin groundwater potential. Based on the study, the following summaries are made;

- Buffalo catchment is characterized by shallow unconfined aquifer hosted by its alluvial sediments, fractured, and weathered sandstone. The sub-basins are characterized by varying hydraulic properties across their sub-basins.
- The sub-basins associated with dolerite intrusion reveal the existence of a fault system. The zones with high relief are characterized by flooding potential.
- The possibility of uneven rainfall distribution which favors the basins with high relief and steeply topography can be inferred from some of the morphometric parameters.
- The Quencwe basin indicates the potential for rainwater harvest. The basin has the potential to develop flash floods. It has heterogeneous hydraulic property, low infiltration, and high erosion potential which may have an influence on its groundwater potential.
- Tshoxa and Mgqakwebe sub-basins were shown to be important groundwater capture zones. Flooding potential in the basin may be due to the favorable rainfall distribution; however, this is balanced by the lithological property with high infiltration capacity. This was shown to be a weathered and fractured sandstone lithosome.
- Yellowwoods basin indicates the potential for streamflow sustenance despite the premature status of the drainage. This can be linked with the groundwater potential of the headwater which is characterized by well-developed infiltration capacity. There is no adequate information on the groundwater potential of the sub-basin.
- Ngqokweni basin shows high groundwater vulnerability.



University of Fort Hare

Together in Excellence

Chapter 8: Investigation for groundwater potential zonation

8.1 Introduction

This chapter reports the results of integration of geologic, hydrologic, geomorphic and environmental factors for exploration of groundwater potential. The results of model validation, interpretation and implications are also presented with an attempt to motivate conjunctive approaches and improve the integrity of an effective regional groundwater exploration program.

8.2 Attributes of thematic maps

8.2.1 Dominant surficial lithology

The surficial lithology map has been prepared using the geological map sheet of the Council of Geological Survey at 1:250,000 scale as the base map (Figure 8.2).

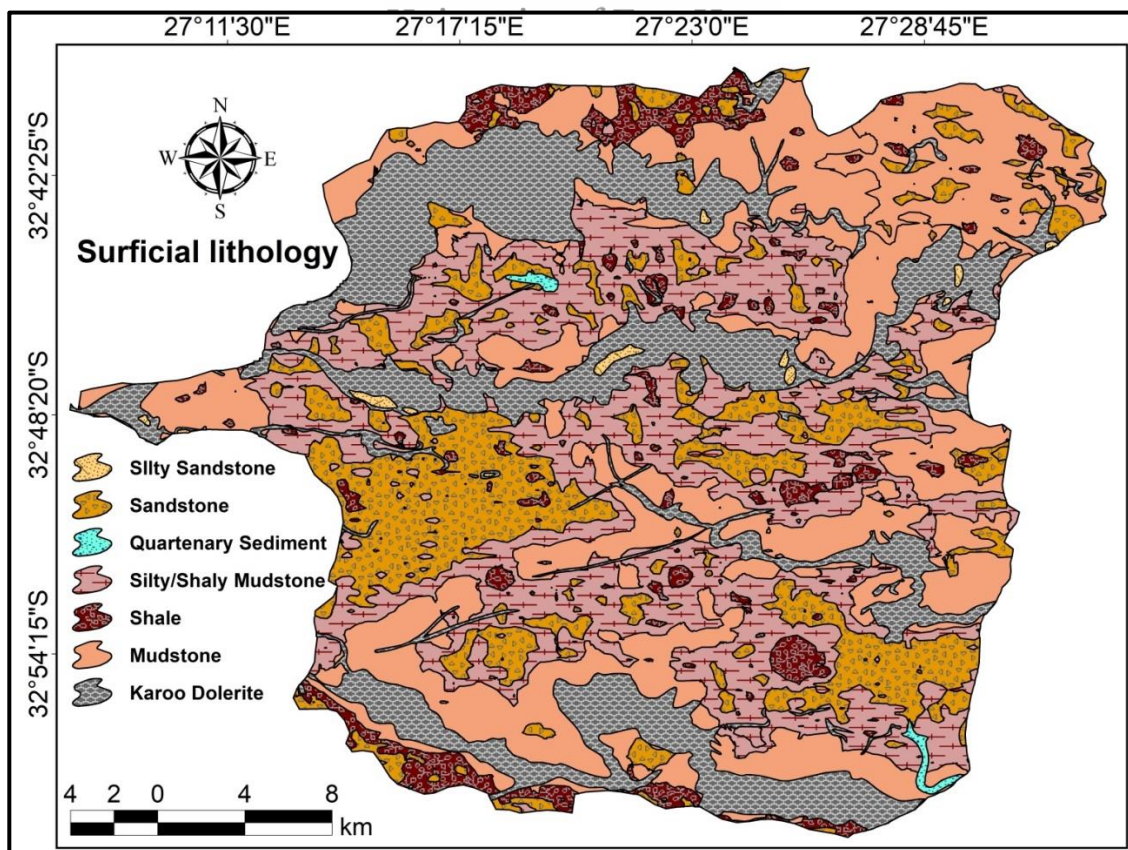


Figure 8. 1: Map of dominant surficial lithology.

The surficial lithology is dominated by Mudstone (359 km²) covering 29% of the area. Dolerite (281 km²), sandstone (189 km²), shale (56 km²), and Quaternary sediment (4 km²) covers 23%, 15%, 5% and 0.3% of the river catchment. The silty sandstone and silty/sandy mudstone intercalation units were estimated to cover approximately 340 km² and 8 km² of the area respectively. Hydraulic conductivity is one of the foremost aquifer properties that determine groundwater recharge and storage potential of a lithology. According to Domenico and Schwartz (1990), Quaternary Sediment was considered as the highest important for groundwater storage on account of its high hydraulic conductivity, followed by sandstone, silty sandstone, and silty/sandy mudstone. The least important for the groundwater storage is the dolerite rock, followed by the shale and the mudstone.

8.2.2 Lineament density

The lineament density map is classified into five; the very high (4%), high (10), moderate (17), low (25), and the very low/none lineament density area (Figure 8.3).

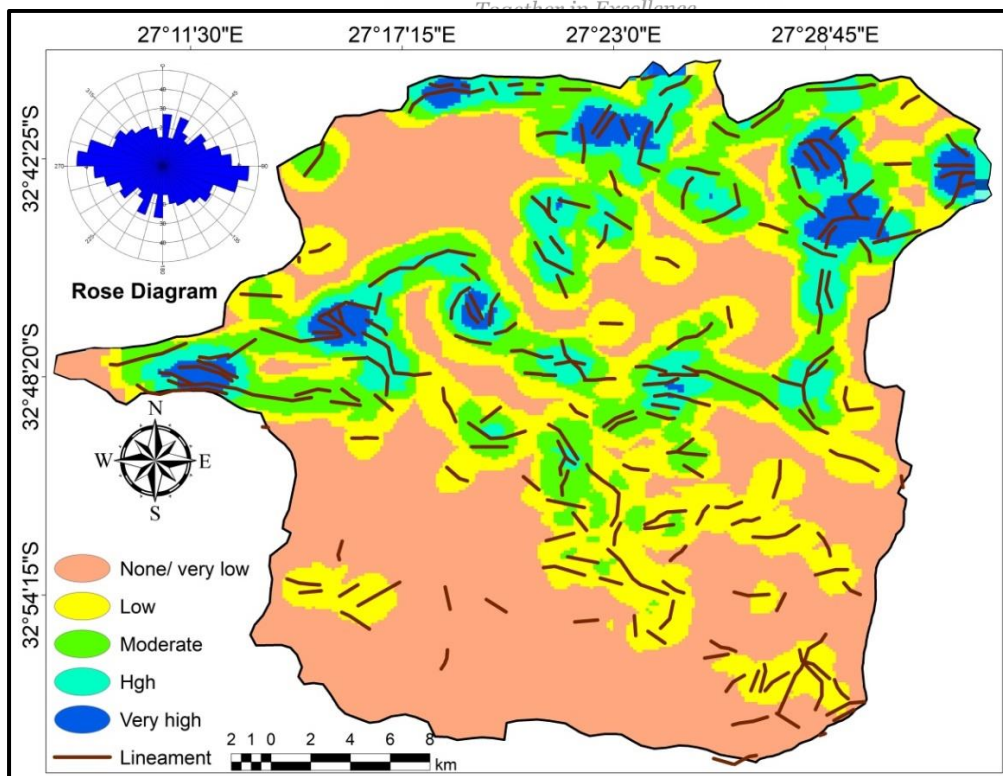


Figure 8. 2: Lineament density map of Buffalo basin headwater showing areas of variable lineament density.

The map shows the biasness of lineament concentration to the North. This aligns with the topographic complexity in the North where the relief is steep and abrupt. Importantly, the zones of very high to moderate lineament density lie around with the edges of the Karoo Dolerite where the intrusion of magma creates a contact zone between the dolerite and the pre-existing sedimentary rock. Areas of extensive fracture system have been shown to be replicated by high lineament density (Mostafa and Bishta, 2005; Khosroshahizadeh et al., 2016; Meixner et al., 2018). Hence, the zones of effectively high/moderate lineament density therefore serve as modifier for high-drained fractured dolerite that was ranked as very poor for groundwater potential under the surficial lineament. Rose diagram shows that the dominant trend of the surficial lineaments is WNW-ESE. This therefore conforms to the direction of the Neotectonic structure shown on study area geology map (Figure 4.4B). Zones of higher lineament density are expected to have higher potential for groundwater accumulation; hence, they are ranked higher.



University of Fort Hare
Together in Excellence

8.2.3 Drainage density

The drainage density map was classified into four with areas of high concentration surrounding the river confluence where enormous groundwater discharge to the water course indicates a negative influence on aquifer development (Figure 8.4). The four spots of very high drainage density in the South and one at the North can be associated with the existence of spring in close proximity to a possible leaky aquifer. The high drainage spot in the north shows a connection with a contact zone on account of proximity to a zone of high lineament density. As a result, areas of higher drainage density are inversely ranked while the areas of very low drainage density are assigned higher rank.

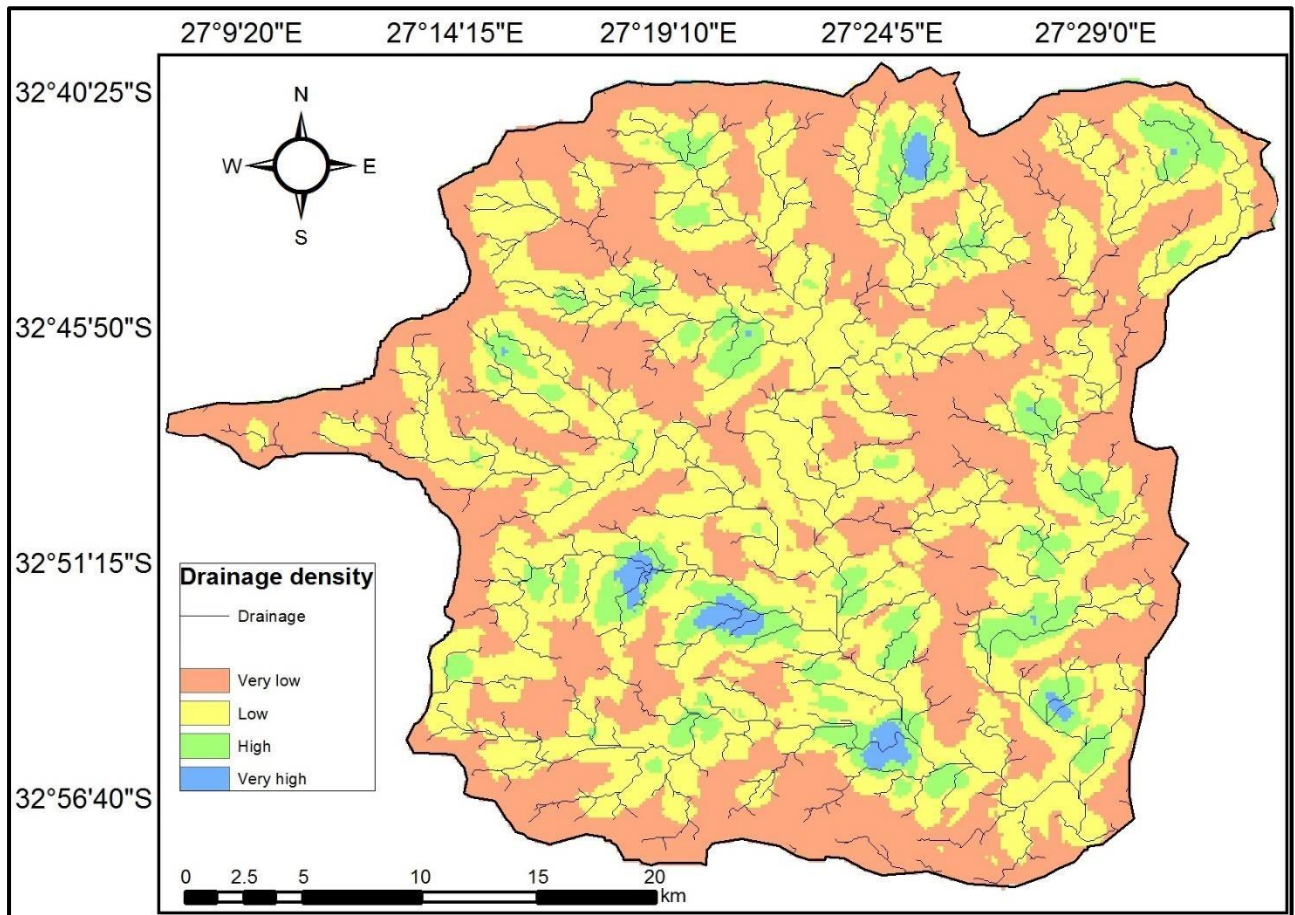


Figure 8. 3: Reclassified drainage density map of Buffalo basin headwater showing areas of high and low drainage density.

8.2.4 Rainfall

The average annual rainfall for hydrologic year record of 1989 to 2016 in the study area ranges from 544 mm to 610 mm (Figure 8.5). The rainfall trend shows a positive linear variation with relief in a NW-SE trend. This suggests the possible influence of relief on atmospheric circulation in such a way that favors orographic downpour at the high relief. In a similar fashion, it was identified in section 6.2 that relief exhibits a linear spatial influence on regional hydro-climatic pattern. The spatial variation in rainfall intensity influences the distribution of groundwater recharge rate across the study area. Due to the high positive influence of rainfall on groundwater recharge, the areas with higher rainfall range are ranked higher.

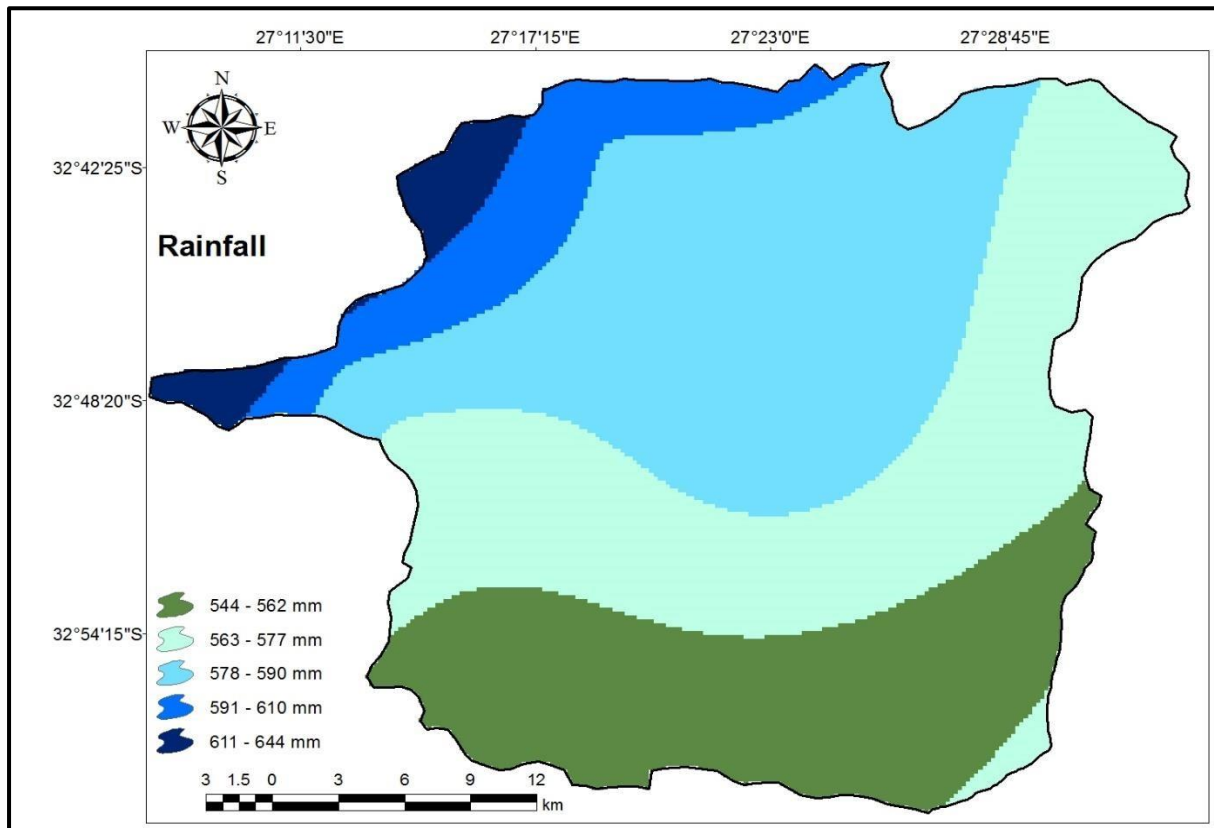


Figure 8. 4: Rainfall map of Buffalo basin headwater showing the rainfall variability.

8.2.5 Land use/ Land cover change map

University of Fort Hare
Together in Excellence

Land use/land cover (LULC) pattern contributes significantly to landform modification through alteration of imperviousness, hydrologic pattern, drainage channels, return flow development, and geologic structures. The result of the LULC mapping among the seven land cover features indicate that the cropland (320 km²), has the highest coverage (Figure 8.6). This is followed by the grassland (295 km²), the built-up (247 km²), the mixed forest (188 km²), the scrubs (145 km²), and the bare ground (37 km²), while water bodies has the least coverage (4 km²). The validity of LULC plot was confirmed using Google Earth features. The Rooikrandsdam and its water course located ny the Quencwe River were distinctly marked out just the same way as portrayed in Google Earth. The dispersed settlement across the Mggakwebe, Tshoxa, a nd Ngqokweni rivers showed similar distal segmentation just as observed in Google Earth. Also the Evergreen nature forest showed similar sectoral demarcation in the Google Earth the same way as mapped in the LULC map.

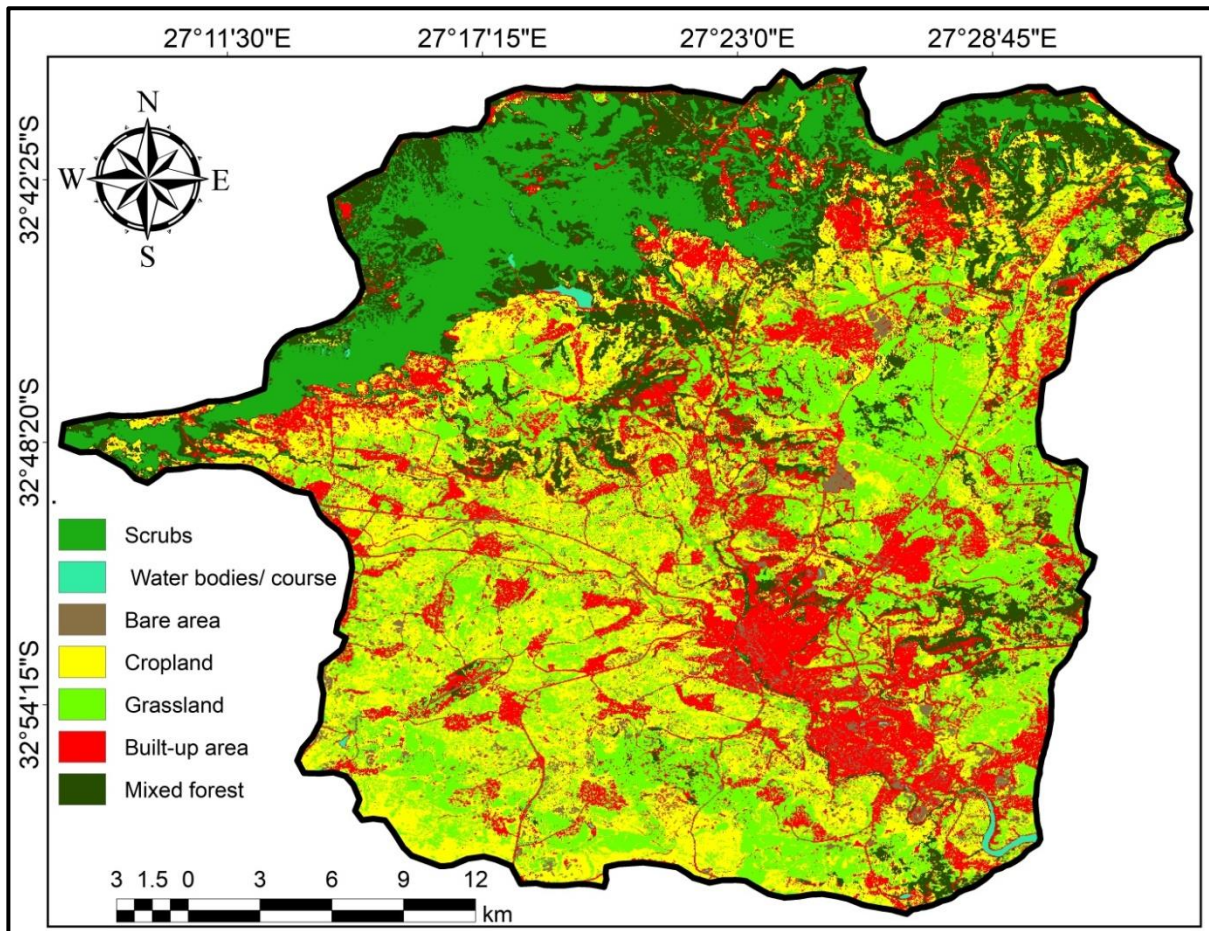


Figure 8. 5: Land use/land cover map of Buffalo basin headwater showing variability in land use and cover type.

Due to the varying impact of LULC changes on groundwater development, the different elements of LULC change are rated based on their significance to groundwater investigation. Mixed forest is a naturally preserved environment and an important indication of groundwater potential. Scrubs and cropland rank second to the indicators of groundwater potential, hence, they are ranked higher than others. Meanwhile, built-up area and water bodies/ course are least important areas for groundwater investigation, followed by bare ground which is vulnerable to evaporation. Grassland is ranked higher than bare ground because of its significance to soil moisture accumulation.

8.2.6 Land surface temperature

The land surface temperature map is classified into four; very low (8 – 13), low (13 – 16), moderate (16 -19), and high (19 – 22) as presented in Figure 8.7.

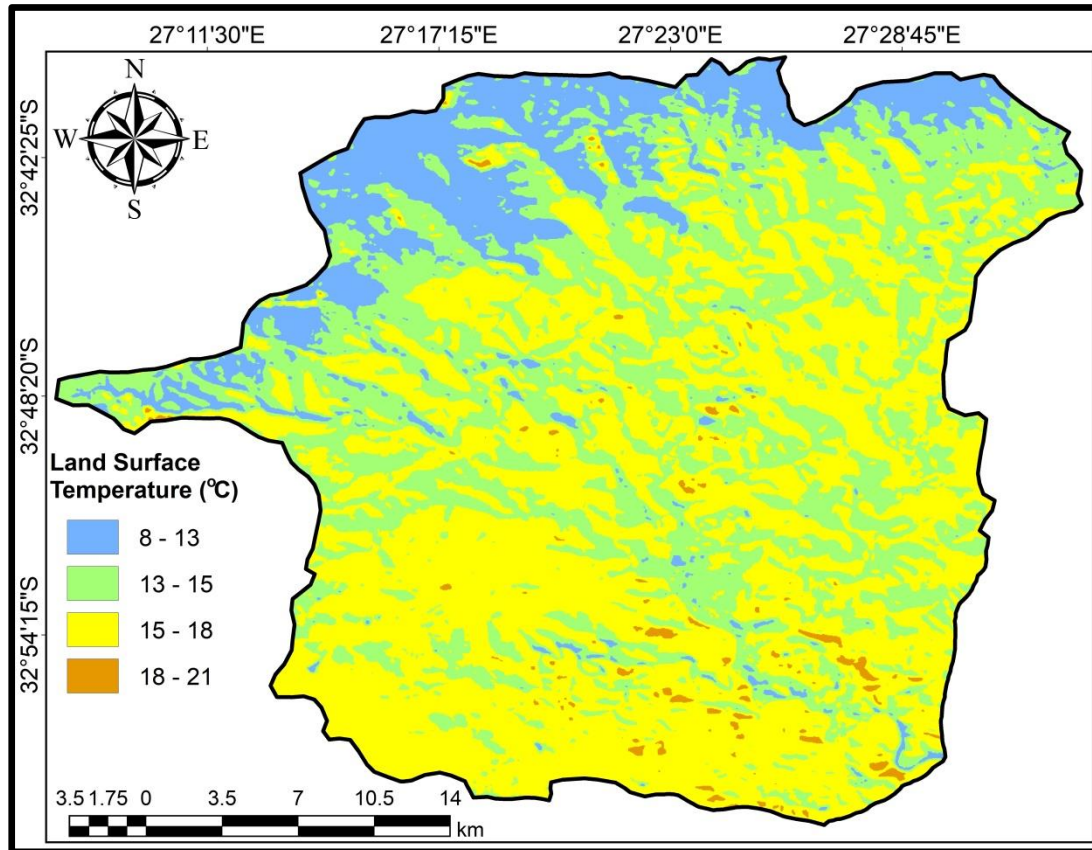


Figure 8. 6: Land surface temperature map showing spatial variability in land surface hotness and coldness.

Areas of low temperature had the largest coverage (102 km²), followed by a moderate temperature class (356 km²), the very low-temperature class (508 km²) and the least which is hot temperature class (272 km²). The similitude in the geospatial attributes of LULC and LST further depicts the relative influence of urbanization in inducing urban heat index which indirectly culminate into the spatial variability in land surface temperature. This therefore conforms to the findings of Orimoloye et al. (2018) on the relationship between LULC system and LST variability. Areas of high temperatures are associated with a high

evaporation rate. Evaporation is a critical issue in a water-scarce country like South Africa. It is a significant factor in soil moisture loss in semi-arid environments and to shallow unconfined aquifers. As a result, areas with high temperatures are assigned the lowest rank while the areas with low temperatures are assigned the highest rank.

8.2.7 Topographic Wetness Index map

The result of topographic wetness index for the study area is presented in Figure 8.8.

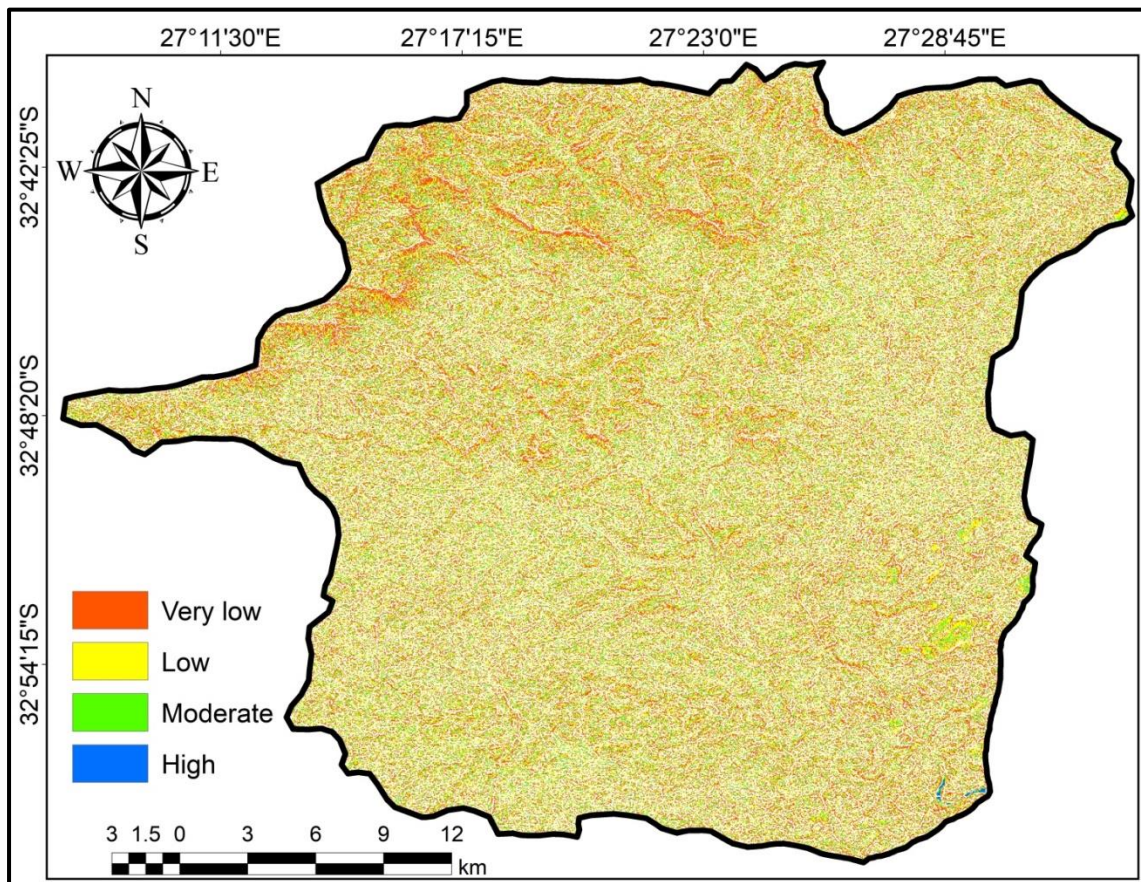


Figure 8. 7: Topographic wetness index map of Buffalo basin headwater showing the areas of potential for topographic influence on wetness.

The complexity of Buffalo topography is evidently revealed by the lines of concentration of the low TWI, which evidently coincides with the edges of dolerite outcrops in the North (Figure 8.2). In a way, the concentrated low TWI patches depicts the influence of dolerite intrusion on the initiation, evolution, and the development of rift (Madi and Zhao, 2013). Consequently, the low TWI areas are more likely to develop an overland flow rather than

enabling groundwater recharge on account of the influence of hillslope factor. Meanwhile, high TWI which lies at the foothill of low TWI is more likely to enable groundwater recharge on account of the tendency for soil moisture accumulation (Figure 8.8). Soil moisture accumulation is a significant indicator of groundwater abundance, although the hydraulic properties of soil/lithologic material are the primary determinant of infiltration (Naghbi et al., 2017). The hillslope may have been due to tectonic uplift caused by dolerite intrusion in the area, hence the low TWI reveals a similar trend as the dolerite intrusion (Figure 1.1 and 8.2).

TWI has been employed to decipher the average groundwater level in a watershed characterized by low permeability soils (Rinderer et al., 2014). Since, Buffalo catchment is dominated by argillaceous sedimentary material, TWI is therefore considered applicable to groundwater potential mapping here too. The very low TWI that suggest the tendency for overland flow was assigned the lowest rank while the very high TWI that indicates the tendency for soil moisture accumulation zone was assigned the highest rank.



University of West Indies
Together in Excellence

8.3 Normalization of features of GWPZ mapping

Relevant weights were assigned to the seven themes based on the influence on groundwater development based on the criteria weight provided by AHP as presented in Table 8.2.

Table 8. 1: Pairwise comparison matrix

	SL	Rainfall	LST	LD	DD	TWI	LULC	Critical Weight	Consistency measure
SL	1.00	2.00	9.00	1.00	6.00	4.00	0.50	0.22	7.61
Rainfall	0.50	1.00	7.00	0.50	6.00	4.00	4.00	0.24	8.23
LST	0.11	0.14	1.00	0.11	0.50	0.33	0.17	0.02	7.78
LD	1.00	2.00	9.00	1.00	5.00	3.00	0.50	0.21	7.67
DD	0.17	0.17	2.00	0.20	1.00	0.50	0.25	0.04	7.57
TWI	0.25	0.25	3.00	0.33	2.00	1.00	0.33	0.06	7.45
LULC	2.00	0.25	6.00	2.00	4.00	3.00	1.00	0.21	7.52
Total	5.03	5.81	37.00	5.14	24.50	15.83	6.75	100.07	7.69
								Consistency index	0.12
								Random index	1.32
								Consistency ratio	0.09

The value of CR obtained is 0.09, implying that the criteria weight was based on a reasonable level of consistency. The factors and its classes are presented in Table 8.3.

Table 8. 2: Classification of parameters for weighted overlay analysis

Factors	Classes
Surficial	Quaternary sediment
Lithology (LD)	Sandstone Silty sandstone Silty/ sandy mudstone Mudstone Shale Dolerite
Lineament	Very high
Density (LD)	High Moderate Low Very low/ None
Drainage density	Very low Low High Very high
Rainfall (mm/yr)	610 - 644 591 - 610 578 - 591 563 - 578 544 - 563
Land surface	8 – 13
Temperature (°C)	13 – 16 16 – 19 19 – 22
Topographic Wetness Index (TWI)	High Moderate Low Very low
Land use/ land Cover (LULC)	Mixed Forest Cropland Scrubs Grassland Bare Built-up/ Water bodies



University of Fort Hare
Together in Excellence

8.4 Delineation of Groundwater Potential Zones

The potential zone of groundwater was classified into five; good (187 km²), moderate (338 km²), fair (406 km²), poor (185 km²), and very poor zones (121 km²) as shown in Figure 8.9.

The study shows that the potential for groundwater varies from the northwest to southeast within short distance. Overall, zones with high groundwater potential are dominant in the northwest, while the extremely poor groundwater potential zone is dominant at the south and southeast.

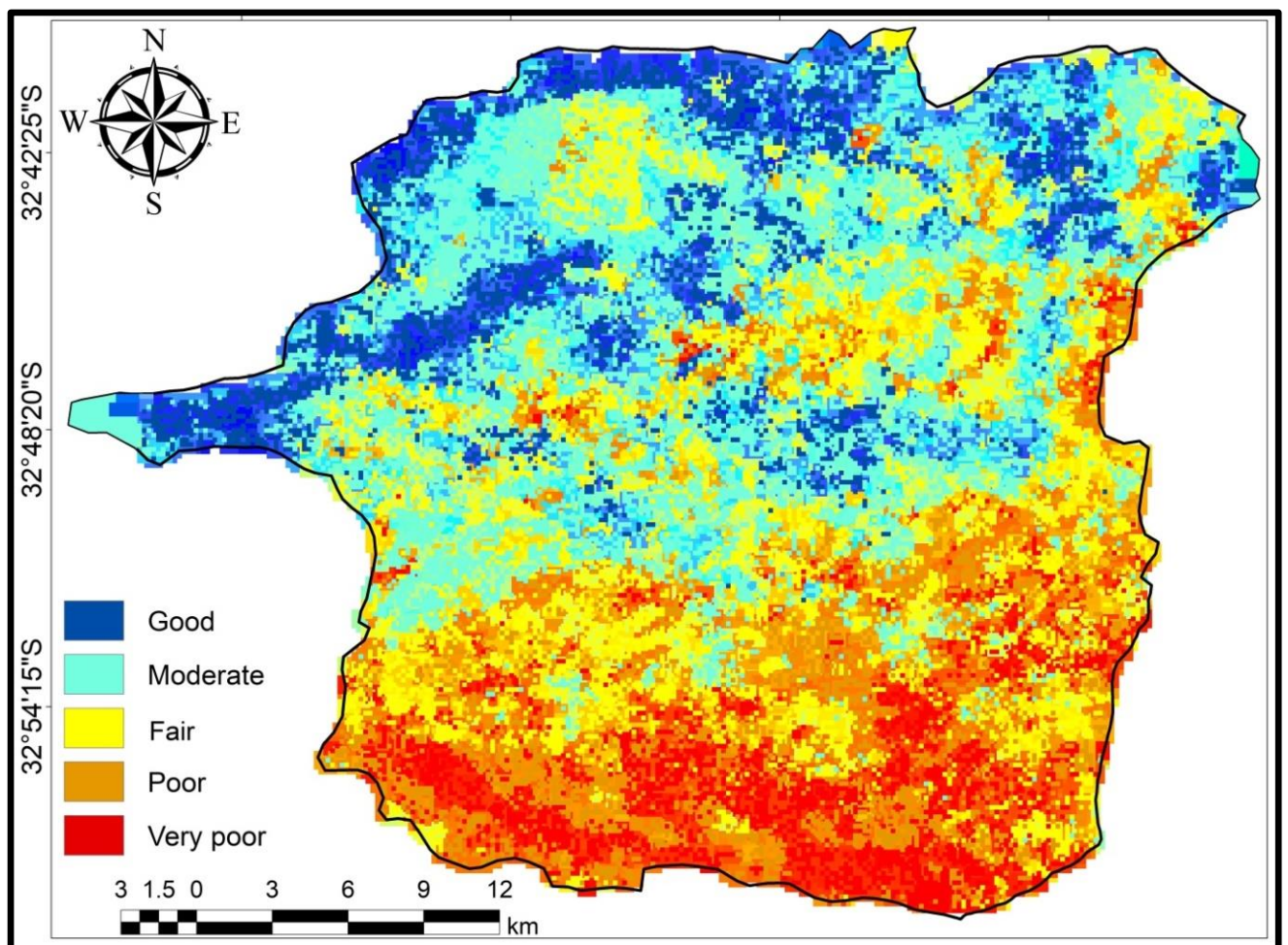


Figure 8. 8: Map showing groundwater potential zone of the study area.

8.5 Validation and corroboration of groundwater potential zones

The scientific significance of models depends on validation reports; hence it is considered the most important stage of scientific research. The spatial distribution of exploration borehole

yield employed is presented in Figure 8.10. Its related gridcode extracted from the Arcmap is presented in Table 8.4.

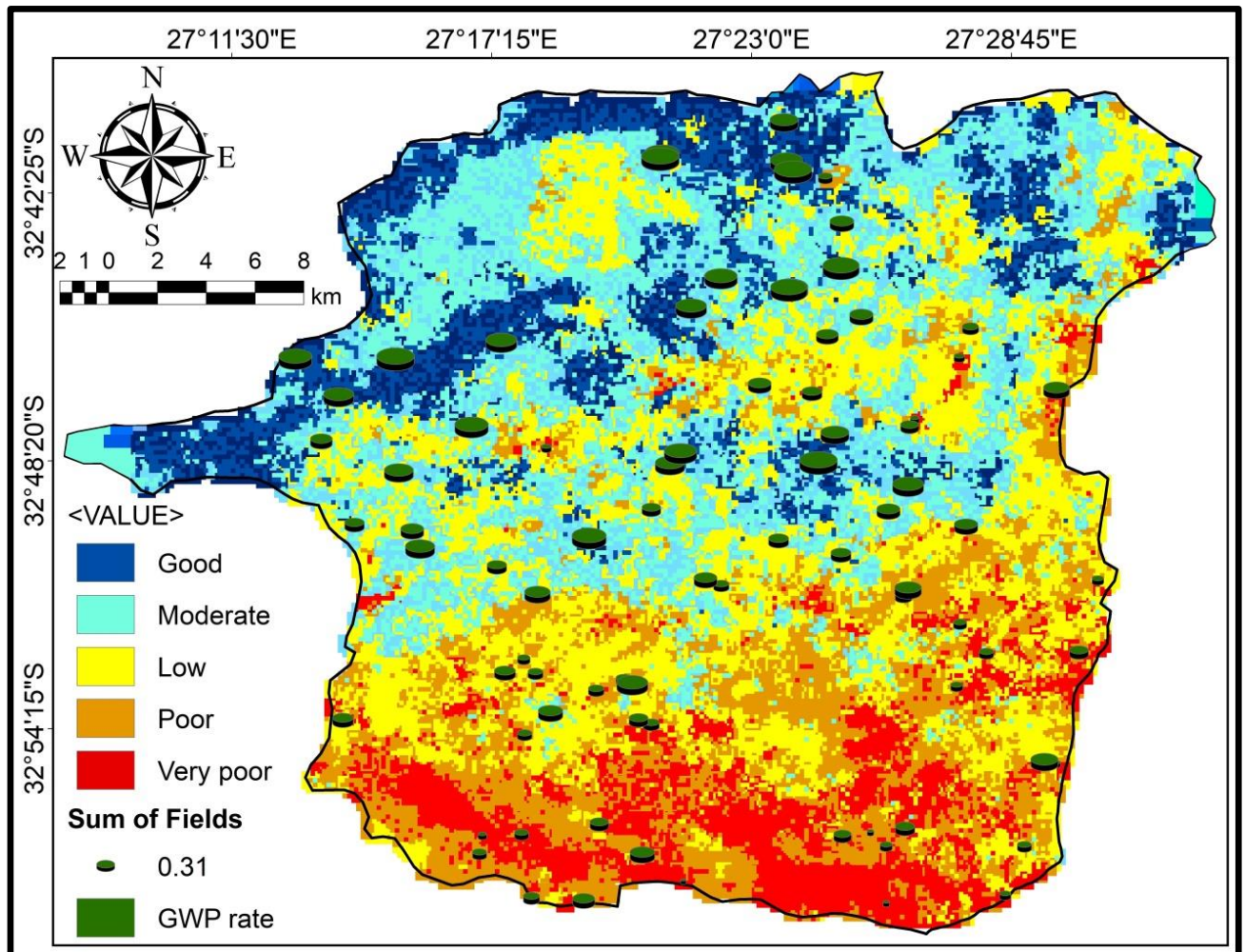


Figure 8. 9: Map showing the overlay of borehole yield and GWPZ.

The coefficient of determination ($R^2 = 0.901$) obtained from the scattered diagram indicates that the GWPZ model is an excellent fit for characterization of zones groundwater yield as it explains the borehole yield variability around its mean (Figure 8.10). This was further established by the coefficient of correlation and the test for significance (p -value < 0.01) for the model which that the modeling procedure shows a very significant and strong positive relationship with the borehole yield. That is, the model can provide relevant and applicable information on the availability of groundwater in place of borehole yield. A more expository relationship between borehole yield and GWP rate is presented in the box-and-whisker plots

Table 8. 3: Table indicating the relative value of GWP rate to borehole yield

Lat.	Long.	Yield (l/s)	GW P	Lat.	Long.	Yield (l/s)	GW P	Lat.	Long.	Yield (l/s)	GWP	Lat.	Long.	Yield (l/s)	GW P
-32.758	27.436	0.03	4.6	-32.875	27.469	0.38	4	-32.797	27.224	1.26	5.2	-32.778	27.49572	3.63	4
-32.883	27.303	0.04	4	-32.908	27.299	0.38	4.3	-32.871	27.369	1.28	5.6	-32.853	27.30431	3.63	7.6
-32.865	27.460	0.04	4	-32.884	27.326	0.38	4.6	-32.919	27.399	1.36	4	-32.792	27.44161	3.64	5.9
-32.825	27.457	0.06	4	-32.848	27.511	0.41	4	-32.889	27.326	1.36	4.3	-32.916	27.44961	3.79	4
-32.847	27.433	0.06	4.3	-32.908	27.485	0.42	4.3	-32.828	27.462	1.36	4.3	-32.882	27.2923	3.79	4
-32.968	27.433	0.07	3.4	-32.852	27.441	0.46	4	-32.887	27.339	1.36	5	-32.905	27.29823	3.79	4.6
-32.854	27.439	0.08	4	-32.879	27.269	0.46	5.5	-32.780	27.264	1.36	6.6	-32.750	27.421	3.79	6.3
-32.852	27.503	0.09	3.7	-32.818	27.397	0.46	5.6	-32.964	27.476	1.39	4	-32.839	27.41628	4.06	6.9
-32.767	27.349	0.11	4	-32.916	27.495	0.5	4	-32.901	27.346	1.39	4.3	-32.958	27.32155	4.58	5.6
-32.921	27.375	0.12	3.4	-32.925	27.396	0.5	4.3	-32.748	27.499	1.46	4.3	-32.823	27.43378	4.61	7
-32.693	27.349	0.13	4.3	-32.877	27.299	0.5	4.6	-32.737	27.372	1.47	5.3	-32.744	27.50349	4.98	5
-32.818	27.501	0.14	4	-32.946	27.492	0.51	4.3	-32.915	27.491	1.5	4.3	-32.80	27.25317	5.64	7.3
-32.818	27.501	0.14	4	-32.748	27.360	0.52	6.9	-32.751	27.415	1.52	5.6	-32.825	27.43772	6.06	6.96
-32.698	27.398	0.15	5	-32.783	27.389	0.53	6.6	-32.943	27.416	1.53	3	-32.873	27.46405	6.31	6
-32.717	27.416	0.17	4.9	-32.875	27.504	0.54	4	-32.834	27.393	1.64	4.3	-32.805	27.40794	7.21	6.6
-32.946	27.432	0.19	3.7	-32.885	27.336	0.56	5.3	-32.938	27.327	1.67	4.3	-32.897	27.30913	7.22	6.3
-32.941	27.427	0.19	4	-32.849	27.511	0.58	4.3	-32.800	27.307	1.83	5.3	-32.737	27.48794	7.24	4.9
-32.852	27.440	0.19	4	-32.945	27.289	0.63	4.6	-32.671	27.502	1.83	7.6	-32.837	27.261	7.45	8
-32.948	27.301	0.19	4.3	-32.949	27.282	0.63	4.6	-32.756	27.464	1.84	4.3	-32.804	27.35711	7.67	7.6
-32.694	27.396	0.2	4.9	-32.866	27.340	0.67	4.6	-32.921	27.432	1.89	4	-32.804	27.35405	8.06	7.6
-32.965	27.302	0.2	5.6	-32.766	27.459	0.71	4	-32.760	27.452	1.89	5.3	-32.744	27.406	8.06	8
-32.73	27.456	0.21	4.3	-32.909	27.249	0.76	4.3	-32.730	27.507	1.89	5.3	-32.761	27.291	8.21	7.6
-32.933	27.293	0.23	4.3	-32.878	27.299	0.76	4.6	-32.751	27.423	1.9	6.3	-32.846	27.50767	8.33	5.3
-32.729	27.456	0.23	4.3	-32.942	27.29	0.81	5	-32.794	27.432	1.9	6.6	-32.792	27.28989	8.83	8
-32.943	27.284	0.23	4.9	-32.905	27.299	0.82	4.3	-32.850	27.372	1.97	4.3	-32.767	27.252	8.96	8
-32.964	27.477	0.25	4	-32.779	27.495	0.83	4	-32.713	27.467	2	5.3	-32.781	27.231	9.03	8
-32.871	27.266	0.25	4.3	-32.830	27.465	0.88	4.6	-32.700	27.410	2.05	5.3	-32.847	27.335	9.31	8
-32.963	27.466	0.25	4.6	-32.895	27.275	0.92	3.4	-32.737	27.522	2.08	4	-32.814	27.441	9.38	8
-32.843	27.289	0.25	5	-32.897	27.290	0.92	3.7	-32.917	27.395	2.08	4.3	-32.748	27.316	9.56	8
-32.918	27.416	0.27	4	-32.900	27.341	0.92	6.9	-32.789	27.479	2.08	6.3	-32.743	27.407	9.87	8
-32.919	27.418	0.29	4	-32.900	27.366	0.93	4	-32.805	27.358	2.15	6.9	-32.795	27.414	9.87	8
-32.888	27.459	0.31	3.4	-32.691	27.350	1	5.6	-32.825	27.437	2.17	6.9	-32.766	27.36572	10	7
-32.751	27.421	0.33	4.9	-32.867	27.286	1.01	5.3	-32.819	27.335	2.2	5.3	-32.762	27.3602	10	7.6
-32.833	27.399	0.34	4	-32.769	27.447	1.01	6	-32.908	27.485	2.22	4.3	-32.767	27.215	11.4	7.6
-32.729	27.491	0.34	5.3	-32.779	27.496	1.05	4	-32.940	27.439	2.27	5.3	-32.676	27.491	13.2	8
-32.822	27.479	0.35	4.3	-32.789	27.443	1.08	4.9	-32.867	27.266	2.27	5.9	-32.9669	27.34323	3.61	4.9
-32.962	27.353	0.36	4	-32.870	27.339	1.11	4.3	-32.923	27.432	2.44	4	-32.673	27.396	3.2	6.3
-32.864	27.460	0.36	4	-32.900	27.232	1.11	5.3	-32.874	27.438	2.52	4.4	-32.766	27.347	2.75	5.6
-32.942	27.282	0.37	5	-32.931	27.387	1.26	4	-32.7336	27.41628	2.52	6.3	-32.940	27.493	2.59	5.3
-32.767	27.482	2.53	4.6	-32.828	27.236	3.12	6.5	-32.708	27.533	3.25	5.6	-32.829	27.262	3.18	6.5
-32.766	27.507	2.53	4.6	-32.848	27.366	3.15	6	-32.9212	27.42461	3.28	4	-32.7769	27.38627	3.55	7

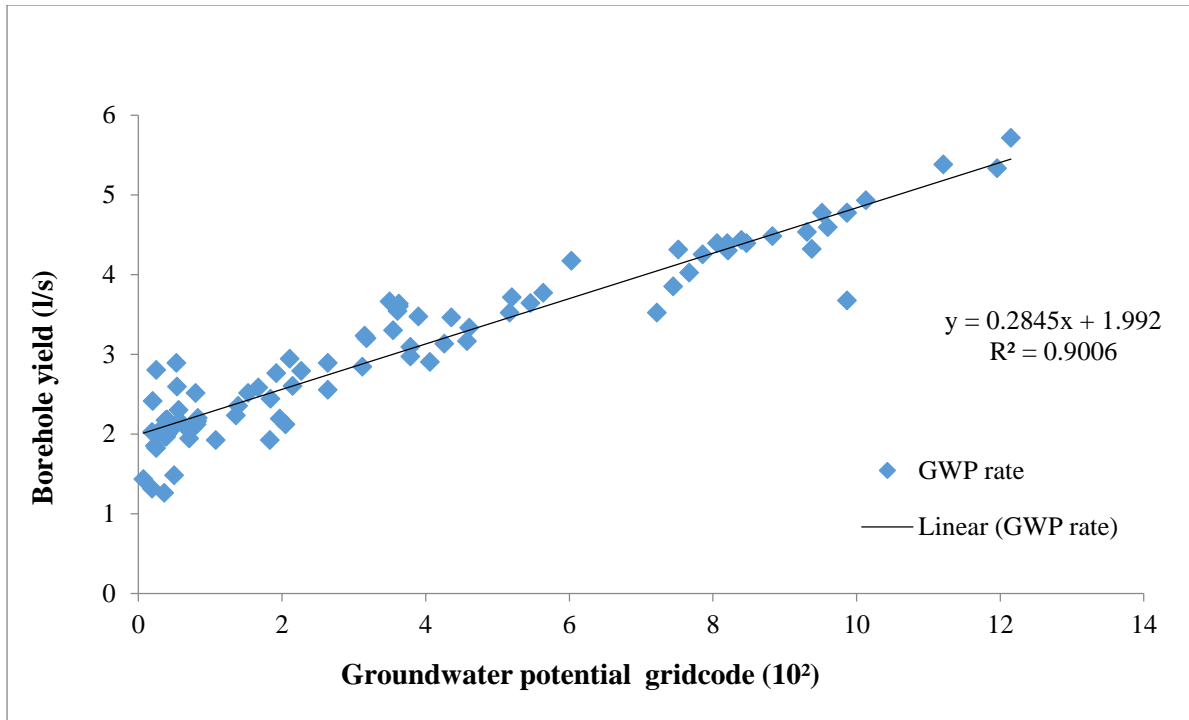


Figure 8. 10: Scattered plots of groundwater potential zone mapping of Buffalo catchment.



Table 8. 4: Results of the model assessment

Test parameters	Estimate
Number of Samples	164
Degree of freedom	162
Correlation coefficient (R)	0.949
t-value	27.255
p-value	1.777E-43

Meanwhile, the statistical summary reports a significant and excellently positive relationship between the model and borehole yield ($p\text{-value} < 0.01$; $7 \leq R \leq 9$; Figure 8.11; Table 8.5). A more expository relationship between borehole yield and GWP rate is presented in the box-and-whisker plots in Figure 8.12. The good GWPZ class reports a high level of agreement with borehole yield, whereby more than half of its class is 9.3 l/sec. The moderate GWPZ class is associated the widest range and highest yield standard deviation with an average value is 5.5 l/sec. The fair, poor and very poor GWPZ classes are associated with 3.2, 0.8 and 0.4 l/s average yield which are not consider economical for groundwater development where

water demand is high. The plot reveals that groundwater borehole exploitation sited on the good and moderate GWPZ area are most likely to provide considerable yield.

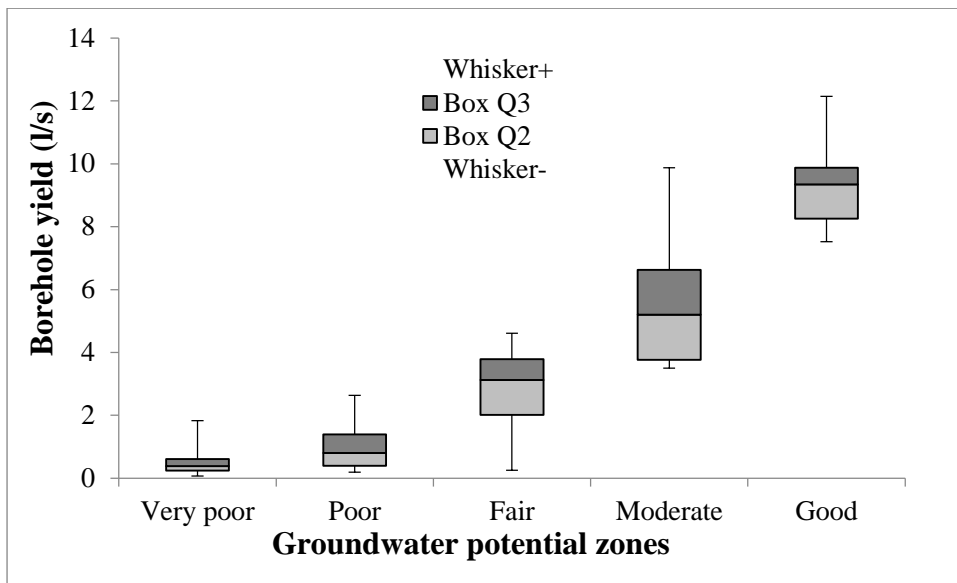


Figure 8. 11: Box-and-whisker plot reporting the relationship between the GWPZ and borehole yield.

8.6 Integrated hydrogeological conceptualization

Three-dimensional projection of the total residual magnetization confirms that the northern half is associated with spikes of dolerite intrusion which possibly influence the development of the complex topographic system (Figure 8.13). The uplift in the north, resulting from the emplacement of dolerite, may have influenced the development of extensional stress and the morpho-tectonic specs responsible for high surficial lineament density. The differential dolerite intrusion varies in gradient to the south in an opposite manner to the geomorphic configuration, which is therefore in conformity with the gradient of the depth slice (Figure 4.10).

The findings from the integrated mapping of GWPZ together with field geologic structure mapping reveal that the shallow hydrogeological system is mainly hosted by fractured and the intergranular hydrostratigraphy (Figure 8.2 and 8.13). This occurs within the permeable

contact zones that lie at the edges of the fractured dolerite intrusion and the thick layer of sandstone and silty-sandstone deposits of the Permian-Triassic (Figure 4.10).

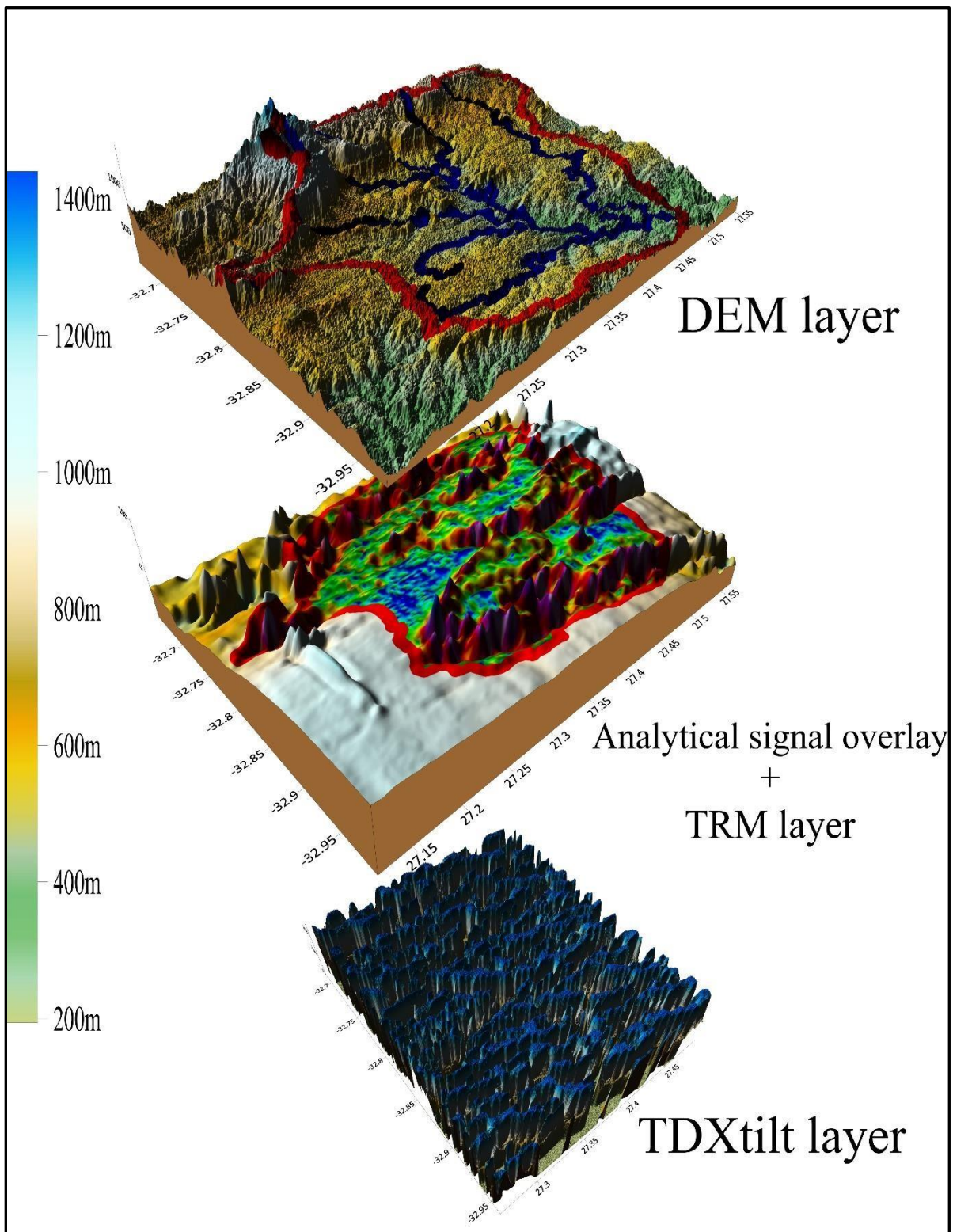


Figure 8. 12: Three-dimensional presentation of actual landform (DEM), magnetic anomaly map (analytical signal on total residual magnetic layer) and lineament (TDXtilt) structure within.

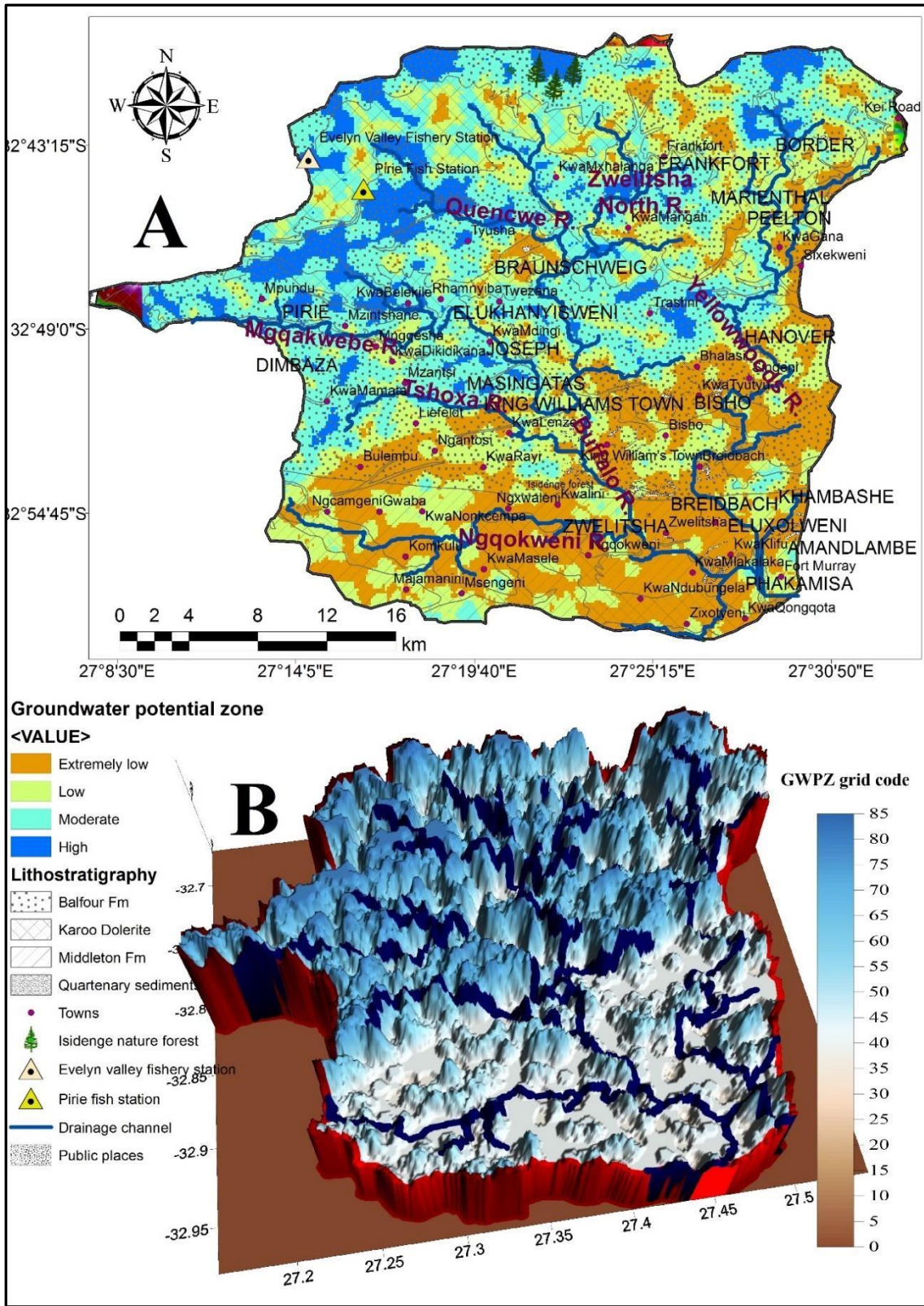


Figure 8.13: Map showing: A. the spatial demarcation of GWPZ in relation to the surficial geology, the watershed drainage, and some townships; B. GWPZ association with drainage.

The area associated with high lineament density within the catchment area is the main recharge center for the aquifer. These are west, north, and north-west of the catchment. The analytical signal map indicates the possibility of the dolerite dykes constituting the fractured aquifer boundaries most especially at the south and some part of the north (Figure 8.13). More so, the traverse flow of the Buffalo River across the groundwater flow-path constitutes a significant variable head boundary to the aquifer. Connectivity of the aquifer to Tshoxa, Mgqakwebe, and Buffalo may have facilitated the high baseflow discharge reported in section 6.2.4.

Figure 8.13 reveals that the magnetic field strength which indicates the magnetite-rich resistant rocks has a lower gradient at the north and very high gradient in the south. This may have influenced the spatial disparity in surficial and subsurface lineaments which varies from north to south. The spikes of magnetic amplitude at the north reveal that the intrusion of the dolerite outcrop and how it may have influenced the development of the complex topographic system in the north. The uplift in the north, resulting from the emplacement of dolerite, may have influenced the development of extensional stress and tectonic specs responsible for high surficial lineament density (Figures 7.2). The strikes of the lineament (Figure 8.12) indicate that the groundwater flow-net direction is in a west-east trend. The hydraulic gradient infers that groundwater flows from west to east (Figure 8.11) owing to the lack of data on borehole piezometric level. The TDXtilt layers reveal the influence of tectonic structures on the water table and groundwater flow within the aquifer. There are possibilities of the total independent flow of groundwater in each lineament space.

8.7 Summary

This section demonstrates the mapping of the zone of groundwater potential in a semi-arid environment using geoinformatics. The integrated approach involving the use of remote sensing for groundwater has proven efficient in terms of cost-effectiveness, aptness, and

explicitness. Eleven different thematic layers were reported using indicators of geologic, hydrologic, geomorphic, and meteorological factors.

Discussions on interrelationship across the various thematic maps used, the result of the analysis and linkage with literature were extensively presented in chapter 9. However, the result presents multi-influencing factors and the eleven indicators as an excellent tool for estimating contributions of groundwater potential parameters. This was based on the coefficient of correlation and determination as well as root mean square assessment which established the significant reliability of the model. Results of the analysis indicate that groundwater potential is high in the north-west and the low in the south and southeast of the study area. The high GWPZ is majorly due to the density of fractures in sandstones (catchment center), dolerite and mudstone (west and north). The south constitutes majorly groundwater discharge centers. The poor groundwater potential in the south is possibly due to limited fractures in the mudstone and dolerite that dominated the region. Overall, the approach adopted here can be readily employed in any semi-arid/arid environment with a similar geologic layout for delineation of zones of groundwater potential.



University of Fort Hare

Chapter 9: Discussion

9.1 Introduction

The integrated study of surface water and groundwater interaction, as well as physiographic perspectives, have enhanced the understanding of spatial and regime variability of surface water in relation to its hydrologic basin. It has enabled the understanding of variability in groundwater discharge to stream through low flow and baseflow index analyses, which has further assisted in deciphering the viable basins of high groundwater potential. The physiographic study has assisted in characterizing the catchment in relation to drainage morphometric attributes. This chapter provides general discussions on the implication of the entire results reported in chapters 4 to 8.



9.2 Evaluation of geologic structures

Geologic structures such as fractures, joints, faults, and bedding planes serve as flow-paths for groundwater. As a result, the hybrid approach of field and GIS-based analysis of sedimentary facies, structures, and lineaments were carried out. More importantly, the tectonic features corresponding to the exploration quest were strongly depicted in autolineament extraction and enhancement of magnetic maps.

9.2.1 Geologic settings of Buffalo catchment

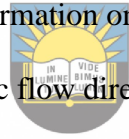
Buffalo lithostratigraphy comprises sedimentary components of sandstone, silty-sandstone, shale and mudstone deposits in the Permian-Triassic period. As a result of the reports of morphometric and structural analysis, the sedimentary facies of Balfour Formation represents a meandering or braided mud-dominated fluvial system. The surface lithology is characterized by exposed Jurassic dolerite at the north and the south. Other sections of the catchment are covered by soil materials such as clay (dominant in the south), sand (dominant

at the center), and alluvium along the river banks. Katemaunga and Gunters (2009) reported on the existence of Oudeberg, Daggaboersnek, Barberskrans, Elandsberg and Palingkloof Members as the unit of Balfour Formation. Mapping of these Members within the catchment reveals features associated with Daggaboersnek, Barberskrans, Elandsberg and Palingkloof Members only. Elandsberg Member had the poorest exposure. The mapping of the Members was achieved with the aid of features that further confirm the existence of these sedimentary facies as paleochannel deposits. The dominance of the sandstone in Barberskrans Members and mudstone lithosomes in Daggaboersnek Members agrees with Oghenekome's (2012) reports on the Balfour Formation within the catchment. The Elandsberg Member within the catchment is dominated by the intercalation of sandstone and red mudstone as its surface.

The densely fractured unstratified sandstone of the Barberskrans Member found in Mpundu (west) stretches to Elukhanyisweni (center - approximately 8 km) and extends to the north at Tyusha (northwest – approximately 3 km). The section reveals the potential for groundwater flow. The sandstone layer of Daggaboersnek Member observed in the south-west, south and south-east of the study area are intercalated with mudstone. Traps of mud-clast within the sandstone matrix were also visible in the south, especially along Ngqokweni dry river bank. This lithologic section is likely to have very low hydraulic conductivity due to the clogging of flow-path. However, at the extreme south-east around the mouth of the Buffalo River, fractured thick layer sandstones of the Daggaboersnek Member were observed. Along the river bank is a thick unconsolidated alluvial plain which may facilitate high groundwater flow potential.

The geomorpho-tectonic analysis reports some important information that can be associated with the lithostratigraphic settings in the Buffalo catchment. The sedimentary facies obtained at Ngqokweni River (south-west and south) which was composed of an upward-fining

succession of thick mudstone and thin sandstone was abridged by trapped mud-clast within thick unstratified sandstone (Figure 4.1B). The unstratified thick-layered sandstone deposit at the west represents the deposition by action of a turbulent meandering channel with moderate frequency (Figure 4.2A-B). The stratified interspersed succession of thick mudstone and narrowing sandstone at the east is the product of a low energy flow regime characterized by suspension and accretion of mud at varying degrees (section 4.1). The deposition at the north-east can be described as being heterolithic due to the fractional balance between mudstone, sandstone, shale, and silty-sandstone among the pyroclastic dispersion of dolerite outcrops. The heterolithic bedding suggests a regulated successive deposition typical of a straight and faster-moving flow. The change in flow energy in the north-east to the south may be due to variation in palaeochannel gradient. The information on attributes of the paleoenvironment provides further information on the potential for variability in groundwater flow on account of the lithostratigraphic flow direction settings.



University of Fort Hare

Baiyegunhi (2015) mentioned the calcareous concretion in the Elandsberg Member near the Cradock area. A similar observation was made in this work around the Pirie fish station in the north-west of the study area. This feature was inferred to have been due to calcrete formation from age-long duricrust of bone or shell-rich fossil. These features were identified in the Permian-Triassic gray mudrock of Katberg Formation by Hiller and Stavrakis (1984), and Smith and Ward (2001). The observation of dispersed lime solution can also be supported by the discovery of calcretes and carbonate precipitates in the shale of lower Katberg Formation (which directly overlies Palingkloof Member) in the work of Khadkikar et al. (1998). Tordiffe (1978) specifically highlighted the occurrence of calcrete or caliche on soils or mudrock dominated area of Elandsberg Member of Balfour Formation, and Katberg Formation.

The analysis of the total residual magnetism revealed that the landscape of the Buffalo catchment possibly evolved from the uplift initiated by the intrusion of dolerite at the north of the catchment (Section 7.1; Figure 8.16). The uplift may have influenced the gaps, folding, overlapping, and fault systems in lithological layers as revealed in the geoelectric sections (Figure 7.5A – E). These may have accounted for the development of the extensional and compressional stress which dominated the Quencwe rock system as shown in Figure 7.2. Madi and Zhao (2013) reported that the Jurassic dolerite intrusion may have probably influenced the tectonic uplift which resulted in Amatole-Swaziland ranges. Wildman et al. (2016) indicated that the structural processes associated with intracontinental rifting can result in long-term geomorphic uplift at the continental hinterlands. Hence, the saturation and exposure of the fractured dolerite may possibly be responsible for weathering of the rock as reported by Madi and Zhao (2013) and as a result, indicates the potential for saturation of the rock system in the north compared to the south.



University of Fort Hare

9.2.2 *Surficial and subsurface lineaments of Buffalo catchment*

The catchment exhibits varieties of lithostratigraphy structures that provides the information on the zones of groundwater potential. These include the surficial tectonic features revealed by autolineaments, the subsurface tectonic apertures revealed by the magnetic edge analysis, and the fracture and fault systems identified on the unstratified and stratified sandstones, mudstone, and dolerite. The findings on the surficial lineaments reveal that the Barberskrans Members of the Balfour Formation is the most fractured. It is therefore possibly the most saturated with appreciable groundwater yield. The auto-lineament analysis also suggests that the dolerite and mudstone in the west and the north of the catchment are excessively fractured and therefore have the potential for high groundwater drainage.

A significant neotectonic lineament which possibly indicates the paleochannel where Barberskrans Members may have been deposited was indicated by reducing-to-pole magnetic analysis. This discovery is in agreement with Katemaunzanga and Elango's (2009) report which noted that the massive sand bodies of the Barsberkrans Member filled in one of the biggest channels in the Daggaboersnek Member. Reports of vertical and TDXTilt derivatives indicate subsurface sections with low magnetic amplitude, and these suggest that the subsurface neotectonic channels or conduits are possibly composed of permeable hydrostratigraphic material. Ferreira et al. (2013) revealed that the vertical and TDXTilt derivatives provide the precise location of the edge of magnetic bodies. The frequency and orientation of the subsurface lineaments are consistent with that of the surficial lineaments. Hence, the subsurface lineament validates the applicability of auto-lineaments for the analysis of surficial lineaments.



Importantly, the subsurface tectonic lineaments indicate the possible influence of geologic layout on groundwater residence and flow-net trend, subject to the hydraulic conductivity of the interstitial material within the channel. The strike and dip of the surficial lineaments are 275° and $5^\circ/25^\circ$, hence the groundwater flow-net has its hydraulic head and flow direction in north-west-east/south-east-east and east-west trends. The groundwater flow is bounded by a fixed no-flow boundary at the south and variable flow boundary at the north. In the south, groundwater flow is low and poor. This is possibly due to the interstitial material of mudstone and the poor fracture system in the dolerite intrusion in the south. The dolerite system in the north is associated with a fracture system. The two large dolerite sills are in east-west trends.

These discoveries agree with the findings of Andreoli et al. (2006), Lewis (2008) and Madi and Zhao (2013). Andreoli et al. (1996, 2006) reported the initiation of neotectonic activity

which was oriented in a north-west/south-east direction from South Angola to South Africa. In this, Chevallier and Woodford (1999) reported that the orientation of dolerite sills and dykes in the Karoo are a substantial identity for inference of neotectonic fractures since the dolerites are emplaced within the neotectonic structures. Lewis (2008) reported the occurrence of the geostructural line in the north-west/south-east orientation. Madi and Zhao (2013) also reported the occurrence of a neotectonic line on weathered layers in King Williams Town. Its orientation was classified with Amatole-Swaziland uplift and reported to be in the northwest/south-east trend.

The use of Landsat 8 OLI with PC2 as a reliable combo for the extraction of geologic lineaments was substantiated in agreement with Adiri et al. (2017). Adiri et al. (2017) compared the application of Landsat 8 OLI and PC2 and Sentinel 1 for extraction of autolineament with a focus on Sidi Flah-Bouskour inlier, Morocco. The use of Landsat 8 OLI and PC2 revealed an effective match with geologic strike and dip in the area while results from Sentinel 1 positioned the extracted lineament on the wrong edge of surficial lineament. Similar combinations involving enhancement of RTP with tilt derivative and total horizontal derivatives have been documented as effective for the detection of anomaly edges and lineament depiction (Baiyegunhi and Gwavava, 2017a; Azaiez et al., 2018).

Effectiveness of analytical signal for enhancement of magnetic maps has been extensively appraised in the works of Li (2006) and Baiyengunhi and Gwavava (2017a). The vital significance of dolerite intrusion as a groundwater divide due to its imperviousness has demanded the mapping of its actual position and extent in the study area, as well as preferential flow along its contact zone with the host rocks. In this study, the tool has assisted in projecting near-surface and outcrops of magnetic-rich signal, identified as dolerite intrusion by Johnson et al. (2006). The previously limited coverage of the magnetite-dominated feature may have been due to limited field exposure, poor visibility of

remote sensors, technical deficiency, regional-scale resolution issues, inaccessibility, and inadequate tool calibrations. Analytical signals have been employed to ascertain the position of dolerite intrusion in the south-eastern Karoo basin in the work of Baiyegunhi and Gwavava (2017a). This study, therefore, conforms to the findings of Baiyegunhi and Gwavava (2017a).

The analytical map was analyzed for delineation of synclinal structure which could be inferred as an aquifer. As a result, the various gradation in tones was interpreted through borehole-logs coinciding with the magnetic amplitudes and reports drawn from groundtruthing of exposures (Figure 4.11-13). The areas with low magnetic amplitude are the regions associated with a magnetic material deficit and high hydraulic properties. The area with high magnetic amplitude is mainly due to enrichment of magnetic minerals like magnetite and apatite minerals in the rock (Apukhtina et al., 2016). Implications of findings in this section were further discussed together with other findings in this research in the hydrogeological characterization section.



University of Fort Hare
Together in Excellence

9.3 Spatio-temporal variability and recession of streamflow

The assessment of streamflow variability revealed the dissimilarity in hydro-climatic behaviors and streamflow heterogeneity across the watershed. Examination of autocorrelation and the existence of white noise in this study revealed that Buffalo streamflow varies in a stochastic manner across the hydrological time series. The spatial variability in streamflow hydrodynamics suggests the influence of physiographic settings and the land cover system on the drainage pattern of the sub-basins.

The baseflow index (BFI) plots revealed that Buffalo streamflow is perennial. The perennial attribute of the streamflow indicates the existence of connection of the streamflow to a groundwater system. The streamflow recession analyses using FDC and BFI present results

that conform to the streamflow variability results reported by Parde plots, and the trend analysis. The confluence of the drainage system at Buffalo catchment favors the viability of streamflow at the station. The pseudo-section of geoelectric sounding data also indicates that the lithostratigraphy of the Buffalo capture zone is highly saturated, thus indicating the groundwater potential in the area (Figure 7.5E). Within the sub-basin, the report indicates that Yellowwoods and Tshoxa streamflow are perennial while Mgqakwebe, Quencwe, and Ngqokweni are ephemeral. However, it also implies that rainfall has a major influence on the groundwater system of the Buffalo watershed. The BFI results are consistent with Xu et al.'s (2002) assertion on baseflow and stages of a river in South Africa.

The multiple distortions on the DMC plot, the high skewness and kurtosis, the distinct prewhitening, and homogeneity results of Quencwe streamflow suggest that the flow is occasionally turbulent, and with high erosive potential. This is mainly due to the high relief and hillslope influence on the flow velocity. On the contrary, the Ngqokweni streamflow is possibly characterized with extreme river diminution, no-flow regime, variable low flow velocity, trend distortion, insensitive and high deviation from precipitation. The result indicates that the Ngqokweni basin is possibly deficient in groundwater potential. Since high baseflow enables the sustenance of streamflow in dry seasons, conversely, the streamflow deficit in Ngqokweni station indicates poor baseflow contribution. This was also indicated by the low flow section of the FDC and baseflow index plot.

The information from homogeneity tests and plots of DMC, FDC, BFI, and Parde coefficients indicates that the temporal trend of Mgqakwebe, Tshoxa, and Yellowwoods streamflow are uniformly controlled by regional hydro-climatic trends. The tendency for the three stations to replicate similar hydrodynamic responses despite the lithostratigraphic heterogeneity indicates that the three stations are possibly regulated by the same groundwater

aquifer at approximately the same discharge frequency. The high discharge proportion of discharge in Tshoxa station as reported by the descriptive analysis was confirmed by the FDC (low and high sections) plots. The result indicates the existence of favorable groundwater potential in the Basin. Mqgakwebe and Yellowwoods streamflow variability results also indicate the existence of groundwater potential; however, the baseflow discharge in Mqgakwebe is low compared to Tshoxa station. This is possibly due to the alteration influence of the LULC system on soil moisture (Figure 8.6). A typical example is the ecological use of basin for forestry and fishing at the Pirie Mission.

The variability in streamflow pattern in Buffalo catchment is possibly due to the sensitivity of land use/land cover system which is peculiar to a semi-arid environment. The finding here is consistent with the report of Kilment and Matoušková (2009), Choi et al. (2016) and Peng et al. (2016). Kilment and Matoušková (2009) demonstrated a positive change in a land cover which positively alters runoff generation. This may contribute a significant influence on hydrologic alteration in the south. Choi et al. (2016) and Peng et al. (2016) reported the influence of urbanization and complex topography on the streamflow temporal variability.

Urbanization is very high in the south of the catchment compared to the north where the natural ecological system such as woodland and natural vegetation dominates. LULC reports the dominance of dense vegetation, reservation of some portion of the land for forestry and use of some portion of the land for plantation (Figure 8.6 and 8.14). The ecological management of the land lowers the impact of evaporation in the Quencwe basin compared to the Ngqokweni basin which is dominated by sparse vegetation and urbanization. The exposure of the Ngqokweni basin may also influence the quality of drainage and net soil moisture antecedent on account of high evaporate rate as shown by the land surface temperature (LST) map (Figure 8.7). This corresponds to the report of Urqueta et al. (2018)

on evaporation in areas with high LST. Hence, Ngqokweni streamflow can be regarded as a climate-sensitive flow and, as a result, it is ephemeral in status. The existence of climate-sensitive streamflow was first reported by Lins and Slack (1999) based on the result of 395 streamflow stations in the United States based on streamflow variability. Shadmani et al. (2012) also revealed the influence of climate on 11 synoptic stations in arid regions of Iran, while Zhang et al. (2015) also depicted these using streamflow characterizations of 16 stations within Heihe River Basin, north-west China.

The variability in soil moisture content in Quencwe and Ngqokweni basins can also be associated with the orographic influence of relief on atmospheric circulation. The influence of the relief system on the high hydrodynamic response of headwater associated with high relief such as Quencwe, Tshoxa and Mggakwebe stations was reported by the Pc plot. The possible influence of topographic relief on rainfall distribution was reported by Bookhagen and Strecker (2008). Bookhagen and Strecker (2008) indicated that the rainfall peak can be influenced by elevation difference. It also noted that rainfall-topography relations can be controlled by base-level condition and that moisture influx can be influenced by orogeny. In this work, trends of moisture content vary proportionately through the relief system in agreement with Bookhagen and Strecker's reports. The Ngqokweni drainage system lies at a planar topography while Quencwe is associated with high relief. The Quencwe flow may have been driven by the hillslope factor, hence run-off can possibly be influenced by gravity while the Ngqokweni flow is subject to flow resistance and ponding. More so, the wide gap in the extremity of rainfall in the great escarpment to the escarpment interior and low relief in Eastern Cape, South Africa has been established in the work of Jury and Levey (1993). The findings here reveal a strong significant relationship on the trend of streamflow, rainfall and soil moisture as shown by variability assessment, rainfall map (Figure 8.5) and elevation map (Figure 8.16). Reed et al. (2009) report the triangular relationship between rainfall, moisture

development as a result of topographic control and vegetation types. Reed et al. (2009) revealed that a significant relationship and positive association between vegetation diversity and average rainfall while vegetation diversity and topographic moisture indices revealed a negative linear relationship.

The variability in the performance of the BFI employed in this study conforms to the findings of Rutledge (1998), Eckhardt (2008) and Barlow et al. (2015) on calibration variability in metrics of BFI approaches. The estimations of Two-parameter digital filter, PART approaches and BFI programs reveals significant discrepancy in estimation which indicates the possibility of either an overestimation by Two-parameter digital filter and PART programs or an underestimation in BFI programs. The long term average BFI result reveals the decreasing order of baseflow consistent with the size of the watershed. In general, the BFI result is consistent with low flow assessment in order to generalize the significance of baseflow during the dry season.



University of Fort Hare

The entire results further establish the variability in the performance of watershed, which could be used in determining the exploitation potential of streamflow. The BFI analysis reports that Buffalo station has a high proportion of baseflow discharge and, as a result, it reveals the existence of aquifer. The analysis also indicates that there is a high proportion of baseflow discharge in Tshoxa station, that is, the river gains water from a connected groundwater system. Ngqokweni River is reported to have the lowest proportion of groundwater discharge. This is possibly due to the low groundwater potential of its headwater or possibly the exceedance of evaporation potential to infiltration potential. The high-flow analysis of Ngqokweni, however, suggests that the Ngqokweni sub-basin is possibly affected by unfavorable hydro-climate and land use/land cover systems. Some parts of the Ngqokweni basin are covered with dolerite outcrops (Figure 8.2) which is possibly

unfractured as indicated by the surficial lineament map (Figure 4.4). This may possibly complicate the potential for groundwater recharge within the sub-basin.

9.4 Geomorpho-tectonic and geo-electric section analyses

The evolution of drainage networks depended on the dissolution of a petrologic network of weak debris interstice for the creation of hydrodynamic flow-path through geologic architectures and alteration of morpho-tectonic settings of the area. The landscape and the lithologic setting of Buffalo catchment possibly evolve from fluvio-deltaic deposition initiated by flood in the Mesozoic era. This was inferred from the account of braided channelfill structures of the sedimentary facies reported in section 4.1 and the multi-layering system of the lithology revealed by the pseudo-sections of Ngqokweni and Yellowwoods stations (Figure 7.5 A & D). The geomorphic maturity and the deltaic dissection property of the basin drainage which depicts a hyperpycnal flow type at the mouth of the watershed as accounted for in section 7.2.1 further revealed the evolution from fluvio-deltaic deposition. This report conforms to the finding of Catuneanu and Elango (2001) whose investigation on litho-facies of the Beaufort group was based on physical and paleontologic observation. Further, Mutti et al. (2000) revealed that flood-dominated fluvio-deltaic systems are often associated with alluvial successions of tectonically active sedimentary basins. A similar observation was made in this work. The reports on the water level indicated that the water-table across most of the VES stations lies in the alluvial layer of the lithologic log.

9.4.1 Morpho-tectonics of the sub-basins and implications

The result of the morphometric analysis of the Buffalo basin indicates the imprints of drainage fluvial style on the carved petrologic network of weak interstice. The analysis reports the maturation of curves of the drainage networks, the physiographic and lithologic impact on the drainage system (Singh et al., 2013).

Quencwe basin represents the upper course of the river stage where the intense erosive activity takes place. This can be inferred from the bifurcation ratio and the physiographic reports of the basin. The dissection attributes of the drainage, as revealed by the bifurcation ratio, indicates that the drainage is possibly associated with the turbulent flow (Ghany, 2015). Based on the physiographic reports, stream channel which contains cobbles and boulders is possibly associated with highly energetic streamflow. This, therefore, indicates the tendency for flooding in the basin. The tendency for flooding has been indicated by streamflow variability analysis associated with the hydrodynamic flow pattern in the Quencwe basin (section 6.2.2). The streamflow in Quencwe is associated with high efficiency as reported by the elongation ratio in Table 7.2 (Yadav et al., 2014). This also aligns with the impact of the hillslope factor. The high erosive activity probably improves the infiltration potential through the abrasive action of erosion loads on the stream channel and banks. This may have accounted for the fracture and fault system in the basin as indicated by the ruggedness ratio and infiltration number (Pareta and Pareta, 2011; Rai et al., 2017). This is further validated by the thickness of the weathered sandstone layer in the basin lithology (Figure 7.6C). Weathering of the sandstone layer within the basin lithology may have been promoted by the turbulence and abrasive action of eroded boulders. The geoelectric section of the Quencwe basin indicates that the groundwater system in the basin is shallow, hence the river is connected to the basin and possibly gaining from the groundwater system (Barlow and Leake, 2012). A fault system was indicated in the pseudo-section of the geo-electric section carried out in the Quencwe basin. This information suggests that the Quencwe basin has a high potential for groundwater, despite the dolerite outcrops which cover the major part of the basin. The reports on the geo-electric section analysis suggest that the dolerite intrusion is possibly fractured and with a flow-path for groundwater flow. However, the poor lithological control on surface permeability as suggested by the constant of channel maintenance

(Abdulkareem et al., 2018) may be due to the turbulent action of the flow and hillslope factor. Due to the intensive erosion activity and flood potential, the Quencwe catchment mouth can serve as a suitable capture zone for surface water harvest.

Yellowwoods sub-station has the youngest geomorphological development based on its circularity ratio (Wilson et al., 2012). This is contrary to its stream segment and total stream length which are due to its drainage size. The low development in the drainage can be linked with its low energy fluvial style typical of streams with a gentle flow pattern as accounted for by its physiographic report. This also aligns with its low dissection attributes indicated by the bifurcation ratio (Ghany, 2015). Kaliraj et al. (2015) established that drainage basins with long orders and less density of orders are associated with less porous watershed and more permeable layers and vice versa. Based on this, Yellowwoods is dominated by a mudstone deposit at the lower section of the drainage. This is reported by the drainage density, stream frequency and infiltration number which indicate the possibility of low infiltration capacity of the drainage (Yadav et al. 2014; Rai et al. 2017). The ruggedness number report can be linked to the existence of a fracture system in the lithologic material of the basin in some sections of the basin. This finding conforms with the report of auto-lineament analysis in section 4.2 (Figure 4.4) and to the geo-section which provides information on the possibility of a high fault system in the subsurface lithologic layer (Figure 7.7D). There is the possibility of dual river stages in Yellowwoods drainage as indicated by the physiographic reports. The headwater of the drainage indicates the area of relatively high energetic flow which is probably influenced by the possibility of high groundwater discharge in the north and east, while the south is the area of relatively gentle flow. The coarseness of the drainage as reported by drainage texture (Yadav et al., 2014) is probably associated with the discharge at the headwater. Hence, the basin indicates that it has the potential for groundwater drainage at the headwater.

Mgqakwebe drainage represents a middle course stage of a river with less turbulent drainage efficiency as indicated by its elongation ratio (Yadav et al., 2014). However, it has a better constant of channel maintenance, which indicates the possibility of groundwater connection to the streams which enhances the seasonality of the drainage. This was actually true as Table 7. 4B indicates that the stream is connected to the shallow groundwater system. Its form factor reports indicate that the basin surface lithology is characterized with permeable lithology material (Yadav et al., 2014). This high hydraulic conductivity of Mgqakwebe material has been reported by the analytical signal results of residual magnetism of the basin in section 4.3.3. The length of overland flow indicates that the station is likely to serve as a natural aquifer recharge center and indicates the evidence of a local connection to a localized aquifer. The borehole logs within the basin reveal that sandstone thickness within the basin ranges from 12 m at the west to about 75 m at the west. This was confirmed by the pseudosection of VES sounding carried out in the basin.



University of Fort Hare

Ngqokweni sub-basin registered the lowest stream order, stream length, slightly low form factor, ruggedness number, and the lowest watershed texture ratio. Its fluvial style not only indicates a weak and low energy sinuosity but an ephemeral flow with high vulnerability to climate change. It reveals the risk for river diminution, riparian and biodiversity loss. The relative relief ratio indicates that its relief may have been the major factor responsible for its poor drainage system. Ground-truthing also indicates that it is vulnerable to desertification due to the high-temperature incidence in the environment. Ground-truthing and pseudosection results suggest the high impact of groundwater evapotranspiration on account of the thick dry sandstone section in the lithological profile which agrees with the stream frequency and drainage density estimate. The land use/ land cover system looks good with respect to low settlements and urbanization rate but is highly vulnerable due to the veld and bare ground percentage. The low dynamism of hydro-climate and streamflow in Ngqokweni

over geologic time may have enhanced the build-up of high-density interstice which rendered the sandstone of Middleton Formation impermeable. Some of the well-log across Ngqokweni sub-basin indicates the existence of near-surface dolerite intrusion.

The morpho-tectonic assessment revealed Tshoxa sub-basin has a mature drainage system. Its potential for infiltration as indicated by its texture ratio is balanced by its run-off efficiency in conformity to the form factor result. Its stream order-segment ratio informs on its high sustainability and viability for perennial flow. The deduction from stream frequency information suggests that Tshoxa drainage seasonality is supported by a major aquifer. And there are possibilities that the recharge that occurs in the Mgqakwebe sub-basin is partly discharged in Tshoxa drainage from the secondary aquifer connected to the primary aquifer at Mgqakwebe at fair depth.

9.4.2 Buffalo morpho-tectonics



On the broader scale, the Buffalo station indicates a lower stage of the river course. Buffalo catchment has a dendritic drainage pattern. The ordering of Buffalo streams into five indicates the variability in the hydrogeologic and physiographic property of the Buffalo basin from high altitude to the low altitude (Singh et al., 2013). Its dissection property is based on the drainage structure of the headwater. The drainage density plot indicates that the Tshoxa basin has the strongest hydrodynamic influence on Buffalo flow. The efficiency of flow at the station may have been due to streamflow contribution from tributaries. Its fine drainage texture confirms the maturity of the drainage which is indicated by its circularity ratio. Its low infiltration potential and infiltration number can be linked with the unfractured mudstone and dolerite intrusion which possibly dominated the lithology (Johnson et al., 2006; Oghenekome et al., 2016). However, the pseudo-section reveals that the shallow geologic layer is highly saturated. This may have been due to the dominance of alluvial fans within the shallow geology. The river is possibly connected to the shallow water-table at 3 m. Hence,

Buffalo drainage is possibly perennial. The hydro-geomorpho-tectonic settings reveal the three major stages of rivers;

- a. the upper course, where flow turbidity is high and there are possibly minimal groundwater recharge due to hillslope at the far north;
- b. the middle course, where groundwater recharge and discharge are relatively balanced depending on the lithological and aquifer properties, at the west, through the center to the east;
- c. the lower course of the river, where groundwater discharge occurs and river channels become wide and the flow is gentle.

9.5 Eco-environmental analysis of groundwater potential zone mapping

The soil type reveals the general influence of altered morphogenesis of the study area. The local relationship between the soil map and the lithological variation was difficult to establish because of the high resolution of the soil map used. The topographic wetness index (TWI) has been projected in order to reveal the accumulation potential of surface water due to gradient, abrupt downslope, accumulation tendency and gravitational force influence of surface water infiltration as noted by Radula et al. (2018). Corresponding to this, TWI plots reveal areas with potentials for high and low soil moisture. Hence, here high TWI in the north, just as it is for the area with dense vegetation potential, implies the tendency for more groundwater accumulation in the north compared to the south where there are high concentrations of low TWI patches and sparse vegetation potential. It also suggests the high impact of topographic control on groundwater circulation and movement in the watershed.

The LULC map result revealed a varying land-use system that may influence landscape potential for groundwater, hydrologic balance/alteration and morphogenetic changes on the natural pattern of land cover (Figure 8.7). The area with woodland and vegetation cover in

the northern half has a more positive influence on the groundwater potential result as natural conservation of the landform and geologic structures enable infiltration and groundwater transport. The region also indicates the potential for low evaporation rate compared to the south, hence, the plot aligns with the land surface temperature (LST) variability shown by the LST plot (Figure 8.7) and reported in section 8.2.12 and section 9.3. High urbanization has been associated with an increase in total impervious area and reduced potential for infiltration (Rothenberger et al., 2009). Although changes in LULC are not the focus of the study, the result suggests the likely influence of urbanization concentration on the drainage system of the study area as revealed in a visual comparison of the maps (Figure 8.4 and 8.6). This situation agrees with the findings of Rothenberger et al. (2009) on urbanization influence on drainage systems.



9.6. Integrated hydrogeological conceptualization

The GWPZ mapping reveals that Buffalo groundwater resources are hosted by two hydrostratigraphic units; the fractured unit, dominant in the permissive contact zones of dolerite and the inter-granular unit comprising of the arenaceous sedimentary materials (Figure 8.1 and 8.8). This dominant borehole yield falls within the range of 2 – 5 l/s, the fair GWPZ (Figure 8.11), covering 33% of the study area. These findings agree with the report of Vegter (2006) on the hydrogeology of the regional water management area of Buffalo Catchment. However, excellent borehole yield are regionally biased in the study, thus occupying the Northern half of the study area, where the lineament densities are localized. Hence, the localization and distribution of groundwater in the study area is controlled by the permissive contact zone, which also possibly flow in the WNW-ESE direction (Figure 4.4). This study therefore confirms the assertion of Chevallier et al. (2001) on the groundwater potential of weathered and fractured dolerite as a viable aquifer. The poor potential of the

dolerite outcrop in the South is due to limited/non-existence of surficial lineaments in the area (Figure 8.2). It has been previously noted that Buffalo streamflow is a perennial flow and possibly sustained the existence of springs or leaky aquifer. The drainage density map (Figure 8.3) confirms the existence of the springs while the direction of groundwater flow suggested by the lineaments dominant orientation further confirms the possibility of discharges from the local aquifer (Figure 8.2).

The computation approach used in this work, presents the GIS-based GWPZ model as an excellent tool for exploring the prospective spots of groundwater for site-specific geologic investigation. In this work, a significant 90% plus assessment accuracy was obtained by the R^2 and R. This not only validated the applicability of AHP computation, but also accredited the quality of influencing factors employed and the proficiency of pairwise weightage assignment. In conclusion, the computational approach exhibited in this work can be adopted for characterization of groundwater potential zones and areas requiring conservative use against groundwater contamination based on the seven parameters employed..



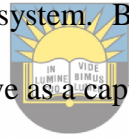
Chapter 10: Conclusions and recommendation

Groundwater exploration in a fractured aquifer of a semi-arid environment is complex. The need for improvement of conceptual knowledge in the delineation of groundwater potential zone in such an environment has led to the integration of hydro-climatic, environmental, geomorphic, and geologic factors using the GIS-based approach. In doing so, the study has been able to present a technically feasible approach involving geohydrodynamic perspectives for the exploration of the groundwater potential zone.

The study showed the possibility of adopting a simpler analytic exploration technique for dominant geologic structures that determine groundwater occurrence and transport. The autolineament extraction revealed the dominance of the surficial lineament in the north and center of the Buffalo catchment. It indicated that the strike and dip of surficial tectonic fault system is in N-W-W 280° / S-E-E 100° and north/south direction respectively, and dominantly within the Barberskrans Member of the Balfour Formation. Digital processing of total residual magnetism lineament suggests the possible orientation of subsurface lineaments and reveals that groundwater flow-net is possibly in a west to east trend based on the strike of the subsurface lineament. The existence of geologic structures that control groundwater flow was also indicated by the pseudo-section of geo-electric data analysis.

The study of spatio-temporal variability of streamflow through the analysis of seasonality of flow and their trends of the flow suggest the variability in the contribution of baseflow. The assessment characterized the six stations assessed into two types; the consistent flows being Tshoxa, Mgqakwebe and Yellowwoods flow and the inconsistent flows being Quencwe, Buffalo and Ngqokweni flows. The major factors identified to have influenced flow variability across the stations are mainly atmospheric circulation, physiography and land use/land cover systems.

The information on groundwater-surface water interaction was drawn from FDC and BFI analyses. The analyses revealed that streamflow recession attributes and groundwater discharge characteristics are consistent with the topography of the environment. The BFI analyses indicate that the Buffalo River is perennial and that the flow is regulated in dry seasons by discharge from a moderate-yield aquifer. In general, there is high variability in baseflow discharge across the rivers on account of the heterogeneity of hydraulic properties of the catchment geologic materials. Tshoxa and Yellowwoods stations reveal a relatively high potential for stormflow and baseflow discharge due to aquifer saturation and basin sizes respectively. Quencwe station indicates flooding potential which may be influenced by high rainfall intensity and the possibility of occasional dam release. Ngqokweni station indicates poor stormflow and low recession attributes which may be due to the location of the headwater and land use/land cover system. Buffalo station reveals excellent recession attributes which indicate that it can serve as a capture zone for surface water exploitation.



University of Fort Hare

Analysis of morphometric parameters reveals the geomorpho-tectonic features consistent with the Buffalo watershed evolution. The analyses revealed that Buffalo catchment evolved from fluvio-deltaic deposition while its present landscape is possibly due to uplift from dolerite intrusion in the north of the catchment. The geomorphic maturity and dissection property of the basin were important indicators of the palaeoenvironmental deposition history. The flow history accounts for the alluvial lithologic cover along the river channel. Buffalo mouth was further revealed as an important highly drained capture zone for both surface water and groundwater. Geo-electric section analysis indicated that the watershed is associated with a fault system that may enhance the effective development of the groundwater system. Quencwe River represents the upper course of the Buffalo River stage. It showed the potential to develop a flash flood possibly influenced by the hillslope factor.

Tshoxa River is a gaining stream whose flow system is regulated by high groundwater discharge or possible existence of spring. Its high dissection property indicates its potential for perennial flow. Mgqakwebe River is a gaining stream whose flow system is controlled by effective baseflow discharge, and with the attributes of the middle course of the river stage. Yellowwoods River represents a drainage basin that transcends from the middle course to lower course due to dual geomorphic development of its drainage, from highly drainage headwater to poorly drained discharge outlet. Ngqokweni River depicts the attributes of a disconnected stream. Its geo-electric section revealed the possibility of decline in water level which may account for its disconnection from the water table. Hence, the river depicts the potential for vulnerability to diminution.

The integration of the geologic property of the Buffalo catchment with other groundwater influencing factors in the environment for groundwater potential zone mapping revealed an important discovery on the spatial variation in groundwater potential across the watershed. Groundwater availability varies abruptly from the north to the south. The north is associated with excellent potential for groundwater while the south is dominated by zones of poor groundwater potential. The abrupt variation has a strong link with the fracture system which is dominant in the northern half of the catchment and atmospheric circulation that favors high rainfall intensity in the north, hence the high saturation of geologic structures. Urbanization, evaporation and land use/land cover may have also contributed to the poor infiltration to a minimal extent. The aquifer system of Buffalo possibly flows from the west to the east based on the yield which suggests high groundwater elevation in the west. The dolerite intrusion at the extreme north and south of the catchment with west-east strike may have constituted the low to no flow boundary for groundwater flow, while the Buffalo River and other connected river systems in the basin constituted a varying head boundary for the groundwater system.

Due to the shallowness of the aquifer and degree of urbanization in the east and south of Buffalo catchment, analysis of the groundwater quality and its suitability for drinking purposes in relation to South Africa national standard have to be considered.

Validation of the GIS-based groundwater potential zone mapping reveals a strong positive and significant relationship with borehole yield, which indicates high precision of the model to the actual field situation. Hence, the approach can be adopted to improve the water resource management system and exploration scheme based on the recommendation made in this work. This project identified the possibility of developing a groundwater system from a high yield sandstone aquifer domain in Tshoxa basin, at the north of Liefldt, and north and south of KwaMamata. The headwater of Mggakwebe basin, around Mpundu, KwaBelekile and the south of Twezana are also important sweet spot of groundwater capture with possibility of high groundwater yield from the intergranular and fractured aquifer. Tyusha, the south of Pirie Fish Station and the Northeast of Frankfurt are zone of high-drained fractured aquifer. Exploitation of groundwater in the areas would ease the social and economic pressure on transfer scheme, and enhance adequate management of surface water. Surface water has been the main source of water supply. The areas identified as the possible capture zone for groundwater should also be considered as being vulnerable to groundwater contamination. Groundwater contamination are not easily remediated, hence, water resource policy which will ensure the protection of the zones of excellent groundwater potentials should be sure. For example, nuclear and radioactive waste from industries, farm practices which involves the releases of contaminants, cesspools, cemeteries, sewer pipes, and gas pipes may have to be reallocated in the zones of poor groundwater potential in order to prevent the risk of contamination of the aquifers. This project is therefore instrumental for water resource management and watershed management since it involved an integrated



University of Fort Hare

approach and a case designed within a catchment scale in compliance with the requirements of the integrated water resource management scheme.

It is recommended that further research involving an integrated approach for surface and subsurface water flow exploration should include numerical modeling. This will help to reveal the role of the intrinsic groundwater aquifer properties in geohydrodynamic flow systems. For a further reconstruction of a geologic unit in the study area, incorporation of provenance and diagenetic analyses of the rock mass is recommended. This enables the definition of the actual geologic unit and decipherment of the actual palaeoenvironment processes. The mathematic and geographic information system methods provided here is a one-and-two-dimensional hybrid approach. For a detailed groundwater exploration program, the adoption of this method would need further point analysis such as deep-hole vertical electric sounding for actual geophysical logging of borehole depth and aquifer thickness.



University of Fort Hare
Together in Excellence

More analysis of the relationship between surficial lineaments and tectonically active seismic lines is recommended in order to improve knowledge on the adoption of surficial lineaments.

More information on the morphometric parameters and hydraulic properties of lithology is recommended as these can improve the application of GIS tools in hydrogeological investigations.

High urbanization in the east and south of Buffalo catchment indicates a high potential for contamination and hydrochemical alteration. Hence, it is recommended that further analysis incorporate groundwater-surface water interaction based on hydrochemical interaction.

Variation in water quality may also consider the use of environmental isotopes. Variation in environmental isotopes across the hydrologic regime may also provide more information on the degree of baseflow discharge or aquifer recharge and residence time of water in the aquifer.

References

- Abdulkareem, J.H., Pradhan, B., Sulaiman, W.N.A. and Jamil, N.R., 2018. Quantification of runoff as influenced by morphometric characteristics in a rural complex catchment. *Earth Systems and Environment*, 2(1), pp.145-162.
- Adiri, Z., El Harti, A., Jellouli, A., Lhissou, R., Maacha, L., Azmi, M., Zouhair, M. and Bachaoui, E.M., 2017. Comparison of Landsat-8, ASTER, and Sentinel 1 satellite remote sensing data in automatic lineaments extraction: A case study of Sidi Flah-Bouskour inlier, Moroccan Anti Atlas. *Advances in Space Research*, 60(11), pp.2355-2367.
- Aher, P.D., Adinarayana, J. and Gorantiwar, S.D., 2014. Quantification of morphometric characterization and prioritization for management planning in semi-arid tropics of India: a remote sensing and GIS approach. *Journal of Hydrology*, 511, pp.850-860.
- Ahmad, N.H. and Deni, S.M., 2013. Homogeneity test on daily rainfall series for Malaysia. *Matematika*, 29, pp.141-150.
- Ali, Z. and Bhaskar, S.B., 2016. Basic statistical tools in research and data analysis. *Indian Journal of Anaesthesia*, 60(9), p.662.
- Amin, A. and Fazal, S., 2017. Assessment of forest fragmentation in District Shopian using multitemporal land cover (A GIS Approach). *Journal of Geosciences and Geomatics*, 5(1), pp.12-23.
- Andreoli, M.A.G., Doucouré, M., Van Bever Donker, J., Brandt, D. and Andersen, N.J.B., 1996. Neotectonics of southern Africa—a review. *Africa Geoscience Review*, 3(1), pp.1-16.
- Andreoli, M.A., Hart, R.J., Ashwal, L.D. and Coetzee, H., 2006. Correlations between U, Th content and metamorphic grade in the western Namaqualand Belt, South Africa, with implications for radioactive heating of the crust. *Journal of Petrology*, 47(6), pp.1095-1118.



- Anibas, C., Verbeiren, B., Buis, K., Chromanski, J., De Doncker, L., Okruszko, T., Meire, P. and Batelaan, O., 2012. A hierarchical approach on groundwater-surface water interaction in wetlands along the upper Biebrza River, Poland. *Hydrology and earth system sciences.Katlenburg-Lindau*, 16(7), pp.2329-2346.
- Ansari, Z.R., Rao, L.A.K. and Yusuf, A., 2012. GIS-based morphometric analysis of Yamuna drainage network in parts of Fatehabad area of Agra district, Uttar Pradesh. *Journal of the Geological Society of India*, 79(5), pp.505-514.
- Apukhtina, Olga B., Vadim S. Kamenetsky, Kathy Ehrig, Maya B. Kamenetsky, Jocelyn McPhie, Roland Maas, Sebastien Meffre et al., "Postmagmatic magnetite–apatite assemblage in mafic intrusions: a case study of dolerite at Olympic Dam, South Australia." *Contributions to Mineralogy and Petrology* 171, no. 1 (2016): 2.
- Aquilué, N., De Cáceres, M., Fortin, M.J., Fall, A. and Brotons, L., 2017. A spatial allocation procedure to model land-use/land-cover changes: Accounting for the occurrence and spread processes. *Ecological Modelling*, 344, pp.73-86.
- Arnold, J.G., Muttiah, R.S., Srinivasan, R. and Allen, P.M., 2000. Regional estimation of base flow and groundwater recharge in the Upper Mississippi river basin. *Journal of Hydrology*, 227(1-4), pp.21-40.
- Asfaw, A., Simane, B., Hassen, A. and Bantider A., 2018. Variability and time series trend analysis of rainfall and temperature in Northcentral Ethiopia: A case study in Woleka subbasin. *Weather and Climate Extremes*, 19(2018), pp.29-41.
- Attwa, M. and Ali, H., 2018. Resistivity Characterization of Aquifer in Coastal Semiarid Areas: An Approach for Hydrogeological Evaluation. In *Groundwater in the Nile Delta*. Springer, Cham. pp. 213-233
- Attwa, M., El-Bastawesy, M. and El-fattah, A.M., 2016. How Efficient is an Integrative

Approach of GIS and Resistivity Data in Groundwater Exploration? A Case Study of Esna, Luxor, Egypt.

Avinash, K., Deepika, B. and Jayappa, K.S., 2014. Basin geomorphology and drainage morphometry parameters used as indicators for groundwater prospect: insight from geographical information system (GIS) technique. *Journal of Earth Science*, 25(6), pp.1018-1032.

Azaiez, H., Gabtni, H., Bédir, M. and Campbell, S., 2018. Aeromagnetic study of buried basement structures and lineaments of Sahel region (Eastern Tunisia, North Africa). *Arabian Journal of Geosciences*, 11(7), p.140.

Bailey, G.N., Reynolds, S.C. and King, G.C., 2011. Landscapes of human evolution: models and methods of tectonic geomorphology and the reconstruction of hominin landscapes. *Journal of Human Evolution*, 60(3), pp.257-280.

Baiyegunhi, C., 2015. Geological and Geophysical Investigation of the Southeastern Karoo Basin, South Africa (*Doctoral dissertation, University of Fort Hare*).

Baiyegunhi, C. and Gwavava, O., 2017a. Magnetic investigation and 2½ D gravity profile modelling across the Beattie magnetic anomaly in the southeastern Karoo Basin, South Africa. *Acta Geophysica*, 65(1), pp.119-138.

Baiyegunhi, C., Liu, K. and Gwavava, O., 2017b. Sedimentation rate and subsidence history of the southeastern Karoo Basin, South Africa, using 1D backstripping method. *Arabian Journal of Geosciences*, 10(10), p.225.

Banzhaf, S., Krein, A. and Scheytt, T., 2013. Using selected pharmaceutical compounds as indicators for surface water and groundwater interaction in the hyporheic zone of a low permeability riverbank. *Hydrological Processes*, 27(20), pp.2892-2902.

Barath, S., 2015. Delineation of Groundwater Region 65: Zululand Coastal Plain Aquifer,

KwaZulu-Natal (*Doctoral dissertation, North-West University (South Africa), Potchefstroom Campus*).

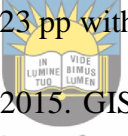
- Barlow, P.M. and Leake, S.A., 2012. Streamflow depletion by wells: understanding and managing the effects of groundwater pumping on streamflow (p. 84). Reston, VA: *US Geological Survey*.
- Barlow, P.M., Cunningham, W.L., Zhai, Tong, and Gray, Mark, 2015. U.S. Geological Survey Groundwater Toolbox, a graphical and mapping interface for analysis of hydrologic data (version 1.0)—User guide for estimation of base flow, runoff, and groundwater recharge from streamflow data: *U.S. Geological Survey Techniques and Methods*, book 3, chap. B10, 27 p.,
- Barros, A.P., Hodes, J.L. and Arulraj, M., 2017. Decadal climate variability and the spatial organization of deep hydrological drought. *Environmental Research Letters*, 12(10), p.104005.
- Barthel, R. and Banzhaf, S., 2016. Groundwater and surface water interaction at the regionalscale—a review with focus on regional integrated models. *Water resources management*, 30(1), pp.1-32.
- Batalla, R.J., Gomez, C.M. and Kondolf, G.M., 2004. Reservoir-induced hydrological changes in the Ebro River basin (NE Spain). *Journal of Hydrology*, 290(1-2), pp.117-136.
- Bates, B.C. and Davies, P.K., 1988. Effect of baseflow separation procedures on surface runoff models. *Journal of Hydrology*, 103(3-4), pp.309-322.
- Bencala, K.E. and Walters, R.A., 1983. Simulation of solute transport in a mountain pool and riffle stream: A transient storage model. *Water Resources Research*, 19(3), pp.718-724.
- Beven, K., 2002. Towards an alternative blueprint for a physically based digitally simulated hydrologic response modelling system. *Hydrological Processes*, 16(2), pp.189-206.

- Beven, K., 2012. Causal models as multiple working hypotheses about environmental processes. *Comptes Rendus Geoscience*, 344, 77-88.
- Bonetto, S., Facello, A. and Umili, G., 2017. A new application of CurvaTool semi-automatic approach to qualitatively detect geological lineaments. *Environmental & Engineering Geoscience*, 23(3), pp.179-190.
- Bookhagen, B. and Strecker, M.R., 2008. Orographic barriers, high-resolution TRMM rainfall, and relief variations along the eastern Andes. *Geophysical Research Letters*, 35(6).
- Bormann, H., 2010. Runoff regime changes in German rivers due to climate change. *Erdkunde*, pp.257-279.
- Bracken, L.J., Wainwright, J., Ali, G.A., Tetzlaff, D., Smith, M.W., Reaney, S.M. and Roy, A.G., 2013. Concepts of hydrological connectivity: research approaches, pathways and future agendas. *Earth-Science Reviews*, 119, pp.17-34.
- Bredenkamp, D.B., Botha, L.J., van Tonder, G.J. and van Rensburg, H.J., 1995. Manual on Quantitative Estimation of Groundwater Recharge and Aquifer Storativity. *WRC Report TT 73/95*, Pretoria, South Africa, pp. 407.
- Bredenkamp, D.B., Schutte, J.M. and Dutoit, G.J., 1974. Recharge of a dolomitic aquifer as determined from tritium profiles. *Isotope Techniques in Groundwater Hydrology*, IAEA, Vienna, pp. 73-94.
- Bredenkamp, D.B. and Vogel, J.C., 1970. Study of a dolomitic aquifer with carbon-14 and tritium. *Isotope Hydrology 1970*, Proc. Symp. IAEA, 9-13 March, 1970, 349-371.
- Broquet, C.A., 1992. The sedimentary record of the Cape Supergroup: A review. Inversion tectonics of the Cape Fold Belt, Karoo and Cretaceous basins of southern Africa, 159, p.183.

- Burbery, L.F., Moore, C.R., Jones, M.A., Abraham, P.M., Humphries, B.L. and Close, M.E., 2018. Study of connectivity of open framework gravel facies in the Canterbury Plains aquifer using smoke as a tracer. *Geological Society, London, Special Publications*, 440(1), pp.327-344.
- Burn, D.H. and Elnur, M.A.H., 2002. Detection of hydrologic trends and variability. *Journal of Hydrology*, 255(1-4), pp.107-122.
- Caló, F., Notti, D., Galve, J., Abdikan, S., Görüm, T., Pepe, A., and Balik Şanlı, F. (2017). Dinsar-based detection of land subsidence and correlation with groundwater depletion in konya plain, Turkey. *Remote Sensing*, 9(1), 83.
- Catuneanu, O., 2004. Retroarc foreland systems—evolution through time. *Journal of African Earth Sciences*, 38(3), pp.225-242.
- Catuneanu, O. and Elango, H.N., 2001. Tectonic control on fluvial styles: the Balfour Formation of the Karoo Basin, South Africa. *Sedimentary Geology*, 140(3-4), pp.291-313.
- Catuneanu, O., Hancox, P.J. and Rubidge, B.S., 1998. Reciprocal flexural behaviour and contrasting stratigraphies: a new basin development model for the Karoo retroarc foreland system, South Africa. *Basin Research*, 10(4), pp.417-439.
- Catuneanu, O., Wopfner, H., Eriksson, P.G., Cairncross, B., Rubidge, B.S., Smith, R.M.H. and Hancox, P.J., 2005. The Karoo basins of south-central Africa. *Journal of African Earth Sciences*, 43(1-3), pp.211-253.
- Chapman, T., 1999. A comparison of algorithms for stream flow recession and baseflow separation. *Hydrological Processes*, 13(5), pp.701-714.
- Chen, Y., Guan, Y., Shao, G. and Zhang, D., 2016. Investigating trends in streamflow and precipitation in Huangfuchuan Basin with wavelet analysis and the Mann-Kendall test. *Water*, 8(3), p.77.

- Chhetri, P.K., 2018. Predicting upslope expansion of sub-alpine forest in the Makalu Barun National Park, Eastern Nepal, with a hybrid cartographic model. *Journal of Forestry Research*, 29(1), pp.129-137.
- Chevallier, L. and Woodford, A., 1999. Morpho-tectonics and mechanism of emplacement of the dolerite rings and sills of the western Karoo, South Africa. *South African Journal of Geology*, 102(1), pp.43-54.
- Choi, W., Nauth, K., Choi, J. and Becker, S., 2016. Urbanization and rainfall–runoff relationships in the Milwaukee River Basin. *The Professional Geographer*, 68(1), pp.14-25.
- Chung, I.M., Kim, N.W., Lee, J. and Sophocleous, M., 2010. Assessing distributed groundwater recharge rate using integrated surface water-groundwater modelling: application to Mihocheon watershed, South Korea. *Hydrogeology Journal*, 18(5), pp.1253-1264.
- Cimen, M. and Saplioglu, K., 2004, May. A Procedure For Separation Of Baseflow. In Conference of Water Observation and Information System for Decision Support (BALWOIS) (pp. 25-29).
- Cobbing, J., 2014. Groundwater for rural water supplies in South Africa. *Nelson Mandela Metropolitan University and SLR Consulting (Pty) Ltd.*
- Cobbing, J.E. and de Wit, M., 2018. The Grootfontein aquifer: Governance of a hydro-social system at Nash equilibrium. *South African Journal of Science*, 114(5-6), pp.1-7.
- Collischonn, W., and Fan, F. M., 2013. Defining parameters for Eckhardt's digital baseflow filter. *Hydrological Processes*, 27(18), 2614-2622
- Coney, L., Reimold, W.U., Hancox, P.J., Mader, D., Koeberl, C., McDonald, I., Struck, U.,

- Vajda, V. and Kamo, S.L., 2007. Geochemical and mineralogical investigation of the Permian–Triassic boundary in the continental realm of the southern Karoo Basin, South Africa. *Palaeoworld*, 16(1-3), pp.67-104.
- Conway, D., Van Garderen, E.A., Deryng, D., Dorling, S., Krueger, T., Landman, W., Lankford, B., Lebek, K., Osborn, T., Ringler, C. and Thurlow, J., 2015. Climate and southern Africa's water–energy–food nexus. *Nature Climate Change*, 5(9), p.837.
- Cook, P.G., 2003. A guide to regional groundwater flow in fractured rock aquifers. *CSIRO Land and Water*, Australia.
- Cooper, G.R., 2014. The automatic determination of the location, depth, and dip of contacts from aeromagnetic data. *Geophysics*, 79(3), pp.J35-J41.
- Corgne, S., Magagi, R., Yergeau, M. and Sylla, D., 2010. An integrated approach to hydrogeological lineament mapping of a semi-arid region of West Africa using Radarsat-1 and GIS. *Remote Sensing of Environment*, 114(9), pp.1863-1875.
- Crocker, K.M., Young, A.R., Zaidman, M.D. and Rees, H.G., 2003. Flow duration curve estimation in ephemeral catchments in Portugal. *Hydrological Sciences Journal*, 48(3), pp.427-439.
- Dahl, M., Nilsson, B., Langhoff, J.H. and Refsgaard, J.C., 2007. Review of classification systems and new multi-scale typology of groundwater–surface water interaction. *Journal of Hydrology*, 344(1-2), pp.1-16.
- Das, S., Gupta, A. and Ghosh, S., 2017. Exploring groundwater potential zones using MIF technique in semi-arid region: a case study of Hingoli district, Maharashtra. *Spatial Information Research*, 25(6), pp.749-756.
- De Coning, C., 2006. Overview of the water policy process in South Africa. *Water Policy*, 8(6), pp.505-528.

- Demers, J.D., Yavitt, J.B., Driscoll, C.T. and Montesdeoca, M.R., 2013. Legacy mercury and stoichiometry with C, N, and S in soil, pore water, and stream water across the upland - wetland interface: The influence of hydrogeologic setting. *Journal of Geophysical Research: Biogeosciences*, 118(2), pp.825-841.
- Dhansay, T., Brandl, G. and De Wit, M.J., 2016. Fractal geometry of the fault network across the Soutpansberg Mountains, Limpopo, South Africa. *South African Journal of Geology* 2016, 119(1), pp.235-242.
- Dickinson, W.R., 1974. Plate tectonics and sedimentation.
- Dijkshoorn JA, van Engelen VWP and Huting JRM 2008. Soil and landform properties for LADA partner countries (Argentina, China, Cuba, Senegal and The Gambia, South Africa and Tunisia). *ISRIC report 2008/06 and GLADA report 2008/03, ISRIC – World Soil Information and FAO*, Wageningen (23 pp with data set)
- Dixon, B., Uddameri, V. and Ray, C., 2015. GIS and Geocomputation for Water Resource Science and Engineering. *John Wiley & Sons*.  **University of Fort Hare**
excellence
- Djuric, P.M. and Míguez, J., 2010. Assessment of nonlinear dynamic models by Kolmogorov–Smirnov statistics. *IEEE Transactions on Signal Processing*, 58(10), pp.5069-5079.
- Domenico, P.A. and Schwartz, F.W., 1990, Physical and chemical hydrogeology
- Dougherty, E.R., Kim, S. and Chen, Y., 2000. Coefficient of determination in nonlinear signal processing. *Signal Processing*, 80(10), pp.2219-2235.
- Douglas, E.M., Vogel, R.M. and Kroll, C.N., 2000. Trends in floods and low flows in the United States: impact of spatial correlation. *Journal of Hydrology*, 240(1-2), pp.90-105.
- DWA (Department of Water Affairs, South Africa), 2010. Groundwater Strategy 2010. *Department of Water Affairs*, Pretoria.

- Eckhardt, K., 2005. How to construct recursive digital filters for baseflow separation. *Hydrological Processes: An International Journal*, 19(2), 507-515.
- Eckhardt, K., 2008. A comparison of baseflow indices, which were calculated with seven different baseflow separation methods. *Journal of Hydrology*, 352(1-2), pp.168-173.
- Eckhardt, K., 2012. Analytical sensitivity analysis of a two parameter recursive digital baseflow separation filter. *Hydrology and Earth System Sciences*, 16(2), pp.451-455.
- Entholzner, A. and Reeve, C. eds., 2016. Building climate resilience through virtual water and nexus thinking in the southern African development community. *Springer*.
- Esralew, R.A. and Lewis, J.M., 2010. Trends in base flow, total flow, and base-flow index of selected streams in and near Oklahoma through 2008 (No. 2010-5104). *US Geological Survey*.
- Evangelin, R., Selvakumar, R., Rajasimman, U. and Victor, R., 2015. Morphometric analysis of sub-watershed in parts of Western Ghats, South India using ASTER DEM. *Geomatics. Nature Hazard Risk*, 6, pp.326-341.
- Faiz, M.A., Liu, D., Fu, Q., Li, M., Baig, F., Tahir, A.A., Khan, M.I., Li, T. and Cui, S., 2018. Performance evaluation of hydrological models using ensemble of General Circulation Models in the northeastern China. *Journal of Hydrology*, 565, pp.599-613.
- Feijth, J., Cevallos, C., Rudge, T. and Parsons, M., 2019. Three-dimensional interpretation of tectono-sedimentary evolution and hydrocarbon prospectivity by the integration of airborne gravity gradiometer, regional gravity, magnetic, and two-dimensional seismic data in the Canning Basin, Western Australia. *AAPG Bulletin*, 103(3), pp.569-604.
- Fenta, A.A., Kifle, A., Gebreyohannes, T. and Hailu, G., 2015. Spatial analysis of groundwater potential using remote sensing and GIS-based multi-criteria evaluation in Raya Valley, northern Ethiopia. *Hydrogeology Journal*, 23(1), pp.195-206.

- Ferreira, F.J., de Souza, J., de B. e S. Bongioiolo, A. and de Castro, L.G., 2013. Enhancement of the total horizontal gradient of magnetic anomalies using the tilt angle. *Geophysics*, 78(3), pp.J33-J41.
- Fetter, C.W., 2018. Applied hydrogeology. *Waveland Press*.
- Galloway, D.L., 2010. The complex future of hydrogeology. *Hydrogeology journal*, 18(4), pp.807-810.
- Gebre, T., Kibru, T., Tesfaye, S. and Taye, G., 2015. Analysis of watershed attributes for water resources management using GIS: The case of Chelekot micro-watershed, Tigray, Ethiopia. *Journal of Geographic Information System*, 7(02), p.177.
- Ghany, M.K.A., 2015. Quantitative Morphometric Analysis of Drainage Basins between Qusseir and Abu Dabbab Area, Red Sea Coast, Egypt using GIS and Remote Sensing Techniques. *International Journal of Advanced Remote Sensing and GIS*, 4(1), pp.1295132.
- Gilluly, J., 1976. Lineaments; ineffective guides to ore deposits. *Economic Geology*, 71(8), pp.1507-1514.
- Gimblett, R., 1989. Innovations in computer labs. Linking perception research, visualsimulations and dynamic modeling within a GIS framework: The ball state experiencecomputers. *Environment and Urban Systems*, vol. 13(2), pp. 109–123.
- Glose, T.J., Lowry, C.S. and Hausner, M.B., 2019. Vertically _integrated hydraulic conductivity: a new parameter for groundwater_surface water analysis. *Groundwater*.
- Graf, A., Bogena, H.R., Drüe, C., Hardelauf, H., Pütz, T., Heinemann, G. and Vereecken, H., 2014. Spatiotemporal relations between water budget components and soil water content in a forested tributary catchment. *Water Resources Research*, 50(6), pp.4837-4857.



University of Fort Hare

- Grimm, N.B. and Fisher, S.G., 1984. Exchange between interstitial and surface water: implications for stream metabolism and nutrient cycling. *Hydrobiologia*, 111(3), pp.219-228.
- Haitjema, H.M., 1995. Analytic element modeling of groundwater flow. *Elsevier*.
- Hashim, M., Ahmad, S., Johari, M.A.M. and Pour, A.B., 2013. Automatic lineament extraction in a heavily vegetated region using Landsat Enhanced Thematic Mapper (ETM+) imagery. *Advances in Space Research*, 51(5), pp.874-890.
- Hayashi, M. and Rosenberry, D.O., 2002. Effects of ground water exchange on the hydrology and ecology of surface water. *Groundwater*, 40(3), pp.309-316.
- Hayashi, M., van der Kamp, G. and Rosenberry, D.O., 2016. Hydrology of prairie wetlands: understanding the integrated surface-water and groundwater processes. *Wetlands*, 36(2), pp.237-254.
- Hiller, N. and Stavrakis, N., 1980. Distal alluvial fan deposits in the Beaufort Group of the Eastern Cape Province. *Transactions of the Geological Society of South Africa*, 83, pp.353-360.
- Hiller, N. and Stavrakis, N., 1984. Permo-Triassic fluvial systems in the southeastern Karoo basin, South Africa. *Palaeogeography, Palaeoclimatology, Palaeoecology*, 45(1), pp.1-21.
- Hirsch, R.M. and Slack, J.R., 1984. A nonparametric trend test for seasonal data with serial dependence. *Water Resources Research*, 20(6), pp.727-732.
- Hoffmann, J. and Sander, P., 2007. Remote sensing and GIS in hydrogeology. *Hydrogeology Journal*, vol. 15(1), pp. 1–3
- Hojati, M. and Mokarram, M., 2016. Determination of a topographic wetness index using high resolution digital elevation models. *European Journal of Geography*, 7(4), pp.41-52.



University of Fort Hare

South Africa

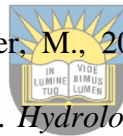
- Holland, M. and Witthüser, K.T., 2011. Evaluation of geologic and geomorphologic influences on borehole productivity in crystalline bedrock aquifers of Limpopo Province, South Africa. *Hydrogeology Journal*, 19(5), pp.1065-1083.
- Hong, H., Tsangaratos, P., Ilija, I., Liu, J., Zhu, A.X. and Chen, W., 2018. Application of fuzzy weight of evidence and data mining techniques in construction of flood susceptibility map of Poyang County, China. *Science Of The Total Environment*, 625, pp.575-588.
- Horton, R.E., 1945. Erosional development of streams and their drainage basins; hydrophysical approach to quantitative morphology. *Geological Society Of America Bulletin*, 56(3), pp.275-370.
- Hu, D.L., Chan, B. and Bush, J.W., 2003. The hydrodynamics of water strider locomotion. *Nature*, 424(6949), p.663.
- Hughes, D.A., Kapangaziwiri, E. and Baker, K., 2010. Initial evaluation of a simple coupled surface and groundwater hydrological model to assess sustainable groundwater abstractions at the regional scale. *Hydrology Research*, 41 (1), 1-12.
- Hughes, D.A., Gush, M., Tanner, J.L. and Dye, P., 2013. Using targeted short-term field investigations to calibrate and evaluate the structure of a hydrological model. *Hydrological Processes*, DOI: 10.1002/hyp.9807.
- Hughes, Z.J., FitzGerald, D.M., Wilson, C.A., Pennings, S.C., Więski, K. and Mahadevan, A., 2009. Rapid headward erosion of marsh creeks in response to relative sea level rise. *Geophysical Research Letters*, 36(3).
- Institute of Hydrology (Great Britain), 1980. Low Flow Studies Reports. *Institute of Hydrology*.
- James, O.B. and Hedenquist, J.W., 1978. Consortium breccia 73255: Petrology of aphanitic lithologies (abs). Lunar Planet. Sci. IX. *Lunar Planetary Institute, Houston*, pp.



University of Fort Hare
Together in Excellence

585-587

- Jewitt, G.P.W. and Schulze, R.E., 1999. Verification of the ACRU model for forest hydrology applications. *Water SA*, 25(4), pp.483-489.
- Johnson, M.R., 1976. Stratigraphy and sedimentology of the Cape and Karoo sequences in the Eastern Cape Province.
- Johnson, M.R., Van Vuuren, C.J., Hegenberger, W.F., Key, R. and Show, U., 1996. Stratigraphy of the Karoo Supergroup in southern Africa: an overview. *Journal of African Earth Sciences*, 23(1), pp.3-15.
- Johnson, M.R., Van Vuuren, C.J., Visser, J.N.J., Cole, D.I., Wickens, H.D.V., Christie, A.D.M., Roberts, D.L. and Brandl, G., 2006. Sedimentary rocks of the Karoo Supergroup. *The Geology of South Africa*, pp.461-499.
- Kalbus, E., Reinstorf, F. and Schirmer, M., 2006. Measuring methods for groundwater? surface water interactions: a review. *Hydrology and Earth System Sciences Discussions*, 10(6), pp.873-887.
- Kaliraj, S., Chandrasekar, N. and Magesh, N.S., 2015. Morphometric analysis of the River Thamirabarani sub-basin in Kanyakumari District, South west coast of Tamil Nadu, India, using remote sensing and GIS. *Environmental Earth Sciences*, 73(11), pp.7375-7401.
- Kanagaraj, G., Elango, L., Sridhar, S.G.D. and Gowrisankar, G., 2018. Hydrogeochemical processes and influence of seawater intrusion in coastal aquifers south of Chennai, Tamil Nadu, India. *Environmental Science and Pollution Research*, 25(9), pp.8989-9011.
- Kapangaziwiri, E. and Hughes, D.A., 2008. Towards revised physically-based parameter estimation methods for the Pitman monthly rainfall-runoff model. *Water SA*, 32 (2), 183191.
- Katemaunzanga, D. and Gunter, C.J., 2009. Lithostratigraphy, sedimentology, and provenance of the Balfour Formation (Beaufort Group) in the Fort Beaufort–Alice area,



University of Fort Hare
Together in Excellence

- Eastern Cape Province, South Africa. *Acta Geologica Sinica-English Edition*, 83(5), pp.902-916.
- Kazemi, R. and Davoodi, H., 2011. The role of structural elements in reconnaissance of karst hydrology in the Lar catchment's, Iran. in Asian trans-disciplinary karst conference 2011 (p. 92).
- Kelbe, B. and Germishuysen, T., 2010. Groundwater/surface water relationships with specific reference to Maputaland. *Water Research Commission Report*, (1168/1), p.10.
- Kendall, M.G., 1948. Rank correlation methods.
- Kienzle, S.W., 2006. The use of the recession index as an indicator for streamflow recovery after a multi-year drought. *Water Resources Management*, 20(6), pp.991-1006.
- Kilment, Z. and Matoušková, M., 2009. Runoff changes in the Šumava Mountains (Black Forest) and the foothill regions: extent of influence by human impact and climate change. *Water Resources Management*, 23(9), pp.1813-1834.
- Kisi, O. and Ay, M., 2014. Comparison of Mann-Kendall and innovative trend method for water quality parameters of the Kizilirmak River, Turkey. *Journal of Hydrology*, 513, pp.362-375.
- Kocal, A., Duzgun, H.S. and Karpuz, C., 2004. Discontinuity mapping with automatic lineament extraction from high resolution satellite imagery. *ISPRS XX, Istanbul*, pp.12-23.
- Krause, S., Boano, F., Cuthbert, M.O., Fleckenstein, J.H. and Lewandowski, J., 2014. Understanding process dynamics at aquifer-surface water interfaces: An introduction to the special section on new modeling approaches and novel experimental technologies. *Water Resources Research*, 50(2), pp.1847-1855.
- Krzywinski, M. and Altman, N., 2014. Points of significance: visualizing samples with box plots.

- Lanci, L., Tohver, E., Wilson, A. and Flint, S., 2013. Upper Permian magnetic stratigraphy of the lower Beaufort group, Karoo basin. *Earth and Planetary Science Letters*, 375, pp.123134.
- Lane, P.N., Best, A.E., Hickel, K. and Zhang, L., 2005. The response of flow duration curves to afforestation. *Journal of Hydrology*, 310(1-4), pp.253-265.
- Le Maitre, D.C and Colvin, C.A., 2008. Assessment of the contribution of groundwater discharges to rivers using monthly flow statistics and flow seasonality. *Water SA*, 34 (5), 549-564.
- Leake, S.A. and Barlow, P.M., 2013. Understanding and managing the effects of groundwater pumping on streamflow. US Department of the Interior, *US Geological Survey*.
- Lesage, G., Byrne, K., Morris, W.A., Enkin, R.J., Lee, R.G., Mir, R. and Hart, C.J., 2019. Interpreting regional 3D fault networks from integrated geological and geophysical data sets: An example from the Guichon Creek batholith, British Columbia. *Journal of Structural Geology*, 119, pp.93-106.
- Levy, J. and Xu, Y., 2012. Groundwater management and groundwater/surface-water interaction in the context of South African water policy. *Hydrogeology Journal*, 20(2), pp.205-226.
- Lewis, C.A., 2008. Glaciations and glacial features. Geomorphology of the Eastern Cape, South Africa. 2nd ed. NISC, Grahamstown, pp.127-148.
- Li, X., 2006. Understanding 3D analytic signal amplitude. *Geophysics*, 71(2), pp.L13-L16.
- Li, Y., Zhang, Q., Yao, J., Werner, A.D. and Li, X., 2013. Hydrodynamic and hydrological modeling of the Poyang Lake catchment system in China. *Journal of Hydrologic Engineering*, 19(3), pp.607-616.
- Lillesand, T., Kiefer, R.W. and Chipman, J., 2014. Remote sensing and image interpretation.

John Wiley & Sons.

Lindeque, A., de Wit, M.J., Ryberg, T., Weber, M. and Chevallier, L., 2011. Deep crustal profile across the southern Karoo Basin and Beattie Magnetic Anomaly, South Africa: an integrated interpretation with tectonic implications. *South African Journal of Geology*, 114(3-4), pp.265-292.

Lins, H.F. and Slack, J.R., 1999. Streamflow trends in the United States. *Geophysical Research Letters*, 26(2), pp.227-230.

Lott, D. A., and Stewart, M. T., 2013. A power function method for estimating base flow. *Groundwater*, 51(3), 442-451. <https://doi.org/10.1111/j.1745-6584.2012.00980.x>

Luo, M., Chen, Z., Zhou, H., Zhang, L. and Han, Z., 2018. Hydrological response and thermal effect of karst springs linked to aquifer geometry and recharge processes. *Hydrogeology Journal*, 26(2), pp.629-639.




Lyle, J. and Stutz, F.P., 1983. Computerised land use suitability mapping. *The Cartographic Journal*, vol. 20(1), pp.39-49.

MacDonald, A.M. and Davies, J., 2000. A brief review of groundwater for rural water supply in sub-Saharan Africa.

Machiwal, D. and Jha, M.K., 2009. Time series analysis of hydrologic data for water resources planning and management: a review. *Journal of Hydrology and Hydromechanics*, 54(3), pp.237-257.

Machiwal, D., Jha, M.K. and Mal, B.C., 2011. Assessment of groundwater potential in a semiarid region of India using remote sensing GIS and MCDM techniques. *Water Resources Management*, vol. 25(5), pp. 1359–1386.


- Madi, K, and Zhao, B., 2010. Neotectonics and its applications for the exploration of groundwater in the Karoo fractured aquifers in the Eastern Cape, South Africa. MSc dissertation, University of Fort Hare, South Africa.
- Madi, K. and Zhao, B., 2013. Neotectonic belts, remote sensing and groundwater potentials in the Eastern Cape Province, South Africa. *International Journal of Water Resources and Environmental Engineering*, 5(6), pp.332-350.
- Mahajan, S. and Sivakumar, R., 2018. Evaluation of physical and morphometric parameters for water resource management in Gad Watershed, Western Ghats, India: an integrated geoinformatics approach. *Environmental Earth Sciences*, 77(15), p.556.
- Mahan, M.Y., Chorn, C.R. and Georgopoulos, A.P., 2015. White Noise Test: detecting autocorrelation and nonstationarities in long time series after ARIMA modeling. In Proceedings 14th Python in Science Conference (Scipy 2015), Austin, TX.
- Mair, A. and Fares, A., 2011. Time series analysis of daily rainfall and streamflow in a volcanic dike-intruded aquifer system, O'ahu, Hawai'i, USA. *Hydrogeology Journal*, 19(4), pp.929-944.
- Mann, H.B., 1945. Nonparametric tests against trend. *Econometrica: Journal of the Econometric Society*, pp.245-259.
- Marghany, M. and Hashim, M., 2010. Lineament mapping using multispectral remote sensing satellite data. *International Journal of Physical Sciences*, 5(10), pp.1501-1507.
- Marghany, M., Hashim, M. and Mansor S., 2009. Geologic mapping of United Arab Emirates using multispectral remotely sensed data. *American Journal of Engineering and Applied Sciences*, vol. 2(2), pp. 476-480.

- Masoud, M.H., 2016. Geoinformatics application for assessing the morphometric characteristics' effect on hydrological response at watershed (case study of Wadi Qanunah, Saudi Arabia). *Arabian Journal of Geosciences*, 9(4), p.280.
- Maughan, E.K. and Perry Jr, W.J., 1986. Lineaments and Their Tectonic Implications in the Rocky Mountains and Adjacent Plains Region: Part I. Regional Overview.
- McBride, M.S. and Pfannkuch, H.O., 1975. The distribution of seepage within lakebeds. *Journal of Reservoir, US Geological Survey*, 3(5), pp.505-512.
- McKeen, S.A., Wilczak, J., Grell, G., Djalalova, I., Peckham, S., Hsie, E., Gong, W., Bouchet, V., Menard, S., Moffet, R., McHenry, J., McQueen, J., Tang, Y., Carmichael, G. R., Pagowski, M., Chan, A., Dye, T., Frost, G., Lee, P. and Mathur, R., 2005. Assessment of an ensemble of seven realtime ozone forecasts over eastern North America during the summer of 2004, *Journal of Geophysical Research*, vol. 110(21), pp. 1984-2012.
- Mishra, A.K. and Singh, V.P., 2010. Changes in extreme precipitation in Texas. *Journal of Geophysical Research: Atmospheres*, 115(D14).

 University of Fort Hare
 Geographical Science
- Montgomery, D.R. and Dietrich, W.E., 2002. Runoff generation in a steep, soil-mantled landscape. *Water Resources Research*, 38(9), pp.7-1.
- Moody, J.D. and Hill, M.J., 1956. Wrench-fault tectonics. *Geological Society of America Bulletin*, 67(9), pp.1207-1246.
- Mutti, E., Tinterri, R., di Biase, D., Fav, L., Mavilla, N., Angella, and Calabrese, L., 2000. Delta-front facies associations of ancient flood-dominated fluvio-deltaic systems. *Review of Social Geology*. Espana, 13 (2): 165-190
- Müller, M. F., Dralle, D. N., and Thompson, S. E., 2014. Analytical model for flow duration curves in seasonally dry climates. *Water Resources Research*, 50(7), 5510-5531.
<https://doi.org/10.1002/2014WR015301>

- Mwaniki, M.W., Matthias, M.S. and Schellmann, G., 2015. Application of remote sensing technologies to map the structural geology of central Region of Kenya. *IEEE Journal of Selected Topics in Applied Earth Observations and Remote Sensing*, 8(4), pp.1855-1867.
- Naghibi, S.A., Pourghasemi, H.R., Pourtaghi, Z.S. and Rezaei, A., 2015. Groundwater qanat potential mapping using frequency ratio and Shannon's entropy models in the Moghan watershed, Iran. *Earth Science Informatics*, 8(1), pp.171-186.
- Nampak, H., Pradhan, B. and Manap, M.A., 2014. Application of GIS based data driven evidential belief function model to predict groundwater potential zonation. *Journal of Hydrology*, 513, pp.283-300.
- Neilson, B.T., Cardenas, M.B., O'Connor, M.T., Rasmussen, M.T., King, T.V. and Kling, G.W., 2018. Groundwater flow and exchange across the land surface explain carbon export patterns in continuous permafrost watersheds. *Geophysical Research Letters*, 45(15), pp.7596-7605.
- O'leary, D.W., Friedman, J.D. and Pohn, H.A., 1976. Lineament, linear, lineation: some proposed new standards for old terms. *Geological Society of America Bulletin*, 87(10), pp.1463-1469.
- Ochoa-Rodriguez, S., Wang, L.P., Gires, A., Pina, R.D., Reinoso-Rondinel, R., Bruni, G., Ichiba, A., Gaitan, S., Cristiano, E., van Assel, J. and Kroll, S., 2015. Impact of spatial and temporal resolution of rainfall inputs on urban hydrodynamic modelling outputs: A multicatchment investigation. *Journal of Hydrology*, 531, pp.389-407.
- Oghenekome, M.E., 2012. Sedimentary environments and provenance of the Balfour Formation (Beaufort Group) in the area between Bedford and Adelaide, Eastern Cape Province, South Africa (*Doctoral dissertation, University of Fort Hare*).
- Oghenekome, M.E., Chatterjee, T.K., Hammond, N.Q. and van Bever Donker, J.M., 2016. Provenance study from petrography of the late Permian–Early Triassic sandstones of the

- Balfour Formation Karoo Supergroup, South Africa. *Journal of African Earth Sciences*, 114, pp.125-132.
- Ohlson, J.A. and Kim, S., 2015. Linear valuation without OLS: the Theil-Sen estimation approach. *Review of Accounting Studies*, 20(1), pp.395-435.
- Orimoloye, I.R., Mazinyo, S.P., Nel, W. and Kalumba, A.M., 2018. Spatiotemporal monitoring of land surface temperature and estimated radiation using remote sensing: human health implications for East London, South Africa. *Environmental Earth Sciences*, 77(3), p.77.
- Oshmarin, R.A., Ostankov, A.V., Kompaniets, S.V. and Tokareva, O.V., 2016. Capabilities and Limitations of Electromagnetic Techniques in Eastern Siberia. In SPE Russian Petroleum Technology Conference and Exhibition. *Society of Petroleum Engineers*.
- Ozdemir, A. and Altural, T., 2013. A comparative study of frequency ratio, weights of evidence and logistic regression methods for landslide susceptibility mapping: Sultan Mountains, SW Turkey. *Journal of Asian Earth Sciences*, 64, pp.180-197.
- Pacheco, F.A.L. and Fallico, C., 2015. Hydraulic head response of a confined aquifer influenced by river stage fluctuations and mechanical loading. *Journal of Hydrology*, 531, pp.716-727.
- Pángaro, F. and Ramos, V.A., 2012. Paleozoic crustal blocks of onshore and offshore central Argentina: New pieces of the southwestern Gondwana collage and their role in the accretion of Patagonia and the evolution of Mesozoic south Atlantic sedimentary basins. *Marine and Petroleum Geology*, 37(1), pp.162-183.
- Pardé, M., 1947. Les chemins de fer des États-Unis. In *Annales de géographie* (Vol. 56, No. 304, pp. 274-294). *Société de géographie*.
- Pareta, K. and Pareta, U., 2011. Quantitative morphometric analysis of a watershed of Yamuna basin, India using ASTER (DEM) data and GIS. *International journal of*

- Geomatics and Geosciences*, 2(1), pp.248-269.
- Patel, D.P., Gajjar, C.A. and Srivastava, P.K., 2013. Prioritization of Malesari miniwatersheds through morphometric analysis: a remote sensing and GIS perspective. *Environmental Earth Sciences*, 69(8), pp.2643-2656.
- Peddie, N.W., 1982. International geomagnetic reference field. *Journal Of Geomagnetism And Geoelectricity*, 34(6), pp.309-326.
- Peng, D., Qiu, L., Fang, J. and Zhang, Z., 2016. Quantification of climate changes and human activities that impact runoff in the Taihu Lake basin, China. *Mathematical Problems in Engineering*, 2016.
- Pettitt, A.N., 1979. A non-parametric approach to the change-point problem. *Journal of the Royal Statistical Society: Series C (Applied Statistics)*, 28(2), pp.126-135.
- Pettyjohn, W. A., and Henning, R. J., 1979. Preliminary estimate of regional effective ground-water recharge rates in Ohio. Ohio State University. *Water Resources Center*.
- Pietersen, K., Beekman, H.E., Holland, M. and Adams, S., 2012. Groundwater governance in South Africa: A status assessment. *Water SA*, 38(3), pp.453-460.
- Pohlert T., 2016. Non-parametric trend tests and change-point detection. CC BY-ND. 2016 May 14;4.
- Prabu, P. and Baskaran, R., 2013. Drainage morphometry of upper Vaigai river sub-basin, Western Ghats, South India using remote sensing and GIS. *Journal of the Geological Society of India*, 82(5), pp.519-528.
- Prudic, D.E., 1989. Documentation of a computer program to simulate stream-aquifer relations using a modular, finite-difference, ground-water flow model.
- Pryshlak, T.T., Sawyer, A.H., Stonedahl, S.H. and Soltanian, M.R., 2015. Multiscale hyporheic exchange through strongly heterogeneous sediments. *Water Resources*

- Research*, 51(11), pp.9127-9140.
- Rai, P.K., Mishra, S., Ahmad, A., Mohan, K., 2014. A GIS-based approach in drainage morphometric analysis of Kanhar River Basin, India. *Applied Water Science*.
- Rai, P.K., Mishra, V.N. and Mohan, K., 2017. A study of morphometric evaluation of the Son basin, India using geospatial approach. *Remote Sensing Applications: Society and Environment*, 7, pp.9-20.
- Raudkivi, A.J., 1979. *Hydrology*. 479 pp.
- Reed D N, Anderson T M, Dempewolf J, Metzger K, and Semeels S., 2009. The spatial distribution of vegetation types in the Serengeti ecosystem: the influence of rainfall and topographic relief on vegetation patch characteristics. *Journal of Biogeography* 36.4 (2009): 770-782.
- Renner, M., Seppelt, R. and Bernhofer, C., 2011. A simple water-energy balance framework to predict the sensitivity of streamflow to climate change. *Hydrology & Earth System Sciences Discussions*, 8(5).
-  University of Fort Hare
Together in Excellence
- Rinderer, M., Van Meerveld, H.J. and Seibert, J., 2014. Topographic controls on shallow groundwater levels in a steep, prealpine catchment: When are the TWI assumptions valid?. *Water Resources Research*, 50(7), pp.6067-6080.
- Robinson, G.M., Gray, D.A., Healey, R.G. and Furley, P.A., 1989. Developing a geographical information system (GIS) for agricultural development in Belize, Central America. *Applied Geography*, vol. 9(2), pp. 81–94.
- Ross, A., 2018. Speeding the transition towards integrated groundwater and surface water management in Australia. *Journal of Hydrology*, 567, pp.e1-e10.
- Rothenberger, M.B., Burkholder, J.M. and Brownie, C., 2009. Long-term effects of changing land use practices on surface water quality in a coastal river and lagoonal estuary. *Environmental Management*, 44(3), pp.505-523.

- Roy, D.P., Wulder, M.A., Loveland, T.R., Woodcock, C.E., Allen, R.G., Anderson, M.C., Helder, D., Irons, J.R., Johnson, D.M., Kennedy, R. and Scambos, T.A., 2014. Landsat-8: Science and product vision for terrestrial global change research. *Remote sensing of Environment*, 145, pp.154-172.
- Rubidge, B.S., Hancox, P.J. and Catuneanu, O., 2000. Sequence analysis of the Ecca—Beaufort contact in the southern Karoo of South Africa. *South African Journal of Geology*, 103(1), pp.81-96.
- Rudra, R.P., Ahmed, S.I., Khayer, M., Dickinson, W.T. and Gharabaghi, B., 2010. The Relationship between Watershed Physiography, Tile Flow, and Streamflow Characteristics. In 9th International Drainage Symposium held jointly with CIGR and CSBE/SCGAB Proceedings, 13-16 June 2010, Québec City Convention Centre, Quebec City, Canada (p. 1). *American Society of Agricultural and Biological Engineers*.
- Rutledge, A. T., 1998. Computer programs for describing the recession of ground-water discharge and for estimating mean ground-water recharge and discharge from streamflow records: Update
- Rutledge, A.T., 2007. Update on the use of the RORA program for recharge estimation. *Groundwater*, 45(3), pp.374-382.
- Sahoo S., Dhar A., Kar A., and Ram P., 2017. Grey analytic hierarchy process applied to effectiveness evaluation for groundwater potential zone delineation. *Geocarto International*, 32(11), pp.1188-1205.
- Sahu, N., Reddy, G.O., Kumar, N., Nagaraju, M.S.S., Srivastava, R. and Singh, S.K., 2017. Morphometric analysis in basaltic Terrain of Central India using GIS techniques: a case study. *Applied Water Science*, 7(5), pp.2493-2499.
- Sakher, C., Mantilla-Pimiento, A.M., Jimenez-Berrocoso, A., Cascone, L., Chaabouini, A., Parsons, M. and Weber, J., 2015, June. Reducing the Exploratory Risk in Northern

- Tunisia: Integrating HRes Gravity, Magnetic and Seismic Data. *In 77th EAGE Conference and Exhibition 2015*.
- Samal, D.R., Gedam, S.S. and Nagarajan, R., 2015. GIS based drainage morphometry and its influence on hydrology in parts of Western Ghats region, Maharashtra, India. *Geocarto International*, 30(7), pp.755-778.
- Sankarasubramanian, A., Vogel, R.M. and Limbrunner, J.F., 2001. Climate elasticity of streamflow in the United States. *Water Resources Research*, 37(6), pp. 1771-1781.
- Santos, M. and Fragoso, M., 2013. Precipitation variability in Northern Portugal: data homogeneity assessment and trends in extreme precipitation indices. *Atmospheric Research*, 131, pp.34-45.
- Sawyer, A. H. and Cardenas, M. B., 2009. Hyporheic flow and residence time distributions in heterogeneous cross-bedded sediment. *Water Resources Research* 45.
- Sayemuzzaman, M., and Jha, M. K., 2014. Seasonal and annual precipitation time series trend analysis in North Carolina, United States. *Atmospheric Research*, 137, 183-194;
- Schaake, J. C. 1990. From climate to flow. Climate change and US water resources., 177206. Hydrologic Services Division, National Weather Service, NOAA Silver Spring, Maryland, USA. ISBN; 0471618381. Record Number: 19911959039. *John Wiley and Sons Inc*.
- Scheiber, T., Fredin, O., Viola, G., Jarna, A., Gasser, D. and Łapińska-Viola, R., 2015. Manual extraction of bedrock lineaments from high-resolution LiDAR data: methodological bias and human perception. *GFF*, 137(4), pp.362-372.
- Searcy, J.K. and Hardison, C.H., 1960. Double-mass curves.
- Sen, P.K., 1968. Estimates of the regression coefficient based on Kendall's tau. *Journal Of The American Statistical Association*, 63(324), pp.1379-1389.

- Shadmani, M., Marofi, S. and Roknian, M., 2012. Trend analysis in reference evapotranspiration using Mann-Kendall and Spearman's Rho tests in arid regions of Iran. *Water Resources Management*, 26(1), pp.211-224.
- Shamuyarira, K.K., 2017. Determination of recharge and groundwater potential zones in Mhinga area, South Africa (*Doctoral Dissertation*).
- Shaw, E., 2014. Hydrology in practice. CRC Press.
- Singh, P., Thakur, J.K. and Singh, U.C., 2013. Morphometric analysis of Morar River Basin, Madhya Pradesh, India, using remote sensing and GIS techniques. *Environmental Earth Sciences*, 68(7), pp.1967-1977.
- Singhal, B.B.S. and Gupta, R.P., 2010. Applied hydrogeology of fractured rocks. *Springer Science & Business Media*.
- Sivapalan, M., 2003. Prediction in ungauged basins: a grand challenge for theoretical hydrology. *Hydrological Processes*, 17(15), pp.3163-3170.
- Shumway, R.H. and Stoffer, D.S., 2017. Time series analysis and its applications: with R examples. *Springer*.
- Silvester, P.P., 1990. RL Ferrari. Finite Elements for Electric Engineers", *Cambridge*.
- Singh, P., Thakur, J.K. and Singh, U.C., 2013. Morphometric analysis of Morar River Basin, Madhya Pradesh, India, using remote sensing and GIS techniques. *Environmental Earth Sciences*, 68(7), pp.1967-1977.
- Singhal, B.B.S. and Gupta, R.P., 2010. Applied hydrogeology of fractured rocks. *Springer Science & Business Media*.
- Slaughter, A.R., Mantel, S.K. and Hughes, D.A., 2014. Investigating possible climate change and development effects on water quality within an arid catchment in South Africa: a comparison of two models.

- Smakhtin, V.U., 2001. Low flow hydrology: a review. *Journal Of Hydrology*, 240(3-4), pp.147-186.
- Smit, P.J., 1978. Groundwater recharge in the dolomite of the Ghaap Plateau near Kuruman in the Northern Cape, Republic of South Africa. *Water SA*, 4(2), pp.81-92.
- Smith, L.C., 1997. Satellite remote sensing of river inundation area, stage, and discharge: A review. *Hydrological Processes*, 11(10), pp.1427-1439.
- Smith, R.B., 2006. Progress on the theory of orographic precipitation. *Special Papers Geological Society Of America*, 398, p.1.
- Smith, R.M. and Botha-Brink, J., 2014. Anatomy of a mass extinction: sedimentological and taphonomic evidence for drought-induced die-offs at the Permo-Triassic boundary in the main Karoo Basin, South Africa. *Palaeogeography, Palaeoclimatology, Palaeoecology*, 396, pp.99-118.
- Smith, R.M. and Ward, P.D., 2001. Pattern of vertebrate extinctions across an event bed at the Permian-Triassic boundary in the Karoo Basin of South Africa. *Geology*, 29(12), pp.1147-1150.
- Sophocleous, M., 2002. Interactions between groundwater and surface water: the state of the science. *Hydrogeology Journal*, 10(1), pp.52-67.
- Souza, O., Silva, A.M., Mccafferty, A. and Perrotta, M., 2009, August. The Use of Airborne Magnetics in Hydrogeology: An Example from Northeast Brazil. *In 11th International Congress of the Brazilian Geophysical Society*.
- Sreedevi, P.D., Subrahmanyam, K. and Ahmed, S., 2005. The significance of morphometric analysis for obtaining groundwater potential zones in a structurally controlled terrain. *Environmental Geology*, 47(3), pp.412-420.



- Srivastava, P.K. and Bhattacharya, A.K., 2006. Groundwater assessment through an integrated approach using remote sensing, GIS and resistivity techniques: a case study from a hard rock terrain. *International Journal of Remote Sensing*, 27(20), pp.4599-4620.
- Stanford, J.A. and Ward, J.V., 1988. The hyporheic habitat of river ecosystems. *Nature*, 335(6185), p.64.
- Stephens, D.B., 2018. Vadose zone hydrology. *CRC press*.
- Steven, E.J., Adepitan, A.E. and Suleiman, A., 2018. Geological, Multispectral and Aeromagnetic Expressions of Pegmatite Hosted Mineralization of Keffi Sheet 208 NE, North-Central Nigeria. *American Journal of Modern Physics and Application*, 5(4), pp.53-69.
- Stewart, M.K., Morgenstern, U. and McDonnell, J.J., 2010. Truncation of stream residence time: how the use of stable isotopes has skewed our concept of streamwater age and origin. *Hydrological Processes*, 24(12), pp.1646-1659.
- Strahler, A.N., 1957. Quantitative analysis of watershed geomorphology. *Eos, Transactions American Geophysical Union*, 38(6), pp.913-920.
- Stroebel, D.H., Thiart, C. and de Wit, M., 2018. Towards defining a baseline status of scarce groundwater resources in anticipation of hydraulic fracturing in the Eastern Cape Karoo, South Africa: salinity, aquifer yields and groundwater levels. *Geological Society, London, Special Publications*, 479, pp.SP479-3.
- Su, N., 1995. The unit hydrograph model for hydrograph separation. *Environment International*, 21(5), pp.509-515.
- Sultan, S.A., Essa, K.S.A.T., Khalil, M.H., El-Nahry, A.E.H. and Galal, A.N.H., 2017.



University of Fort Hare

Together in Excellence

Evaluation of groundwater potentiality survey in south Ataq-northwestern part of Gulf of Suez by using resistivity data and site-selection modeling. *NRIAG Journal of Astronomy and Geophysics*, 6(1), pp.230-243.

Sun, W., Song, X., Mu, X., Gao, P., Wang, F., and Zhao, G., 2015. Spatiotemporal vegetation cover variations associated with climate change and ecological restoration in the Loess

Plateau. *Agricultural and Forest Meteorology*, 209, 87-99.

Suresh, S., Ajay, S.V. and Mani, K., 2016. Estimation of land surface temperature of high range mountain landscape of Devikulam Taluk using Landsat 8 data. *International Journal of Reservoir Engineering. Technol*, 5, pp.92-96.

Suter, J.F., Rouhi Rad, M., Manning, D., Moore, L.K. and Goemans, C., 2019. The Impact of Groundwater on Economic Outcomes in the Ogallala Region.

Tang, L., Sheng, J., Hatcher, B.G. and Sale, P.F., 2006. Numerical study of circulation, dispersion, and hydrodynamic connectivity of surface waters on the Belize shelf. *Journal of Geophysical Research: Oceans*, 111(C1).


Tankard, A.J., Martin, M., Eriksson, K.A., Hobday, D.K., Hunter, D.R. and Minter, W.E.L., 2012. Crustal evolution of southern Africa: 3.8 billion years of earth history. *Springer Science & Business Media*.

Tankard, A., Welsink, H., Aukes, P., Newton, R. and Stettler, E., 2009. Tectonic evolution of the Cape and Karoo basins of South Africa. *Marine and Petroleum Geology*, 26(8), pp.1379-1412.

Tanner, J.L., 2013. Understanding and modelling of surface and groundwater interactions (*Doctoral Dissertation, Rhodes University*).

- Tanner, J.L. and Hughes, D.A., 2015. Surface water–groundwater interactions in catchment scale water resources assessments—understanding and hypothesis testing with a hydrological model. *Hydrological Sciences Journal*, 60(11), pp.1880-1895.
- Taylor, C.J. and Greene, E.A., 2008. Hydrogeologic characterization and methods used in the investigation of karst hydrology. *US Geological Survey*.
- Telford, W.M., Telford, W.M., Geldart, L.P., Sheriff, R.E. and Sheriff, R.E., 1990. Applied geophysics (Vol. 1). *Cambridge University Press*.
- Theil, H., 1950. A rank-invariant method of linear and polynomial regression analysis (parts 1-3). *In Ned. Akad. Wetensch. Proc. Ser. A* (Vol. 53, pp. 1397-1412).
- Tordiffe, E.A.W., 1978. Aspects of the hydrogeochemistry of the Karoo Sequence in the Great Fish River basin, eastern Cape Province, with special reference to the groundwater quality (*Doctoral Dissertation, University of the Free State*).
- Toth, J., 1963. A theoretical analysis of groundwater flow in small drainage basins. *Journal of Geophysical Research*, 68(16), pp.4795-4812.
- Turner, S.P., Peate, D.W., Hawkesworth, C.J., Eggins, S.M. and Crawford, A.J., 1999. Two mantle domains and the time scales of fluid transfer beneath the Vanuatu arc. *Geology*, 27(11), pp.963-966.
- Urqueta, H., Jódar, J., Herrera, C., Wilke, H.G., Medina, A., Urrutia, J., Custodio, E. and Rodríguez, J., 2018. Land surface temperature as an indicator of the unsaturated zone thickness: A remote sensing approach in the Atacama Desert. *Science of The Total Environment*, 612, pp.1234-1248.
- Van Wyk, E., Van Tonder, G.J. and Vermeulen, D., 2012. Characteristics of local groundwater recharge cycles in South African semi-arid hard rock terrains: Rainfall–groundwater interaction. *Water SA*, 38(5), pp.747-754.

- Vasanthavigar, M., Srinivasamoorthy, K., Vijayaragavan, K., Gopinath, S. and Sarma, S., 2011. Groundwater Potential Zoning in Thirumanimuttar Sub-Basin Tamilnadu, India—A GIS and Remote Sensing Approach. *Geo-spatial Information Science*, vol. 14(1), pp. 17-26
- Vegter, J.R. and Pitman, W.V., 2003. Recharge and stream flow. In Xu, Y. and Beekman, E. (eds.) Groundwater recharge estimation in southern Africa. *UNESCO IHP Series*, 64, 109123. UNESCO, Paris.
- Verma, R. K., Murthy, S., Verma, S., and Mishra, S. K., 2017. Design flow duration curves for environmental flows estimation in Damodar River Basin, India. *Applied Water Science*, 7(3), 1283-1293. <https://doi.org/10.1007/s13201-016-0486-0>
- Veevers, J.J., Walter, M.R. and Scheibner, E., 1997. Neoproterozoic tectonics of AustraliaAntarctica and Laurentia and the 560 Ma birth of the Pacific Ocean reflect the 400 my Pangean supercycle. *The Journal of Geology*, 105(2), pp.225-242.
- Viezzoli, A., Tosi, L., Teatini, P. and Silvestri, S., 2010. Surface water-groundwater exchange in transitional coastal environments by airborne electromagnetics: the Venice Lagoon example. *Geophysical Research Letters*, 37(1).
- Visser, J.N.J. and Dukas, B.A., 1979. Upward-fining fluvial megacycles in the Beaufort Group, north of Graaff-Reinet, Cape Province. *South African Journal of Geology*, 82(1), pp.149-154.
- Vittecoq, B., Reninger, P.A., Violette, S., Martelet, G., Dewandel, B. and Audru, J.C., 2015. Heterogeneity of hydrodynamic properties and groundwater circulation of a coastal andesitic volcanic aquifer controlled by tectonic induced faults and rock fracturing—Martinique island (Lesser Antilles—FWI). *Journal of Hydrology*, 529, pp.1041-1059.
- Vogel, R.M. and Kroll, C.N., 1992. Regional geohydrologic-geomorphic relationships for the estimation of low-flow statistics. *Water Resources Research*, 28(9), pp.2451-2458.

- Wagener, T. and Gupta, H.V., 2005. Model identification for hydrological forecasting under uncertainty. *Stochastic Environmental Research and Risk Assessment*, 19(6), pp.378-387.
- Wang, N., Zhang, C., Xiao, Y., Jin, G. and Li, L., 2018. Transverse hyporheic flow in the cross-section of a compound river system. *Advances in Water Resources*, 122, pp.263-277.
- Wendt, L., Hilberg, S., Robl, J., Dirnberger, D., Strasser, T. and Braun, A., 2016. Remote Sensing in Hydrogeology: A short summary of methods and constraints for groundwater exploration.
- Werner, A.D., Bakker, M., Post, V.E., Vandenbohede, A., Lu, C., Ataie-Ashtiani, B., Simmons, C.T. and Barry, D.A., 2013. Seawater intrusion processes, investigation and management: recent advances and future challenges. *Advances in Water Resources*, 51, pp.3-26.
- Whitehead, N. and Musselman, C., 2008.  Montaj Grav/Mag Interpretation: Processing, Analysis and Visualization System for 3D Inversion of Potential Field Data for Oasis montaj v6. 3, Geosoft Incorporated, 85 Richmond St. W., Toronto, Ontario, M5H 2C9, Canada.
- Wildman, M., Brown, R., Beucher, R., Persano, C., Stuart, F., Gallagher, K., Schwanethal, J. and Carter, A., 2016. The chronology and tectonic style of landscape evolution along the elevated Atlantic continental margin of South Africa resolved by joint apatite fission track and (U.Th.Sm)/He thermochronology. *Tectonics*, 35(3), pp.511-545.
- Wilson, A., Flint, S., Payenberg, T., Tohver, E. and Lanci, L., 2014. Architectural styles and sedimentology of the fluvial lower Beaufort Group, Karoo Basin, South Africa. *Journal of Sedimentary Research*, 84(4), pp.326-348.
- Wilson, J.J. and Ch, N., 2012. Morphometric Analysis of Major Sub-Watersheds in Aiyar & Karai Pottanar Basin, Central Tamil Nadu, India Using Remote Sensing & GIS

- Techniques. *Bonfring International Journal of Industrial Engineering and Management Science*, 2 (Special Issue Special Issue on Geospatial Technology Development in Natural Resource and Disaster Management), pp.08-15.
- Wilson Jr, C.W., 1936. Geology of Nye-Bowler lineament, Stillwater and Carbon counties, Montana. *AAPG Bulletin*, 20(9), pp.1161-1188..
- Wilson, J.T., 1950. On the growth of continents. *In Papers and Proceedings of the Royal Society of Tasmania* (pp. 85-111).
- Winter, T.C., Harvey, J.W., Franke, O.L., Alley, W.M., 1998. Groundwater and surface water - a *single resource* vol 1139. USGS
- Wittenberg, H., 1999. Baseflow recession and recharge as nonlinear storage processes. *Hydrological Processes*, 13(5), pp.715-726.
- Woessner, W.W., 2000. Stream and fluvial plain ground water interactions: rescaling hydrogeologic thought. *Groundwater*, 38(3), pp.423-429.
- Wysocki, D.A. and Schoeneberger, P.J., 2016. Soils in Geomorphologic Research. *International Encyclopedia of Geography: People, the Earth, Environment and Technology: People, the Earth, Environment and Technology*, pp.1-19.
- Xevi, E., Christiaens, K., Espino, A., Sewnandan, W., Mallants, D., Sørensen, H. and Feyen, J., 1997. Calibration, validation and sensitivity analysis of the MIKE-SHE model using the Neuenkirchen catchment as case study. *Water Resources Management*, 11(3), pp.219-242.
- Xu, Y. and Beekman, H.E. eds., 2003. Groundwater recharge estimation in Southern Africa.
- Xu, Y. and van Tonder, G.J., 2001. Estimation of recharge using a revised CRD method. *Water SA*, Vol.27, No. 3, 341-343.
- Xu, Y., Titus, R., Holness, S.D., Zhang, J. and van Tonder, G.J., 2002. A

- hydrogeomorphological approach to quantification of groundwater discharge to streams in South Africa. *Water SA*, 28 (4), 375-380
- Yadav, S.K., Singh, S.K., Gupta, M. and Srivastava, P.K., 2014. Morphometric analysis of Upper Tons basin from Northern Foreland of Peninsular India using CARTOSAT satellite and GIS. *Geocarto International*, 29(8), pp.895-914.
- Yap, W.K., 2015. Flood forecasting in Langat river basin using stochastic Arima model (*Doctoral dissertation, UTAR*).
- Ye, L., Ding, W., Zeng, X., Xin, Z., Wu, J. and Zhang, C., 2018. Inherent Relationship between Flow Duration Curves at Different Time Scales: A Perspective on Monthly Flow Data Utilization in Daily Flow Duration Curve Estimation. *Water*, 10(8), p.1008.
- Yokoo, Y. and Sivapalan, M., 2011. Towards reconstruction of the flow duration curve: development of a conceptual framework with a physical basis. *Hydrology and Earth System Sciences*, 15(9), pp.2805-2819.
- Zhang, A., Zheng, C., Wang, S. and Yao, Y., 2015. Analysis of streamflow variations in the Heihe River Basin, northwest China: trends, abrupt changes, driving factors and ecological influences. *Journal of Hydrology: Regional Studies*, 3, pp.106-124.
- Zhang, Y., Singh, V. and Byrd, A., 2017. Entropy Parameter M in Modeling a Flow Duration Curve. *Entropy*, 19(12), p.654.
- Zhou, Y., Shi, C., Fan, X. and Shao, W., 2015. The influence of climate change and anthropogenic activities on annual runoff of Huangfuchuan basin in northwest China. *Theoretical and Applied Climatology*, 120(1-2), pp.137-146.
- Ťugaj R., 2015, Hidrologija, Sveu ilište u Zagrebu, Rudarsko-geološko-naftni fakultet, 2nd edition, Zagreb, 538 pp

APPENDIX

Borehole lithological log used in Chapter 4 and Chapter 7

ID	Latitude	Longitude	Event Date	DepthToTop	DepthToBottom	Litho Name
A1	-32.9082	27.29961	10/18/1949	0	1.83	SOIL
A1	-32.9082	27.29961	10/18/1949	1.83	57.91	Sandstone
A2	-32.9497	27.28294	9/7/1949	0	1.22	SOIL
A2	-32.9497	27.28294	9/7/1949	1.22	45.72	Sandstone
A3	-32.9902	27.36628	7/19/1949	0	1.22	SOIL
A3	-32.9902	27.36628	7/19/1949	1.22	45.72	Sandstone & Shale
A4	-32.9335	27.12184	10/26/1949	0	1.22	SOIL
A4	-32.9335	27.12184	10/26/1949	1.22	53.04	Sandstone
A5	-32.9419	27.57461	5/24/1951	0	1.22	SOIL
A5	-32.9419	27.57461	5/24/1951	1.22	79.25	Sandstone
A6	-32.8292	27.33461	2/13/1951	0	13.72	SOIL
A6	-32.8292	27.33461	2/13/1951	13.72	50.9	Sandstone & Shale
A6	-32.8292	27.33461	2/13/1951	50.9	60.96	Sandstone
A7	-32.8669	27.34072	1/26/1951	0	0.91	SOIL
A7	-32.8669	27.34072	1/26/1951	0.91	4.88	Boulders
A7	-32.8669	27.34072	1/26/1951	4.88	60.96	Sandstone
A8	-32.7336	27.41628	3/19/1951	0	1.22	SOIL
A8	-32.7336	27.41628	3/19/1951	1.22	46.33	Shale
A9	-32.9319	27.38738	1/22/1952	0	3.35	SOIL
A9	-32.9319	27.38738	1/22/1952	3.35	10.67	Dolerite
A9	-32.9319	27.38738	1/22/1952	10.67	41.45	Sandstone
A10	-32.6927	27.55295	10/2/1951	0	7.01	SOIL
A10	-32.6927	27.55295	10/2/1951	7.01	13.41	Shale
A10	-32.6927	27.55295	10/2/1951	13.41	20.73	Shale
A10	-32.6927	27.55295	10/2/1951	20.73	23.77	Sandstone
A10	-32.6927	27.55295	10/2/1951	23.77	26.82	Sandstone
A11	-32.6927	27.55294	10/12/1951	0	1.22	SOIL
A11	-32.6927	27.55294	10/12/1951	1.22	21.34	Sandstone
A11	-32.6927	27.55294	10/12/1951	21.34	28.65	Sandstone
A12	-32.6927	27.55295	10/22/1951	0	0.61	SOIL
A12	-32.6927	27.55295	10/22/1951	0.61	22.86	Sandstone & Shale
A12	-32.6927	27.55295	10/22/1951	22.86	38.71	Sandstone
A13	-32.8258	27.43772	1/10/1952	0	1.83	SOIL
A13	-32.8258	27.43772	1/10/1952	1.83	11.28	Shale
A13	-32.8258	27.43772	1/10/1952	11.28	15.85	Shale

A13	-32.8258	27.43772	1/10/1952	15.85	24.38	Sandstone
A14	-32.73	27.45628	7/2/1952	0	12.19	Sandstone
A14	-32.73	27.45628	7/2/1952	12.19	16.46	Dolerite
ID	Latitude	Longitude	Event Date	DepthToTop	DepthToBottom	Litho Name
A14	-32.73	27.45628	7/2/1952	16.46	18.29	Sandstone
A14	-32.73	27.45628	7/2/1952	18.29	28.96	Dolerite
A15	-32.658	27.57378	8/18/1954	0	2.44	SOIL
A15	-32.658	27.57378	8/18/1954	2.44	3.66	Shale
A15	-32.658	27.57378	8/18/1954	3.66	14.63	Sandstone
A15	-32.658	27.57378	8/18/1954	14.63	28.04	Sandstone
A15	-32.658	27.57378	8/18/1954	28.04	30.18	Sandstone
A16	-32.708	27.60655	7/9/1968	0	3	Clay
A16	-32.708	27.60655	7/9/1968	3	48.77	Dolomite
A16	-32.708	27.60655	7/9/1968	48.77	76.5	Dolomite
A17	-32.8436	27.55433	5/5/1969	0	5.79	Sandstone
A17	-32.8436	27.55433	5/5/1969	5.79	21.34	Sandstone
A17	-32.8436	27.55433	5/5/1969	21.34	30.48	Shale
A17	-32.8436	27.55433	5/5/1969	30.48	54.86	Sandstone
A17	-32.8436	27.55433	5/5/1969	54.86	60.96	Sandstone
A17	-32.8436	27.55433	5/5/1969	60.96	91.74	Sandstone
A18	-32.8472	27.53988	5/12/1969	0	6.1	Sandstone

**Sub-basins monthly streamflow in Buffalo basin headwater used in chapter 5 and 6
(Courtesy of DWA)**

Date	Buffalo	Yellowwoods	Nggokweni	Mgqakwebe	Quencwe	Tshoxa
Jan-89	49.623	7.516	2.233	23.582	17.008	54.851
Feb-89	33.989	2.548	0.142	7.535	3.138	32.402
Mar-89	31.661	7.314	0.794	4.659	8.262	34.559
Apr-89	76.33	17.452	3.933	17.741	16.726	97.102
May-89	26.638	3.096	1.605	5.307	4.334	23.093
Jun-89	8.068	1.072	0.761	1.172	1.403	4.789
Jul-89	6.412	0.862	0.309	0.807	1.328	2.006
Aug-89	3.979	0.734	11.803	1.461	0.562	1.035
Sep-89	3.853	0.355	58.562	1.336	0.333	0.815
Oct-89	46.65	78.061	20.549	31.766	19.895	161.358
Nov-89	210.181	210.309	48.639	128.695	77.054	592.137
Dec-89	70.157	14.818	5.818	15.665	7.606	51.471

Jan-90	19.039	5.28	1.705	5.52	3.111	13.601
Feb-90	10.939	2.67	0.111	3.237	2.554	8.049
Mar-90	111.75	19.393	2.907	31.591	20.766	155.181
Apr-90	48.106	5.206	1.527	11.197	9.354	42.64
May-90	9.412	1.537	0.428	2.469	1.612	5.871
Jun-90	5.487	1.101	0.163	1.451	0.782	2.335
Jul-90	5.605	1.26	0.284	1.066	0.978	2.146
Aug-90	4.808	0.955	0.119	0.571	1.056	1.42
Date	Buffalo	Yellowwoods	Nggokweni	Mgqakwebe	Quencwe	Tshoxa
Sep-90	7.566	2.13	0.447	0.593	0.699	2.343
Oct-90	12.732	2.692	1.904	1.754	1.657	5.846
Nov-90	5.845	0.958	0.904	1.317	0.917	2.942
Dec-90	6.779	1.197	25.862	1.756	0.972	3.723
Jan-91	14.534	0.623	34.242	9.025	1.174	10.848
Feb-91	23.825	5.76	6.279	13.224	2.938	19.06
Mar-91	10.963	1.105	3.957	4.189	1.264	6.046
Apr-91	5.4	0.304	0.743	1.298	0.327	2.992
May-91	7.73	0.325	0.543	0.543	0.419	5.159
Jun-91	7.971	0.612	0.245	0.431	0.31	4.865
Jul-91	6.009	0.582	0.245	0.282	0.353	3.378
Aug-91	3.757	0.695	0.2	0.298	0.398	0.554
Sep-91	3.867	0.48	0.354	1.143	0.264	0.212
Oct-91	45.668	36.525	9.025	30.127	9.423	52.809
Nov-91	66.387	14.415	2.639	25.916	9.321	45.115
Dec-91	11.017	2.093	10.971	2.846	1.046	5.647
Jan-92	28.347	0.514	1.607	1.192	0.77	2.191
Feb-92	17.705	0.489	3.617	1.625	0.328	4.504
Mar-92	9.3	0.715	3.503	0.711	13.381	2.636
Apr-92	9.704	0.712	1.785	0.551	12.764	1.283
May-92	7.484	0.34	0.945	0.618	1.052	0.173
Jun-92	9.24	0.702	2.033	0.546	0.612	0.144
Jul-92	7.39	0.578	8.702	1.806	0.469	0.093
Aug-92	11.01	1.768	2.852	1.183	97.462	0.735
Sep-92	20.997	0.438	27.092	0.101	4.861	0.106
Oct-92	18.484	2.633	8.524	1.945	7.924	3.182

Nov-92	42.612	3.756	3.486	3.753	1.566	4.236
Dec-92	119.111	0.225	32.996	3.873	27.09	3.456
Jan-93	22.642	5.821	3.302	11.696	23.315	16.461

King Williams town precipitation information used in Chapter 5 (Courtesy of SAWS)

Year	Jan	Feb	Mar	Apr	May	Jun	Jul	Aug	Sep	Oct	Nov	Dec
1989	60.8	50.8	52.9	124.2	5.6	5.4	11.6	1.8	17.1	124.7	324	22.2
1990	60.2	46.6	108.4	15.5	2.1	16.9	0.4	11.3	40.1	60.3	20	65.7
1991	56.9	60	33.6	9	19.1	4.2	1.7	13.5	25	173.7	66.6	67.4
1992	6.9	66.9	36.2	24.6	1	6.7	2.1	52.1	11.9	83.9	43.6	34.2
1993	78.1	35.9	9.4	47.1	1.6	45.9	1.2	13.2	93.4	23	101.3	182.6
1994	48.4	39.6	97.9	10.5	3.7	2.7	25.4	39.4	7.3	49.7	9.5	161.1
1995	92.2	83.2	95.7	37	24.6	11.7	6.5	0	41.5	72	80.9	150.3
1996	100.7	81.1	67.5	15.3	11.3	1.1	11	6.8	11.7	40.6	234.6	64
1997	47.7	16.2	51	104.5	48.6	142.7	5.6	8.9	21.1	43.8	35.4	17.2
1998	80.9	100.4	134	51.7	24.6	0.4	4.9	63.4	33.3	43.3	133.5	72.2
1999	148.4	0	0	61.3	3.3	0	74	2.1	19.5	52.1	29.7	56
2000	110.5	61.5	238.7	46.6	10	19.2	0	0	67	55.3	128.4	43.5
2001	62.2	44.9	105.7	96.3	13.9	1.5	28	31.7	63.1	54.6	0	75.3
2002	106	14.4	49.4	52.9	6.8	24	64.2	96.8	120.7	11.8	28.6	94.9
2003	34.6	54.5	137.6	34.5	27.6	3.4	4.1	14.3	17.2	24.3	39.6	46.8
2004	100.9	34.8	77.2	31.9	10.4	3.1	18.3	15.5	166.4	8.6	35.1	189.7
2005	132.4	55	60.4	79	26.6	9.2	7.5	75.3	5.1	25.7	186.8	10.4
2006	76.6	80.2	37.1	55.9	86.8	9	8.5	115.4	55.1	163.4	32.8	68.7
2007	50.5	20.9	44.3	33.1	14.2	3.7	3.4	12.9	13.3	26.3	76.4	83.5
2008	141.3	57.8	60.7	49.9	4	39.9	0	35.6	9.2	33.6	105.4	40.4
2009	74.6	66.5	69.6	26.6	10	13.2	50.5	10.6	18.2	79.3	42.4	33.3
2010	58.3	36.8	20.2	60.3	3.1	56.9	6.1	9.5	8.2	71.2	68.3	121.4
2011	120.3	12.8	76.3	13.6	118	105.9	86.7	15.1	0.9	74.1	53	131.6
2012	16.3	101.4	90.1	2.9	12.5	38.4	0	34.6	58.5	45.3	29.9	88.8
2013	24.6	70.3	45	61.7	31.3	11.3	11.8	0	0.5	52.7	108.4	108.1
2014	71.9	81.8	37.3	27.6	2.5	0	0	65.2	60.7	41.2	63.8	39.7
2015	54.4	88.3	59.7	107.5	3	98.1	114.1	22.9	53	19.8	90.9	5.5
2016	28.2	100.1	109.7	26.3	23.5	7.7	69.4	11.5	25.8	19.9	74	30

Borehole discharge rate used in Chapter 8 for validation of groundwater potential zone map

Latitude	Longitude	Date And Time	Discharge Rate	Well ID
-32.9983	27.33267	2/23/1990 0:00	1.53	316

-32.9974	27.50713	6/1/1974 0:00	0.23	672
-32.9969	27.50099	12/2/1980 15:00	1.69	645
-32.9969	27.50099	12/2/1980 23:00	1.69	646
-32.9969	27.501	11/8/1956 0:00	0.53	647
-32.9967	27.32111	1/30/1980 9:00	1.11	303
-32.9967	27.32111	1/30/1980 12:00	1.11	304
-32.9967	27.32111	1/30/1980 4:00	1.21	305
-32.9967	27.32111	1/30/1980 3:00	1.43	306
-32.9966	27.48877	12/15/1970 0:00	5.05	606
-32.9966	27.48877	11/8/1956 0:00	2.52	605
-32.9966	27.48877	1/12/1946 0:00	0.23	604
-32.9966	27.48878	11/27/1956 0:00	0.76	607
-32.9966	27.48879	6/20/1949 0:00	3.79	608
-32.9966	27.4888	2/14/1946 0:00	0.04	609
-32.9961	27.28352	11/27/1968 0:00	2.53	248
-32.9944	27.09322	3/8/1983 14:00	0.47	48
-32.9944	27.09322	3/8/1983 13:00	0.69	49
-32.9944	27.09322	3/8/1983 12:00	0.77	51
-32.9944	27.09322	3/8/1983 11:00	1.02	54
-32.9944	27.09322	3/8/1983 10:00	1.14	55
-32.9944	27.09322	3/8/1983 9:00	1.27	56
-32.9944	27.09322	3/8/1983 8:00	1.62	57
-32.9941	27.47267	10/8/1968 0:00	1.26	557
-32.9941	27.47269	1/6/1939 0:00	0.04	558
-32.9939	27.23574	6/11/1975 0:00	0.14	188
-32.9938	27.23573	3/3/1952 0:00	2.27	187
-32.9938	27.23574	1/29/1985 0:00	1.67	189
-32.993	27.29822	11/26/1968 0:00	0.29	271
-32.9927	27.23933	7/12/1957 0:00	0.38	191
-32.9927	27.23933	3/3/1952 0:00	2.27	192
-32.9925	27.47072	5/8/1968 0:00	0.53	555
-32.9924	27.47072	5/14/1945 0:00	1.07	556
-32.9902	27.36628	7/19/1949 0:00	3.79	394
-32.9897	27.35747	9/14/1977 0:00	0.42	375
-32.9891	27.08295	11/11/1949 0:00	0.63	31
-32.9887	27.23047	9/16/1977 0:00	0.28	184
-32.9884	27.38323	7/19/1949 0:00	3.79	411

-32.9869	27.07447	11/11/1949 0:00	0.63	29
-32.9844	27.2676	7/12/1957 0:00	0.38	212
-32.9832	27.16661	11/18/1980 0:00	0.73	107
-32.9817	27.2638	9/1/1976 0:00	0.06	199
-32.981	27.26888	5/27/1987 10:00	0.33	213
-32.981	27.26888	5/27/1987 11:00	0.33	214
-32.981	27.26888	5/27/1987 12:00	0.33	215
-32.981	27.26888	5/27/1987 13:00	0.33	216
-32.981	27.26888	5/27/1987 14:00	0.33	217
-32.981	27.26888	5/27/1987 15:00	0.33	218
-32.981	27.26888	5/27/1987 9:00	0.36	219
-32.981	27.26888	5/27/1987 8:00	0.56	220
-32.981	27.26888	5/27/1987 7:00	0.72	221
-32.981	27.26888	5/27/1987 6:00	0.92	222
-32.9808	27.56349	2/7/1974 0:00	0.33	790
-32.9808	27.26905	1/29/1985 14:00	1.67	228
-32.9808	27.26905	1/29/1985 18:00	1.67	229
-32.9808	27.26905	1/29/1985 10:00	1.83	230
-32.9808	27.26905	1/29/1985 9:00	3.67	231
-32.9748	27.06847	4/20/1954 0:00	2.53	25
-32.9734	27.31742	2/17/2009 8:00	0.04	302
-32.9721	27.61136	5/21/1951 0:00	0.08	820
-32.971	27.30711	11/26/1978 0:00	0.29	293
-32.9702	27.51561	7/27/1965 0:00	0.36	688
-32.9672	27.066	2/17/1975 0:00	0.31	18
-32.9672	27.06661	12/31/1939 0:00	0.51	23
-32.9672	27.06661	3/11/1954 0:00	0.63	24
-32.9669	27.34323	7/29/1975 0:00	3.61	340

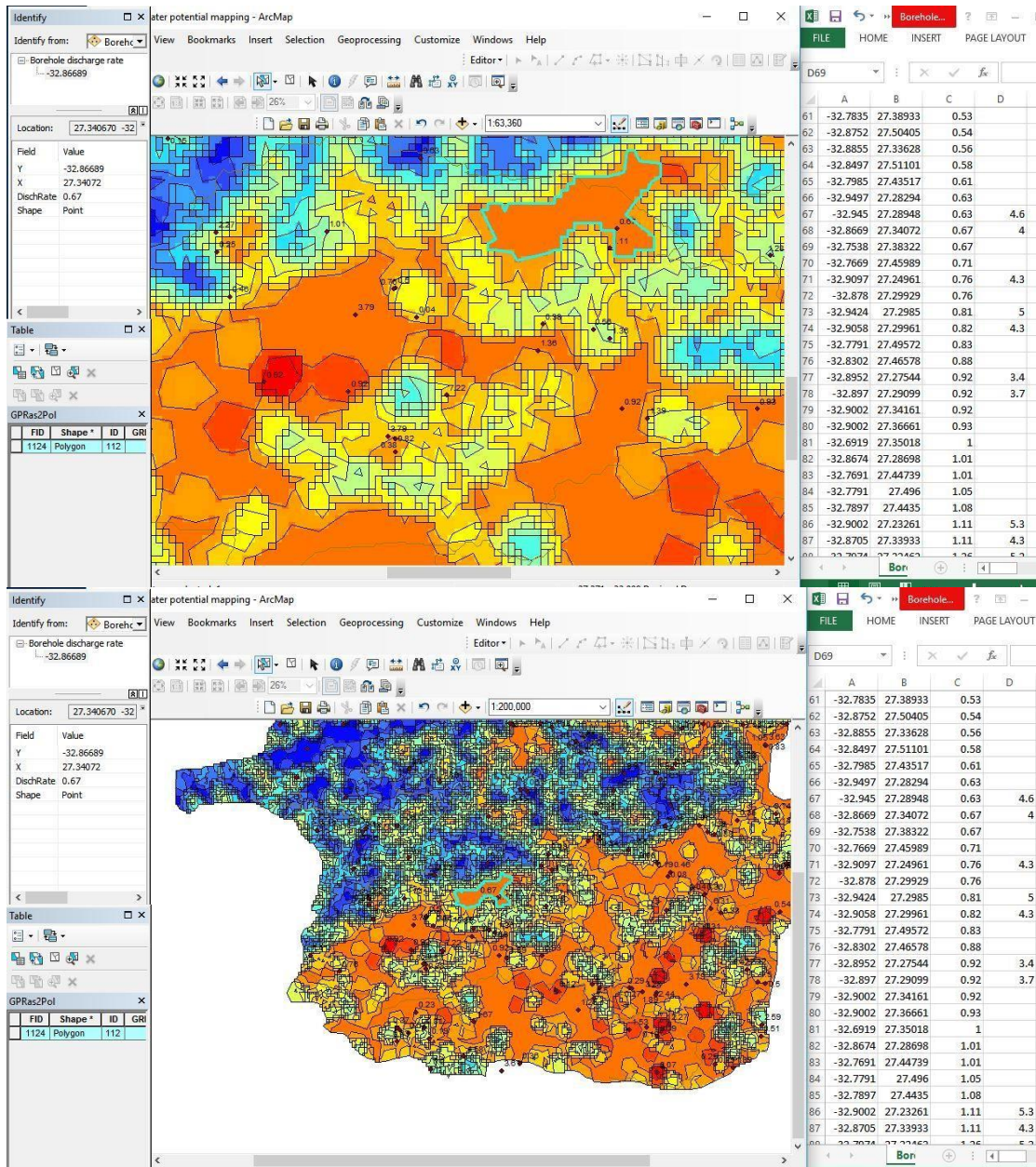


Figure 3. 2. Picture showing manual extraction of integers of GWPZ within the spatial identity of borehole yield in Arcmap 10.5.1 and Excel spreadsheet.